UNIVERSITY OF BIRMINGHAM

MANUFACTURING AND DEVELOPMENT OF IMPLANTABLE DRUG DELIVERY DEVICE FOR THE LOCALISED TREATMENT OF GLIOBLASTOMA

by

GHADEER YOUSEF WAN WAN

A thesis submitted to the University of Birmingham for the degree of

DOCTOR OF PHILOSOPHY

School of Pharmacy

College of Medical and Dental Sciences

University of Birmingham

July 2023

Abstract

Glioblastoma (GBM) is an aggressive brain tumour with low survival rates. The blood-brain barrier (BBB) limits drug penetration into brain tissue, affecting the effectiveness of systemic chemotherapy. Localised drug delivery devices have emerged as a promising solution to address these limitations. This study focuses on developing and investigating biodegradable implantable devices to directly deliver chemotherapeutic drugs to brain tissue, reducing systemic administration and recurrence risk. Irinotecan (IRN) has shown success in clinical trials against GBM. However, large intravenous doses of IRN lead to severe systemic side effects. The study investigates the local delivery of IRN through implantable drug delivery devices to improve therapeutic outcomes while minimising adverse effects. The first study develops IRN-loaded poly(lactic-co-glycolic acid) (PLGA) implants using injection moulding (IM) and hot melt extrusion (HME) techniques. The study compared IM and HME implants, finding that HME implants showed better drug content uniformity and homogeneous drug distribution due to high shear mixing. Factors such as PLGA type, drug load, and implant size influenced drug release behaviour. HME implants exhibited slower drug release due to their denser matrix. Accelerated release studies showed both IM and HME implants had sustained release over seven days, with HME implants considered preferable based on drug content, stability, and distribution results. Pitavstatin (PTV) effectively slows tumour growth, but its limited BBB penetration suggests potential benefits of local administration. The second study involves the development of PTV-loaded PLGA implants using IM and HME techniques. Both IM and HME implants demonstrate an amorphous state of PTV. HME implants show higher drug content and uniformity due to homogeneous drug

distribution facilitated by high shear mixing force, making them preferable over IM. In vitro drug release studies revealed slower drug release from HME implants due to denser matrices, and accelerated release studies confirmed sustained release over seven days for HME implants. In the third study, the high-performance liquid chromatography (HPLC) method was developed and validated for quantifying IRN and PTV in multi-layered implantable drug delivery devices. This method allowed precise drug release quantification, ensuring accurate safety and efficacy assessment of the devices. The final study involves the development of IRN-PTV-loaded PLGA implants as multi-layered devices using HME. The purpose of combining IRN and PTV in these implants is their synergistic effects against the GBM. The multi-layered implants were characterised using HPLC, differential scanning calorimetry (DSC), X-ray diffraction (XRD), and Raman spectroscopy. They demonstrated uniformity in size, weight, and drug content, validating the reliability of the HME technique. XRD and DSC analyses confirmed crystalline IRN in the IRN-PLGA layer and amorphous PTV in the PTV-PLGA layer, suggesting enhanced drug bioavailability and therapeutic effectiveness. Raman mapping reveals homogeneous drug distribution within the implants, ensuring consistent drug release. In vitro studies show biphasic drug release over seven days, characterised as non-Fickian behaviour by the Korsmeyer-Peppas model. This enhances our understanding of the release mechanism. This thesis presents advancements in implantable drug delivery devices for localised GBM treatment, offering valuable insights into formulation compositions and manufacturing techniques. Further research is necessary to assess in vivo performance and therapeutic efficacy.

Acknowledgement

First and foremost, I would like to express my deepest gratitude to my supervisor, Dr. Christopher McConville, for his valuable guidance and instructions throughout this project and over the years of my PhD study. His willingness to give his time so generously has been greatly appreciated. I would also like to extend my gratitude to my family and friends. To my loving parents and siblings, Yousef, Faizah, Hadeel, Ahmed, Anas, Lama, and Hanadi, who initially encouraged me to pursue this PhD. I would not have been able to achieve this accomplishment without them. Special thanks go to my best friend Maab and my amazing cousins – Hana, Heba and Asma – and all other cousins for their endless support, encouraging words, and prayers. I want to express my gratitude to my friends and lab mates, especially Ruba, Manna, Dina, and Shareen, as well as other colleagues at the Pharmacy school. Their kindness and support have truly made my studying and living in the UK an amazing experience. Finally, I would like to acknowledge Umm Al Qura University and the Saudi Arabian Cultural Bureau, Royal Embassy of Saudi Arabia, for their financial support.

In conclusion, I am grateful to everyone who has been a part of my journey and has contributed to my growth and success. Each person mentioned here has played a significant role in shaping my academic and personal development, and for that, I am truly thankful.

Covid-19 impact statement

Due to the onset of the Covid-19 pandemic during the initial stage of the second year of my PhD, there have been some impacts on my project as a result of the lockdown restrictions and the safety measures.

The main impacts are as follows:

- I did not get to test the multi-layered IRN-PTV-loaded PLGA implants in animal studies.
- I did not get to test the in vivo release studies to correlate with the in vitro release behaviour.
- I did not get to test the accelerated stability testing to identify the optimal storage conditions for the drug-delivery device.
- I did not get to optimise the HME manufacturing technique, further optimisation of the extrusion settings, such as temperatures and screw speed, is needed to investigate their ability to predict the drug release rate and timing.

Table of contents

List of Figures

List of Tables

List of Abbreviations

AUC Area Under The Curve

APIs Active Pharmaceutical Ingredients

ALL Acute Lymphoid Leukaemia

BCNU Carmustine

CNS Central Nervous System

CT Computerised Tomography

Cs-131 Caesrium-131

DCM Dichloromethane

DEB Drug Eluting Beads

DMSO Dimethyl Sulfoxide

dH_2O Deionised Water

DSC Differential Scanning Calorimetry

EGFR Epidermal Growth Factor Receptor

FDA Food and Drug Administration

FGFR1 Fibroblast Growth Factor Receptor 1

GBM Glioblastoma

GT Gamma-Tile

HME Hot Melt Extrusion

ICH	International Council For Harmonisation
IDDS	Implantable Drug Delivery System
IDH	Isocitrate Dehydrogenase gene
IM	Injection Moulding
IRN	Irinotecan
MDR-1	Multidrug Resistance Protein 1
Mw	Molecular Weight
MGMT	O6 Methylguanine Methyltransferase
MRI	Magnetic Resonance Imaging
PAT	Process Analytical Technology
PBS	Phosphate Buffered Saline
PCL	Poly (caprolactone)
PLA	Poly (lactide acid)
PLGA	Poly Lactic-Co-Glycolic Acid
PTV	Pitavsatatin
PVA	Biocompatible Polyvinyl Alcohol
RCTs	Phase III Randomised Clinical Trials
RT	Radiation Therapy
TERT	Telomerase Reverse Transcriptase

TMZ Temozolomide

Tg Glass Transition Temperature

WHO World Health Organization

XRD X-ray Powder Diffraction

CHAPTER 1: INTRODUCTION

1.1 Gliomas

Glioma is the most prevalent type of primary brain tumour found in the brain parenchyma of adults (Lee et al., 2018; Lee & Wee, 2022; Wen & Kesari, 2008). They account for approximately 80% of all malignant primary brain tumours and are the most frequent tumours of the central nervous system (CNS) (Agnihotri et al., 2013; Hanif et al., 2017; Messali et al., 2014; Schwartzbaum et al., 2006). The World Health Organization (WHO) has established a classification system for gliomas that relies on layered reports diagnosis approach (Figarella-Branger et al., 2022; Lee & Wee, 2022; Osborn et al., 2022). The layered report includes histological classification, grade determination, and molecular information. The histological classification considers factors such as nuclear atypia, mitotic activity, perivascular proliferation, the degree of necrosis, and clinical results. The 2021 WHO classification has recently undergone a paradigm shift, emphasising molecular information as the primary evidence for classifying gliomas and determining their grade. This significantly differs from the previous reliance on classic histology (Figarella-Branger et al., 2022; Lee & Wee, 2022). This updated classification divides the diffuse glioma into; adult type diffuse glioma, paediatric type diffuse low-grade glioma and paediatric type diffuse high-grade glioma (Osborn et al., 2022). The adult-type diffuse gliomas consist of three main subtypes: astrocytoma with Isocitrate dehydrogenase gene (IDH) mutation, oligodendroglioma with IDH mutation and 1p/19q codeletion, and glioblastoma with IDH wildtype. These subtypes are characterised by specific molecular alterations, irrespective of their morphological characteristics (Komori, 2023; Osborn et al., 2022).

1.2 Glioblastoma: description, incidence, and symptoms

Glioblastoma (GBM) is a subtype of adult diffuse glioma, characterised by being IDH wildtype and grade 4 according to the 2021 WHO classification (Canoll & Goldman, 2008; Lee et al., 2018; Louis et al., 2021; Melhem et al., 2022). It is recognised as the most prevalent and aggressive primary malignant tumour of the brain and central nervous system (Grochans et al., 2022; Koshy et al., 2012; Melhem et al., 2022). It accounts for 14.5 percent of all central nervous system tumours and 48.6 percent of malignant central nervous system tumours (Grochans et al., 2022; Koshy et al., 2012). Patients with GBM have poor survival outcomes, with only a 5% to 10% overall survival rate over five years (Lee & Wee, 2022; Ostrom, Cioffi, et al., 2019). The symptoms of GBM are diverse and can vary depending on the location and size of the tumour. Increased pressure within the brain, indicated by common symptoms like headaches, nausea, vomiting, and drowsiness, patients may additionally experience seizures, changes in personality, and visual or speech disturbances (Ellor et al., 2014; Hanif et al., 2017; JOVČEVSKA et al., 2013). The incidence of GBM might vary from 3.19 cases per 100,000 people per year to 4.17 cases per 100,000 people per year, depending on the report, making it challenging to characterise precisely (Fabbro-Peray et al., 2019; Grochans et al., 2022; Perry & Wesseling, 2016; Razavi et al., 2016). Although GBM is a rare disease with a worldwide incidence of less than 10 cases per 100,000 individuals, its poor prognosis and survival rate of only 14–15 months after diagnosis make it a major public health concern (Hanif et al., 2017; Iacob & Dinca, 2009; Lee et al., 2018; Thakkar et al., 2014). The incidence of GBM is influenced by factors such as age, gender, and race/ethnicity, with the incidence rate significantly increasing after age 40. With a

mean age of diagnosis at 65, the incidence is highest between the ages of 75 and 84 years, reaching 15.30 cases per 100,000 individuals. Males have a 1.59 times higher likelihood of developing GBM compared to females, and Caucasians have a 1.99 times higher incidence compared to Africans (Louis et al., 2021; Melhem et al., 2022; Ostrom et al., 2018; Ostrom, Cioffi, et al., 2019).

1.3 Causes and risk factors of GBM

Little is known about the causes of the brain tumours. No underlying genetic causes can be identified. The only risk factor identified to date is high-dose ionising radiation exposure (Bondy et al., 2008; Hanif et al., 2017; Inskip et al., 2001; Ohgaki, 2009). More than 116 cases of GBM linked to radiation exposure have been documented since the 1960s, and it has been predicted, calculated, or estimated that the overall probability of getting GBM after radiotherapy is 2.5% (Hanif et al., 2017; Salvati et al., 2003). Additionally, it has been observed that the relatively low doses of radiation used to treat skin hemangiomas and tinea capitis in children and new-borns have also been linked to relative risks for gliomas (Hanif et al., 2017; Ostrom, Fahmideh, et al., 2019; Wrensch et al., 2002). A significant rise in the risk of glioma in paediatric populations following therapeutic intracranial radiation exposure has also been observed (Hanif et al., 2017; Prasad & Haas-Kogan, 2009). This risk depends on the patient's age, radiation dose, and volume (Hanif et al., 2017; Prasad & Haas-Kogan, 2009). Fewer data are available for adults, although those that are exposed to radiation have a higher risk (Hanif et al., 2017; Prasad & Haas-Kogan, 2009). The effects of ionising radiation after the Japanese populace was exposed to radiation from the atomic bombs in Nagasaki and Hiroshima have also been examined in several studies. They discovered a rise in the frequency of gliomas and all other

forms of brain tumours (Hanif et al., 2017; Prasad & Haas-Kogan, 2009). No proof exists that regular diagnostic radiation exposure to children and adults increases the chance of acquiring GBM (Hanif et al., 2017; Prasad & Haas-Kogan, 2009). Furthermore, patients with acute lymphoid leukaemia (ALL) were more likely to develop GBM, which may be related to side effects from the leukaemia or the chemotherapeutic drugs used to treat ALL (Hanif et al., 2017; Salvati et al., 2003). No significant correlation between GBM and environmental variables such as smoking, nutritional risk factors, electromagnetic fields from mobile phones, serious head injuries, occupational risk factors, or pesticide exposure has been observed (Adamson et al., 2009; Agnihotri et al., 2013; Fisher et al., 2007; Hanif et al., 2017; Inskip et al., 2001; Ohgaki, 2009). However, some agricultural chemicals and insecticides, such as organochlorides and alkylureas mixed with copper sulphates, have been suspected of causing cancer in animal trials. Case-control studies and cohort studies of agricultural labourers have shown outcomes that were equally negative or positive in terms of the risk for brain tumours (Hanif et al., 2017; Wrensch et al., 2002). According to a few studies, ovarian steroid hormones may contribute to the development of GBM (Hanif et al., 2017; Kabat et al., 2010). It has been discovered that gliomas run in families, although the susceptibility gene is unknown (Bondy et al., 2008; Hanif et al., 2017). Only 5–10% of cases have a genetic propensity (Fisher et al., 2007). Researchers discovered an increased incidence of GBM in rare genetic disorders such as neurofibromatosis type 1 and type 2, tuberous sclerosis (Adamson et al., 2009; Bondy et al., 2008; Hanif et al., 2017; Iacob & Dinca, 2009; Ohgaki, 2009). In contrast, case-control studies have demonstrated that a

history of atopic diseases (e.g., eczema, allergies) reduces the incidence of glioma by 30% (Amirian et al., 2016; Melhem et al., 2022).

1.4 GBM location in the brain

GBM often develops in the cerebral hemispheres; 95% of these tumours start in the supratentorial region, compared to a small percentage in the cerebellum, brainstem, and spinal cord (Nakada et al., 2011).

1.5 Characteristics of GBM

GBM is a diffuse glioma with a high tendency to infiltrate the surrounding brain tissue (Ceccarelli et al., 2016). Histological features of GBM include marked hypercellularity, nuclear atypia, microvascular proliferation, and necrosis (D'Alessio et al., 2019). Tumour heterogeneity, another characteristic of GBMs, presents one of the biggest obstacles in treating GBM (Agarwal et al., 2011; Florio & Barbieri, 2012; Furnari et al., 2007; Olar et al., 2012). GBM cells are particularly invasive, proliferative, and angiogenic compared to other types of normal and malignant cells (Karcher et al., 2006). It has been found that the interaction of the integrin heterodimer with the extracellular matrix, which results in alterations to the cytoskeleton's conformation, is what encourages the migration of tumorigenic cells from GBMs to the surrounding tissue (Louis et al., 2016).

1.6 Diagnosis

Magnetic resonance imaging (MRI) has been the primary method for diagnosing GBM for the past few decades to find any abnormal brain structure changes. T1-weighted MRI scans with and without gadolinium, and T2-weighted MRI images are usually used to identify the tumour's size, shape, and location. Several new MRI

methods could produce images with better detail. Diffusion-weighted MRI produces contrast-enhanced MR images by using differential diffusion of water molecules in malignancies and healthy brain tissue. In addition, perfusion-weighted MRI uses a tracer agent to calculate relative cerebral blood flow, volume, and mean transit time to assess the degree of tumour neo-angiogenesis (Korfiatis & Erickson, 2014). Contrast-enhanced "computerised tomography" (CT) scans can be used if MRI technology is not possible (Abd-Elghany et al., 2019). However, MRI is generally considered the primary imaging modality for diagnosing GBM. To confirm the diagnosis, the histological and molecular characterisations are conducted on the surgically removed tumour tissue that is typically removed during the tumour removal procedure (Di Bonaventura et al., 2021). This analysis helps further grade the tumour, identify specific genetic mutations, and classify the specific type of GBM (Di Bonaventura et al., 2021).

1.7 Classification of GBM

GBM is a grade 4 IDH-wildtype diffuse glioma according to the 2021 WHO classification, which serves as the international standard for the nomenclature and diagnosis of gliomas (Guo et al., 2023). The 2021 WHO classification defines three different types of glioma (Guo et al., 2023; Melhem et al., 2022; Osborn et al., 2022)**:**

1. Adult-type diffuse glioma:
    - Astrocytoma, IDH-mutant: This type includes IDH mutations and is graded as 2, 3, or 4 based on histological and molecular characteristics.
    - Oligodendroglioma, IDH-mutant, and 1p/19q-codeleted: This type includes IDH mutations and 1p/19q codeletion and is graded as 2 or 3.

- Glioblastoma, IDH-wildtype: This refers to diffuse gliomas lacking IDH mutations but exhibiting specific molecular features such as microvascular proliferation, necrosis, Telomerase reverse transcriptase (TERT) promoter mutation, epidermal growth factor receptor (EGFR) gene amplification, or specific chromosomal copy number changes (e.g., gain of chromosome 7, loss of chromosome 10), and this glioma is graded as grade 4.

2. Pediatric-type diffuse glioma:
    - Low-grade gliomas occur in young individuals and are characterised by specific genetic alterations such as MYB or MYBL1.
    - High-grade gliomas occur in young individuals and are characterised by specific genetic alterations such as H3K27.
3. Circumscribed Astrocytic Gliomas: This type encompasses specific subtypes of astrocytic gliomas with distinct molecular characteristics, such as BRAF V600E mutations or fibroblast growth factor receptor 1 (FGFR1) alterations.

1.7.1 Molecular subtypes of GBM

GBM has been further classified into three different molecular subtypes (proneural, classical, and mesenchymal) based on gene expression profiles to develop specific clinical strategies. The distinguishing features of proneural transcriptional subtypes are cyclin-dependent kinase 4 (CDK4) and platelet-derived growth factor alpha (PDGFRA). The classical subtype defines the loss of homozygous CDKN2A/B and EGFR amplification. The critical characteristic of the mesenchymal subtype is the loss of neurofibromatosis type 1 (NF1) (Brennan et al., 2013; Ceccarelli et al., 2016; Melhem et al., 2022). In addition to genomic alterations, profiling the epigenome and

methylome has improved the classification of GBM. DNA methylation profiling determined seven distinct entities within GBM. Despite these advances, however, the clinical applicability of these distinct subtypes has yet to be realised (Capper et al., 2018; Melhem et al., 2022).

1.8 Current treatment of GBM

1.8.1 Surgical resection

The current standard treatment for newly diagnosed GBM involves surgically debulking as much of the tumour as possible, followed by radiotherapy and chemotherapy (Kreth et al., 2013; Minniti et al., 2008). Surgical resection is the major component of GBM treatment. Removing a tumour's mass can have several advantages, such as lowering the tumour's burden, lowering seizure frequency, and reducing or even eliminating neurological deficiency. Surgery also plays a diagnostic role because it provides tissue samples for histologic and molecular diagnosis. Moreover, local therapeutic agents can be inserted during surgery to increase the effectiveness of the resection and quality of life (Newton, 2016). However, complete resection is impossible due to the high degree of GBM invasion, which frequently occurs in eloquent areas (Iacob & Dinca, 2009). Therefore, within 2-3 cm of the original tumour, GBM recurrence occurred in 80% of patients (Mrugala, 2013).

1.8.2 Radiation therapy (RT)

Radiotherapy and surgery have been the cornerstone of treatment for GBM since the 1970s, and the combination of the two doubles overall survival in those with malignant gliomas (Walker et al., 1978, 1980; Wick et al., 2018). To allow for adequate wound healing following surgery, RT should not be started until two weeks after surgery (Adamson et al., 2009; Kristiansen et al., 1981). The location, grade,

and histology of the tumour, as well as the extent of the resection surgery, all affect the total dose of radiation (Lapointe et al., 2018). In the current care, the "standard" RT dose for patients with GBM consists of fractionated focused irradiation of 60 Gy with daily fractions of 2 Gray units (Gy), five times per week for six weeks (30 treatment days). Higher doses, different fraction schemes, and radiation sensitisers have all been investigated to increase the therapeutic efficacy of RT, but these efforts have so far been ineffective (Bianco et al., 2017; Buckner et al., 2007a). Nevertheless, Elderly patients are recommended procedures with shorter and hypo-fractionated radiation doses (Bianco et al., 2017; Corso & Bindra, 2016; Patel et al., 2015; Stupp et al., 2014). Patients who simply receive supportive care after surgery had a survival time of 4 to 5 months; however, phase III randomised clinical trials (RCTs) have demonstrated that RT can double that time to 9 to 10 months (Adamson et al., 2009; Kristiansen et al., 1981; Walker et al., 1978). Whole-brain radiation was traditionally used; however, due to most recurrences being found close to the edges of the resection cavity, it became normal to practise irradiating smaller local areas of the brain, minimising potential side effects. Additionally, experience and development led to the introduction of innovative technologies such as focused radiation, intensity-modulated radiotherapy, and 3D-conformal radiotherapy, which made the radiotherapy treatment for the patient more precise and secure as well as stereotactic radiosurgery; however, these are less usually used to treat GBMs (Bianco et al., 2017; Buckner et al., 2007b). Compared to the more targeted and precise three-dimensional conformal RT, whole brain RT did not increase survival. Targeted variants of RT that are highly targeted have been created to be more similar to surgery - hence its generic term, radiosurgery. This procedure is typically

used to treat minor areas (<3 cm), radiographically well-defined lesions in physically inaccessible or eloquent brain regions or in patients with substantial underlying medical conditions who are unsuitable for open resection (Iacob & Dinca, 2009; Kayama et al., 1991). However, Radiation therapy is linked to a number of adverse reactions, including the necrosis of healthy tissues, disruption to the BBB, neurological deficits and headaches (Iacob & Dinca, 2009; Wilson et al., 2014). Resection surgery, radiation therapy, and the drug temozolomide together have been used in the current Stupp protocol for GBM management with better results (Minniti et al., 2008) than resection surgery and radiation therapy alone (Stewart, 2002; Walker et al., 1978).

1.8.3 Systemic chemotherapy

The main administration routes for GBM chemotherapy currently used are oral and intravenous. Although these certainly provide flexibility in administration, treatment of GBM is challenging due to a variety of reasons that frequently prevent drug delivery to the brain:

- High proliferative and infiltrative potential, heterogeneity, and inherent and acquired chemoresistance of GMB cells.
- The tumour microenvironment, such as the capacity to provoke anergic states in surrounding lymphocytes and glial cells, limiting the antitumor immune response.
- The brain macroenvironment, specifically the surrounding BBB and blood-tumour barrier, which restrict the ability of drugs to reach the brain parenchyma (Masui et al., 2016; Tabet et al., 2019).

These systemic chemotherapies have demonstrated some clinical efficacy; however, higher systemic toxicities have been reported because of the high rate of drug diffusion throughout the systemic circulation (Bhandari et al., 2017; Parodi et al., 2019).

1.8.3.1 Temozolomide (TMZ)

TMZ, an oral alkylating chemotherapeutic drug, damages DNA and starts events that kill tumour cells (Day & Waziri, 2012; Wilson et al., 2014). TMZ undergoes intracellular conversion into its active metabolite, MTIC (5-(3-methyl-triazen-1-yl) imidazole-4-carboxamide), which then methylates DNA at the N7 and O6 sites of guanine residues. This process hinders the cell's ability to repair itself and ultimately results in cell death (apoptosis) by breaking down double-stranded DNA (Duwa et al., 2019) (Figure 1.1). The standard care for the treatment of GBM recently included TMZ. Previously, RT alone remained the standard of care following surgical resection because chemotherapy had not been shown to provide any clinically significant advantages (Anton et al., 2012; Wilson et al., 2014).

Clinical research conducted in 2005 found that concurrent radiation therapy plus the drug TMZ, followed by adjuvant TMZ, significantly increased median survival compared to radiation therapy alone (14.6 months versus 12.1 months; $P< 0.001$). In this study's 5-year review, more patients who had received TMZ were still alive (9.8% versus 1.9%; P 0.001) (Minniti et al., 2008; Wilson et al., 2014). These results confirmed the therapeutic effectiveness of TMZ when combined with RT so-called "Stupp regimen," which is now the accepted standard of care for treating GBM (Minniti et al., 2008; Stupp et al., 2006; Wilson et al., 2014). Despite these advancements, the median progression-free survival time is still only seven months

(Clarke et al., 2010). When given TMZ combined with RT, patients get TMZ at a dose of 75 mg/m^2 per day for six weeks. For adjuvant therapy, after RT is finished, patients get 150 mg/m^2/day of TMZ for five days every 28 days for at least six cycles (Minniti et al., 2008; Wilson et al., 2014). As previously stated in the literature, the therapeutic advantage of TMZ is derived from the addition of a methyl group to the purine bases of DNA, which results in DNA damage and sets off a series of events that cause tumour cells to apoptose (Day & Waziri, 2012; Wilson et al., 2014; Zhang et al., 2012). O6 methylguanine methyltransferase, or MGMT, is a DNA repair protein that works to remove methyl groups from the O6 position of guanine and to remove the methyl group that has been added to O6 methylguanine. The removal of this methyl group gives tumour cells resistance to TMZ and other alkylating chemotherapy drugs by protecting cells from the DNA-damaging effects (Kaina et al., 2007; Villalva et al., 2012; Wilson et al., 2014; Zhang et al., 2012). In certain patients, MGMT expression has been reduced or stopped by methylation of the promoter regions of the MGMT gene, inhibiting it from removing methyl groups from the O6 position of guanine (Villalva et al., 2012). As a result, one of the primary factors affecting TMZ sensitivity or resistance in individuals with GBM is the methylation state of the MGMT gene promoter region (Chinot et al., 2007; Hegi et al., 2005; Martinez et al., 2009; van den Bent et al., 2009; Villalva et al., 2012). Unmethylated MGMT patients are much less sensitive to TMZ, but methylated MGMT promotes sensitivity to TMZ in GBM patients. The most frequent adverse effect of TMZ is hematologic toxicity (Gerber et al., 2007; Wilson et al., 2014).

Thrombocytopenia has been observed in approximately 10% to 20% of patients undergoing treatment. Notably, a Phase II clinical trial incorporating a thrombopoietin

receptor agonist, Romiplostin, in adjuvant concurrent chemoradiation treatment (CCRT) demonstrated a higher completion rate of regimens (Le Rhun et al., 2019; Wu et al., 2021). TMZ can cause hepatotoxicity, nausea, anorexia, and other non-hematologic toxicities, which are less frequent (Dixit et al., 2012; Wu et al., 2021). Systemic TMZ is administered in six 5-day, 4-week cycles. In actuality, increasing the number of adjuvant TMZ cycles from 6 to 12 enhances overall survival by 8.4 months but at the expense of increased hematological toxicity (Bhandari et al., 2017; Tabet et al., 2019).

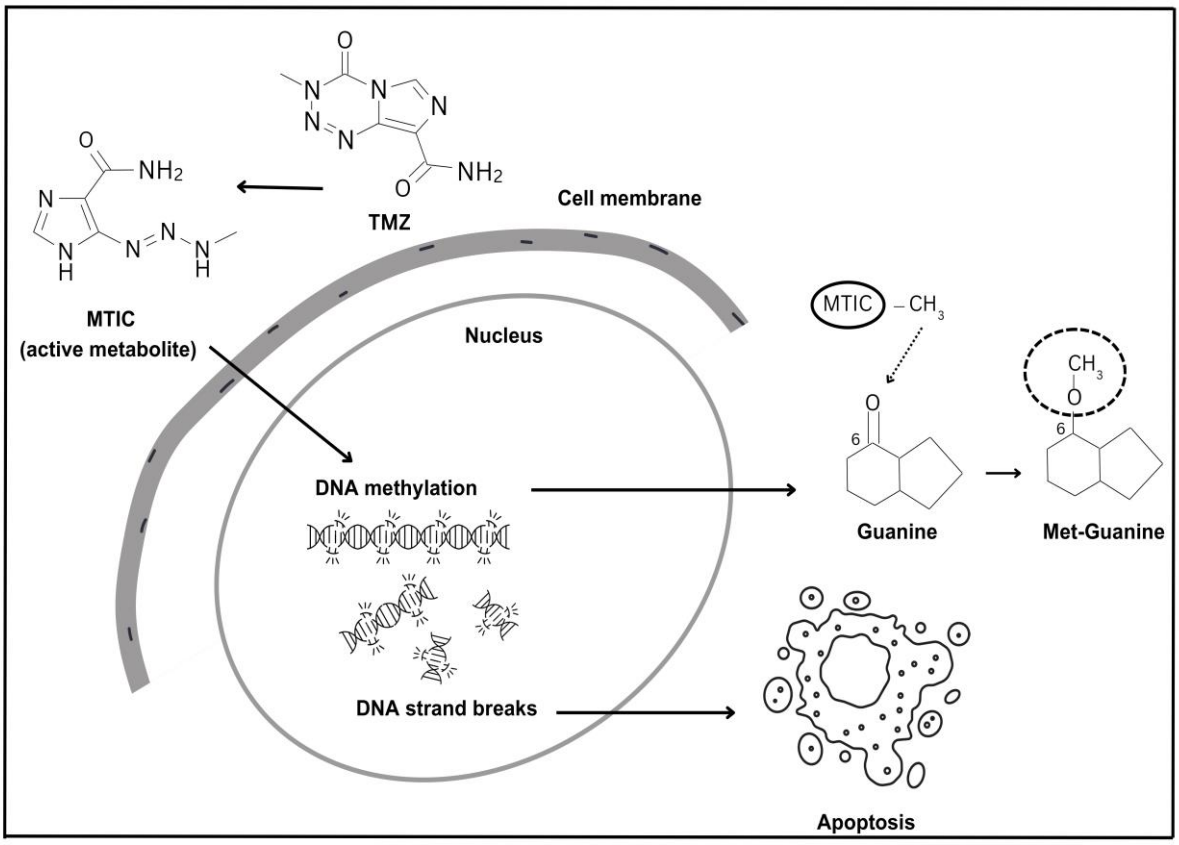

Figure 1. 1 Schematic diagram illustrating the mechanism of action of TMZ. Intracellular conversion of TMZ into its active metabolite, MTIC, initiates the methylation of crucial nucleobases, particularly guanine. This process induces DNA strand breaks, ultimately leading to apoptosis, redrawn and modified from (Duwa et al., 2019; Tomar et al., 2021; Zhang et al., 2012).

1.8.3.2 Carmustine (BCNU)

BCNU was approved for intravenous infusion in 1977 (Bota et al., 2007). BCNU, an alkylating agent, has been utilised as a first-line glioma treatment, much like temozolomide (Engelhard, 2000). BCNU, also known as bis-chloroethyl nitrosourea (BCNU), prevents DNA synthesis and repair by generating interstrand linkages on the DNA chain. Like temozolomide, it acts on the chloroethyl adducts that form at the O6 site of guanine. Chloroethylation displaces a chloride ion from the opposing DNA strand, which develops an ethyl bridge across the DNA strand (Bota et al., 2007). This will stop the DNA from unravelling, which would otherwise restrict DNA replication and cause apoptosis (Dronkert & Kanaar, 2001) (Figure 1.2). Like MGMT mediates resistance to temozolomide, MGMT also mediates resistance to BCNU (Friedman et al., 1998). MGMT does this by eliminating the 30 chloroethyl adducts from the O6 -position of guanine (Esteller et al., 2000). As a result, BCNU is more effective when the MGMT gene is silenced, and MGMT can be artificially depleted using inhibitors like O6-benzylguanine (Wedge & Newlands, 1996). The use of BCNU depends on careful patient group selection because the effectiveness of the medication depends on genes like TP53 and MGMT (Batista et al., 2007; Hegi et al., 2005; Hirose et al., 2001).

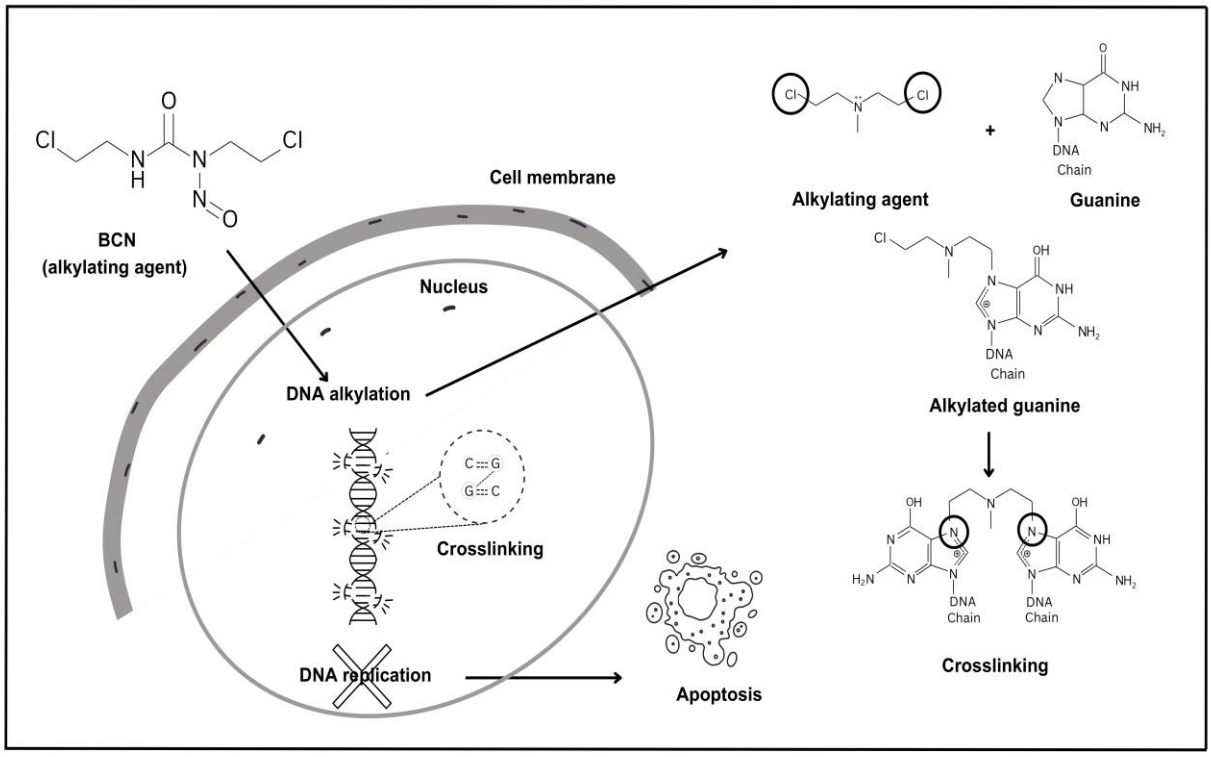

Figure 1. 2 Schematic diagram illustrating the mechanism of action of BCNU, redrawn and modified from (Han et al., 2019; Schjesvold & Oriol, 2021).

1.8.3.3 Lomustine

Lomustine is an additional alkylating anti-tumour drug. Lomustine can pass across the BBB because of its small size and strong lipophilicity. Lomustine is administered orally (Bartzatt, 2013), and its action is connected to the methylation of the MGMT gene, just like TMZ and BCNU (Heiland et al., 2016). Patients are only instructed to administer one dose every six weeks due to the extremely high toxicity, which can have fatal consequences. Lomustine is rarely given for GBM since the introduction of the STUPP regimen because it may result in permanent systemic side effects, such as kidney damage, renal failure, thrombocytopenia, and leukopenia. Patients on lomustine treatment must regularly undergo testing for their electrolyte levels, liver function, and blood count (“Highlights of Prescribing Information.,” 2016).

1.8.3.4 Bevacizumab

Bevacizumab is a humanised monoclonal antibody with anti-angiogenic characteristics, bevacizumab is given intravenously. It binds to and inhibits vascular endothelial growth factor A (VEGF-A), which triggers the formation of new blood vessels when attached to its receptor. Since the levels of VEGF-A in GBM are thought to be 30 times higher than in low-grade astrocytomas, it is a desirable therapeutic target. Bevacizumab does not significantly prolong overall survival for individuals with newly diagnosed GBM, despite treatment apparently prolonging progression-free survival (Khasraw et al., 2010; Wu et al., 2021). Thus, it is mainly applied to the management of recurrent GBM. The combination of Irinotecan (IRN), a small-molecule prodrug that transforms into a topoisomerase I inhibitor, has been investigated (Friedman et al., 2009; Ozel et al., 2016; Wu et al., 2021). However, leukopenia and hypertension are the two side effects of bevacizumab most frequently reported (Brandes et al., 2016; Diaz et al., 2017; Wu et al., 2021).

1.9 Problems associated with systemic chemotherapy

The main factor in their failure is that most GBM therapies are either administered orally or intravenously. Due to the BBB, systemic delivery of chemotherapy drugs to the brain is challenging (Reese & Karnovsky, 1967). Only low molecular weight, electrically neutral, hydrophobic molecules can pass the BBB (Abbott & Romero, 1996; Gawley et al., 2020b; Kemper et al., 2003; Seelig et al., 1994). The majority of chemotherapeutic drugs are large, ionically charged, hydrophilic molecules that make it difficult for them to pass the BBB at the levels needed for therapeutic action, requiring a substantial systemic dose (Abbott & Romero, 1996; Gawley et al., 2020; Greig, 1987; Siepmann et al., 2006; Wang et al., 2002). After systemic delivery, maintaining stable drug levels in the brain might be challenging even if the drug crosses the BBB because it can quickly diffuse back (Gawley et al., 2020b). Local administration would deliver the chemotherapy drug to the tumour directly, providing benefits such as enhanced bioavailability, direct transport to the site of action, a lower amount of drug needed, and fewer adverse effects because systemic circulation would not be involved (Gawley et al., 2020b; Wolinsky et al., 2012). Additionally, given that 80 to 90 percent of GBM returns within 2 cm of the site of resection, local drug delivery may be appropriate for treating GBM (Gawley et al., 2020; Wang et al., 2002). As a result, many local delivery techniques have been researched for direct administration into the brain parenchyma of the resection cavity, including polymer millirods (Gawley et al., 2020b; McConville et al., 2015; Qian et al., 2001; Weinberg et al., 2008), gels (Jackson et al., 2000; Krupka et al., 2006; Vogl et al., 2002; Vukelja et al., 2007), micro and nanoparticle formulations (Béduneau et al.,

2007; Cruickshank et al., 2015; Gawley et al., 2020; Koo et al., 2011; Menei et al., 2005; Meyers et al., 2013; Reguera-Nuñez et al., 2014; Wang, 2012).

1.9.1 Local chemotherapy

As a result of the complications associated with systemic chemotherapy, local chemotherapy has emerged. Local chemotherapy involves the direct administration of chemotherapeutics to the tumour location, as opposed to systemic administration through intravenous injection or oral route (Nam et al., 2018). Local drug delivery would help increase the drug concentration at the tumour site, reducing the side effects associated with systemic chemotherapy (De Souza et al., 2010; Nam et al., 2018). Localised delivery vehicles can also be created in the form of depots, a type of pharmaceutical dosage form that releases the active ingredient of a drug over an extended period of time. Localised drug depots offer a variety of benefits in the delivery of anticancer medications: (1) they enhance the stability of the chemotherapeutic drugs, (2) they produce longer and regulated drug release patterns, which improve drug level control and lower the number of invasive drug administrations, (3) can combine poorly soluble chemicals within the depot, (4) reduce the overall amount of drug in the formulation, and (5) minimise the side effects of chemotherapy (Nam et al., 2018; Wolinsky et al., 2012). The local delivery strategy appears to have additional advantages for treating GBM and other brain disorders since it can avoid the BBB and concentrate higher amounts of a drug in the cancerous tissues (Chakroun et al., 2018; Nam et al., 2018). In addition, to target the remaining cells when there is the least tumour burden. Two main delivery technologies have been created to date for local delivery of chemotherapies to target residual disease: Gliadel wafers and brachytherapy.

1.9.1.1 Gliadel wafer

Gliadel wafer, a local delivery device, was created first to increase the therapeutic effectiveness of BCNU by administering the drug locally. BCNU stability was extended, and the dosage required was reduced as a result of avoiding large drug distribution and rapid liver elimination rates (Fleming & Saltzman, 2002; Wait et al., 2015). It is a disc-shaped, 200 mg biodegradable wafer (Siepmann et al., 2006; Wolinsky et al., 2012; Zembko et al., 2015) manufactured using 1,3-bis(p-carboxyphenoxy) propane: sebacic acid (20:80 ratio) polymer and containing 3.85 % w/w of the chemotherapy drug BCNU (Attenello et al., 2012). These wafers have a diameter of 14.5 mm, a thickness of 1 mm, and contain a total of 7.7 mg of BCNU (Domb et al., 1999). Following surgical removal, a maximum of 8 wafers can be inserted into the tumour bed (Figure 1.3), releasing the drug over five days as the wafers swell and eventually break down (Domb et al., 1999; Wolinsky et al., 2012). Local delivery of chemotherapeutic drugs into the resection cavity is a very promising method since surgical resection plays a crucial role in GBM therapy and because 80–90% of recurrences are located within 2 cm of the original site of the tumour (Hochberg & Pruitt, 1980; Wang et al., 2002; Westphal et al., 2003). The Food and Drug Administration (FDA) approved the Gliadel® wafer in 1996 to manage recurrent GBM (Fleming & Saltzman, 2002; Valtonen et al., 1997). Initial research demonstrated the effectiveness of these wafers in treating recurrent GBM in patients, with improved overall survival (OS) of 31 weeks as compared to 23 weeks (placebo wafers) (Brem et al., 1995), which, coupled with other clinical trials, resulted in FDA approval for recurrent GBM in 1997. Additional clinical studies on newly diagnosed GBM resulted in expanded FDA approval in 2003 (Ashby et al., 2016; Westphal et

al., 2003). Similar to TMZ, Gliadel wafers extended patient survival by two months (in a subset of patients) as compared to radiation (RT) alone (Ashby et al., 2016).

However, not all patients are suitable for Gliadel wafers. Wafers can only be implanted if the resection cavity's size, shape, and site enable it. A wide resection cavity is needed to fit eight wafers considering that they are each 1.45 cm in diameter and 1 mm thick (Desai & Lee, 2008). Besides, It results in post-implant problems such as tumour cyst formation, intracranial abscess, meningitis, delayed wound healing, cerebrospinal fluid leak, seizures, and cerebral abscess (Engelhard, 2000). In addition, Gliadel wafers can only penetrate a few millimetres (1mm or less) due to the dependence on drug diffusion from the device into the brain parenchyma. According to a study by Fung et al., drug penetration from the wafer in rats reached a maximum of 5 mm in the first three days after implantation. This dispersion decreased to 1 mm from the implant site after 3 to 14 days (Fung et al., 1998). Previous studies show that recurrence, however diffuse, frequently occurs within 2 cm of the initial tumour (De Bonis et al., 2013). As a result, the limited diffusion and high BCNU transcapillary penetration limit the potential of this local delivery device. Gliadel wafers release the majority of the drug content within the first week, and after this initial large bolus release, the adverse effects of this technique start to manifest (Domb et al., 1995; Fleming & Saltzman, 2002; Fung et al., 1998; Grossman et al., 1992; Tabet et al., 2019). A stiffer matrix does not necessarily indicate a prolonged release in vivo (Tabet et al., 2019).

Figure 1. 3 Gliadel Wafers inserted intracranially into a cavity used to treat a GBM adopted from (Wolinsky et al., 2012).

1.9.1.2 Brachytherapy

Brachytherapy is a localised treatment where a sealed radioactive source or seed is inserted into the tumour or surgical cavity that degrades over time, releasing radiation to surrounding tissue. In GBM, brachytherapy has been most often utilised with iodine-125, although two phase III randomised trials found no improvement in survival (Barbarite et al., 2017; Gawley et al., 2020b; Laperriere et al., 1998; Waqar et al., 2022). Additionally, brachytherapy technology advancements have increased its safety, which has raised support for its use. Gamma-Tile® (GT), a new brachytherapy technology, contains seeds of caesium-131 (Cs-131) embedded in absorbable radioisotope carrier systems (Gessler et al., 2020; Waqar et al., 2022). The radioactive seed has a physical length of 4.5 mm and an exterior diameter of 0.8 mm (Ferreira et al., 2021; Murphy et al., 2004; Rivard et al., 2017). GT delivers 120–150 Gy at the cavity surface, and at 5 mm depth, it maintains 60–80 Gy (Brachman et al., 2019; Gessler et al., 2020). GT offers a cumulative radiation boost earlier than

radioisotopes like iodine-125 from an efficacy standpoint because it has a shorter half-life (Gessler et al., 2020; Waqar et al., 2022). GT is approved as a treatment for newly discovered malignant and recurrent brain tumours (Gessler et al., 2020; Rivard, 2007; Youssef et al., 2017).

However, one of the drawbacks of this treatment for these tumours has been the frequent occurrence of radiation necrosis in malignant gliomas treated with high-dose radiation (Marriott et al., 1998; Vitaz et al., 2005; Wald et al., 1997). Additionally, brachytherapy dosage distributions do not reach GBM cells that are more distantly invasive (Giordano et al., 2019; Waqar et al., 2022). This therapy is unlikely to be effective on tumour cells more than 5-8 mm away from the resection cavity where the GT is placed (Gessler et al., 2020).

1.10 Selected drugs suitable for local drug delivery to treat GBM

1.10.1 Irinotecan (IRN)

IRN is a semi-synthetic analogue of camptothecin that was discovered in 1983 in Japan in *Camptotheca acuminata* Chinese plants (Rothenberg, 2001). IRN is metabolised into the active form of 7-ethyl-10-hydroxycamptothecin (SN-38) (Figure 1.4), a topoisomerase I inhibitor and 100–1000 times more potent than IRN (Xu & Villalona-Calero, 2002). Topoisomerase I enzymes work within the cell to cause transient breaks in one or both DNA strands, enabling the DNA to uncoil for transcription and replication (Gawley et al., 2020b; Sinha, 1995). Topoisomerase I creates a covalent bond with DNA during this step, allowing it to form a cleavable complex (Gawley et al., 2020b; Sinha, 1995). In this way, SN-38 binds to Topoisomerase I and prevents the enzyme from reconnecting the DNA strands, leading to S-phase-specific cell death (Gawley et al., 2020; Sinha, 1995;

Vredenburgh et al., 2009; Xu & Villalona-Calero, 2002). IRN has been approved for the first and second-line therapy of colorectal cancer and other solid tumours (Potmesil, 1994; Ramesh et al., 2010). IRN has demonstrated clinical activity against colorectal, lung, stomach, cervical, and ovarian cancers, as well as malignant lymphoma and other malignancies (Masuda et al., 1992; Ohno et al., 1990; Ramesh et al., 2010; Shimada et al., 1993).

IRN has been used as a second or alternative line treatment for GBM for patients who do not act in response to the treatment with TMZ or BCNU (Iacob & Dinca, 2009). Treatment with TMZ plus BCNU may result in resistance or severe unfavourable side effects. As a result, the ability of IRN to cross the BBB (Hasselbalch et al., 2010) and the differential mechanism of action from temozolomide are useful in overcoming GBM resistance to temozolomide (Hasselbalch et al., 2010; Vredenburgh et al., 2007). A study showed that after receiving IRN intravenously, 55 percent of 60 glioma patients responded for 12 to 42 weeks (Friedman et al., 1999). However, IRN can pass through the BBB, it requires high intravenous doses of between 125 and 500 mg/m^2 to reach therapeutic levels in the brain. This can have severe systemic adverse effects, such as gastrointestinal toxicity that can cause both early and late-onset diarrhoea and severe neutropenia (Gawley et al., 2020b; Hecht, 1998). All these issues with the systemic administration of IRN have led to the development of novel drug-delivery techniques for transferring IRN to the brain (Gawley et al., 2020a). Local delivery of IRN might improve therapeutic results by delivering a larger dose locally to the tumour resection site and minimising systemic concentrations, which would minimise the aforementioned side effects.

Drug Eluting Beads (DEB) implanted into the brains of healthy and tumour-bearing BD IX rats were manufactured from a modified, biocompatible polyvinyl alcohol (PVA) hydrogel and contained either doxorubicin or IRN, according to histology and survival studies (Baltes et al., 2010). When IRN or doxorubicin DEB was administered to the rats, they demonstrated a substantial difference in survival compared to the placebo group. Although there was no statistically significant difference between the survival curves of doxorubicin and IRN DEB, there was some local toxicity associated with the use of doxorubicin DEB, which led to noticeable haemorrhage around the area of implantation of the beads. IRN had no such impact (Baltes et al., 2010; Gawley et al., 2020b). According to the results of this study, compared to the pattern often seen with Gliadel® wafers, there was no evidence of swelling, inflammation, or any indication that a pseudo-abscess had formed. This suggests lower local toxicity and a lower risk of infection. This is because IRN is less toxic than BCNU, making it better suitable for local administration to the brain. It is also injected directly into the brain parenchyma rather than deposited in the resection cavity. This study shows that local distribution into the brain parenchyma provides a safe therapeutic benefit over systemic delivery in treating GBM if the medication selection and administration technique are adequate. Although most of the DEB gel formulation was forced out of the brain parenchyma and into the bed of the resection cavity, the DEBs could only supply IRN for up to 72 hrs. Because of this, manufacturing solid implants with PLGA polymers might supply drugs for a much longer time and will stay inside the brain parenchyma.

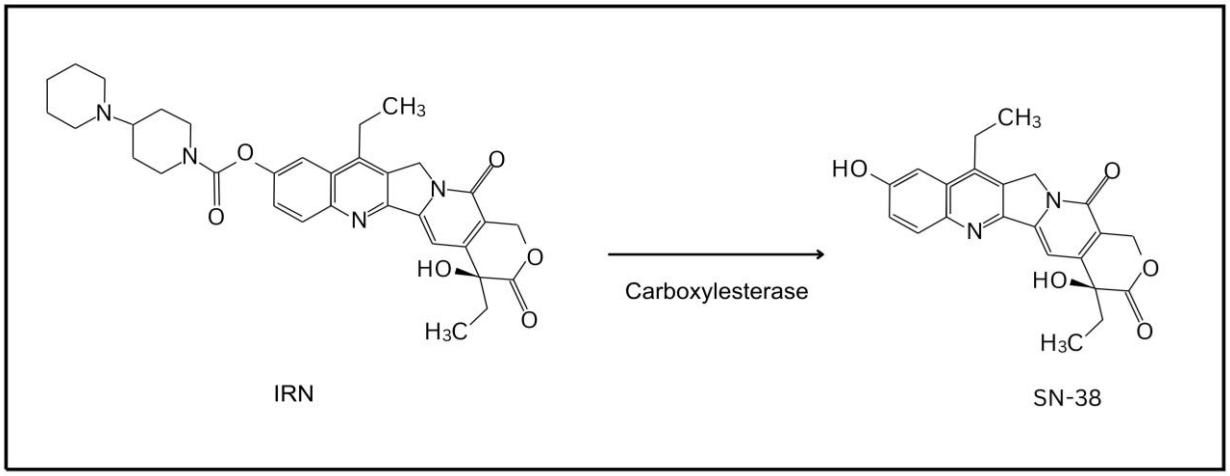

Figure 1. 4 Chemical structure of IRN and its active metabolite SN-38, adopted and redrawn from (ISHIMINE et al., 2020).

1.10.2 Pitavastatin (PTV)

PTV (Figure 1.5), a drug from the statin group, is often used to treat high blood cholesterol levels (Stein, 2003; Voss et al., 2021). PTV inhibits the liver's HMG-CoA (3-hydroxy-3-methyl-glutaryl-CoA) reductase, which regulates cholesterol production (Ose, 2011). Multiple studies have shown statin drugs, such as PTV, to be effective in slowing the growth of tumours (Jiang et al., 2014; Nielsen et al., 2012; Thurnher et al., 2012). According to a study, PTV reduced multidrug resistance protein 1 (MDR-1) and promoted cellular autophagy in GBM tumour cells (Jiang et al., 2014). The mechanism of action was postulated to involve PTV's effects on the metabolism of cholesterol, a substance found in cell membranes, and tumour cell signalling, both of which are critical for developing tumours. Since GBMs are highly proliferative cells, they need a lot of cholesterol, which may cause them to respond to statin therapy (Jiang et al., 2014). Additional research suggests that statins can cause GBM cells to apoptosis by targeting LDL cells and acting via the ERK/AKT pathway (Guo et al., 2011; Yanae et al., 2011).

The findings on the cytotoxicity of statins against GBM cells stated above have prompted scientists to investigate the cytotoxicity of the IRN and PTV dual therapy. PTV has proven more effective than other statin drugs and produces synergistic effects when combined with IRN (Jiang et al., 2014). One mechanism for drug resistance in GBM is the overexpression of the MDR-1, often referred to as the permeability glycoprotein pump or P-glycoprotein 1 (PGP) (Nabors et al., 1991; Nakai et al., 2009). This protein creates an active transporter that carries cytotoxic agents like IRN out of the cell using ATP (Garrigues et al., 2002; Jiang et al., 2014). When PTV and IRN are used together, there is an increased level of apoptosis. This is

because PTV decreases the glycosylation of MDR-1, inhibiting its function and allowing a higher IRN concentration to enter the GBM cells. This synergistic effect was verified in mice during an in-vivo study (Jiang et al., 2014).

Moreover, it has been suggested that PTV treatment for glioma cells inhibits nuclear factor-kappa B activation, which inhibits autophagy and causes autophagic cellular death (Koukourakis et al., 2016; Tsuboi et al., 2009). A high throughput drug screening assay of GBM cell lines was used by Fan et al. to screen PTV and IRN separately and in combination (Fan et al., 2016). Results showed that the combination medication treatment using IRN and PTV was more successful than using either drug alone. The ability of PTV to pass the BBB is expected to be restricted, with a calculated logarithm value of brain to plasma concentration ratio (-log BB) of -0.6499 (Jiang et al., 2014). Therefore, PTV delivery by oral or intravenous routes will produce sub-therapeutic concentrations in the brain and is not a suitable mode of administration for treating GBM. Local delivery would be the greatest choice.

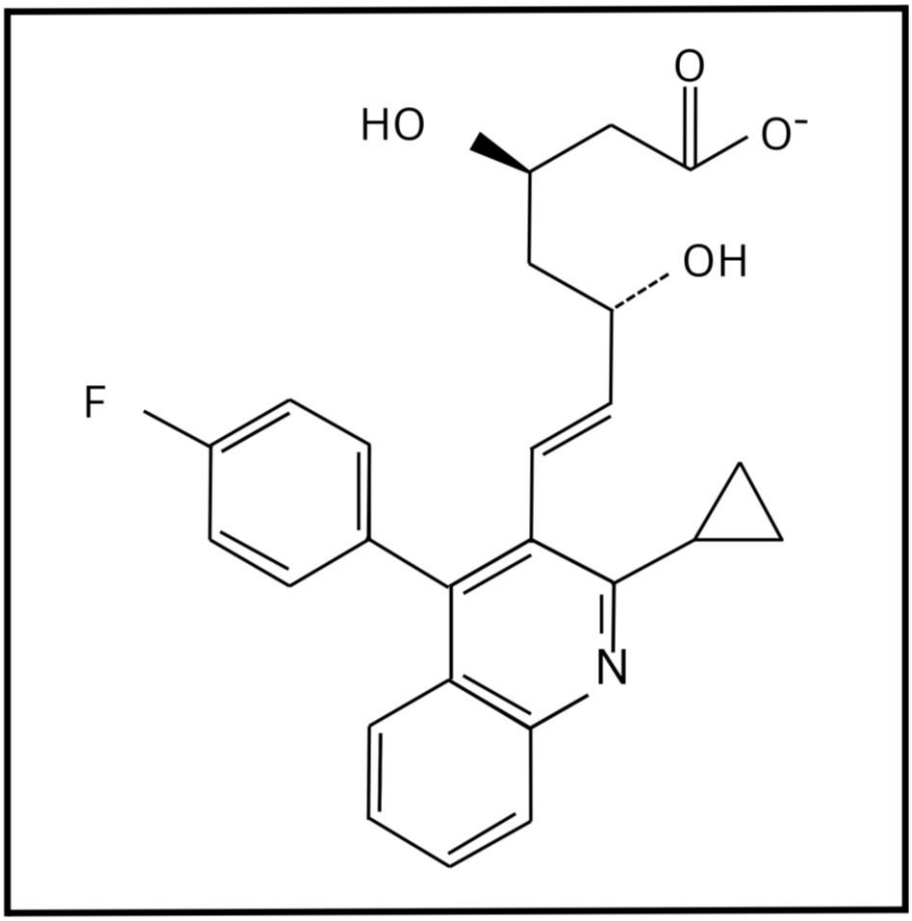

Figure 1. 5 Chemical structure of PTV, adopted and redrawn from (Davignon, 2012).

1.11 Implantable drug delivery system (IDDS)

Polymeric implantable devices are a viable alternate delivery route for drug molecules. IDDS provide localised and targeted drug delivery. They may achieve high local concentrations of active ingredients while reducing or avoiding systemic toxicity (Dash & Cudworth, 1998; Fialho & Silva Cunha, 2005; Langer, 1990; Rajgor et al., 2011; S. Stewart et al., 2018). In the 1960s, IDDS, which uses polymers as delivery vehicles, began to be developed, providing a new idea in drug delivery (Kamaly et al., 2016; Kleiner et al., 2014). Since then, significant efforts have been undertaken to enhance their formulation and release characteristics. These systems allow for the prolonged, continuous, and predictable delivery of drugs, which is particularly helpful for treating chronic disorders requiring repeated treatments (Fung & Saltzman, 1997). The systems were built utilising nondegradable polymers and were first designed to transport hormones, among other therapies (Fung & Saltzman, 1997; Kamaly et al., 2016). They were based on biocompatible polymers with suitable physical properties. The term IDDS refers to both nondegradable and degradable systems. The first controlled-release devices were built on nonbiodegradable polymeric materials such as silicone elastomers (Folkman & Long, 1964; Fung & Saltzman, 1997). The consequence was the development of reservoir drug delivery systems, which release the drug through the polymer wall of the delivery device via controlled diffusion (Brown et al., 1986). The drug was released in a controlled manner, however, a medical practitioner needs to remove the device after the treatment period. After the reservoir IDDS, solid polymer matrices were used for long-term drug release. The need to develop biodegradable IDDS that can degrade into compatible biological components under physiological conditions has

been a significant incentive (Kleiner et al., 2014; Markland & Middleton, 2015). One of the benefits is that the implant does not need to be removed at the end of treatment, which enhances patient compliance, especially when dealing with chronic diseases that require prolonged therapeutic periods and multiple treatments to control the disease. These systems consist of natural or synthetic biodegradable polymers, typically polymers that can be disintegrated in vivo, either enzymatically, nonenzymatically, or both, to yield biocompatible, endogenous metabolites that the body's natural metabolic pathways can remove without toxic effects (Makadia & Siegel, 2011). Biodegradable polymers are widely utilised in matrix implants to create delivery devices by physically trapping drug molecules in matrices. Because biodegradable polymers disintegrate following implantation and drug release, they undergo degradation along with drug release, making it possible to regulate some elements of device degradation and erosion by carefully selecting suitable polymer properties (Fung & Saltzman, 1997). The main benefit of this method over micro and nanoparticles is related to the capability to be removed in the incidence of unfavourable adverse outcomes since the matrix implants retain a degree of reversibility which is not present in depot injections (Makadia & Siegel, 2011; Rabin et al., 2008; SIEGEL et al., 2006).

1.12 Requirements for Implantable drug delivery system (IDDS) in GBM

GBM is a highly complex brain tumour that presents challenging requirements for developing a suitable IDDS. The first step in effectively treating tumours is to provide suitable drug release kinetics in combination with an effective drug. As a result, applied systems should ideally have zero-order controlled release to sustain a constant drug concentration within the therapeutic window at the cancerous site for an extended period of time (Fenton et al., 2018; Hauck et al., 2022). However, there is a growing debate on the potential benefits of incorporating a burst release to deliver a high initial dose of the drug. A burst release strategy may help target and kill the majority of cancer cells while also increasing the diffusion of the drug into the brain parenchyma to reach deep seated tumour cells (Gawley et al., 2020b). Here, the drug release kinetics depend on several factors, including drug loading and solubility, drug diffusion coefficient, and matrix breakdown rates for biodegradable systems (Hauck et al., 2022; Stewart et al., 2018). Furthermore, IDDS should be biocompatible and not harm brain tissue. This involves having appropriate mechanical properties that correspond to the stiffness of the brain tissue, consequently preventing a foreign body reaction (Hauck et al., 2022; Moshayedi et al., 2014). The most widely used polymers, such as poly (lactide acid) (PLA), poly (caprolactone) (PCL), alginate, and poly (lactic-co-glycolic acid) (PLGA), have FDA approval and are well known for their biocompatibility, non-toxic attributes, and biodegradability (Hauck et al., 2022; Mansour et al., 2010). The insertion of the IDDS into the tumour cavity is one of the most important parts of the treatment plan; it is preferable if the IDDS conformally adheres to the surface of the cavity to facilitate

drug penetration into the brain tissue. Additionally, biodegradable devices are helpful since they prevent the need for surgery to remove the IDDS.

1.13 PLGA copolymers used for Implantable drug delivery device

PLGA is a biodegradable and biocompatible copolymer of PLA and PGA (Maurus & Kaeding, 2004; Stewart et al., 2018). The popularity of PLGA has increased among the several polymers used in drug delivery systems because of its biodegradability, biocompatibility, ease of manufacture, and superior mechanical feature (Zhang et al., 2013). This polymer breaks into its primary monomers, lactic and glycolic acids, which are non-toxic and easily excreted from the body through hydrolysis of ester linkages (Fialho & Silva Cunha, 2005; Jain, 2000). Owing to its superior biocompatibility, biodegradability, and drug compatibility, PLGA has become one of the biodegradable polymers that have received FDA approval (Klose et al., 2008). A study by Makadia and Siege (Makadia & Siegel, 2011) demonstrated that PLGA has excellent mechanical properties that enable processing into any shape and size. The study also mentioned that it could be processed into implants using solvent-casting, compression moulding, and extrusion, or it can be manufactured into micro/nanoparticles (AVERINENI et al., 2012; Fonseca et al., 2002; Jin et al., 2009; Mu & Feng, 2003) by solvent evaporation, phase separation, and spray drying. PLGA foams (Ong et al., 2009), films (Steele et al., 2011), electrospun fibres (Xie & Wang, 2006), and hydrogels (SHIM et al., 2007) have also been successfully created for drug delivery applications. Several physical and chemical factors, including pH, ionic strength, temperature, crystallinity, and the presence of drugs, can influence how rapidly these polymers degrade. The nature of the polymer, such as the molecular weight (Mw) and proportion of the lactic and glycolic monomers, can also affect how

well the drug is released (Fialho & Silva Cunha, 2005). It is possible to change the physical properties of the polymer by changing the lactide-to-glycolide ratio and polymer Mw (Makadia & Siegel, 2011; Stewart et al., 2018). PLA has side methyl groups, which increases the copolymer's hydrophobicity. As a result, PLGA copolymers with a high PLA content exhibit greater hydrophobicity and, as a result, degrade at a slower rate. The advantages of PLGA include a higher degradation rate than PLLA but a lower degradation rate than PDLA; and the absence of acidic by products created during degradation (Maurus & Kaeding, 2004; Stewart et al., 2018). The Mw of the PLGA molecules and the composition of the monomers directly affect the polymer's crystallinity. The polymer's degree of crystallinity significantly impacts both the mechanical properties and the rates of degradation. The degree of crystallinity of PLGA decreases with increasing PGA concentration, whereas the rate of hydration/hydrolysis increases. The highest degradation rates are shown in PLGAs, which contain 50:50 PLA:PGA. PLGA copolymers have glass transition temperature (Tg) values above 37°C, displaying a relatively solid chain structure that is suitable for the manufacturing of implants (Stewart et al., 2018). Finally, due to its biocompatibility, mechanical strength, and ease of formulation, PLGA is the biodegradable polymer that is most frequently used for biomedical purposes (Luckachan & Pillai, 2011; Stewart et al., 2018).

1.14 PLGA matrix implant

Matrix implants are solid, rigid objects that often take the form of cylindrical rods millimetres in length and less than a millimetre in diameter. In PLGA matrix implants, a drug is homogeneously dispersed throughout the matrix, making them similar to monolithic implants (Iyer et al., 2006; Sequeira et al., 2018). They are dosage forms that, depending on the type of polymer utilised in their manufacture, provide the controlled release of a drug over an extended time of months or years (Markland & Middleton, 2015; Sequeira et al., 2018). The system does not require additional surgery to remove the implant at the end of the therapeutic period (Iyer et al., 2006; Sequeira et al., 2018).

1.15 Mechanism of PLGA degradation

As previously stated, PLGA degrades through hydrolytic cleavage of its poly (ester) backbone (Houchin & Topp, 2008), as shown in (Figure 1.6). Polymer chains are broken down into oligomers, which are shorter chains (Lao et al., 2011). The matrix's mass is then reduced due to the latter's transformation into CO_2 and water, a process known as erosion (Lao et al., 2011). PLGA is a bulk-eroding polymer (Kapoor et al., 2015; Lao et al., 2011), which consists of four main stages and is a homogenous process in which degradation occurs across the polymer matrix (Lao et al., 2011). First, a polymer swells after absorbing water, which enters secondary or tertiary structures previously held together by hydrogen bonds and van der Waals forces are destroyed. Second, the covalent ester bonds in the polymer backbone begin to break down by hydrolysis, producing an increasing amount of carboxylic end groups that can autocatalyse the process and speed up the breakdown of the polymer backbone. At this stage, the molecular mass starts to decrease, and the mechanical strength begins to decline. Third, the backbone covalent bonds continue to disintegrate massively. Significant mass loss takes place when the Mw reaches a certain point. At the same time as this process occurs, physical and mechanical integrity is lost. Fourth, oligomer solubilisation into the surrounding media causes the polymer to lose a significant mass. The polymer disintegrates into several tiny fragments, which will then undergo hydrolysis to produce free acids (Hines & Kaplan, 2013; Lao et al., 2011).

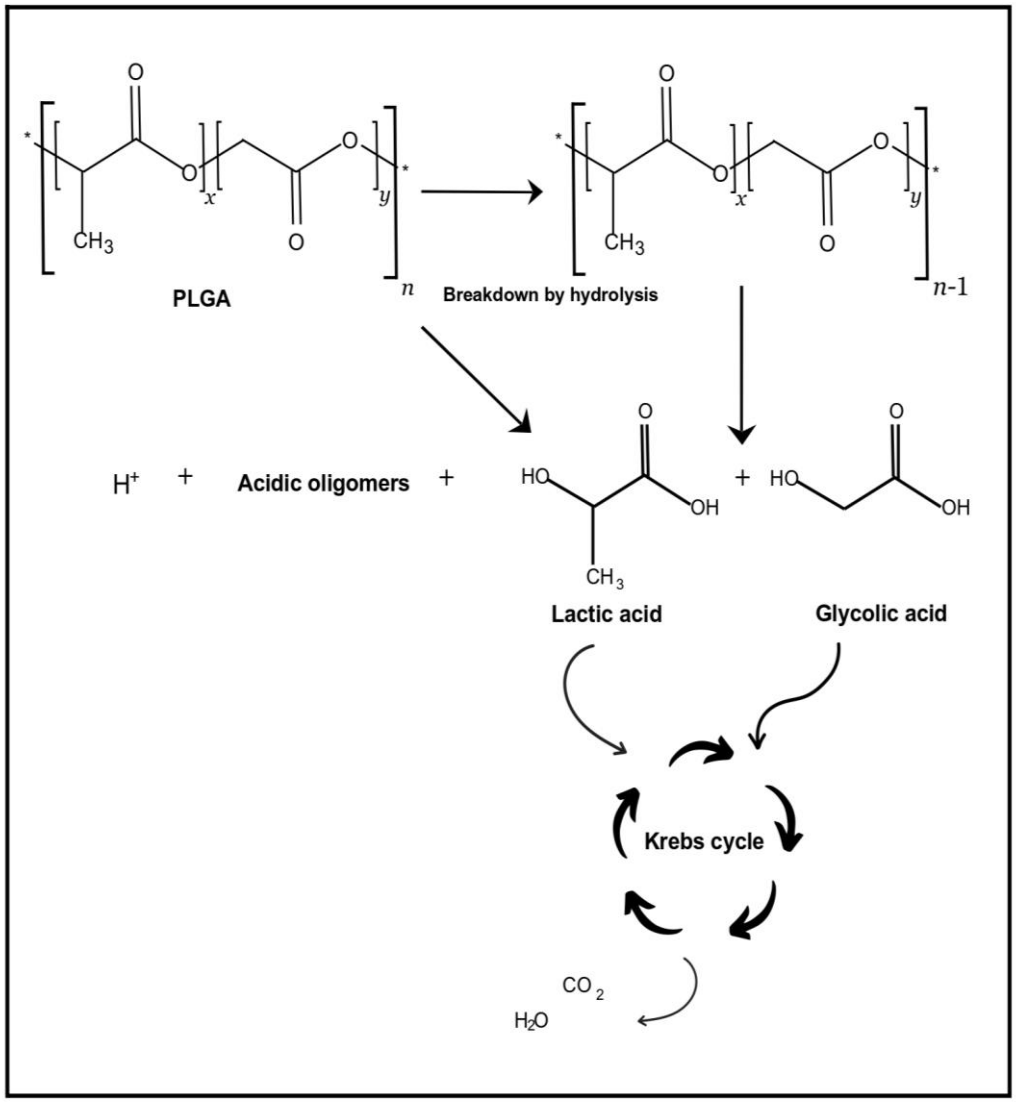

Figure 1. 6 Mechanism of PLGA degradation, adopted and redrawn from (Sequeira et al., 2018).

1.16 Mechanism of drug release from PLGA

Despite degradation by bulk-eroding being a feature of PLGA polymers and is what enables a drug entrapped in a matrix to be released, drugs are typically released from macroscale PLGA-matrix implants through a mixture of three mechanisms: diffusion-controlled release, drug-carrier affinity, and degradation of the matrix material (Kamaly et al., 2016; Kearney & Mooney, 2013). The drug release is diffusion-driven and can be influenced by concentration gradients, matrix swelling, and diffusion distance in relation to the implant's shape (Kamaly et al., 2016). Because of this, the release also mainly depends on the matrix's size. There might be variations in the release if the matrix has pores. Other processes, such as water penetration and solubilisation following the device's first immersion in an aqueous environment, erosion and diffusion of PLGA polymer fragments, and the rate of drug diffusion, may also play a role in the release mechanism. These actions may occur simultaneously, so that the releasing method may be complicated (Hines & Kaplan, 2013).

1.16.1 Release profile of PLGA Matrix implant

Due to the heterogeneous degradation, a macroscopic PLGA matrix implant typically exhibits a release profile with three phases. It is commonly known as a tri-phasic profile. Phase I, frequently described as a burst release, has been related to drug particles on the matrix's surface that is rapidly dissolved by the surrounding aqueous media at the implantation site. Phase II is commonly a slow-release phase, sometimes known as the lag phase. Drug diffusion occurs gradually during this phase through the distributed pores or the relatively dense polymer. While polymer hydration and degradation are already causing quicker drug release, which is

frequently linked to the start of erosion, polymer chains still have enough length to entrap the drug. The drug is typically released quickly during this phase, commonly described as the second burst. It might also result from the matrix forming cracks. The formulation optimisation can enable alterations to the conventional tri-phasic release profile. Degradation of PLGA is a dynamic process; properties and behaviour change while the degradation occurs. The conditions that lead to slow release are also changing as the pH and other properties of the matrix change throughout degradation; a pore-forming process may take place over pore closure. The type of PLGA utilised will also affect the speed of drug release. Since the beginning of rapid drug release was discovered to be correlated with swelling, erosion, and distortion of the device and, consequently, the more accessible hydration of the PLGA matrix, this rapid release might begin in Phase II rather than in Phase III. Phases may also be overlaid, so using the release profile alone to make predictions about the drug release is insufficient (Fredenberg et al., 2011). Numerous mathematical models have been created to explain drug release from PLGA matrix implants (Siepmann & Siepmann, 2012). Mathematical modelling is a helpful technique that can be used to determine release mechanisms, characterise the essential transport processes involved, estimate unknown parameters, such as the diffusion coefficient when diffusion is involved, decrease experimentation, and offer predictive capabilities (Hines and Kaplan, 2013). These models can predict the release behaviour of a specific formulation and help clarify the driving release mechanisms (Siepmann & Siepmann, 2012).

1.17 Methods of PLGA Implant Manufacture

PLGAs have properties of low-melting thermoplastics that soften and melt when heated over their Tg. With pressure and mild to high temperatures, they can be easily moulded into macroscopic (or even microscopic) forms, allowing the fabrication of devices with various morphologies (Hines & Kaplan, 2013; Jain, 2000). Thermoplastic polymers, including PLGA, can be manufactured into implants using compression, solvent casting, hot melt extrusion (HME), injection moulding (IM) or 3D printing techniques (Fialho & Silva Cunha, 2005; Stewart et al., 2018). Different implant manufacturing techniques produce PLGA under various processing conditions. Differences in the moulding process, shearing forces generated, and thermal treatments at the end may modify the polymer's final molecular weight, crystallinity, or microporous structure, resulting in variations in the degradation of the final implant (Rothen-Weinhold, 1999; Rothen-Weinhold et al., 1999). As a result, it will have various in vivo and in vitro release profiles (Fialho & Silva Cunha, 2005; Stewart et al., 2018). The degradation characteristics of the polymers, the manufacturing techniques, and the device's drug-loading ratio define the in vivo performance of the PLGA matrix implant delivery system (Rothen-Weinhold, 1999; Rothen-Weinhold et al., 1999; Rothen-Weinhold et al., 1997). Most of the final matrix implant's properties result from the manufacturing method.

1.17.1 Compression

Compression as a manufacturing process does not require heat or solvents, making it a valuable method for manufacturing implants containing components that are sensitive to heat or solvents, such as proteins or peptides (Jivraj et al., 2000). However, implants made with this method usually have a faster release profile than those made with other manufacturing methods. It may be necessary to use additional procedures, such as covering the implant, to delay drug release. Additionally, as demonstrated by Fialho et al., implants formed by compression had an irregular surface with numerous pores and channels (Fialho & Silva Cunha, 2005), which may cause an unstable release from an implant produced in this technique.

1.17.2 Solvent casting

The solvent casting process involves dissolving the polymer in a suitable solvent first, then casting the formed solution into a mould and eliminating the solvent through evaporation (Makadia & Siegel, 2011). This technique frequently produces films or laminar implants (Dorta et al., 2002; Santoveña et al., 2006; Umeki et al., 2011). The drawback of this technique is the large amount of organic solvent required, which might impact the toxicity and stability of the drugs and cause significant environmental problems (Makadia & Siegel, 2011).

1.17.3 Hot Melt Extrusion (HME)

HME is the process of melting, mixing, and forcing a polymer through a narrow hole known as a die (Makadia & Siegel, 2011). It is a continuous process where a mixture of polymer and drug via a die produces implants with constant diameter without using solvents (Makadia & Siegel, 2011; Wang et al., 2010). The HME requires that the polymers used be thermoplastic (Breitenbach, 2002a). PLGA is a thermoplastic polymer and can be processed using this technique (Breitenbach, 2002a). Above the

Tg, the mixture is melted and pushed through a die. If necessary, pre-mixing can be performed to help in generating a homogenous extrudate. It is the most suitable method for creating matrix systems since the drug is uniformly distributed throughout the implant. The drug stability and Mw of the polymer could be affected by a change in the temperature that is being employed. As a result, the extrusion procedure restricts the drugs used depending on their melting point, thermal stability, polymorph stability, and chemical interactions with PLGA (Makadia & Siegel, 2011).

1.17.4 Injection moulding (IM)

IM is a technique that is well suited for large-scale industrial production. This manufacturing method enables the production of implants of various shapes while ensuring a suitable polymer and drug mixing process. A particular designed IM machine is commonly used, with a mould of the desired shape and size for the finished required form. The polymer and drug mixture is first heated to a suitable temperature to become flexible. Then it is injected under pressure and heated again to provide it with the desired shape. The manufactured implants are allowed to cool at a significantly lower temperature (Rothen-Weinhold, 1999; Rothen-Weinhold et al., 1999). It is not just a continuous process but also very reproducible and automatable. Again, high temperatures are necessary for this method, and a decrease in PLGA's Mw is commonly found. As was previously stated, this might cause some active ingredient degradation (Rothen-Weinhold, 1999; Rothen-Weinhold et al., 1999).

1.17.5 3D printing

3D printing is usually used to manufacture dental implants, prostheses and orthopaedic implants (Shi et al., 2014). This approach could be very promising for producing implantable drug delivery devices because it is inexpensive, accurate, and highly flexible (Shi et al., 2014). 3D printing might be used to form the biodegradable implant structure, which would be loaded with the drug and released from the implant, controlled by degradation of the implant structure or rate-controlling membranes that cover pores in the implant. 3D printing is a promising technique and could be particularly valuable in the fast development of prototypes for research. Its viability as a manufacturing process for mass production is still yet to be determined. But once the FDA approved a 3D-printed drug in 2015, the viability of 3D printing for the production of pharmaceutical dosage forms took a step forward (Norman et al., 2017).

1.18 Factor affecting degradation and drug release from PLGA matrix

1.18.1 Type of polymer

The type of polymer used, among other crucial factors, is the main factor affecting the degradation and, consequently, the drug-release mechanism of a matrix implant (Fredenberg et al., 2011). A particular drug release behaviour could be achieved by altering some polymer properties (Hines & Kaplan, 2013).

1.18.2 Polymer composition

In terms of the PLA-PGA ratio, the polymer composition is considered the most significant factor influencing the degradation rate (Alexis, 2005; Washington et al., 2017). An increase in the ratio of hydrophilic glycolic acid in PLGA composition speeds up weight loss because specific chain scission glycolic links lead to

preferential degradation of those units over lactic acid units (Makadia & Siegel, 2011). The hydrophilicity of the PLGA matrix increases with PGA content, which causes the rate of PLGA backbone disintegration to increase due to hydrolytic scission. This results in a faster drug release (Makadia & Siegel, 2011). In contrast, a rise in the lactic acid residue ratio accelerates backbone breakdown by raising the crystallinity of PLGA. According to reports, PLGA with high initial crystallinity, i.e., a high amount of L-PLA not subject to any process that could cause crystallinity loss, such as compression moulding or quenching processes, had a faster rate of Mw decrease when subjected to hydrolysis (Alexis, 2005).

1.18.3 Crystallinity

There is a correlation between crystallinity and Tg. It depends on the proportion of PGA and PLA units (Makadia & Siegel, 2011). It is more crystalline if the PLGA contains more L-PLA or PGA.

1.18.4 Molecular weight (Mw)

Since PLGAs with higher Mw have longer polymer chains, they consume longer to hydrolyse and decompose completely (Makadia & Siegel, 2011). The converse is true for L-PLA because of their high crystallinity, which increases with Mw (Makadia & Siegel, 2011). It is well known that PLGA chains with low Mw have faster biodegradation rates and release drugs faster than PLGA chains with high Mw (Alexis, 2005). The Tg drops along with this behaviour. L-PLA exhibits the opposite behaviour because of the high level of crystallinity that develops when the Mw decreases. Less hydrophobic PLGA is produced by low Mw, a low PLA-PGA ratio, and uncapped end groups. This PLGA has higher water absorption rates, hydrolysis, and erosion (Fredenberg et al., 2011; Tracy et al., 1999). However, as was

previously stated, those properties change as the polymer degrades and releases the drug. PLGA is dynamic during these processes because it degrades, changing its properties and behaviour. The transition from hydrophobic, high Mw, and slow-degrading PLGA to hydrophilic, low Mw, and fast-degrading PLGA will eventually occur (Fredenberg et al., 2011).

1.18.5 Morphology of the matrix

The matrix degradation increases with the surface area-to-volume ratio, especially for large devices (Grizzi et al., 1995; Kapoor et al., 2015). Bulk degradation will occur more quickly, causing a rapid release of the drug (Makadia & Siegel, 2011). The presence of pores in the matrix can predict drug release if the initial pores have sufficient size to enable drug molecules to be released by diffusion when water enters the pores following implantation.

1.18.6 Manufacturing technique

The implant manufacturing technique will affect the final PLGA properties because of the processing parameters used, which will impact degradation (Hines & Kaplan, 2013).

1.18.7 Drug type

The type of drug incorporated could modify the matrix's degrading mechanism and rate of degradation (Makadia & Siegel, 2011; SIEGEL et al., 2006). The drug of choice can significantly impact the release mechanism due to its chemical properties. Lower drug loadings, salts, and chemicals that stimulate hydrolysis caused the matrix to degrade more rapidly. The drug and polymer may interact, which could slow down the rate of release (Hines & Kaplan, 2013). Some drugs, including caffeine and salicylic acid, can decrease the Tg when dissolved in a PLGA matrix. In contrast,

others can interact with the carboxyl groups produced by the PLGA degradation process (as observed for quinidine) (Alexis, 2005).

1.18.8 pH

Strongly alkaline and acidic media promote the degradation of PLGA. As PLGA degrades, the accumulation of carboxylic end groups will act as an auto catalyst for the degradation by hydrolysing the ester bonds (Makadia & Siegel, 2011).

1.18.9 Drug load

The polymer-to-drug ratio affects the rate and duration of release when drugs are entrapped in a PLGA matrix. A higher polymer-to-drug percentage increases the rate and duration of release; however, this will result in a higher burst release if present in the mechanism of release (Makadia & Siegel, 2011). When the drug is released, the space left will result in a pore in the matrix. As the medium enters the pore, it will enable more drugs to be released by diffusion (Fredenberg et al., 2011).

Other factors influencing the degradation and, subsequently, the drug-release mechanism of PLGA include flow rate, sterilisation of the final pharmaceutical form, strain, the presence of plasticisers, and the presence of enzymes, despite multiple findings related to the function of body enzymes with the degradation of PLGA (Alexis, 2005).

1.19 Aim and objectives

The problem – The systemic delivery of chemotherapeutic drugs to the brain is difficult due to the BBB, which acts as a barrier to large, ionically charged, hydrophilic molecules. And a high systemic dose is needed because most chemotherapeutic drugs could not cross the BBB at concentrations required for therapeutic effect. Additionally, approximately 80 to 90% of cases experience recurrence within 2 cm of the resection site.

The research idea – To develop a range of biodegradable implantable devices of varying parameters formulated by different manufacturing techniques, IM and HME, for localised delivery of chemotherapeutic drugs to the brain. Identifying the most promising biodegradable implantable device by investigating physical and physiochemical characterisation. The localised delivery of chemotherapeutic drugs to the brain will overcome the issues associated with systemic administration of chemotherapy and relapse of GBM.

Objectives:

- To provide insight that could be used for the local treatment of GBM with a view to possible discovery and helpful variations and improvements in drug choice, polymer type, and manufacturing techniques of this implantable drug delivery device.
- Develop a range of single-layer sustained-release implantable devices containing anticancer drugs with varying drug loading and grades of PLGA.
- Study the impact of using different drug loading and different grades of biodegradable PLGA on drug release.
- Develop a multi-layer implantable device containing anticancer drugs with varying drug loadings.
- Develop and optimise different manufacturing techniques for manufacturing implantable drug delivery devices.
- Evaluate implantable drug delivery devices by investigating the size uniformity, drug content, drug release from implants, drug distribution, thermal stability and crystallinity.
- Study the impact of using different manufacturing techniques on drug release, homogeneity, crystallinity, and drug content.

CHAPTER 2: DEVELOPMENT AND CHARACTERISATION OF SINGLE-LAYER IMPLANTABLE DELIVERY DEVICE (IRINOTECAN-LOADED PLGA) FORMULATED BY USING INJECTION MOULDING AND HOT MELT EXTRUSION TECHNIQUES

2.1 Background

PLGA is commonly utilised as a polymeric matrix former to control the release of drugs from implants and microparticles. Numerous implantable pharmaceutical products of PLGA have been on the market for many years. The success of this polymer can be attributed to its (i) good biocompatibility (Anderson & Shive, 2012; Grund et al., 2011; Nair & Laurencin, 2007), (ii) biodegradability (iii) ability to give desirable drug release rates across a range of times periods, from a few hours to several months (Dorta et al., 2002; Schreiner et al., 2021). The choice of the most appropriate biodegradable matrix form for a particular application depends on a number of variables, such as the material's processability, the desired/required mechanical characteristics of the delivery system, the targeted release period and drug release profile. Importantly, PLGA-based implants can be prepared using a variety of techniques, such as HME, IM, solvent extrusion, compression and 3D printing (DESAI et al., 2008; Hamoudi-Ben Yelles et al., 2017; Kempe & Mäder, 2012; McConville et al., 2015; Takahashi et al., 2004). The type of manufacturing technique used and the chosen process parameters can substantially impact the dosage forms' inner and outer structure and, consequently, the drug release kinetics (Andhariya et al., 2019; Bassand et al., 2022; Vay et al., 2011). Additionally, the device's composition can have a significant impact, depending on the drug loading and drug properties (such as solubility, hydrophilicity and affinity of PLGA) (Bassand et al., 2022; Do et al., 2015; Grizić & Lamprecht, 2020; Hamoudi-Ben Yelles et al., 2017; C. Wu et al., 2018), PLGA type (such as average polymer molecular weight, end group type) (Bassand et al., 2022; Xiao et al., 2020; Zolnik & Burgess, 2008), presence of potential additives (Bassand et al., 2022; Lehner et al., 2019; Schliecker

et al., 2004; Thalhauser et al., 2020) and size of the dosage form (Lin et al., 2018). It is crucial to investigate the mechanism by which the type of drug affects the properties of PLGA. The choice of drug entrapped in PLGA matrices plays a crucial role in altering matrix degradation mechanisms and affecting the rate of degradation (Makadia & Siegel, 2011; SIEGEL et al., 2006). The behaviour of the release mechanism is intimately related to the chemical properties of the chosen drug. For instance, lower drug loadings, salts, and drugs assessing hydrolysis processes could accelerate matrix degradation, leading to alterations in the release mechanism (Hines & Kaplan, 2013). Certain drugs, when dispersed in a PLGA matrix, exhibit additional effects such as decreasing the Tg or interacting with carboxyl groups generated during PLGA degradation, further influencing the drug release mechanism (Alexis, 2005). Understanding how the drug interacts with the PLGA matrix is fundamental. It extends beyond release kinetics, impacting the mechanical and thermal properties of the polymer. Ascertaining these mechanisms is essential for tailoring drug release profiles and optimising the performance of PLGA-based drug delivery systems.

PLGA is a thermoplastic polymer that can be simply shaped when it is molten. As a result, PLGA is frequently utilised as a thermal binder in the manufacturing of biodegradable implants through IM or HME (QUINTEN et al., 2009).

In this work, HME and IM techniques were chosen since these techniques offer an interesting potential for the preparation of homogeneous drug-polymer blends (Bassand et al., 2022; Breitenbach, 2002b; Duque et al., 2018; Lehner et al., 2019; QUINTEN et al., 2009). IM is the process of converting the molten material under high pressure into a compact and shape-specific mould. When the material solidifies,

the mould is opened to generate the final product (Quinten et al. 2009). HME has become an innovative processing method for producing molecular dispersions of active pharmaceutical ingredients (APIs) into different polymer matrices, which has allowed this technique to provide time-controlled, modified, extended, and targeted drug delivery (Maniruzzaman et al., 2012; Repka et al., 2007, 2008, 2012). In addition, it complies with the requirements of the US FDA Process Analytical Technology (PAT) scheme for designing, analysing, and controlling the manufacturing process through quality control measurements made during the active extrusion process (Maniruzzaman et al., 2012). HME has been shown to be a reliable method for developing various drug delivery systems. Hence it has also been shown to be helpful in the pharmaceutical industry (Maniruzzaman et al., 2012). For the manufacturing of solid rod-shaped PLGA implants, HME is a suitable and frequently used technique. Implants are molecularly distributed or suspended drug matrix systems (Ghalanbor et al., 2010; Zhou et al., 1998).

IRN, a semi-synthetic pro-drug (Ramesh et al., 2010), inhibits the Topoisomerase I group of enzymes through its active metabolite, 7-ethyl-10-hydroxycamptothecin (SN-38) (Xu & Villalona-Calero, 2002). IRN is proven to be transformed to SN-38 following intratumoral administration to gliomas (Wang et al., 2011). It has been demonstrated to be successful in the clinic against GBM both as a monotherapy (Batchelor et al., 2004; Buckner et al., 2003; Chamberlain, 2002; Cloughesy et al., 2002, 2003; Friedman et al., 1999; Gilbert et al., 2003; Prados et al., 2004, 2006; Raymond et al., 2003; Turner, 2002) and in combination with TMZ (Gruber & Buster, 2004; Yung et al., 2005), BCNU (Brandes et al., 2004; Quinn et al., 2004; Reardon et al., 2004), and bevacizumab (Bokstein et al., 2008; Friedman et al., 2009b; Goli et

al., 2007; Mesti et al., 2015; Ozel et al., 2016b; Purow & Fine, 2004; Raval et al., 2007; Vredenburgh, Desjardins, Herndon, Dowell, et al., 2007; Vredenburgh, Desjardins, Herndon, Marcello, et al., 2007). IRN can cross the BBB, but large intravenous doses of between 125 and 500 mg/m^2 are needed to reach therapeutic levels in the brain, which can have serious systemic adverse effects, including gastrointestinal toxicity that can cause early and late onset diarrhoea and severe neutropenia (Hecht, 1998). The issue of severe side effects such as diarrhoea and neutropenia and the required to increase the dose level of IRN in the brain has provoked new developments in enhancing IRN's ability to pass through the BBB. Local delivery of IRN could enhance therapeutic outcomes by enabling the delivery of a higher dose of IRN locally at the site of the tumour removal, reducing systemic concentrations, and hence minimising the aforementioned side effects.

2.2 Aims and objectives

The aim of this chapter was to develop an IRN-loaded PLGA implantable delivery device by using IM and HME for localised treatment of GBM.

The objectives were:

- To determine the manufacturing processing parameters for chosen material that can be manufactured by IM and HME techniques.
- To produce PLGA matrix implants containing IRN by using IM and HME techniques.
- To characterise the implants using differential scanning calorimetry (DSC), X-ray Powder Diffraction (XRD) and Raman.
- To investigate the IRN content of the implants.
- To investigate the stability of IRN in various solvents for in vitro release studies.
- To study the impact of the drug load, type of PLGA, size of implant, release media and manufacturing techniques on the in vitro drug release from implants.

2.3 Materials & Methods

2.3.1 Chemicals

Irinotecan hydrochloride was purchased from LGM Pharma, Memphis TN, USA. Kolliphor P188 and Sodium hydroxide were purchased from Sigma-Aldrich, Saint Louis, USA. Polymer PLGA from Corbion Purac, Amsterdam, Netherlands. Acetonitrile, Methanol HPLC grade and Potassium dihydrogen phosphate analytical reagent grade were obtained from Fisher Scientific, Loughborough, United Kingdom. Ortho-phosphoric acid 99% was obtained from Merck, Darmstadt, Germany. Potassium dihydrogen phosphate, 98+%, was obtained from Alfa Aesar, England. Phosphate buffered saline (Dulbecco A) was obtained from OXOID, Hampshire, England.

2.3.2 Methods

2.3.2.1 HPLC analysis

Quantification of IRN was performed using an Ultimate 3000 Autosampler HPLC (Thermo Scientific Inc., Germering, Germany) with a Zorbax Eclipse XDB-C18 4.6 x 150 mm, 3. uM particle size column (Agilent Technologies, USA). The column temperature time was set at 25°C. The mobile phase consisted of a mixture of 0.02 M potassium di-hydrogen orthophosphate pH adjusted to 3.5 with the ortho-phosphoric acid, methanol and acetonitrile (60:20:20 v/v/v). The flow rate of the mobile phase was 1.0 ml/min, while the wavelength detection was 220 nm. The total run time was 10 min, and the retention time of IRN was 4.7 minutes. The calibration curve for IRN was plotted over a concentration range of 4–100 µg/mL.

2.3.2.2 Rheological measurements

Rheological analysis of the polymers, drug and polymer blends, and polymers and plasticiser P188 (1, 5, 10 & 20%) blends was performed to determine the melt viscosity and processing parameters as a function of temperature for IM and HME. The experiments were performed on a Discovery hybrid parallel plate rheometer (T.A. Instruments, USA) using a 20 mm cross-hatch steel plate and a 500 µm gap height. The rheometer was calibrated for zero gap before analysing a sample. Initially, an oscillation amplitude sweep was performed for each sample to determine the linear viscoelastic region. Each test was performed at an angular frequency (10 rad/s) with stress between 0.01 and 10,000 pa.s and seven temperature measurements (80, 100, 110, 120, 130, 140, and 150°C). Then, Flow temperature ramp tests were performed to determine an ideal extrusion temperature. The test was conducted from 80-200°C at a ramp rate of 5 °C/min, with constant stress 1000 pa.s (viscoelastic zone), and a time of 30 seconds was used for all measurements.

2.3.2.3 Manufacturing of IRN-Loaded PLGA implant

2.3.2.3.1 Injection moulding (IM)

A 500 mg mixture consisting of the required amount of the drug (10, 20, 30 (w/w)) and PLGA with plasticiser Kolliphor P188 was weighed into a small glass beaker and mixed using a spatula for approximately 10 minutes. The active mix was placed into a 1 mL syringe with a piece of 2 mm diameter and 70 mm length silicon tubing attached. The syringes and tubing were placed in a vacuum desiccator to remove air and subsequently placed into an oven at 110°C for 40 minutes. Upon removal from the oven, the active mix was injected into the silicon tubing and left to cool at room temperature for 20 minutes. Each implant rod was cut to produce an IRN-loaded implant rod 2 mm in diameter and 3 mm or 6 mm in length.

2.3.2.3.2 Hot Melt extrusion (HME)

The appropriate amount of drug (10, 20, 30% (w/w)), PLGA 5004 and plasticiser kolliphor 20% P188 were weighed into a sealed plastic container and roll mixed for approximately 10 minutes to ensure uniform blending of API and excipients. The active mix was subsequently fed into a twin-screw minilab extruder (Kapex Manufacturing, USA) at a feed rate of 5 g per hour. The extruder's feeding, mixing and metering zones were set at 65°C, 87°C and 60°C, respectively, with a screw speed of 20 RPM. The melt was extruded through a 2 mm die and subsequently cut into a rod implant of 3 mm or 6 mm in length to produce 10, 20, and 30% (w/w) IRN-loaded PLGA implant rods. Temperatures of the extruder were sited according to the rheology studies.

2.3.2.4 Physical characterisation of implants

2.3.2.4.1 Determination of the lengths, diameters and weights of IRN-loaded PLGA implants

The length and diameter of each implant rod were measured using a digital vernier calliper. The diameters of the implant rods were measured at both ends and, in the middle, with the results averaged to obtain the average (n=10) diameter of each rod. The lengths of the implant rods were measured (n=10), and the results were averaged to obtain the average length of each implant rod. The weights of implant rods (n=10) were measured using an electronic balance, and the results were averaged to obtain the average weight of each implant rod.

2.3.2.5 Physiochemical characterisation

2.3.2.5.1 Determination of drug content

Each implant (n=6) was accurately weighed and placed into a glass vial. 5ml of Dichloromethane (DCM) was added to each vial and left for 1 hour to dissolve the implant. Then, the DCM was evaporated in a water bath at 65°C. Once completely dry, 10 ml of the mobile phase was added to the IRN/PLGA residue. The vial was placed into the ultrasonic bath for 10 minutes, followed by vortex mixing for 2-3 minutes, causing the PLGA and plasticiser to precipitate while the IRN remained soluble in the solution. The sample was then filtered using a 0.45 uM syringe filter and transferred into the HPLC vials for analysis. The samples were analysed by the IRN HPLC method to determine the content of the drug, and the results were compared to the theoretical content, which was calculated from the implant's total mass to determine the manufacturing process's reliability. An acceptable limit was determined as ±10% of the theoretical content.

2.3.2.5.2 Determination of the Physical State of IRN in the PLGA implants by using Raman

Raman spectroscopy and Raman imaging were performed using a Thermo Scientific™ DXR Raman Imaging Microscope (Waltham, USA) using a 780 nm laser operated at 20 mW power on the solid-state samples were collected at room temperature on a microscope objective of 10X magnification. A 400-groove per millimetre grating was used. The resulting resolution was 2.4– 4.4 cm^{-1} across the spectrum. Data acquisition and processing were carried out using the Thermo Scientific OMNICxi software.

2.3.2.5.3 Drug distribution in PLGA implant by using Raman mapping

The surface of the implants was Raman mapped using a Thermo Scientific™ DXR Raman (Waltham, USA) with a 780 nm laser operated at 20 mW power. Each spectrum was the co-addition of three 5-second exposures collected from 200 to 3200 cm^{-1}. An Olympus 10× objective with a 25 µm confocal pinhole was used to collect the Raman signal. The spectra were collected with a step size of 106 µm in both the x- and y directions.

2.3.2.5.4 Crystallinity studies using X-ray Powder Diffraction (XRD)

X-ray powder diffraction patterns of the implants (ground to a fine powder), formulation blends and pure IRN, PLGA and P188 were filled into a flat sample holder and scanned with a 2θ range of 3–50° and step size of 0.02, and the voltage was 30 kV and 15 mA current. Samples were recorded using a Rigaku MiniFlex 600 (Rigaku, USA) with a Cu Kα X-ray source (λ=1.5418 Å) and with software Miniflex Guidance version 1.2.01.

2.3.2.5.5 Thermal stability studies using Differential Scanning Calorimetry (DSC)

A Thermo analytical study was performed using a T.A. instrument Q200 (DSC) (T.A. Instruments, New Castle, DE, USA) to investigate the physical state of the incorporated IRN in the moulded and extruded implants. The sample was weighed (5–10 mg), placed into an aluminium pan, and sealed, with an empty aluminium pan used as a reference. Each sample was heated from 25°C to 300°C at a 10°C/min heating rate. Nitrogen was used as a purge at a flow rate set at 50 ml/min.

2.3.2.6 In vitro dissolution studies

2.3.2.6.1 Solubility experiments

The saturation solubility of IRN was investigated in Phosphate buffered saline (PBS), Deionised water (dH_2O), 50% Dimethyl sulfoxide (DMSO), 70% DMSO and 80% DMSO to ensure maintenance of sink conditions in all experimental setups. A saturated solution was prepared by dissolving an excess amount of IRN in 1 ml of each media in a glass flask (n=3) and vortex mixed for 30s then transferred to a shaker incubator and maintained at 37°C for (72 h) to reach equilibrium. After three days, samples were transferred into microtubes and centrifuged for 10 minutes. The supernatants were diluted and analysed by HPLC. Results were represented as a mean (n=3) ± standard deviation (S.D.).

2.3.2.6.2 In vitro stability of IRN in the different release media

The purpose of the stability testing was to determine the stability of the IRN over time in different media (dH_2O, PBS and DMSO) and temperatures (8°C, 20°C and 37°C). Standard solutions (100 ug/ml) of IRN in each media were prepared and transferred into glass vials and stored under various conditions, room temperature (20°C), cold room (8°C) and incubator (37°C) for 36 days. IRN has been previously reported to be light sensitive (Kumar et al., 2012), therefore, all samples were protected from the light. Samples were taken daily starting from day 0 up to day 36 and analysed by HPLC. The results were represented as a mean (n=3) ± standard deviation (S.D.).

2.3.2.7 In vitro drug release studies

2.3.2.7.1 Effect of polymer type (PLGA grades) on drug release

In vitro release study was conducted to investigate drug release from different PLGA grades (5002, 5004, 5010 and 7507) implants manufactured by IM. Each implant (10% w/w) loading with varying PLGA grades (5002, 5004, 5010, 7507) 2x6 mm (n=3) was placed into a sealed flask containing 10 mL of PBS (pH 7.4) and placed into an orbital shaking incubator at 37°C and 100 rpm. 1 mL of the release media was sampled at 1, 2, 4, 5, 6, 9, 11, 14, 18, and 21 days and replaced with the same volume of PBS. The samples were filtered using a 0.45 uM filter and analysed using the IRN HPLC method.

2.3.2.7.2 Effect of drug loading ratio on the release

In vitro release study was conducted to investigate the effect of drug loading on the release of IRN from PLGA IM implants. Each 2 × 6 mm PLGA5004 implant with varying (10, 20, and 30% w/w) loadings (n=3) was placed into a sealed flask containing 10 mL, 20ml and 30ml of PBS (pH 7.4) and placed into an orbital shaking incubator at 37°C and 100 rpm. Those volumes provide complete sink conditions for the drug with varying (10, 20, and 30% w/w) loadings. 1 mL samples were taken at time intervals of 1, 2, 4, 5, 6, 9, 11, 14, 18, and 21 days and replaced with the same volume of PBS. The withdrawn samples were filtered using a 0.45 uM filter and analysed using the IRN HPLC method.

2.3.2.7.3 Effect of implant dimensions on drug release

In vitro release study was conducted to investigate the effect of implant dimensions on the release of IRN from PLGA IM implants. Each 30%IRN loaded PLGA 5004 implant (n=3) with two different dimensions, 2X6 mm and 2X3 mm, was placed into a sealed flask containing 15 mL and 30ml of PBS (pH 7.4) and placed into an orbital

shaking incubator at 37°C and 100 rpm. Those volumes provide sink conditions for the drug with varying dimensions of 2X3 mm and 2X6 mm. 1 mL samples were taken at time intervals of 1, 2, 4, 5, 6, 9, 11, 14, 18, and 21 days and replaced with the same volume of PBS. The withdrawn samples were filtered using a 0.45 uM filter and analysed using the IRN HPLC method.

2.3.2.7.4 Effect of manufacturing procedure on the release of IRN

In vitro release study was conducted to investigate the effect of manufacturing procedure on the release of IRN from PLGA implants. Each 10%IRN loaded PLGA 5004 implant why (n=3) formulated by IM and HME was placed into a sealed flask containing 10 ml of PBS (pH 7.4) and placed into an orbital shaking incubator at 37°C and 100 rpm. 1 mL samples were taken at time intervals of 1, 2, 3, 5, 7, 10, 15, 20, 25 and 30 days and replaced with the same volume of PBS. The withdrawn samples were filtered using a 0.45 uM filter and analysed using the IRN HPLC method.

2.3.2.7.5 Long-term in vitro release

Each 10%IRN loaded PLGA 5004 implant (n=3) formulated by IM and HME was placed into a sealed flask containing 10 ml of PBS (pH 7.4) and placed into an orbital shaking incubator at 37°C and 100 rpm. 1 mL samples were taken at time intervals of 1, 2, 3, 5, 7, 10, 15, 20, 25, 30, 35, 40, 45, 50, 55, and 60 days and replaced with the same volume of PBS. The withdrawn samples were filtered using a 0.45 uM filter and analysed using the IRN HPLC method. All the measurements were conducted in triplicate, and the results were represented as mean % cumulative release ± SD.

2.3.2.7.6 Accelerated short-term release (Effect of the various release media on the drug release)

Drug release testing under various types of release media (dH_2O, 50%DMSO, 70% DMSO and 80% DMSO) at 37°C was investigated in order to develop a suitable accelerated in vitro release testing method. Each implant was placed into a sealed flask containing different release media (dH_2O, 50%DMSO, 70% DMSO and 80% DMSO) (volumes provide sink conditions) and placed into an orbital shaking incubator at 37°C and 100 rpm. 1 mL samples were taken at time intervals of 1, 2, 3, 5, 7, 10, 15, 20, 25, 30, 35, 40, 45, 50, 55, and 60 days and replaced with the same volume of release media. The cumulative percentage of IRN released into each release media is plotted as a function of time to generate the IRN release profile under different release media. Drug stability under different release media such as (PBS, dH_2O and DMSO) was obtained in order to understand whether IRN was stable under different release media.

2.3.2.8 Statistical Analysis

The statistical analysis was conducted using GraphPad Prism version 9 and Microsoft Excel 2016. The mean, SD and %RSD were calculated. Two-way analysis of variance (ANOVA) was performed for multiple comparisons, followed by post-hoc comparisons of means using Tukey's Honestly Significance Difference test. A significance level of $p < 0.05$ was assumed significant for all analyses. In addition, a 2-sample t-test was used to determine statistical significance between two values at the same time point, with p values less than 0.05 assumed significant.

2.4 Results and discussion

2.4.1 HPLC analysis

Figure 2.1 illustrates the IRN standard curve at seven different concentrations quantified by the HPLC. The correlation between the IRN concentration and the HPLC area under the curve (AUC) was very good, with the R^2 values at 0.9997 ranging from 4 to 100 µg/ml. The high R^2 value indicates a strong linear relationship between the IRN concentrations and the AUC, confirming the accuracy and reliability of the HPLC method for IRN quantification in the samples.

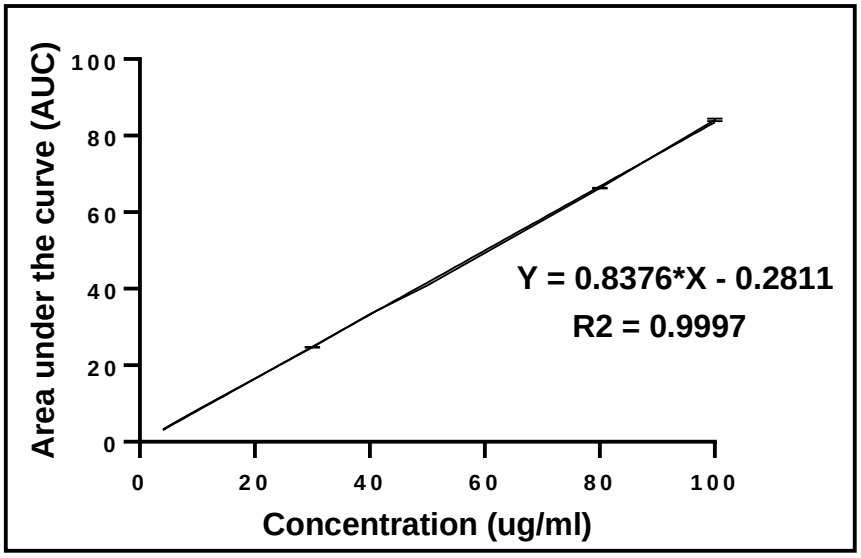

Figure 2. 1 Standard Curve of IRN using HPLC (n= 3).

2.4.2 Rheology

Rheology is the study of how materials flow, and it can be used to predict the behaviour of a material when subjected to stress (Phan-Thien & Mai-Duy, 2017). Applied heat, screw speed, and pressure can improve a material's flow properties in pharmaceutical manufacturing processes such as HME or IM. Rheology can measure a material's flow under these conditions, which is useful for predicting processing parameters and developing a formulation that can be manufactured (Campanella et al., 2002). The melt viscosity determines the processing temperature of the polymer or its mixtures with the drugs (Gupta et al., 2014). Typically, a viscosity between 10^3-10^4 Pa.s is required for extrusion, and the processing temperature is determined accordingly (Gupta et al., 2014). It is crucial to determine an optimal processing temperature to avoid drug degradation during manufacturing (Gupta et al., 2014). Some APIs are unsuitable for high-temperature processing because of thermal decomposition, which could result in a loss of pharmacological

activity. Therefore, reducing the risk of degradation is a major challenge during extrusion processing (Follonier et al., 1994; Kulkarni et al., 2018). One approach is to add plasticisers to lower the Tg and melt viscosity, enabling extrusion to be performed at lower temperatures (Ghebremeskel et al., 2007; Gupta et al., 2014; Kulkarni et al., 2018; Repka et al., 2008). The addition of plasticisers, such as Kolliphor P188, plays a crucial role in altering the mechanical and thermal properties of the polymer matrix during extrusion (Fița et al., 2022; Gupta et al., 2014; Jha, 2020). Plasticisers, low molecular weight compounds added to polymers, interact with polymer chains, effectively lowering the Tg and enhancing the flexibility of the matrix. This reduction in Tg, coupled with improved chain mobility, leads to lowered melt viscosities, enabling extrusion at lower temperatures (Lim & Hoag, 2013; Pradhan et al., 2007). Kolliphor P188, a plasticiser chosen for its low melting point (below 60°C) and excellent thermal binding ability, facilitates the flow of polymer chains, making the extrusion process more efficient and viable at lower temperatures (Fița et al., 2022). Kolliphor P188 is a bio-compatible and non-ionic linear copolymer, enhances its plasticising and solubilising effects, making it a suitable choice for optimising the extrusion process (Chen et al., 2022; Curry et al., 2004; Gawley et al., 2020). Understanding the mechanisms by which plasticisers, specifically Kolliphor P188, impact the polymer matrix is fundamental for tailoring processing conditions, reducing the risk of drug degradation, and ensuring the success of pharmaceutical manufacturing processes.

In this study, the rheological properties of a physical mixture of polymer and the IRN as a function of temperature were investigated to determine an appropriate processing temperature for moulding and extrusion.

2.4.3 Rheological measurements

Polymer PLGA 50:50 with different grades (5002, 5004, 5010) and PLGA75:20 grade (7507) were selected because of their short-term drug release (1-2 months) & (4-5 months), respectively, minimising the possibility of significant differences in drug release between the drugs and enable any drugs with slow diffusion rate to release (Major et al., 2019). First, the melt rheology of the following polymers; PLGA 50:50 with different grades (5002, 5004, 5010) and PLGA75:20 grade (7507) were investigated. A viscosity-temperature sweep was performed on each polymer to model each polymer extrusion profile and its manufacturing processing parameters. For all polymers, viscosity decreased with an increase in temperature (Figure 2.2). The Mw impacted the melt viscosity profile; a higher Mw produced a higher viscosity profile. PLGA 5002, 5004, 5010 and 7507 molecular weights are 16,500 g mol^{-1}, 40,800 g mol^{-1}, 126,000 g mol^{-1}, and 91,400 g mol^{-1}, respectively (Casalini et al., 2019). The ideal viscosity range for a small-scale pharmaceutical extruder is between 10^3-10^4 Pa.s (Gupta et al., 2014, 2015, 2016; Solanki et al., 2018) since greater viscosities would demand high amounts of torque and lower viscosities would result in an extrudate that is too fluid and would not accept the shape of the die (Kolter et al., 2012). To obtain an ideal viscosity range from 10^3-10^4 Pa.s, the processing temperature for the IM method should not exceed 110^{o}C because the syringe used in this method could be melted at a temperature above 110^{o}C. Figure 2.2 shows that only polymer PLGA 5002 has its melt viscosity range of 10^3-10^4 Pa.s. at low

temperatures of 85 to 99^{o}C, which is acceptable to be extruded. While the other three PLGA polymers (5004, 5010 and 7507), their melt viscosities range from 10^{3}-10^{4} Pa.s. at very high temperatures, 110 - 138^{o}C, > 180^{o}C, 126 - 159^{o}C, respectively.

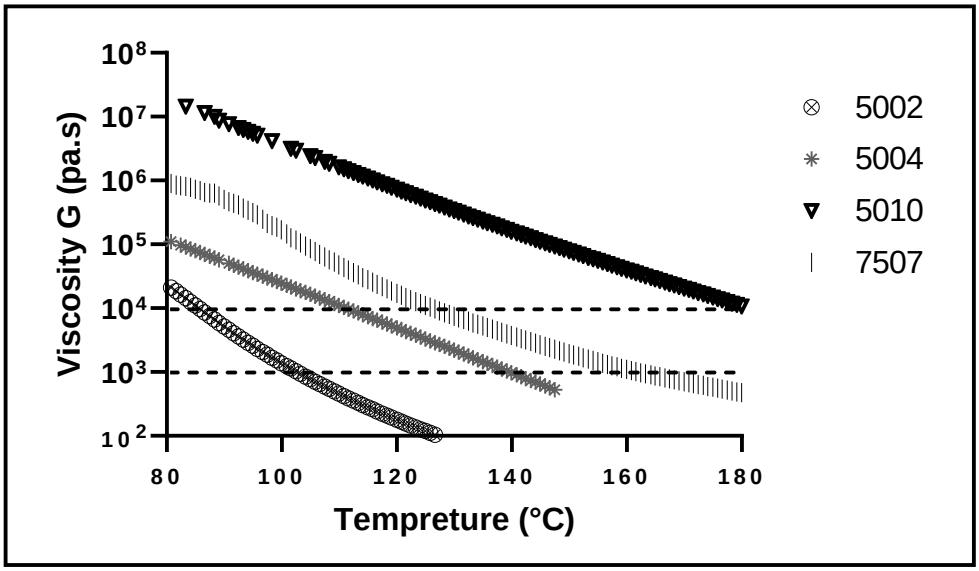

Figure 2. 2 Rheology of different PLGA polymers 5002, 5004, 5010 and 7507 Temperature sweep data between 80 to 180^{o}C for PLGA 5002, 5004, 5010 and 7507. Dashed lines represent the Ideal viscosity range for extrusion (10^{3}-10^{4} Pa.s). There was a decrease in viscosity observed with an increase in temperatures.

The viscosity of the polymer melt is affected by the presence of additives such as drugs (Gupta et al., 2015). Each drug has different physiochemical properties (molecular weight, hydrophilicity, melting point and charge), and adding a drug to the PLGA polymer might affect its melt viscosity and processing temperature. It is crucial to understand how the drugs or plasticisers affect the melt viscosity and extrudability of polymers. Therefore, melt rheology of IRN with a maximum drug loading of 30% w/w mixed with each PLGA polymer (5002, 5004, 5010, 7507) was investigated. Higher melt viscosities were observed for the mixtures of 30% w/w IRN with all grades of PLGA (Figure 2.3A to D). The melt viscosity of the 30% IRN with PLGA 5002 reached the 10^3-10^4 Pa.s viscosity range at 122-144^{o}C (Figure 2.3A), while for 30%IRN with PLGA 5004, 5010, and 7507 reached extremely high viscosities >10^5 Pa.s (Figure 2.3B, 2.3C, & 2.3D). According to their melt viscosity curves, it is anticipated that they would require higher extrusion processing temperatures >110^{o}C, which is not applicable to the IM method. Due to this, a plasticiser must be added to lower their melt viscosities and allow for suitable processing temperatures. It has been reported that adding plasticisers can reduce the process temperature (Gupta et al., 2014). Melt viscosities of 30% IRN with PLGA (5002, 5004, 5010 & 5007) were investigated with the addition of P188 Plasticisers at 1, 5, 10 and 20% (w/w) (Figure 2.3A to D). Adding different percentages of P188 Plasticiser were proven to lower their melt viscosities (Figure 2.3A to D). For 5002 (Figure 2.3A), adding 1% w/w P188 plasticiser achieved 10^3-10^4 Pa.s viscosity but within a high-temperature range of 97-118^{o}C. In comparison, adding 5%, 10% & 20% w/w plasticiser P188 achieved 10^3-10^4 Pa.s viscosity within acceptable low-temperature ranges 85-106^{o}C, 85-102^{o}C and 61-76^{o}C, respectively. For 5004 (Figure 2.3B),

adding 1% w/w plasticiser P188 does not achieve 10^3-10^4 Pa.s viscosity and their melt viscosity range from 10^5-10^6 Pa.s. In comparison, adding 5% & 10% w/w plasticiser achieved 10^3-10^4 Pa.s viscosity but within a high-temperature range of 110-145^{o}C and 119-167^{o}C, respectively. Only the addition of 20% w/w plasticiser P188 achieved 10^3-10^4 Pa.s viscosity within the acceptable low-temperature range of 87-106^{o}C. For 5010 (Figure 2.3C), adding 1% and 5% w/w do not achieve 10^3-10^4 Pa.s viscosity and their melt viscosity >10^4 Pa.s. While the addition of 10% & 20% w/w plasticiser P188 achieved 10^3-10^4 Pa.s viscosity but within the high-temperature range of 110-152^{o}C and 82-114^{o}C, respectively. For 7507 (Figure 2.3D), adding 1% w/w plasticiser P188 does not achieve 10^3-10^4 Pa.s viscosity and their melt viscosity range from 10^5-10^7 Pa.s. Addition of 5%, 10% & 20% w/w plasticiser P188 achieving 10^3-10^4 Pa.s viscosity but within a high-temperature range of 163-199^{o}C, 143-167^{o}C, 110-132^{o}C, respectively.

It is demonstrated that only adding the highest concentration of w P188 20% w/w to a mixture of 30%IRN with PLGA 5004 would be appropriate for extrusion at optimum viscosity 10^3 to 10^4 Pa.s at low-temperature extrusion <110^{o}C. While for a mixture of 30%IRN with PLGA 5002, adding different percentages of P188 plasticiser P188 1%, 5% or 20% w/w would be appropriate for extrusion at optimum viscosity 10^3 to 10^4 Pa.s at low-temperature extrusion <110^{o}C. In contrast, increasing the plasticiser loading from 1% to 20% w/w for the 5010 and 7507 polymers does not achieve the required melt viscosities for low-temperature moulding <110^{o}C. Table 2.1 summarises selected mixtures appropriate for extrusion and their processing temperatures.

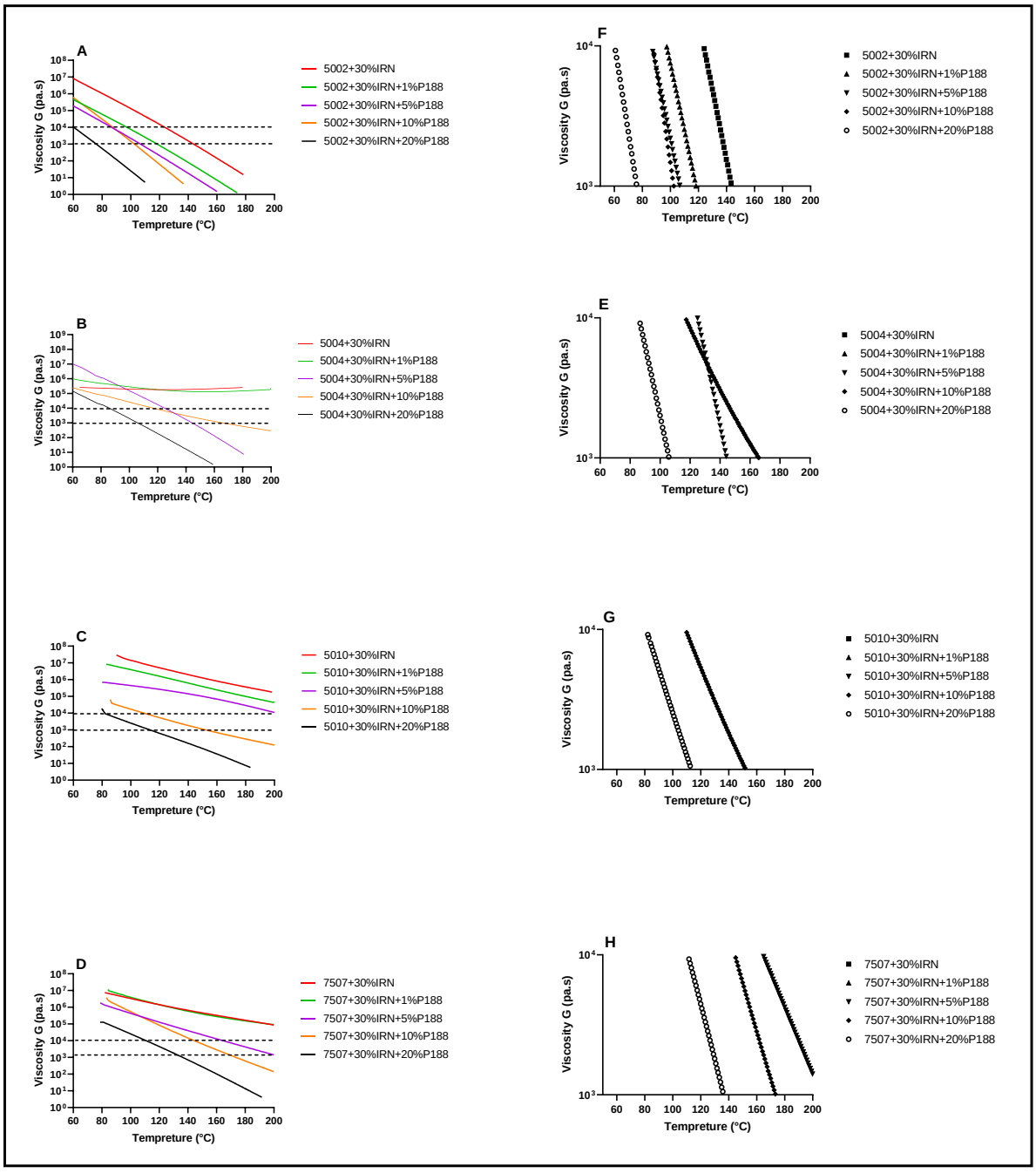

Figure 2. 3 Rheology of different IRN-PLGA-P188 mixtures; 30% IRN w/w with different PLGA polymers (5002, 5004, 5010 & 7507) and different percentages of plasticiser P188 (1, 5, 10, 20%) (A, B, C & D). The temperature sweep was performed at 60-200 ^{o}C. Rheology results were described at the ideal viscosity range for extrusion (10^3 to 10^4 Pa.s) (E, F, G &H).

According to the rheological results (Figures 2.3G & 2.3H), drug load, 30% w/w of IRN, could not be extruded with the Polymer PLGA 5010 and 7507 even with the highest percentage (20% w/w) of plasticiser P188. Therefore, melt rheologies of lower drug load of IRN 10% w/w mixed with each PLGA polymer (5002, 5004, 7507 and 5010) were investigated with plasticiser P188 20% w/w. The percentage of plasticiser P188 (20% w/w) was selected to obtain the exact composition of the extruded formulation of the mixture 30%IRN with PLGA 5004. Thus, study the effect of drug load 30%, 20% and 10% w/w with the same type of Polymer PLGA and the same percentage of P188 (20% w/w) on drug release. Moreover, mixtures of 10% w/w of IRN mixed with each PLGA polymer (5002, 5004, 5010, 7507) and plasticiser P188 20% w/w were investigated for screening polymers for drug release and ability to be extruded.

Figure 2.4 shows the melt rheology of the 10% w/w IRN mixed with each PLGA polymer (5002, 5004, 5010, 7507) and plasticiser P188 20% w/w. Figure 2.4 demonstrated that only PLGA polymers (5002 and 5004), when mixed with 10% w/w of IRN and 20% P188, achieved 10^3-10^4 Pa.s viscosity within acceptable low-temperature range 78-103^{o}C, 79-95^{o}C, respectively. While other PLGA polymers (5010 and 7507), when mixed with 10% w/w of IRN and 20% P188, achieved 10^3-10^4 Pa.s viscosity but within a high-temperature range of 102-118^{o}C and 103-134^{o}C, respectively. Table 2.2 summarises selected mixtures of 10% IRN w/w with 20%P188 and PLGA (5002, 5004, 5010 & 7507) appropriate for extrusion and their processing temperatures.

The processing temperature must be controlled to avoid drug degradation during manufacturing (Gupta et al., 2014). In this work, the processing temperature used

was ≤ 110°C, which is lower than the melting point of the selected drug IRN (250-256°C) (Khan, 2010). Theoretically, when drugs and polymers are mixed, the polymer melts, and the drug particles are dissolved in the molten matrix. As a result, a typical processing temperature is found between the Polymer's Tg and the drug's melting point (Gupta et al., 2014). Hence, the processing temperature was used ≤ 110ºC, which is between the Tg for the PLGA (43°C) and the melting point of the IRN drug.

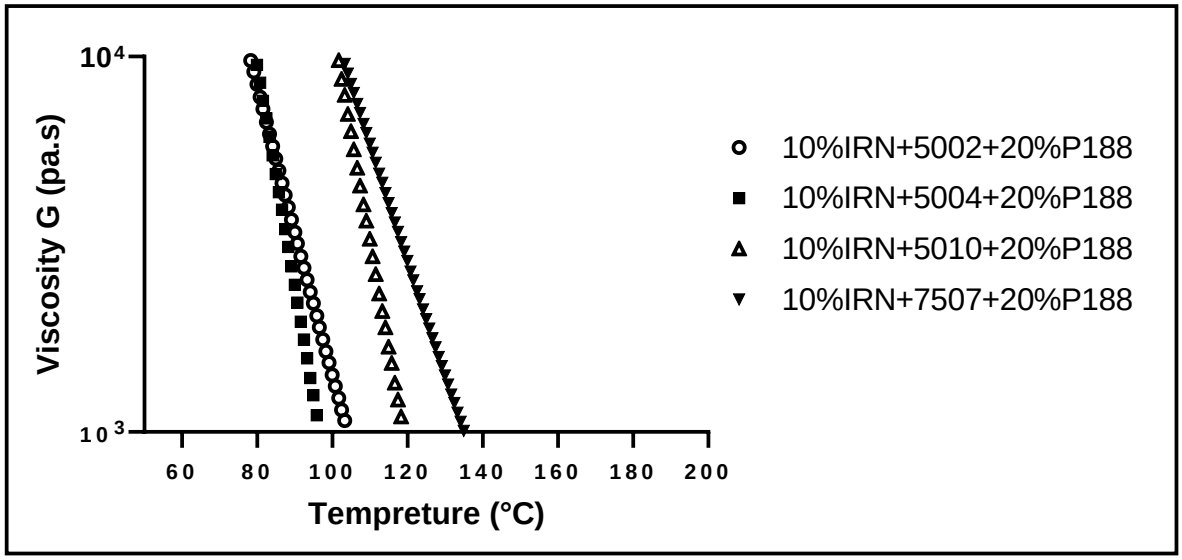

Figure 2. 4 Rheology of the mixtures; 10% IRN w/w, 20%P188 and different PLGA polymers (5002, 5004, 5010 &7507). Temperature sweep data for the IRN-PLGA-P188 mixture of 10% IRN loading with P188 20%. The temperature sweep was performed at 60-200oC. Rheology results were described at the ideal viscosity range for extrusion (10^3-10^4 Pa.s).

Table 2. 1 Selected mixtures of 30% IRN loading, polymers and plasticiser can be extruded at optimum viscosity according to the rheology studies.

Formulations	Temperature°C at Viscosity 10^3 to 10^4 Pa.s
30%IRN+5002+20%P188	61-76
30%IRN+5002+10%P188	85-102
30%IRN+5002+5%P188	85-106
30%IRN+5004+20%P188	87-106

Table 2. 2 Selected mixtures of 10% IRN loading, polymers and plasticiser that can be extruded at optimum viscosity according to the rheology study.

Formulations	Temperature°C at Viscosity 10^3 to 10^4 Pa.s
10%IRN+5002+20%P188	79-103
10%IRN+5004+20%P188	79-95

2.4.4 Physical characterisation of the implants

2.4.4.1 Determination of the lengths, diameters and weights of IRN-loaded PLGA implants

IRN-PLGA implants were manufactured by two different techniques, IM and HME. Size, weight, and content analysis were conducted to evaluate the manufacturing process's reliability. Uniformity of size (diameter and length) and weight measurements for the individual IRN-PLGA implants formulated by IM and HME show that they were consistent in size and weight with a ±10 % deviation. (Table 2.3 & 2.4).

The two-way ANOVA with Tukey's post-hoc tests revealed no significant difference in length, diameter and weight of the 10%, 20%, and 30% IRN-PLGA implants between the two groups (IM and HME) ($p > 0.05$).

Overall the uniformity of size and weight was acceptable across all IRN-PLGA implants formulated by IM and HME.

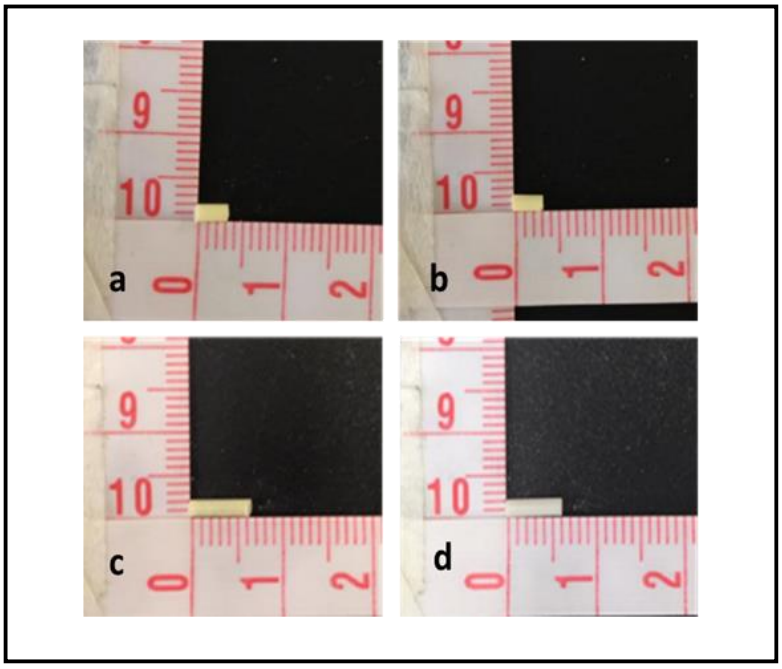

Figure 2. 5 Representative images of single-layered IRN-PLGA-20%P188 implants formulated by IM; 2X3 mm (a) & 2X6 mm (c), single-layered IRN-PLGA-20%P188 implants formulated by HME; 2X3mm (b) & 2X6mm (d).

Table 2. 3 Physical Appearance of IRN-PLGA implants formulated by IM.

IRN-PLGA IM implants			
	10% IRN PLGA 5004 20%P188	**20% IRN** PLGA 5004 20%P188	**30% IRN** PLGA 5004 20%P188
Length (mm) Mean±SD (n=10)	6.0 ± 0.1	6.0 ± 0.1	6.0 ± 0.1
%RSD	1.3%	1.7%	1.9%
Diameter (mm) Mean±SD (n=10)	2.0± 1.3	2.0± 0.1	2.0± 0.1
%RSD	4.5%	3.3%	3.67%
Weight (mm) Mean±SD (n=10)	25.7± 0.6	25.0 ± 0.4	25.5±0.4
%RSD	2.6%	1.9%	0.49%

S.D is the standard deviation, %RSD is the relative standard deviation

Table 2. 4 Physical Appearance of IRN-PLGA implants formulated by HME.

IRN-PLGA HME implants			
	10% IRN PLGA 5004 20%P188	**20% IRN** PLGA 5004 20%P188	**30% IRN** PLGA 5004 20%P188
Length (mm) Mean±SD (n=10)	6.0 ± 0.0	5.9 ± 0.1	6.0 ± 0.0
%RSD	1.3%	1.9%	1.2%
Diameter (mm) Mean±SD (n=10)	2.0± 0.0	2.0± 0.0	2.0± 0.1
%RSD	3.4%	4.7%	5.7%
Weight (mm) Mean±SD (n=10)	26.3± 0.1	25.0 ± 0.1	25.5±0.1
%RSD	0.5%	0.5%	0.49%

S.D is the standard deviation, %RSD is the relative standard deviation

2.4.5 Physiochemical characterisation of implants

2.4.5.1 Determination of drug content

IRN drug was measured for drug content and uniformity within IRN-PLGA implants formulated by IM and HME. All HME implants demonstrated good content uniformity for IRN, with results between 89-95 % and % RSD values below 20 % (Table 2.5). To distinguish between the drug content of the HME and IM implants at different drug loading (10, 20 and 30% w/w), a two-way ANOVA with Tukey's post-hoc test multiple comparisons test was performed. The content analysis for HME implants 10, 20, & 30% IRN show significantly higher IRN drug content ($p < 0.05$), 89 %, 94% and 95%, respectively, with % RSD values below 3 % for all implants (Table 2.5). However, the content analysis for IM implants 10, 20, & 30% IRN show significantly lower IRN drug content ($p < 0.05$), 68 %, 73% and 81%, respectively, with % RSD values below 14 % for all implants (Table 2.5). The content was low for 10%IRN IM implants, measuring less than 70% with the % RSD value of 13 %, demonstrating the lowest drug content among the different implants (Table 2.5). The implants' drug content and uniformity varied depending on the manufacturing techniques and drug loading. The HME implants with 20% and 30% drug loading had similar drug content ($p > 0.05$), but both had significantly higher drug content than the HME implants with 10% drug loading ($p < 0.05$). The IM implants with 10%, 20%, and 30% drug loading had significantly lower drug content than all corresponding HME implants ($p < 0.05$). The %RSD values for the HME implants were lower than those for the IM implants (Table 2.5). This indicates that the HME implants had good content uniformity compared to the IM implants. This can be due to the HME technique permits more precise control over the processing parameters (Major & McConville, 2015), resulting in more constant drug content. Moreover, the HME implants have significantly higher drug

content than IM implants at different drug loading ($p < 0.05$). This can be attributed to the HME technique permitting better drug mixing and distribution in the polymer matrix (Patil et al., 2016) due to the high shear forces of the twin screws (McConville et al., 2015), resulting in a more drug concentration. In contrast, the IM technique may result in an uneven drug distribution within the implant due to no shear in the barrel (McConville et al., 2015), resulting in a lower drug concentration.

The HME technique is preferable to the IM technique. It can produce PLGA implants containing stable IRN at the correct level.

Table 2. 5 IRN content, RSD and %RSD values for each of the 10, 20 and 30% IRN-loaded PLGA implants manufactured by IM and HME. (n=6).

IRN-PLGA IM implants			
	10%IRN	20%IRN	30%IRN
Drug content (%) (n=6)	68.9	73.5	81
RSD	10.71	4.6	11.3
%RSD	13.2	5.5	12.4
IRN-PLGA HME implants			
	10%PTV	20%PTV	30%PTV
Drug content (%) (n=6)	89.2	94.4	95.6
RSD	2.3	1.7	1.3
%RSD	2.5	1.8	1.3

2.4.5.2 Determination of the Physical State of IRN in the IM and HME implants by using Raman

Spectral fingerprints of the IM implant (Figure 2.6A) and HME implant (Figure 2.6B) corresponded fully to the ones of pure IRN used as reference (Figure 2.6D). This confirmed the presence of the solid state of IRN in IM implants and HME implants. The results showed that the crystal form of IRN in both implants did not change, and it was still the crystal form reported in the literature (Chinna Babu et al., 2012). It has been proven that the crystal form of IRN was stable during the moulding and extrusion process.

This study is crucial for monitoring and controlling the entire manufacturing cycle when using a technique that involves melting processes, such as HME and likely dissolution of API in the melt and re-crystallisation. It is essential to understand the novel, non-established pharmaceutical production methods, including HME and is required by regulatory bodies. Finally, understanding how the API crystallises is essential for interpreting dosage form dissolution results (Fanous et al., 2020).

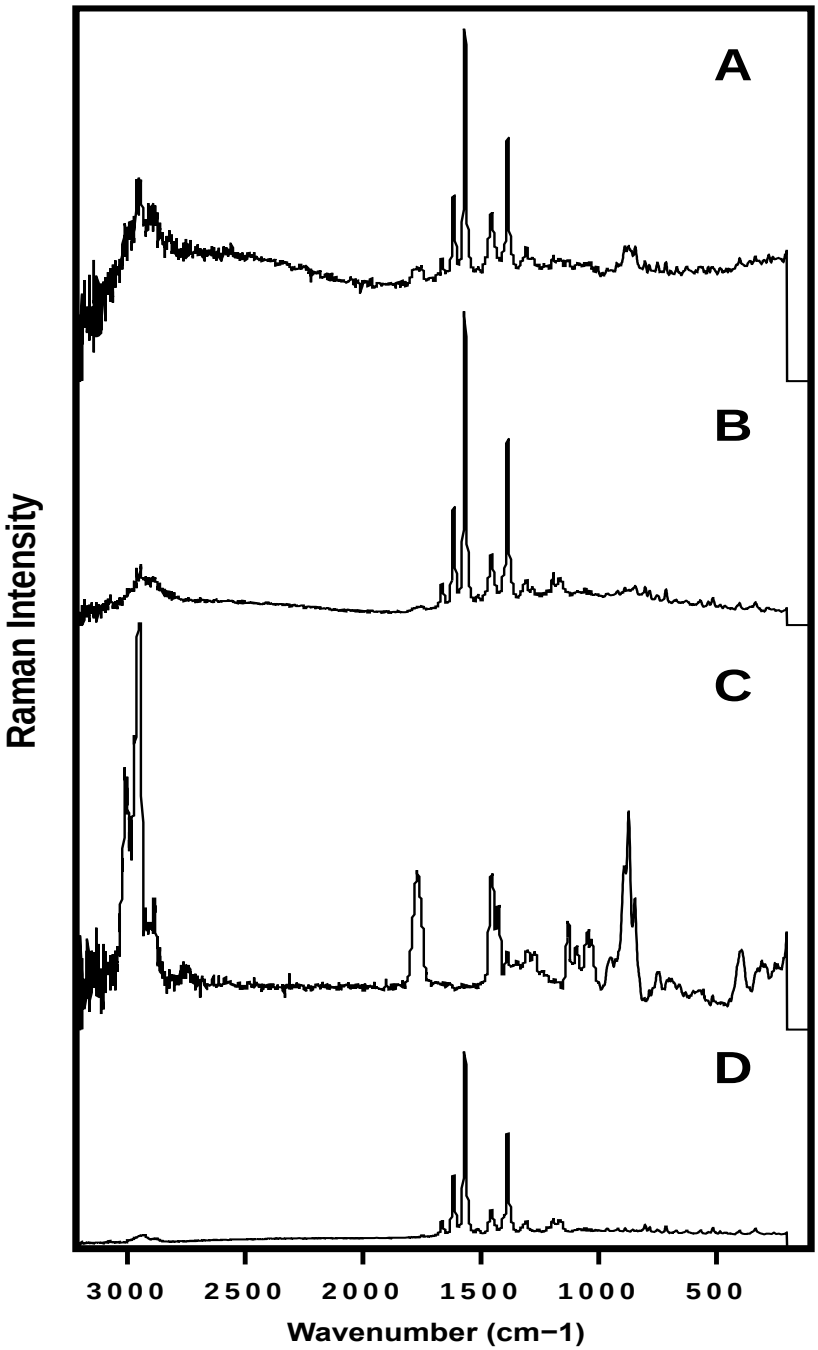

Figure 2. 6 Raman spectrogram of the IM implants (A), HME implant (B), PLGA (C) and API (IRN) (D).

2.4.5.3 Drug distribution in IM implant and HME implant by Raman mapping

To ensure IRN was homogenously distributed throughout the implants, Raman confocal microscopy, a non-descriptive method frequently used to evaluate drug distribution and the amorphous and crystalline content of pharmaceutical implants (Goyanes et al., 2015; Netchacovitch et al., 2017; Scoutaris et al., 2014). Within this study, the entire surface of the IM implant and HME implant were scanned using a Raman microscope. At each point of the formulation mapped, reference IRN and PLGA spectra were inputted into the software and compared with the implant spectra collected. IRN was homogeneously distributed across the entire mapped area of the HME implant (Figure 2.7d), as evidenced by the consistent red areas indicating a uniform IRN presence. In contrast, the IM implants exhibited heterogeneity in IRN distribution (Figure 2.7c), with green areas of varying intensities suggestive of both IRN-rich and IRN-poor regions. Notably, upon closer examination, the intensity maps (Figures 2.7e) revealed significant variations in drug concentration within the IM implants, indicating the presence of hot spots of heightened IRN presence, as well as areas with markedly lower drug levels.

In this study, three samples (n=3) for each implant type were analysed to determine consistency and variability in drug distribution. The IM implants demonstrated considerable variability, with all samples containing variations in drug concentration within the IM implants, pointing towards non-uniformity that may be inherent to the IM manufacturing process. Variability in drug distribution was quantified and visualized on the revised axes of the intensity maps, with the x-axis (um) and the y-axis representing the intensity of the drug IRN. The colour intensity scale has been clarified to reflect the concentration of IRN, with darker regions representing higher

concentrations. Conversely, the uniformity within the HME implants was consistent across all samples, with no significant variability, suggesting a robust and controlled manufacturing process.

The results can be attributed to the fact that the IRN was dispersed entirely throughout the PLGA implant of HME implants due to the high shear mixing of the twin-screw extruder, as reported by McConville et al. (2015). However, in the case of IM implants, the absence of shear forces in the IM processing technique caused the IRN distribution to be heterogenous, resulting in large particles being observed on the implant surface (as shown in Figure 2.7a).

Overall, these results indicate that HME implants are more preferable implants than IM implants due to their homogenous drug distribution.

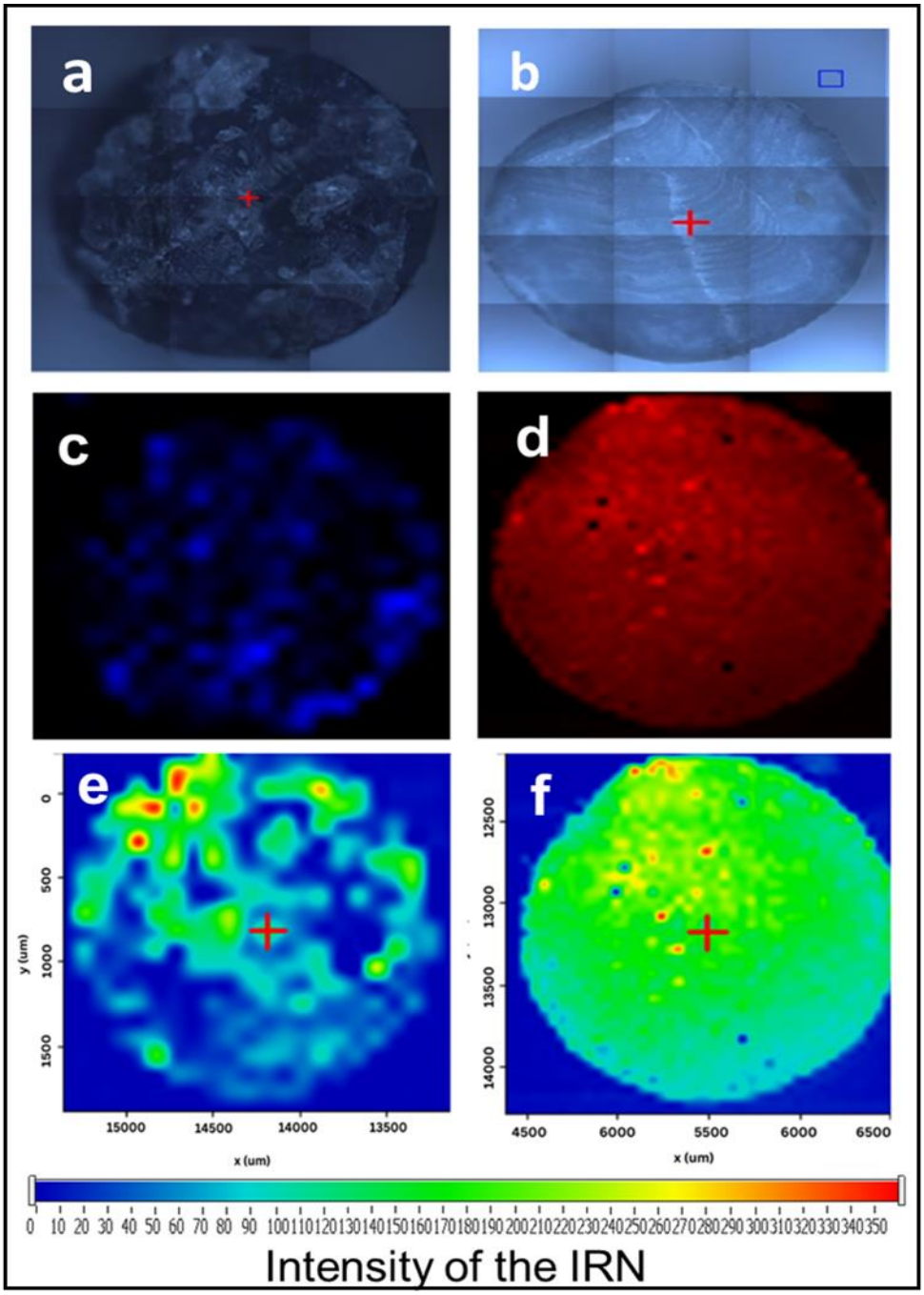

Figure 2. 7 Optical microscopy images of the investigated extrudates entire surface IRN-PLGA implant including IM implant (a) and HME implant (b), Raman mapping of IM implant (c), green areas = IRN distribution in IM implant, Raman mapping of HME implant (d), red areas= IRN distribution in HME implant, Drug intensity on IM implant (e) and in HME implant (f).

2.4.5.4 Crystallinity studies by using Powder X-ray Diffraction (PXRD)

A crystalline state study was conducted after the moulding and extrusion processes. Heating and mixing caused by either moulding or extrusion may change the crystalline state of the drug. The crystalline state affects the implant's dissolution rate and physical stability.

To verify the Raman microscopy findings, PXRD data were collected for pure IRN, PLGA, P188, and physical mixture before and after moulding/extrusion (Figure 2.8). The XRD diffractogram of IRN showed multiple strong-intensity peaks indicating the crystalline nature of IRN. Some of the sharp, intense peaks were at 2Theta = 10°, 13°, 24°, and 26° values (Figure 2.8a), which correspond to IRN (Vangara et al., 2014). The physical mixture of the formulation shows the same peaks in this region, indicating the crystalline nature of the IRN (Figure 2.8d). Both implants (IM and HME) exhibited sharp diffraction peaks and an underlying amorphous halo (Figures 2.8e & 2.8f). The X-ray diffraction patterns of the raw materials are shown in Figures 2.8a, 2.8b & 2.8c for comparison. The IRN powder was crystalline (Figure 2.8a), and the PLGA was amorphous (Figure 2.8b), with similar results reported in the literature (Sepehri et al., 2014) (confirming the Raman spectra data discussed above). Notably, the diffraction peaks observed with the implants corresponded well to the positions observed with the crystalline IRN raw material. The dashed red ovals in Figures 2.8e & 2.8f highlight some of these peaks. In conclusion, based on the obtained Raman spectra and XRD results, these implants were similar to the physical mixture before moulding and extrusion when compared to the pure IRN, demonstrating that the moulding and extrusion processes had no influence on the crystalline state of IRN in the implant.

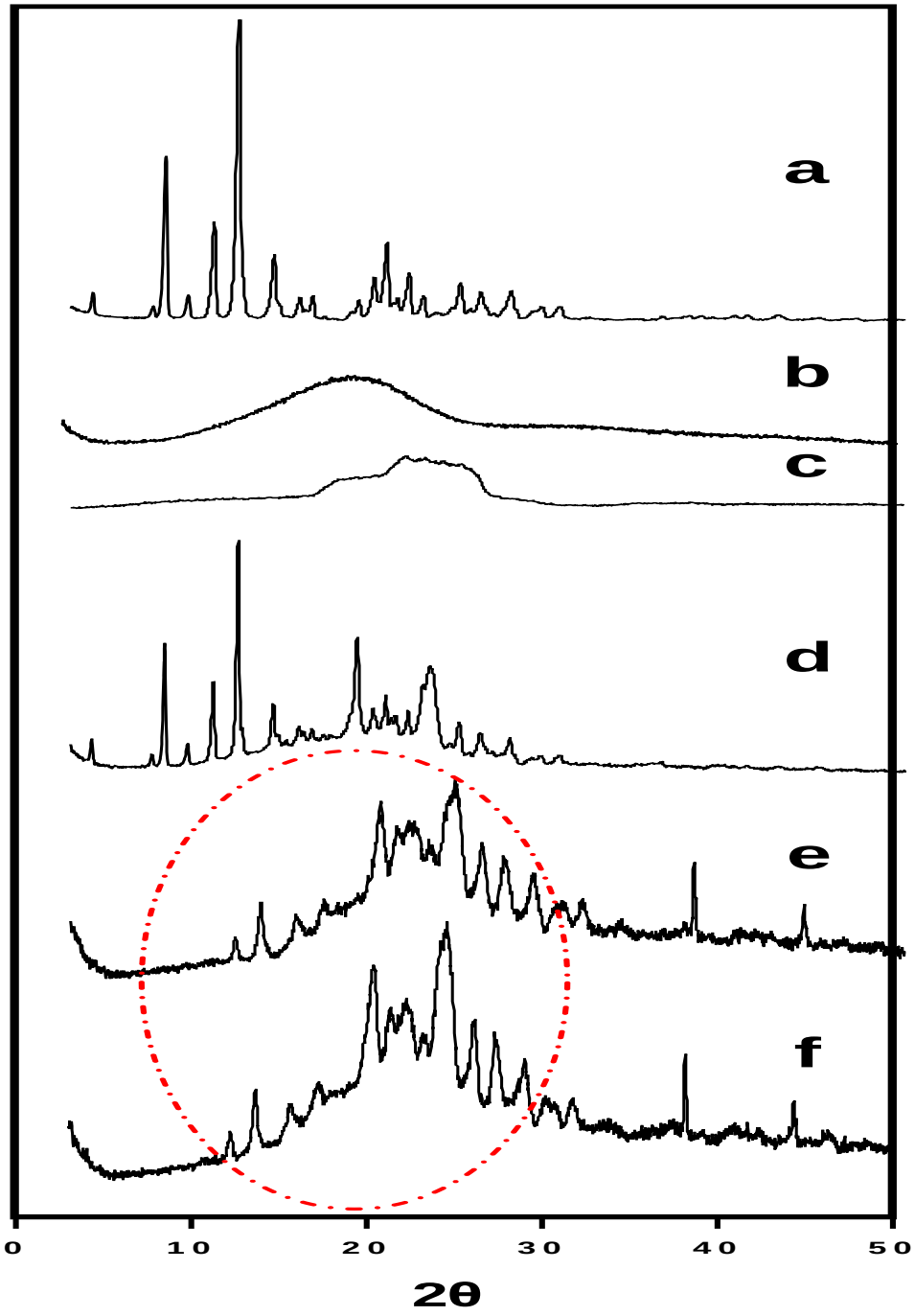

Figure 2. 8 X-ray powder diffraction spectra, pure IRN (a), PLGA (b), P188 (c), Physical mixture before extrusion (d), powdered implants of IM (e) and HME (f).

2.4.5.5 Thermal stability studies using Differential Scanning Calorimetry (DSC)

It is crucial to demonstrate the stability of IRN during the extrusion, considering its susceptibility to various factors, including mechanical stress, heat, moisture and additives (Kollamaram et al., 2018). To define the applicable processing temperature, a range of DSC studies was performed on each drug and excipients individually and in combination to confirm no interactions between the drug and excipients. Peak shifts were indicated as a measure of drug-excipient interactions. The thermograms of the IRN, PLGA, P188, formulation blends, and extrudate implants are represented in (Figure 2.9). Polymer PLGA commonly showed Tg instead of melting temperature (Tm) and was observed as an endothermic peak at 43.6°C (Figure 2.9b). The free IRN showed a sharp endothermic peak at 278°C corresponding to its melting point, indicating its crystalline nature (Figure 2.9a). The broad peak at around 100 -106°C was due to the evaporation of water molecules of the IRN drug (Poudel et al., 2016). The thermogram of free plasticiser P188 has an endothermic melting peak at 53°C during the heating run (Figure 2.9c). All three peaks of IRN, PLGA and P188 were observed in the thermogram of the formulation blends (Figure 2.9d). IRN melting peak was detected in the thermogram of both implants, IM and HME, indicating no transition of the crystalline state to an amorphous state, demonstrating that the drug has not lost its properties and does not show any interactions with the excipients. Additionally, the PLGA glass transition peak and the P188 melting peak were detected at the same temperature. If there were an interaction between IRN and either PLGA or P188, these peaks would also have shifted (Figure 2.9e & 2.9f). These results demonstrated that the preparation process by both techniques, IM and HME, did not affect the stability of the drug and polymer.

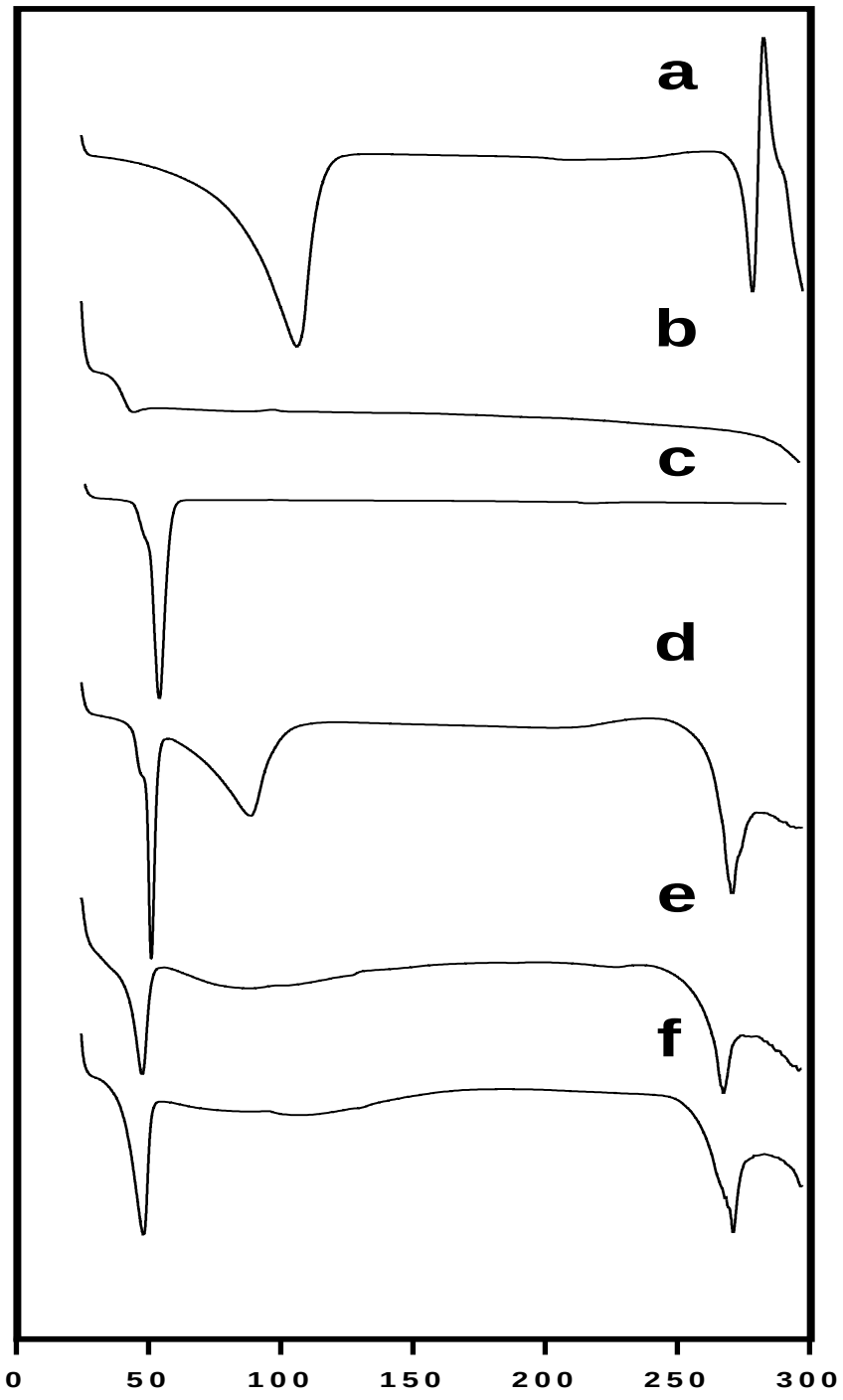

Figure 2. 9 DSC thermograms of Pure IRN (a), PLGA (b), P188 (c), formulation blends (d) and extrudates for two implants; IM implant (e) and HME implant (f).

2.4.6 In vitro dissolution studies

2.4.6.1 Solubility experiments

When selecting the media volumes, the solubility of IRN in the dissolution media was considered to ensure sink conditions throughout the release study. Sink conditions are achieved when the media volume is 3-10 times higher than the volume of solubility (Externbrink et al., 2017). Therefore, before performing the drug release studies, the solubility of IRN in dissolution media (PBS, H_2O, 50%DMSO, 70%DMSO & 80%DMSO) was determined.

Figure 2.10 demonstrates that IRN has a solubility of 0.7 ± 0.0 mg/mL in PBS (pH 7.4). It was observed that IRN is more soluble in dH_2O compared to PBS. However, the solubility of IRN is higher in 80% DMSO compared to dH_2O, 50% DMSO and 70%DMSO. IRN has a solubility of 23.5 ± 0.2 mg/mL, 13.1 ± 0.0 mg/mL, 12.8 ± 0.0 mg/mL and 19.8 ± 0.6 mg/mL in 80% DMSO, dH_2O (pH 5.9), 50% DMSO and 70% DMSO, respectively.

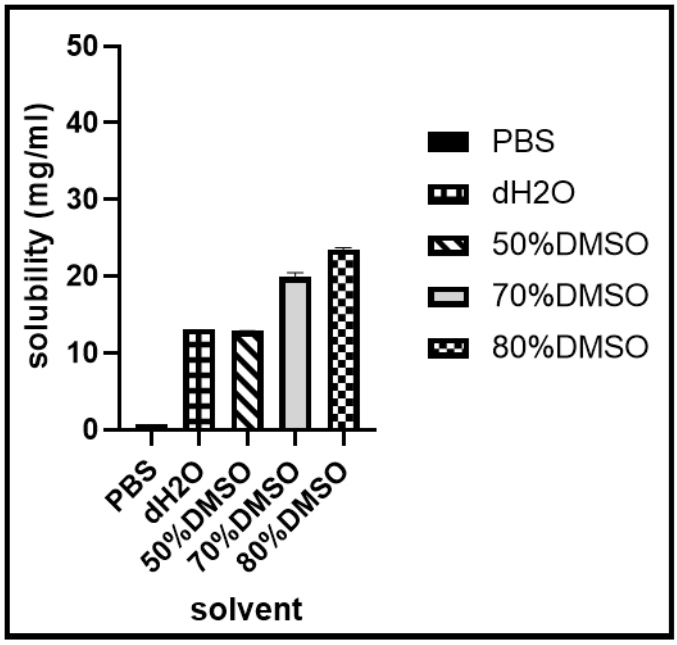

Figure 2. 10 Solubility of IRN in PBS, dH_2O, 50%DMSO, 70%DMSO and 80%DMSO (means ± S.D., n=3).

2.4.6.2 In vitro stability of IRN in the different release media

The stability of IRN in a range of in vitro release solvents (PBS, dH_2O, and DMSO) was investigated (Figure 2.11). It was crucial in this work to identify a suitable solvent in which IRN was stable so that in vitro release tests could be carried out. IRN was found to be stable in all solvents (PBS, dH_2O and DMSO). In this study, a substance was considered stable if it retained 90% of its original concentration. IRN retains 90% to 100% of its stability and remains constant over 36 days under all conditions tested (room temperature, cold room and incubator) (Figure 2.11).

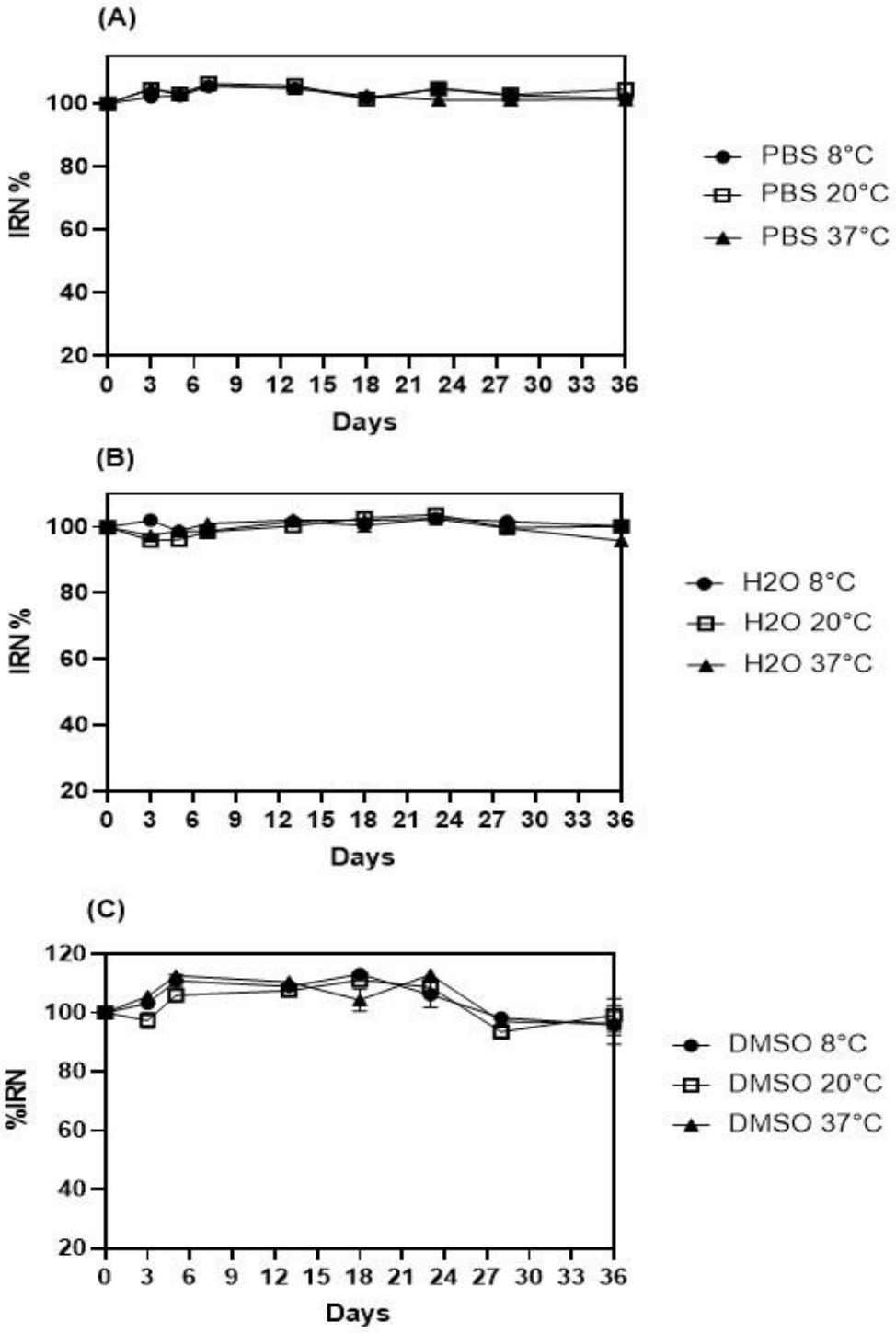

Figure 2. 11 Stability of IRN in PBS (A), H_2O (B) and DMSO (C) over 36 days at 8°C, 20°C and 37°C (means ± S.D., n=3).

2.4.7 In vitro drug release studies

2.4.7.1 Effect of polymer type (PLGA grades) on drug release

In vitro release of IRN from different PLGA grade implants into PBS over 21 days is presented in Figure 2.12 with the 10% (w/w) IRN-loaded IM implants, a day-one burst release is observed for the polymers PLGA 5004, 5010 and 7507. This is due to the drug on the surface of the implants being released immediately. Whereas drug release from polymer 5002 has a no burst release or has a small burst on day 1. The absence of burst release from PLGA 5002 could be attributed to its specific molecular characteristics, such as its lower inherent viscosity (0.2 dl/g) compared to other PLGA grades. The lower melt viscosity at the processing temperature of the IM technique (110°C) may facilitate the melting and homogeneous combination of the PLGA 5002 polymer with the drug, resulting in a slow drug release without a noticeable burst effect. Implants produced by PLGA 5010 exhibited the tri-phasic release profile, which is commonly reported in many PLGA formulations (Berchane et al., 2007; Xu & Czernuszka, 2008; Zolnik et al., 2006) where there is slow diffusion release between day 2 and 4 depending on the polymer, with approximately 25%–35% of the drug being released, followed by an increase in the release rate controlled by the degradation of the polymers and a subsequent slower drug release phase because of the exhaustion of the IRN within the implant. Implants produced by PLGA 5004 and 7507 had a small burst release on day 1 and maintained a slow diffusion-controlled release profile for the entire 21 days. The PLGA 5010 implant released 64% of its IRN content by day 21, whereas the PLGA 5004 and 7507 implants released 20% and 28%, respectively, and PLGA 5002 implant released 88% of its IRN content by day 21. The initial phase of slow diffusion-controlled release is because of the fact that the polymers have not yet started to degrade. However, by

day 4 for the PLGA5004 and 7507 polymers, the second drug release phase begins and continues much faster than the first. This second phase results from the polymers starting to degrade, making the polymer more porous, allowing more release media to diffuse in and more dug to diffuse out. The PLGA 5002 polymer has a bi-phasic release profile with a slow, diffusion-controlled release until day 9, releasing approximately 3.5% of IRN. After day 9, the release rate increases dramatically (second burst release) because of the degradation of the polymer, releasing approximately 88% of its IRN content. The drug release data were analysed using a two-way ANOVA with a Tukey's post-hoc test. The implants produced using the 5010 PLGA polymer achieved significantly faster drug release rates ($p < 0.05$) than those produced using PLGA 7507, 5004, and 5002 at most time points (days 1,2, 4, 5, 6, 9, 11, and 14). According to the literature, each polymer type has different physicochemical properties, a specific Mw and inherent viscosity (Wan et al., 2021). The inherent viscosity midpoint for the PLGA grades: PLGA 5002a, PLGA 5004, PLGA 5010, and PLGA7507 are 0.2 dl/g, 0.4 dl/g, 1.0 dl/g and 0.7 dl/g, respectively. The higher polymer Mw and inherent viscosity have a slower polymer degradation (Makadia & Siegel, 2011). However, these results found the opposite effect. Implants with PLGA5010 have higher Mw and higher inherent viscosity and degrade faster than polymers with lower Mw and lower inherent viscosity (5004 and 5002). The reason for that is because PLGA polymers 5010, when mixed with 10% w/w of IRN and 20% P188, achieved melt viscosity (10^3-10^4 Pa.s) at a high-temperature 118^{o}C (Figure 2.4), which is higher than that processing temperature of IM technique (110^{o}C). Thus, polymer PLGA 5010 would not melt and combine homogeneously with the drug (Figure 2.13), making the drug release from

the PLGA5010 very fast. While with PLGA 5004, when mixed with 10% w/w of IRN and 20% P188, their melt viscosity is at temperatures 79-95^{o}C (Figure 2.4), below the processing temperature of the IM technique (110^{o}C). Therefore, the PLGA 5004 polymer melted and was combined appropriately with the drug. Implants that used PLGA 5010 and 7507 polymers required high processing temperatures for their melt rheology, thus, could not be formulated by an IM technique. In contrast, implants used the polymer PLGA 5002 and 5004, their processing temperature for melt viscosity within the processing temperature used for the IM technique. Therefore, only implants with the polymers 5004 and 5002 would be selected for further characterisation studies.

This data demonstrates that the IRN release from the PLGA implants can be controlled by the choice of polymer used to produce the implants.

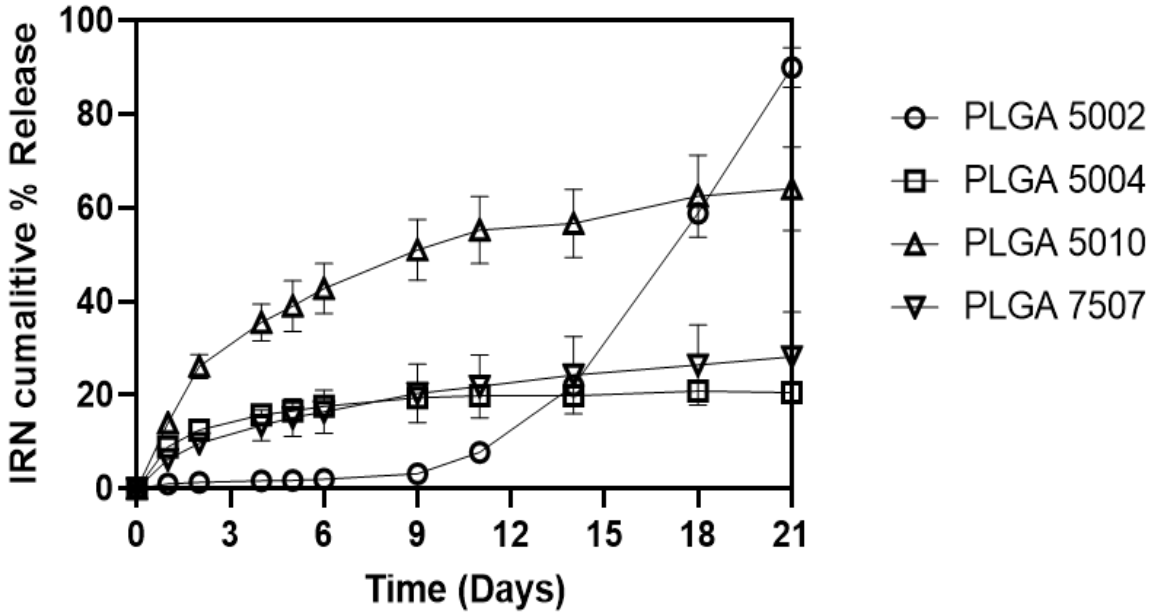

Figure 2. 12 In vitro drug release for 10% IRN-loaded implants used different PLGA (5002a, 5004, 5010 and 7507) manufactured by IM technique (means ± S.D., n=3). significance found using a two-way ANOVA with a Tukey's post-hoc test, * = P<0.05 ** = P<0.01, *** = P<0.001, **** = P<0.0001.

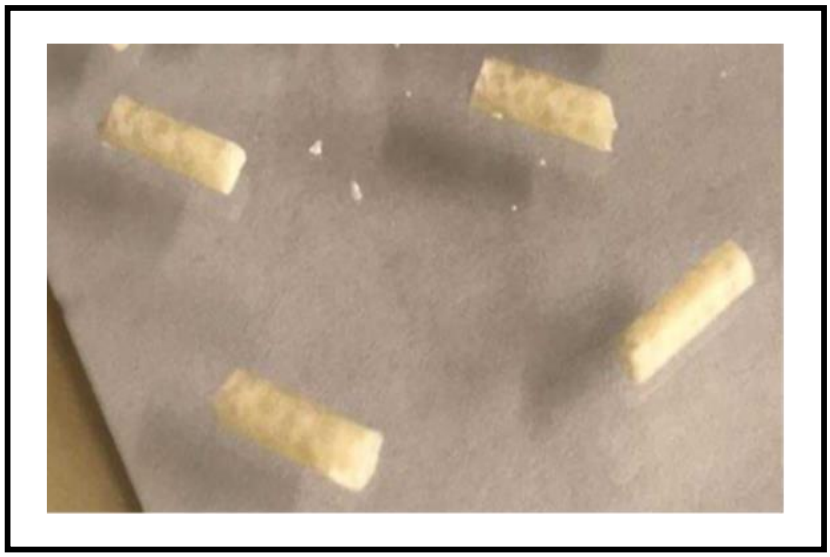

Figure 2. 13 Image of 10% IRN-loaded implants mixed with PLGA 5010 and 20%P188 formulated by an IM technique. PLGA 5010 particles were not melted and can be visually observed.

2.4.7.2 Effect of drug loading ratio on the release

Drug release was biphasic for all drug loadings, comprising an initial diffusive phase and a second erosion phase. The study compared the drug release rate for the 10%, 20%, and 30% w/w loadings implants. A two-way ANOVA followed by Tukey's post-hoc test revealed significant differences in the drug loadings. The 30% w/w loading had a non-significantly greater drug release rate than the 20% w/w loading at most time points ($p > 0.05$) and a significantly greater drug release rate than the 10% w/w loading ($p < 0.05$) at most time points. Additionally, the 20% w/w loading had a significantly greater drug release rate than the 10% w/w loading at most time points ($p < 0.05$). These results were based on data displayed in Figure 2.14. This increase in the release is expected because the more drug in the implant, the greater the polymer's porosity upon drug release, allowing for the imbibition of more release media, thus boosting drug release and degradation (McConville et al., 2015). This

indicates that the release rate of IRN from PLGA implants can be influenced by drug loading.

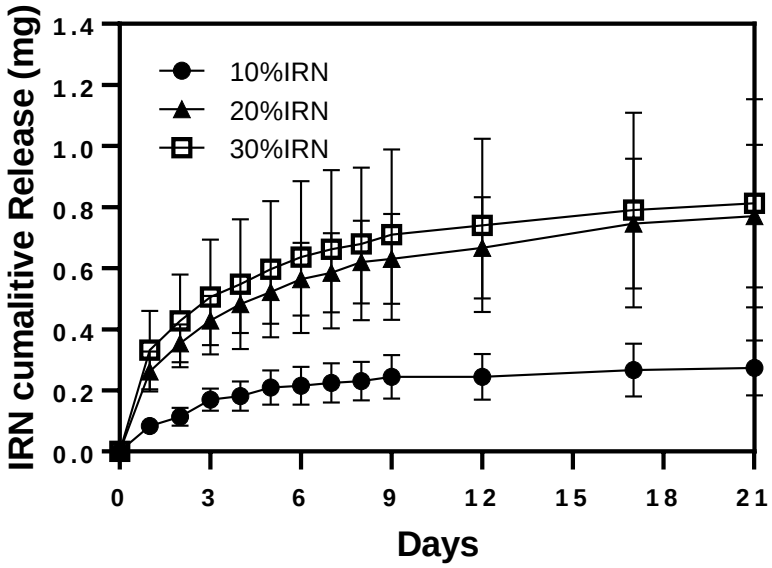

Figure 2. 14 Effect of drug loading on the cumulative amount (mg) of IRN released from PLGA 5004 implants prepared by IM technique (means ± S.D., n=3) significance found using a two-way ANOVA with a Tukey's post-hoc test, * = P<0.05 ** = P<0.01, *** = P<0.001, **** = P<0.0001.

2.4.7.3 Effect of implant dimensions on drug release

The effect of implant dimensions on drug release was investigated. The cumulative drug release over 21 days was determined for 2X3 mm and 2X6 mm implants loaded with 30% IRN in PLGA 5004 (Figure 2.15). Statistical analysis using a two-sample t-test with a 95% confidence level and a significance threshold of ($p<0.05$) was performed to compare the results obtained at each time point. The 2X6 mm implant released 0.3 mg of the drug during the initial burst release on day one, which was significantly higher than the 0.1.8 mg released by the 2X3 mm implant ($p<0.05$). In addition, the total drug release over 21 days was observed to be greater for the 2X6 mm implant (0.8 mg) as compared to the 2X3 mm implant (0.4 mg), which was also statistically significant ($p<0.05$). The increase in initial burst release is expected; as the dimensions of the implant increase, the surface area also increases, leading to increased drug diffusion from the implant and into the surrounding fluid. This increase in surface area may contribute to a burst release of the drug, which could explain the observed increase in drug release on day one. This finding agrees with a previous study (Suh et al., 2021), which indicates that a larger surface area resulted in a higher burst release. In addition, another reason that may contribute to the increase in drug release is the more drug present in the larger dimension implant (2X6mm). As a result, the porosity of the polymer increases upon drug release, allowing more release media to imbibe into the polymer. This further enhances drug release and degradation (Major & McConville, 2015). This may explain the observed increase in drug release on day 21, as the release media continue to be imbibed into the implant.

Overall, the results indicate that implant dimensions can significantly impact drug release from PLGA implants.

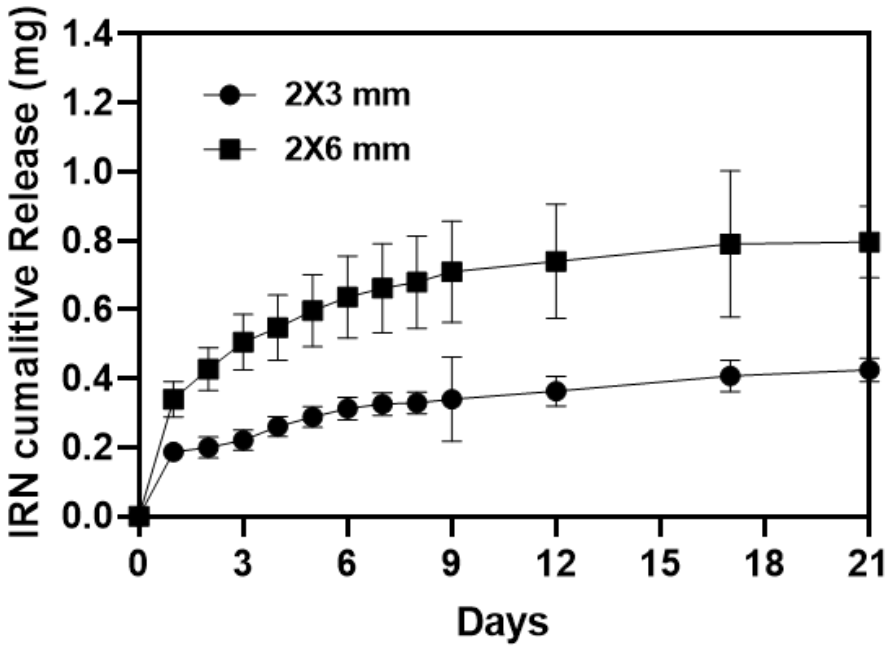

Figure 2. 15 Effect of implant dimensions on the cumulative amount of IRN released (mg) from PLGA 5004 implants prepared by IM technique (means ± S.D., n=3) significance found using a two-sample t-test (* = P<0.05, ** = P<0.01, *** = P<0.001, **** = P<0.0001).

2.4.7.4 Effect of manufacturing procedure on the release of IRN

The influence of the manufacturing procedure on drug release from PLGA 5004 implants containing 10% w/w drug is shown in Figure 2.16. The drug release data were analysed using a two-way ANOVA with a Tukey's post-hoc test. The analysis showed a significant difference in drug release between HME and IM implants ($P < 0.05$). The results indicated that at most time points, drug release was significantly lower for the HME implants compared to the IM implants ($p < 0.05$). This is because of high shear forces of the HME process make the implants denser, more closely packed matrix, as shown in Figure 2.7b, resulting in a slower uptake of the dissolution medium and slower drug release. The absence of burst release from the HME implants was statistically significant on the first day ($p < 0.05$), and the release profile remained slow and diffusion-controlled for the entire 30 days. In contrast, the release from the IM implants was quite rapid during the early stage of drug release due to the lower shear forces of the IM process than HME, which subsequently increases the porosity of the IM implants allowing the release media to imbibe in and the IRN diffuse out at a faster rate thus enhancing degradation and the overall release rate. Drug release from IM implants exhibited a biphasic profile: an initial release followed by a slow release. The initial IRN release of IM on day 1 was from 5%, followed by slow release over 30 days. The drug release from IM was higher than the HME implants, with the IM and HME implants releasing 40% and 6.6%, respectively, over the 30 days ($p < 0.05$). The difference in the initial burst release can be attributed to the higher amount of drug on the surface of the IM implants, as revealed by the Raman data presented in Figure 2.7a. This is due to the absence of shear force and mixing during the manufacturing process. In contrast, the HME implants had lower drug concentrations on the surface, as shown in Figure 2.7b, due

to the effective dispersion of the IRN in PLGA by the high shear forces of the extrusion process.

This data demonstrates that the release rate of IRN from PLGA implants can be influenced by the manufacturing technique used.

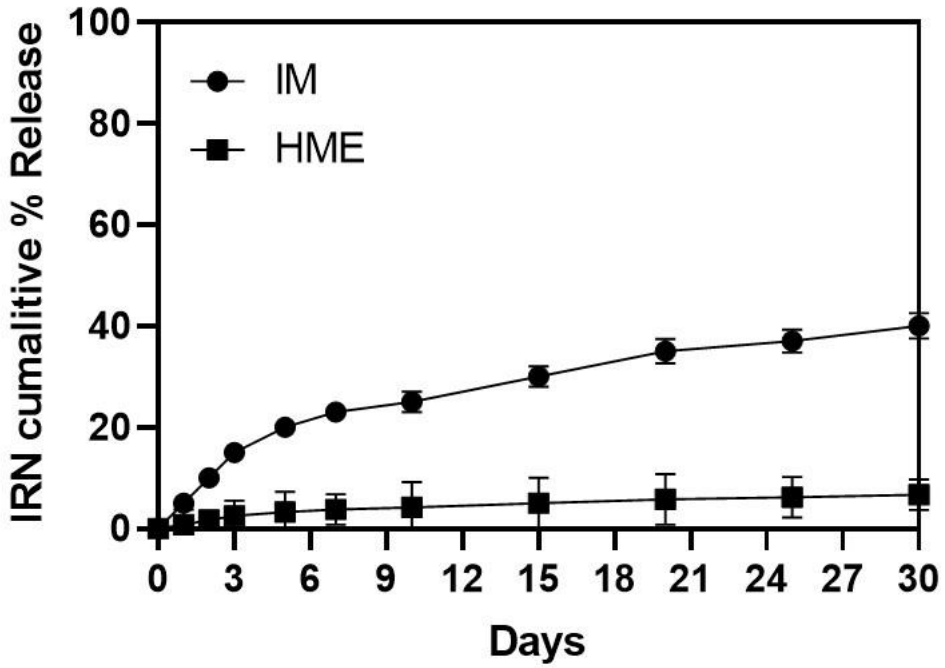

Figure 2. 16 Effect of manufacturing procedure on the release of IRN from PLGA 5004 implants. Results are represented as (means ± S.D., n=3), significance found using a two-way ANOVA with a Tukey's post-hoc test, * = P<0.05 ** = P<0.01, *** = P<0.001, **** = P<0.0001.

2.4.7.5 Long-term in vitro release and accelerated short-term release studies

Long-term (Real-time) in vitro release study is often undertaken to describe the drug release characteristics under physiological conditions (Burgess et al., 2002; Mitra & Wu, 2010). However, (Real-time) in vitro release study for controlled release formulations commonly takes weeks, months, or even years to accomplish (Hoffman, 2008; Mao et al., 2012; Mitragotri et al., 2014; Wang & Burgess, 2012). Furthermore, the drug release durations from PLGA formulations in simulated physiological conditions could range from weeks to months (Zackrisson et al., 1995). This procedure is time-consuming (Zackrisson et al., 1995), and the effective product shelf-life would be reduced if applied to batch-release testing. (Andhariya et al., 2017). Therefore, an accelerated release study (short-term) might be useful (Zackrisson et al., 1995). An accelerated release study can be used as a quality control tool that would promote quicker drug release for extended-release formulations (Goel et al., 2021). The accelerated release study is not intended to be bio-relevant or simulate physiological conditions but to help enable faster formulation development (Goel et al., 2021). Using organic solvents was identified as a potential method to achieve accelerated drug release (Goel et al., 2021). For this work, DMSO:Water with different compositions has been used as a release media, which is expected to increase the drug release similar to the literature (Goel et al., 2021). The goal is to establish an accelerated release study that could release >95% of IRN within seven days.

2.4.7.5.1 Long-term in vitro release

Figure 2.17 illustrates the long-term in vitro release profiles of the IRN from IM implant and HME implant under physiological conditions using PBS (pH 7.4) at 37ºC as a release medium. At each time point, the amount of IRN released into the media was quantified by HPLC. The long-term release profile for IM implant in PBS release media (Figure 2.17 (○)) displays a triphasic release profile characterised by an initial period of sustained release over the first 10 days with a low initial burst release (5%) (A) followed by a lag period with significantly lower IRN release per day (B) followed by a terminal period during which the remaining IRN is released in a controlled manner (C). It is observed that the total cumulative IRN released reached 100% at day 60. The long-term release profile for HME implants in PBS release media maintained a slow, diffusion-controlled-release profile for the entire 60 days, with approximately 16.6% of their IRN loading being released (Figure 2.17(□)). IM implants display a faster drug release than HME, however, both implants (IM and HME) indicate a long-term drug release (months) under physiological conditions using PBS media.

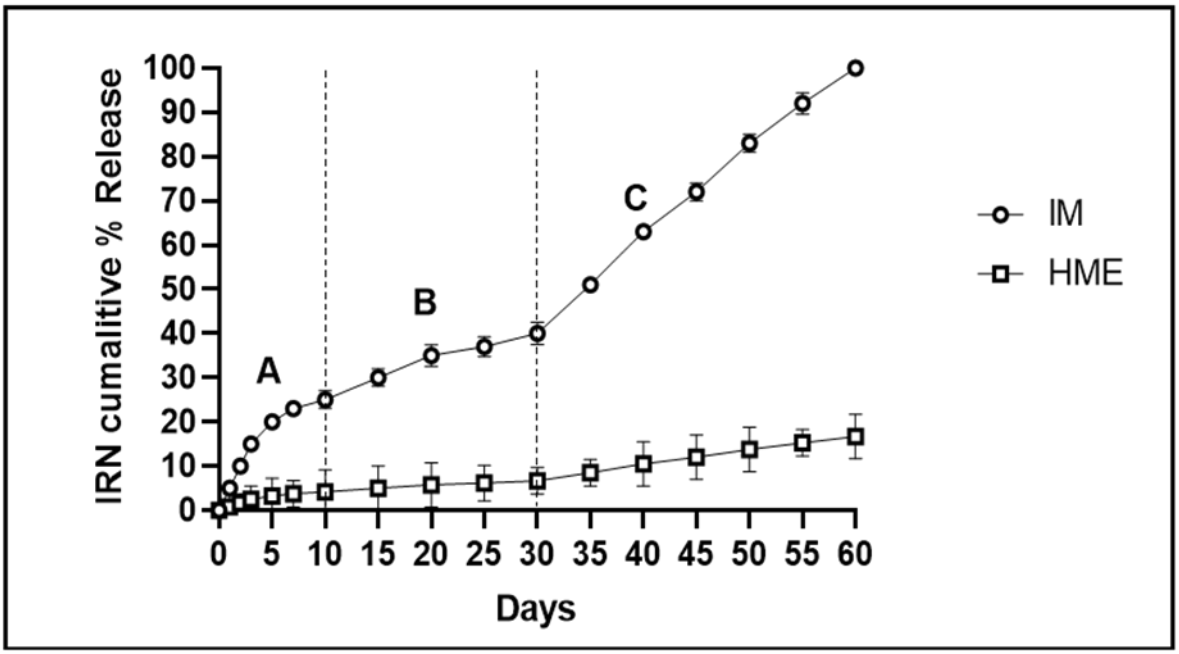

Figure 2. 17 long-term in vitro release of IRN from both IM and HME implants in pH 7.4 PBS at 37°C. The three release phases for IM are marked by 'A', 'B', and 'C' (○), while for HME, the release is represented by a square (□). The means and standard deviations of n=3 samples are shown for both implants.

2.4.7.5.2 Accelerated short-term in vitro release (Effect of the various release media on the drug release)

Figures 2.18 & 2.19 show the effects of the type of release media on the release profile of IRN from PLGA IM implant and HME implant. Figure 2.18 shows that in PBS (pH 7.4) release media, after an initial release (approximately 5%), there is a slower release phase, with the cumulative IRN release from the IM implant increasing to 40% after 30 days. It was then followed by an even slower release over the next 30 days. The typical release media mentioned above could not ensure a 100% release at the required time for drug release (7 days), which was recommended as a specification for an accelerated release. Deionised water and organic solvent (DMSO) with different compositions (50%, 70% and 80%) were used as a release media to speed up the IRN release. Based on the literature, organic solvents (Xie et al., 2015) have been used to accelerate drug release from PLGA (Shameem et al., 1999). It is expected that using organic solvents will increase drug diffusion and have the desired drug release. They can accelerate the drug release rate from polymer matrices due to their tendency to penetrate the matrix and change diffusion characteristics. Compared with the PBS release media, the release rate was significantly faster ($p < 0.05$) in deionised water and organic solvent (DMSO) release media on days 1, 2, 3, 4 and 5. As shown in Figure 2.18, the completed drug release reached 100% in dH_2O, 50%, 70% and 80% DMSO on days 5, 5, 7, and 25, respectively. There was no lag phase in the release curves of deionised water and organic solvents (50%, 70% DMSO) after the initial release. In the release media studied, the release rate in the deionised water was the highest. However, 70% DMSO achieved sustained drug release over 7 days (required time for accelerated drug release). Type of release media and concentration of DMSO influence the

release profile. Therefore, the DMSO 70% was selected for accelerated drug release method as a quality control tool for IM implants. The optimised accelerated release method achieved complete release of IRN from PLGA implant within one week compared to 2 months of real time release.

The release profiles of IRN from the HME implant in different release media, PBS, deionised water and DMSO organic solvent with different concentrations (50%, 70% and 80%, v/v) are shown in Figure 2.19. In PBS and deionised water media, show a slow release over 60 days. The two release media mentioned above could not ensure a 100% IRN release over 60 days. The cumulative release in PBS and deionised water media were 16% and 33% at day 60, respectively. The IRN release in a medium containing a high concentration of DMSO (80%) was higher than in the medium containing lower DMSO concentrations (70% and 50%). As the DMSO concentration increased from 50% to 80%, the cumulative releases were 100%, 100% and 92% at 60, 20, and 7 days, respectively. The release of IRN in the medium with 80% DMSO was significantly higher ($p < 0.05$) compared to the release in PBS, dH_2O, and the medium with 50% DMSO on days 1, 2, 3, 5 and 7. Additionally, the release in the medium with 80% DMSO was not significantly ($p > 0.05$) higher than the release in 70% DMSO medium on days 1, 2, 3, 5 and 7. In 80% of DMSO release media, drug release was sustained over seven days (the required time for accelerated drug release). Its release-promoting effects could be enhanced by increasing its concentration in the release medium. Therefore, the DMSO 80% was selected for the accelerated drug release method for HME implants.

The decision to use these media was driven by their potential to accelerate drug release, as reported in the literature (Goel et al., 2021). Organic solvents, such as DMSO, have been identified for their ability to enhance drug diffusion from PLGA formulations (Xie et al., 2015). The goal was to establish an accelerated release study that could achieve >95% release of IRN within seven days, providing a valuable quality control tool for extended-release formulations. While these media may not fully replicate in vivo conditions, their use in accelerated studies allows for faster formulation development, aligning with previous studies (Goel et al., 2021). It is essential to acknowledge that these media might not perfectly represent physiological conditions; however, their selection was based on their efficacy in promoting rapid drug release. This accelerated approach is particularly relevant for quality control purposes, where achieving timely drug release is crucial for ensuring the effectiveness of the implant. The concentration of DMSO in the release media was optimised based on its influence on release profiles, with DMSO 70% selected as it demonstrated sustained drug release over 7 days for IM implants, meeting the accelerated drug release requirement. For HME implants, the release media achieved sustained release over seven days under 80% DMSO release media.

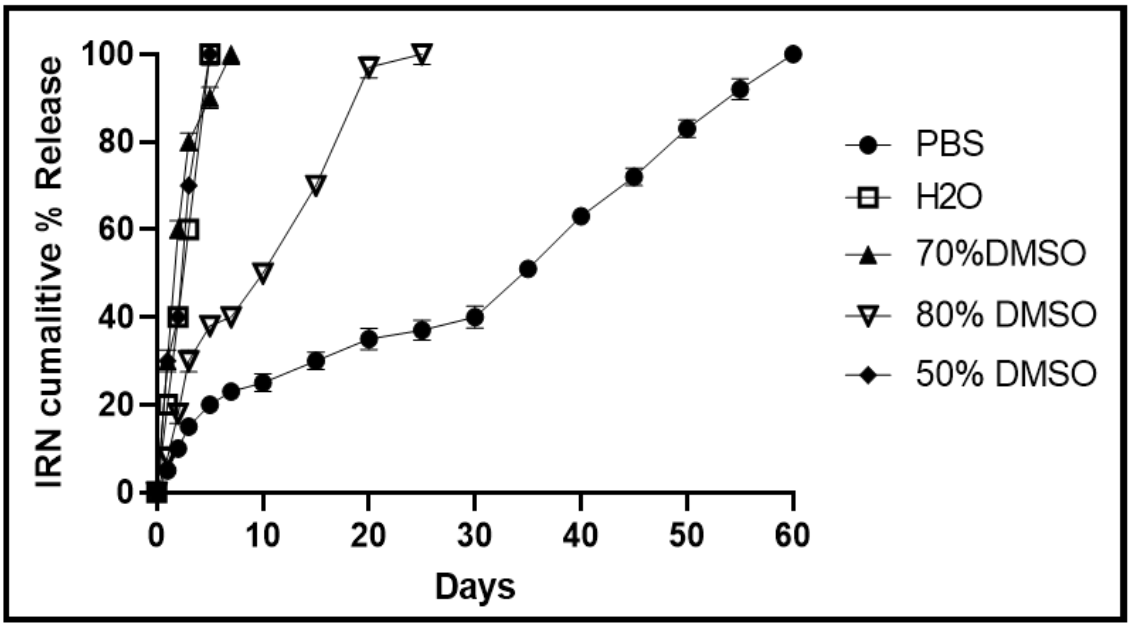

Figure 2. 18 Short- and long-term release profiles of IRN from PLGA IM implant. Short-term (days for x-axis): in different release media: H_2O, 50%DMSO, 70%DMSO and 80% DMSO. Long-term (days for x-axis): in PBS (mean±SD; n=3) significance found using a two-way ANOVA with a Tukey's post-hoc test, * = P<0.05 ** = P<0.01, *** = P<0.001, **** = P<0.0001.

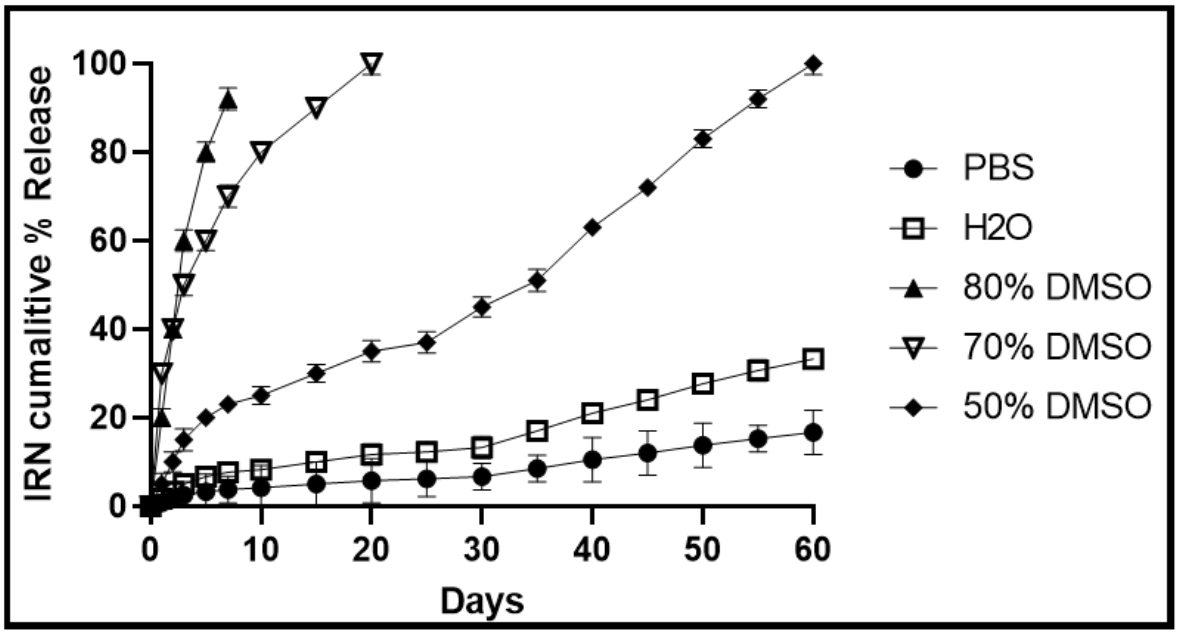

Figure 2. 19 Short-and long-term release profiles of IRN from PLGA HME implant. Short-term (days for x-axis): in different solvents: 80% DMSO, 70%%DMSO. Long-term (days for x-axis): in PBS, H_2O, 50%DMSO (mean±SD; n=3) significance found using a two-way ANOVA with a Tukey's post-hoc test, * = P<0.05 ** = P<0.01, *** = P<0.001, **** = P<0.0001.

2.5 Conclusion

This chapter investigates the effect of IM and HME techniques on the size and weight uniformity, drug content uniformity, drug content, drug distribution, stability, physical state and drug release of IRN-loaded PLGA implants (Table 2.6). The selection of formulation composition and implant manufacturing processes were investigated in the pre-screening step of various variables, including the amount of drug, type of PLGA and amount of plasticiser. Based on the rheology results, the formulations; 30%IRN+5002+5%P188, 30%IRN+5002+10%P188, 30%IRN+5002+20%P188, 30%IRN+5004+20%P188, 10%IRN+5002+20%P188, 10%IRN+5004+20%P188 were appropriate for moulding and extrusion. The resulting IM and HME implants were characterised using various techniques, including HPLC, DSC, XRD, and Raman. The results described in this chapter demonstrate that all IRN-loaded PLGA implants manufactured by IM and HME were consistent in size (diameter and length) and weight. However, HME implants had higher drug content and good content uniformity compared to IM implants. It is demonstrated that neither technique has an adverse effect on the stability of IRN within HME and IM implants. However, Raman mapping confirmed heterogeneous drug distribution within IM implants. In contrast, homogenous drug distribution was observed within HME implants. HME implants were homogenously dispersed within PLGA implants due to the high shear mixing force of the twin screws of the HME. Based on the drug content, stability, and drug distribution results, the HME technique is preferable technique than IM.

In vitro drug release of IM implants and HME implants were investigated. The release of IRN was affected by the type of PLGA, drug load, size of implant, manufacturing techniques and solubility of the drug in release media. The drug release from

PLGA5004 was much faster than from PLGA5002. The results demonstrate that the IRN release from the PLGA implants can be controlled by the choice of polymer used to produce the implants. In addition, the results have shown that 30% w/w IRN loading had an increased release rate compared to the 20% and 10% w/w loaded implants. Increasing the dimensions of 30%IRN loaded PLGA 5004 implants from 2X3 mm to 2X6 mm increased drug release. The release from these HME implants is significantly lower than those manufactured by IM. This is because of high shear forces of the HME process make the implants denser, more closely packed matrix, resulting in a slower uptake of the dissolution medium and slower drug release.

The completed drug release (real-time) for IM and HME implants under physiological conditions using PBS media takes a very long time (more than a month), which is time-consuming. Therefore, accelerated release studies were investigated using various types of release media to speed up drug release. For IM implants, drug release achieved sustained release over seven days under 70%DMSO release media, while for HME implants, release media achieved sustained release over seven days under 80%DMSO release media.

The particular challenge faced by the IM technique, characterised by the absence of significant shear forces present in the twin screws of the HME process, led to lower drug content and uniformity. Addressing this issue would benefit from future investigations exploring potential refinements to the IM process. Strategies such as pre-mixing or optimising the degree of grinding before IM could be implemented to mitigate shear-related challenges, thereby enhancing drug content uniformity and overall performance.

Table 2. 6 Summary comparison of IM and HME techniques for the development and characterisation of IRN-loaded PLGA implants.

Parameter	IM implants	HME implants
Size and weight uniformity	Consistent in size and weight with a ± 10% deviation	Consistent in size and weight with a ± 10% deviation
Drug content uniformity	RSD % (5.5 - 13.2%) Lower drug content uniformity compared to HME implants	RSD % (1.3 - 2.5%) Higher drug content uniformity
Drug content	(67 - 81%) Low drug content level	(89 - 96%) High drug content level
Drug stability	No adverse effect on IRN stability	No adverse effect on IRN stability
Drug distribution	Non-homogenous drug distribution	Homogenous drug distribution
Preferred technique	Not preferred due to lower drug content uniformity and non-homogenous drug distribution	Preferred due to higher drug content uniformity and homogenous drug distribution
Drug release profile	Affected by type of PLGA, drug load, implant size	Generally lower release rate compared to IM due to denser matrix; similar influences as IM
Long term release (PBS media)	Sustained drug release, requires over a month (60 days) for complete drug release	Sustained drug release, requires over a month (>60 days) for complete drug release
Accelerated drug release	Achieved sustained release over 7 days in 70% DMSO media	Achieved sustained release over 7 days in 80% DMSO media

CHAPTER 3: DEVELOPMENT AND CHARACTERISATION OF SINGLE-LAYER IMPLANTABLE DRUG DELIVERY DEVICE (PITAVASTATIN-LOADED PLGA) FORMULATED BY USING INJECTION MOULDING AND HOT MELT EXTRUSION TECHNIQUES

3.1 Background

PTV is a drug that belongs to a class of drugs known as statins and was approved by the FDA in 2009. It is primarily used to treat high cholesterol levels (Stein, 2003; Voss et al., 2021), there is some research supporting its anti-tumour effects in glioma, ovarian and colon cancers, in both in vivo and in vitro studies (Anjum et al., 2017; De Wolf et al., 2017; Jiang et al., 2014; Jiang et al., 2014a, 2014b; Koukourakis et al., 2016; Tsuboi et al., 2009; Zhang et al., 2017). Further studies have stated that statin drugs are effective in slowing the growth of tumours (Jiang et al., 2014b; Nielsen et al., 2012; Thurnher et al., 2012). However, PTV has more potency in reducing tumour growth than other statins (Jiang et al., 2014b). The mechanism of action was postulated to involve PTV's effects on the metabolism of cholesterol, a substance present in cell membranes, and signalling pathways in tumour cells, both of which are critical for developing tumours. Since GBMs are highly proliferative cells, they require significant amounts of cholesterol, which may cause them to respond to statin therapy (Jiang et al., 2014b). A study (Jiang et al., 2014b) stated that PTV reduced MDR-1 and promoted cellular autophagy in GBM tumour cells. Furthermore, it has been reported that PTV treatment for glioma cells inhibits nuclear factor-kappa B activation, which inhibits autophagy and leads to autophagic cellular death (Koukourakis et al., 2016; Tsuboi et al., 2009). However, the ability of PTV to pass the BBB is expected to be limited, with a calculated logarithm value of brain-to-plasma concentration ratio (-log BB) of -0.6499 (Jiang et al., 2014b). Thus, when PTV is administered orally or intravenously, it will result in insufficient levels of the drug in the brain, which makes it an unsuitable route of administration for treating GBM. Furthermore, PTV associated with systemic adverse

effects includes back pain, constipation, diarrhoea, myalgia, and pain in the extremities (Bhatti & Tadi, 2023). This highlights the potential use of local administration of PTV. The local delivery strategy has additional advantages for treating GBM and other brain disorders. It can avoid the BBB and concentrate higher amounts of the drug in the cancerous tissues (Chakroun et al., 2018), thereby potentially reducing systemic exposure and unwanted adverse effects. This chapter focuses on developing PTV loaded PLGA implantable delivery device manufactured by IM and HME techniques for treating GBM. A study (DASARI & MARUVAJALA, 2019) reported that PTV had a high melting point of 139°C. Furthermore, PTV has been shown to be stable at high temperatures up to 198°C (Mikrani et al., 2022), which could be appropriate to be manufactured by IM and HME techniques and able to withstand the high processing temperature required for moulding and extrusion. During the pre-screening phase, various variables will be examined through rheological studies. These variables include the amount of drug, the type of PLGA, and the amount of plasticiser. Consequently, it can provide information on the material's physical properties, allowing us to determine the manufacturing processing parameters and develop a formulation that can be manufactured by IM and HME techniques. Furthermore, the manufacturing technique and process parameters can significantly impact the dosage form's internal and external structure, thereby influencing the drug release kinetics (Andhariya et al., 2019; Bassand et al., 2022; Vay et al., 2011). Thus, the influence effect of manufacturing techniques on the drug content, stability, physical state and drug release will be investigated.

3.2 Aims and objectives

This chapter aimed to develop a PTV-loaded PLGA implantable delivery device using IM and HME for localised treatment of GBM.

The objectives were:

- To determine the manufacturing processing parameters for chosen material that can be manufactured by IM and HME techniques.
- To produce PLGA matrix implants containing PTV by using IM and HME techniques.
- To characterise the implants using DSC, XRD and Raman.
- To investigate the PTV content of the implants.
- To investigate the stability of PTV in various solvents for in vitro release studies.
- To investigate the in vitro drug release from the implants.

3.3 Materials & Methods

3.3.1 Chemicals

Pitavastatin calcium was purchased from LGM Pharma, Georgia, USA. Acetic acid ≥ 99%, HPLC grade from Sigma-Aldrich, Saint Louis, USA. The other materials used in this chapter were the same as those used in chapter 2, section 2.3.1.

3.3.2 Methods

3.3.2.1 HPLC analysis

PTV was quantified using an Ultimate 3000 Autosampler HPLC (Thermo Scientific Inc., Germering, Germany) set at 445 nm. The mobile phase consisted of 0.5% acetic acid/acetonitrile (35/65%, v/v). A Zorbax Eclipse XDB-C18 4.6 x 150 mm, 3. uM particle size column (Agilent Technologies, USA) was used with a 1.0 ml/min flow rate. The column temperature was maintained at 25°C. The total run time was 10 minutes, and the retention time of PTV was 2.1 minutes. The concentration of PTV from each sample was determined from the peak area obtained, based on a calibration curve for the concentration between 4-100 µg/mL (R^2 = 0.9999).

3.3.2.2 Rheological measurements

Melt rheology was performed on the different blends of PTV, polymer and plasticiser (Table 3.1) to determine their melt viscosity and processing parameters as a function of temperature for manufacture via IM and HME techniques. The experiments were performed on a Discovery hybrid parallel plate rheometer (T.A. Instruments, USA) using a 20 mm cross-hatch steel plate and a 500 µm gap height. The method used here is the same rheological method used in Chapter 2, section 2.3.2.2.

Table 3. 1 Summary of different PTV, Polymer, and Plasticiser (P188) blends investigated for melt rheology analysis.

Formulation	PTV (w/w)	Polymer	Plasticiser P188 (w/w)
PTV-5002	10%, 20%, 30%, 40%, 50%	PLGA5002	-
PTV-5004	10%, 20%, 30%, 40%, 50%	PLGA5004	-
PTV-5010	10%, 20%, 30%, 40%, 50%	PLGA5010	-
PTV-7507	10%, 20%, 30%, 40%, 50%	PLGA7507	-
PTV-5004-1%P188	30%	PLGA5004	1%
PTV-5004-5%P188	30%	PLGA5004	5%
PTV-5004-10%P188	30%	PLGA5004	10%
PTV-5004-20%P188	30%	PLGA5004	20%
PTV-5004-20%P188	10%	PLGA5004	20%
PTV-5004-20%P188	20%	PLGA5004	20%
PTV-5004-20%P188	30%	PLGA5004	20%
PTV-5004-20%P188	40%	PLGA5004	20%
PTV-5004-20%P188	50%	PLGA5004	20%

3.3.2.3 Manufacturing of PTV-Loaded PLGA implant

3.3.2.3.1 Injection moulding (IM)

The method used for manufacturing PTV-Loaded PLGA implants by IM is the same method used for manufacturing IRN-Loaded PLGA implants by IM described in Chapter 2, section 2.3.2.3.1.

3.3.2.3.2 Hot Melt extrusion (HME)

The method used here for manufacturing PTV-Loaded PLGA implants by HME is the same method used for manufacturing IRN-Loaded PLGA implants by HME, which was described in Chapter 2, section 2.3.2.3.2, with different extruding parameters (Table 3.2).

Table 3. 2 HME parameters for extruding PTV-PLGA-P188 implants with different drug loads (10, 20, 30% w/w PTV).

PTV-PLGA5004_20%P188 mixtures	Feeding zone temperature ^{o}C	Mixing zone temperature ^{o}C	Metering Zone temperature ^{o}C	Screw Speed (rpm)
10% PTV	75	100	75	20
20% PTV	78	105	81	20
30% PTV	80	110	81	20

3.3.2.4 Physical characterisation of implants

3.3.2.4.1 Determination of the lengths, diameters and weights of PTV-loaded PLGA implants

The method is the same as that described in chapter 2, section 2.3.2.4.1.

3.3.2.5 Physiochemical characterisation

3.3.2.5.1 Determination of drug content

The method used for PTV-PLGA implant content as described in Chapter 2, section 2.3.2.5.1.

3.3.2.5.2 Crystallinity studies using X-ray Powder Diffraction (XRD)

X-ray powder diffraction patterns of IM and HME implants (ground to a fine powder), formulation blends and pure PTV, PLGA and P188 were evaluated using a Rigaku MiniFlex 600 (Rigaku, USA). The method is the same as that described in chapter 2, section 2.3.2.5.4.

3.3.2.5.3 Thermal stability studies using Differential Scanning Calorimetry (DSC)

The method is the same as that described in chapter 2, section 2.3.2.5.5.

3.3.2.5.4 Determination of the Physical State of PTV in the PLGA implants by using Raman

The method used for the determination of the physical state of the PTV in the PLGA implants is the same as that described in chapter 2, section 2.3.2.5.2.

3.3.2.5.5 Drug distribution in PLGA implant by using Raman mapping

The method used for drug distribution in PTV-PLGA implants is the same as that described in chapter 2, section 2.3.2.5.3.

3.3.2.6 In vitro dissolution studies

3.3.2.6.1 Solubility experiments

The method used for the solubility of PTV in different dissolution media is the same as that described in chapter 2, section 3.2.6.1.

3.3.2.6.2 In vitro stability of PTV in the different release media

The purpose of the stability testing was to determine the stability of the PTV over time in different media (dH_2O, PBS and DMSO) and temperatures (8°C, 20°C and 37°C). Standard solutions (100 ug/ml) of PTV in each media were prepared and transferred into glass vials and stored under various conditions, room temperature (20°C), cold room (8°C) and incubator (37°C) for 40 days. PTV has been previously reported to be light sensitive (Jarmużek et al., 2020), therefore, all samples were protected from the light. Samples were taken daily, starting from day 0 up to day 40 and analysed by HPLC. The results were represented as mean (n=3) ± standard deviation (S.D.).

3.3.2.7 In vitro drug release studies

3.3.2.7.1 Effect of manufacturing procedure on the release of PTV

In vitro release study was conducted to investigate the effect of the manufacturing procedure on the release of PTV from PLGA implants. The drug release of the 10% PTV loaded PLGA 5004 implants, manufactured using IM and HME techniques, was performed in PBS (pH 7.4) at 37°C and placed into an orbital shaking incubator at 37°C and 100 rpm over a period of 40 days. 1 mL samples were taken at various time points of 1, 2, 3, 7, 10, 14, 17, 21, 24, 29, 31, 36, 38 and 40 days and replaced with the same volume of PBS. The withdrawn samples were filtered using a 0.45 uM filter and analysed using the PTV HPLC method. The experiments were performed in triplicate (n=3) to ensure the reproducibility of the results.

3.3.2.7.2 Effect of the various release media on the drug release

Drug release testing under different types of release media (dH_2O, 50%DMSO, 70% DMSO and 80% DMSO) at 37°C was investigated to develop a suitable accelerated in vitro release testing method. Each 10%PTV loaded PLGA 5004 implant was placed into a sealed flask containing different release media (dH_2O, 50%DMSO, 70% DMSO and 80% DMSO) and placed into an orbital shaking incubator at 37°C and 100 rpm. 1 mL samples were taken at time intervals of 1, 2, 3, 7, 10, 14, 17, 21, 24, 29, 31, 36, 38 and 40 days and replaced with the same volume of release media. The cumulative percentage of PTV released into each release media is plotted as a function of time to generate the PTV release profile under different release media. Drug stability under different release media such as (PBS, dH_2O, and DMSO) was obtained to understand whether PTV was stable under different release media.

3.3.2.8 Statistical Analysis

The statistical analysis was conducted using GraphPad Prism version 9 and Microsoft Excel 2016. The mean, SD and %RSD were calculated. The two-way analysis of variance (ANOVA) was performed for multiple comparisons, followed by post-hoc comparisons of means using Tukey's Honestly Significance Difference test. A significance level of $p < 0.05$ was assumed significant for all analyses. In addition, a 2-sample t-test was used to determine statistical significance between two values at the same time point, with p values less than 0.05 assumed significant.

3.4 Results and discussion

3.4.1 HPLC analysis

The PTV standard curve is shown in Figure 3.1 at seven different concentrations determined by HPLC. The HPLC area under the curve (AUC) and PTV concentrations had an excellent correlation, with R^2 values at 0.9999 ranging from 4 to 100 g/ml. The high R^2 value indicates a strong linear relationship between the PTV concentrations and the AUC, confirming the accuracy and reliability of the HPLC method for PTV quantification in the samples.

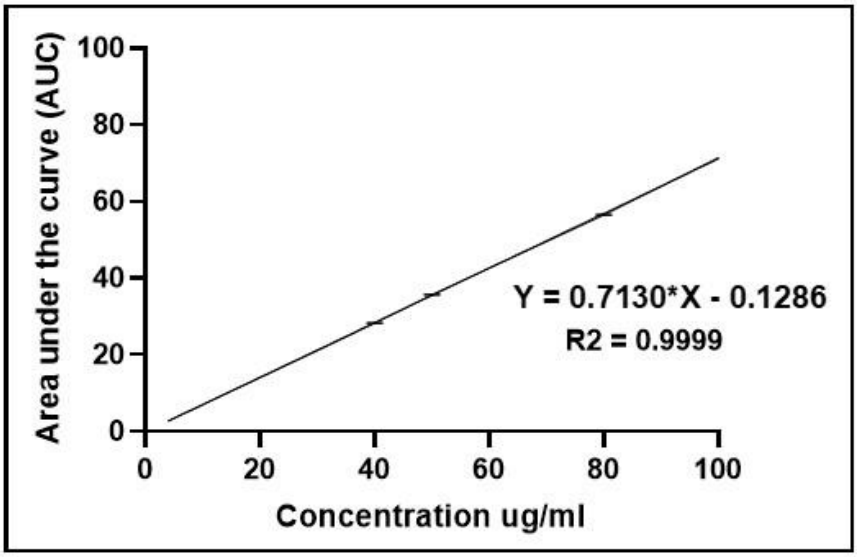

Figure 3. 1 Standard Curve of PTV using HPLC (n= 3).

3.4.2 Rheological measurements

As described previously in chapter 2, the melt viscosity of the polymer is affected by the presence of additives, drugs, drug loading and polymers. The melt viscosity and processing temperature of PLGA may change when PTV is incorporated. Hence, it is crucial to understand how drugs and plasticisers influence polymer melt viscosity and extrudability. Therefore, melt rheology of the selected drug PTV at different loadings (10, 20, 30, 40 and 50% w/w) mixed with each PLGA polymer (5002, 5004, 5010, 7507) was investigated (Figure 3.2). The ideal viscosity of the melt for extrusion has been reported to be in the range of 10^3-10^4 Pa.s. (Gupta et al., 2016). Therefore, those formulations with a melt viscosity within this range at temperatures below 110^{o}C will be considered suitable for moulding and extrusion.

Figure 3.2A shows that only the 10% PTV, when mixed with PLGA5002, achieved a melt viscosity range of 10^3-10^4 Pa.s. within an acceptable temperature range of 74-107^{o}C. The 20, 30, 40 and 50% w/w PTV with PLGA 5002 required temperature ranges of 94-123^{o}C, 100-132^{o}C, 118-147^{o}C and 140-164^{o}C, respectively, to achieve melt viscosities in the range 10^3-10^4 Pa.s. (Figure 3.2A), which is extremely high for our moulding process. Figures 3.2B, 3.2C and 3.2D show that all PTV loadings with PLGA 5004, 5010 and 7507 required temperatures greater than 110^{o}C to achieve melt viscosities in the range of 10^3-10^4 Pa.s. Figure 3.2F demonstrates that PLGA5004, when mixed with 10, 20, 30, 40 and 50% w/w PTV, achieved the melt viscosity range of 10^3-10^4 Pa.s between 116-147^{o}C, 120-155^{o}C, 124-161^{o}C, 138-167^{o}C and 145-172^{o}C, respectively. For PLGA 5010 the temperature range required was 164-192^{o}C, 149-182^{o}C, 148-168^{o}C, 145-172^{o}C and 144-165^{o}C, respectively (Figure 3.2G) and for PLGA7507 they were 141-169^{o}C, 150-173^{o}C, 145-172^{o}C, 155-

178^{o}C and 162-182^{o}C (Figure 3.2H). It was observed that the presence of a greater PTV loading increased the viscosity (Figure 3.2A to D). Table 3.3 summarises selected mixtures from PTV-PLGA mixtures; 10, 20, 30, 40 and 50% (w/w) with different PLGA polymers (5002, 5004, 5010 & 7507) appropriate for moulding and their processing temperatures. Based on the above melt viscosity curves, it is expected that they would require processing temperatures greater than 110^{o}C, which is not suitable for the IM method. For this reason, a plasticiser was needed to minimise melt viscosities and enable processing temperatures. Therefore, melt viscosities of selected PLGA 5004 mixed with 30% w/w PTV were investigated with the addition of different percentages of plasticisers P188 (1, 5, 10 & 20) (w/w) (Figure 3.3). Adding different percentages of P188 Plasticiser were proven to lower their melt viscosities (Figure 3.3). Figure 3.3 shows that adding 1, 5 & 10 % w/w P188 plasticiser to 30% w/w PTV and PLGA 5004 achieved 10^{3}-10^{4} Pa.s viscosity, but within a high-temperature range of 121-154^{o}C, 116-145^{o}C and 100-132^{o}C, respectively and only adding 20% w/w P188 plasticiser to 30% w/w PTV and PLGA 5004 achieved 10^{3}-10^{4} Pa.s viscosity within an acceptable temperature range of 82-110^{o}C.

It was concluded that only adding the highest concentration of plasticiser P188 20% w/w to a mixture of 30%PTV with PLGA 5004 would enable moulding at temperatures below 110^{o}C. Table 3.4 summarises selected mixtures from PTV-PLGA-P188 mixtures; 30% PTV w/w with PLGA5004 and different percentages of plasticiser P188 (1, 5, 10, 20%) appropriate for moulding and their processing temperatures.

The percentage of plasticiser P188 (20% w/w) was selected to obtain the exact composition of the moulded formulation of the mixture PTV with PLGA 5004. Thus, the effects of drug load 10, 20, 30, 40 and 50% w/w PTV with the same type of Polymer PLGA5004 and the same percentage of P188 (20% w/w) on viscosity were investigated for screening mixtures and ability to be extruded and moulded (Figure 3.4). Viscosity measurement revealed that only drug loads 10, 20 and 30% w/w PTV when mixed with PLGA 5004 and 20% w/w P188 plasticiser, achieved 10^3-10^4 Pa.s viscosity below 110^{o}C (Figure 3.4). In comparison, higher drug loads of 40 & 50% w/w PTV when mixed with PLGA5004 and 20% w/w P188 plasticiser achieved 10^3-10^4 Pa.s viscosity but within a high-temperature range of 114^{o}C & 112^{o}C, respectively (Figure 3.4). It is demonstrated that a higher drug load can be added to the mixture PLGA5004 with selected plasticiser 20% P188 is 30% w/w PTV. Table 3.5 summarises selected mixtures from PTV-PLGA-P188 mixtures; 10, 20, 30, 40 & 50% w/w PTV with PLGA5004 and 20% P188 appropriate for moulding and their processing temperatures.

Table 3. 3 Selected mixture from PTV-PLGA; 10, 20, 30, 40 and 50% (w/w) with different PLGA polymers (5002, 5004, 5010 & 7507) can be moulded at optimum viscosity according to the rheology studies.

Formulations	Temperature°C at Viscosity 10^3 to 10^4 Pa.s
10%PTV+5002	74-107

Table 3. 4 Selected mixture from PTV-PLGA-P188; 30% PTV w/w with PLGA5004 and different percentages of plasticiser P188 (1, 5, 10, 20%) can be moulded at optimum viscosity according to the rheology studies.

Formulations	Temperature°C at Viscosity 10^3 to 10^4 Pa.s
30%PTV+5004+20%P188	82-110

Table 3. 5 Selected mixture from PTV-PLGA-P188; 10, 20, 30, 40 and 50% (w/w) PTV with PLGA5004 and 20% P188 can be moulded at optimum viscosity according to the rheology studies.

Formulations	Temperature°C at Viscosity 10^3 to 10^4 Pa.s
10%PTV+5004+20%P188	77-105
20%PTV+5004+20%P188	79-110
30%PTV+5004+20%P188	81-110

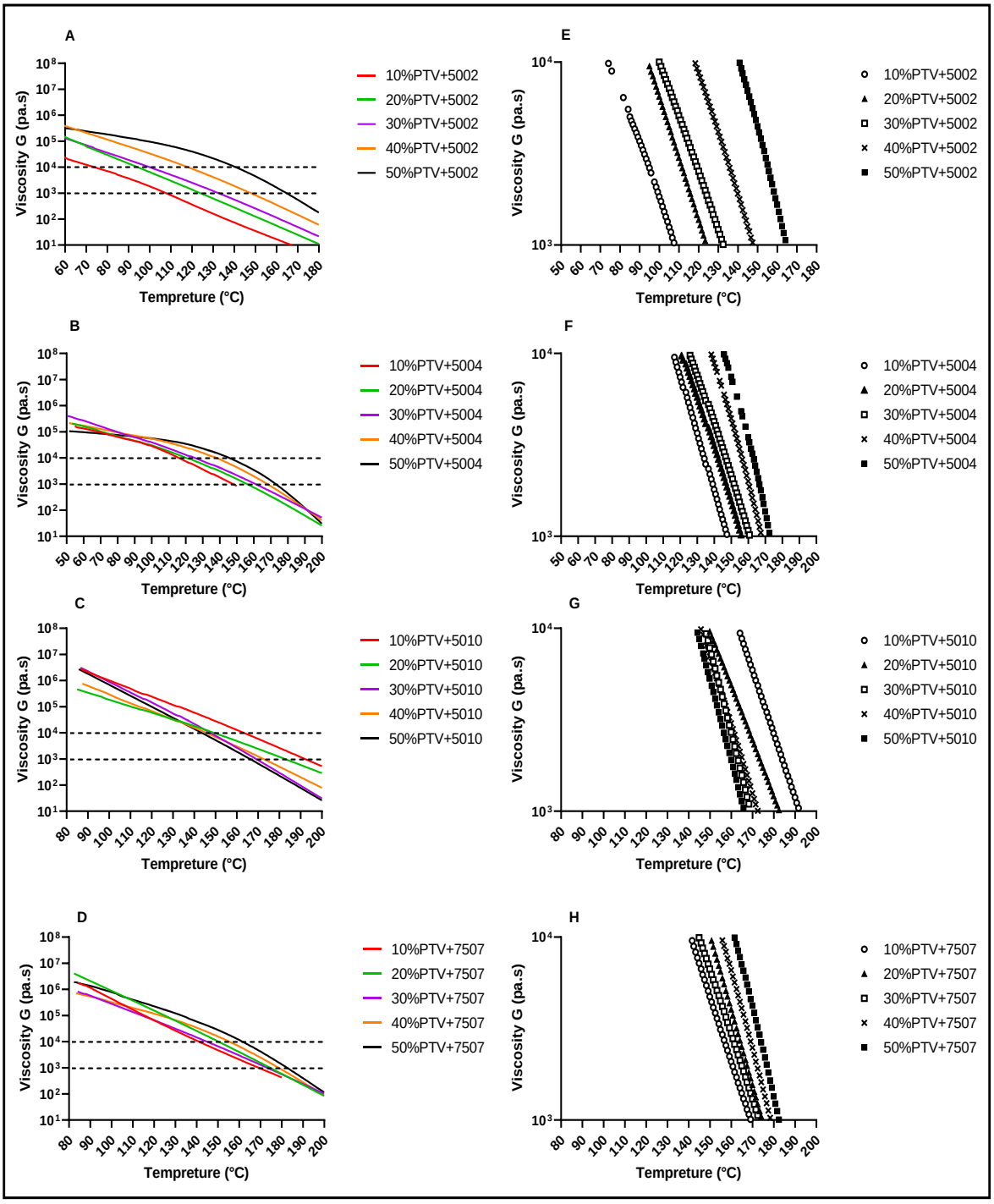

Figure 3. 2 Rheology of different PTV-PLGA mixtures; 10, 20, 30, 40 and 50% (w/w) PTV with different PLGA polymers (5002, 5004, 5010 & 7507) (A, B, C & D). The temperature sweep was performed at 60-200°C. Rheology results were described at the ideal viscosity range for extrusion (10^3 to 10^4 Pa.s) (E, F, G & H).

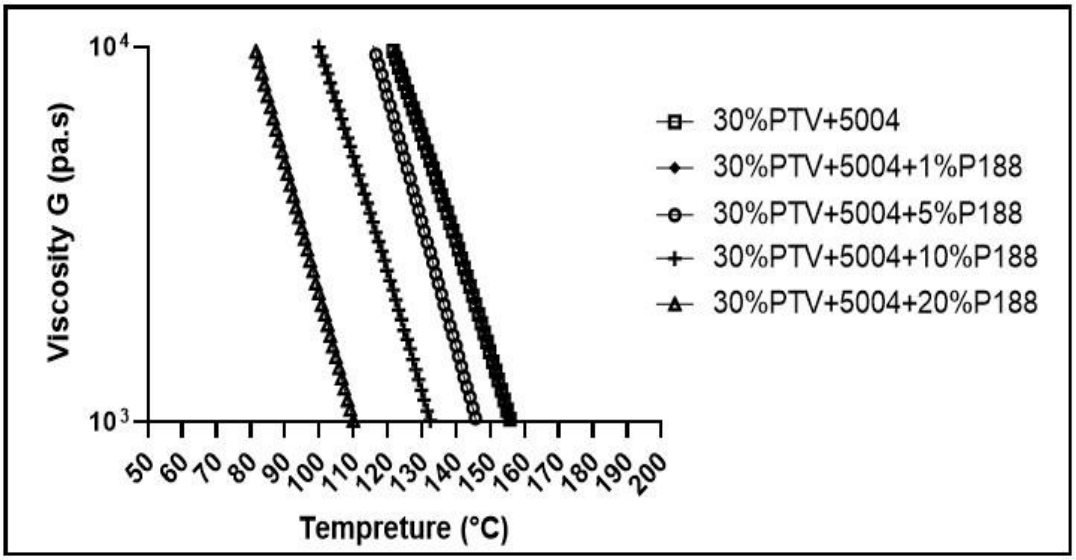

Figure 3. 3 Rheology of different PTV-PLGA-P188 mixtures; 30% PTV w/w with PLGA5004 and different percentages of plasticiser P188 (1, 5, 10, 20%). The temperature sweep was performed at 60-200^{o}C. Rheology results were described at the ideal viscosity range for extrusion (10^{3} to 10^{4} Pa.s).

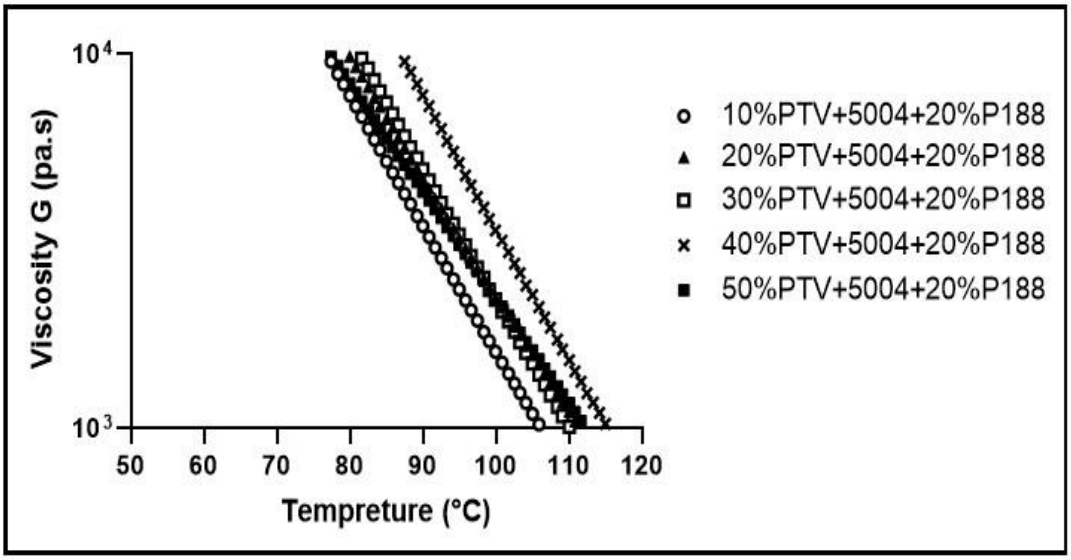

Figure 3. 4 Rheology of different PTV-PLGA mixtures; 10, 20, 30, 40 and 50% (w/w) PTV with PLGA5004 and 20% P188. The temperature sweep was performed at 60-200^{o}C. Rheology results were described at the ideal viscosity range for extrusion (10^{3} to 10^{4} Pa.s).

3.4.3 Physical characterisation of the implants

3.4.3.1 Determination of the lengths, diameters and weights of PTV-loaded PLGA implants

The physical characteristics of PTV-PLGA implants manufactured by IM and HME were evaluated for their dimensions, weight, and content analyses. The results are summarised in Tables 3.6 and 3.7. All IM and HME PTV-PLGA implants had a ±10% deviation in dimensions (diameter and length) and weight, indicating that the implants were consistent.

The two-way ANOVA with Tukey's post-hoc tests revealed no significant difference in length, diameter and weight of the 10%, 20%, and 30% PTV-PLGA implants between the two groups (IM and HME) ($p > 0.05$).

In conclusion, the physical characterisation of the PTV-PLGA implants revealed that the manufacturing process by IM and HME was reliable, and the implants were uniform in relation to dimensions and weight.

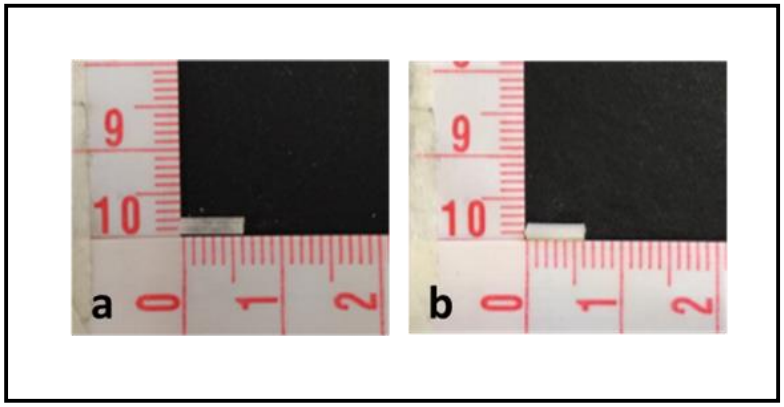

Figure 3. 5 Representative images of single-layered PTV-PLGA-P188 implant 2X6mm formulated by IM (a), single-layered PTV-PLGA-P188 implant 2X6mm formulated by HME (b).

Table 3. 6 Physical Appearance of PTV-PLGA implants formulated by IM.

PTV-PLGA IM implants			
	10%PTV PLGA 5004 20%P188	**20%PTV** PLGA 5004 20%P188	**30%PTV** PLGA 5004 20%P188
Length (mm) Mean±SD (n=10)	6.0 ± 0.1	6.0 ± 0.1	6.0± 0.1
%RSD	2%	1.6%	2.4%
Diameter (mm) Mean±SD (n=10)	2.0± 0.0	2.0± 0.1	2.0± 0.0
%RSD	2.4%	4%	2.5%
Weight (mm) Mean±SD (n=10)	26.1± 0.7	26.1 ± 0.7	26.4±0.2
%RSD	2.7%	2.7%	0.85%

S.D is the standard deviation, %RSD is the relative standard deviation

Table 3. 7 Physical Appearance of PTV-PLGA implants formulated by HME.

PTV-PLGA HME implants			
	10%PTV PLGA 5004 20%P188	**20%PTV** PLGA 5004 20%P188	**30%PTV** PLGA 5004 20%P188
Length (mm) Mean±SD (n=10)	6.0 ± 0.1	6.0 ± 0.1	6.0± 0.1
%RSD	1.6%	1.4%	1.7%
Diameter (mm) Mean±SD (n=10)	2.0± 0.1	2.0± 0.1	2.0± 0.1
%RSD	4%	4%	4%
Weight (mm) Mean±SD (n=10)	26.4± 0.1	26.6 ± 0.1	26.9±0.1
%RSD	0.3%	0.3%	0.5%

S.D is the standard deviation, %RSD is the relative standard deviation

3.4.4 Physiochemical characterisation of the implants

3.4.4.1 Determination of drug content

The drug content of the PTV-PLGA implants manufactured by IM and HME techniques was analysed, and the results are presented in Table 3.8. The drug content of the implants manufactured by IM was determined to be 62%, 67%, and 77.15% for the 10%, 20%, and 30% PTV-PLGA implants, respectively. For the HME technique, the 10%, 20%, and 30% PTV-PLGA implants' drug content was determined to be 91%, 82%, and 82.3%, respectively. The %RSD values for each drug content were also determined. For the IM technique, the %RSD values for the 10%, 20%, and 30% PTV-PLGA implants were 6.2%, 12.2%, and 10.1%, respectively, while for the HME technique, the %RSD values were 1.4%, 0.9%, and 0.4%, respectively. Results indicate that the drug content of PTV-PLGA implants manufactured by HME was higher than PTV-PLGA implants manufactured by IM for all three PTV loadings. This can be attributed to the fact that the HME technique permits better mixing and distribution of the drug in the polymer matrix (Patil et al., 2016) due to the high shear forces of the twin screws (McConville et al., 2015), resulting in a more drug concentration. In contrast, the IM technique may result in an uneven drug distribution within the implant due to no shear in the barrel (McConville et al., 2015), resulting in a lower drug concentration.

The %RSD values for the HME implants were lower than those for the IM implants (Table 3.8). This indicates that the drug content of the HME-produced implants is more consistent and reproducible than the IM-produced implants. This can be due to the fact that the HME technique permits more precise control over the processing parameters (Major & McConville, 2015), resulting in more consistent drug content.

A separate t-test was used for each drug load (10%, 20%, 30%) to compare the drug content between the IM and HME implants. The results suggest that there is a statistically significant difference in drug content for the 10% and 20% PTV-PLGA implants between the two types of implants ($p < 0.05$). However, for the 30% PTV-loaded implants, the difference in drug content between the two types of implants was not statistically significant ($p > 0.05$).

Overall, the results indicate that the HME manufacturing technique may be preferable to the IM technique for achieving higher and more consistent drug content in PLGA implants.

Table 3. 8 PTV content, RSD and %RSD values for each of the 10, 20 and 30% PTV-loaded PLGA implants manufactured by IM and HME (n=6).

PTV-PLGA IM implants			
	10%PTV	20%PTV	30%PTV
Drug content (%) (n=6)	62	67	77.15
RSD	10.07	8.36	8
%RSD	16.2	12.2	10.1
PTV-PLGA HME implants			
	10%PTV	20%PTV	30%PTV
Drug content (%) (n=6)	91	82	82.3
RSD	1.3	0.7	0.3
%RSD	1.4	0.9	0.4

3.4.4.2 Crystallinity studies using X-ray Powder Diffraction (XRD)

X-ray analysis was performed to verify the physical state of PTV in the IM and HME implants. The XRD diffractogram of pure PTV, PLGA, P188, physical mixture, IM implant and HME implant are illustrated in Figure 3.6.

The XRD pattern revealed that pure PTV was crystalline, indicated by strong intensity peaks at 14.28°, 21.06°, 21.86° and 23.95° 2θ values (Figure 3.6a), which correspond to PTV (Pimple et al., 2022). Those peaks were also found in the diffraction pattern of the physical mixture (Figure 3.6d). The XRD pattern of the PLGA indicated the amorphous state of this polymer (Figure 3.6b) and was reported in the literature (Sepehri et al., 2014). The XRD of IM and HME implants (Figures 3.6e & 3.6f) displayed halo-patterns and small peaks at 21.06° and 25°. A reduction in the number of peaks and their intensity indicates a change in the crystallinity of the drug due to heating during the manufacturing processes of IM and HME. It can be hypothesized that the majority of the PTV is dispersed in an amorphous form within the PLGA matrix of the IM and HME implants, while a small amount remains in its crystalline form. Amorphous solids have high molecular mobility compared to the crystalline form, which improves solubility and dissolution rate (Pimple et al., 2022), consequently improving drug release. However, amorphous drug forms are high-energy solids that tend to recrystallise, which can impact the shelf-life of a product and should be evaluated by an accelerated stability analysis (Grohganz et al., 2013).

These findings suggest that the moulding and extrusion process used to produce PTV-PLGA implants can significantly impact the physical properties of the PTV in the implant.

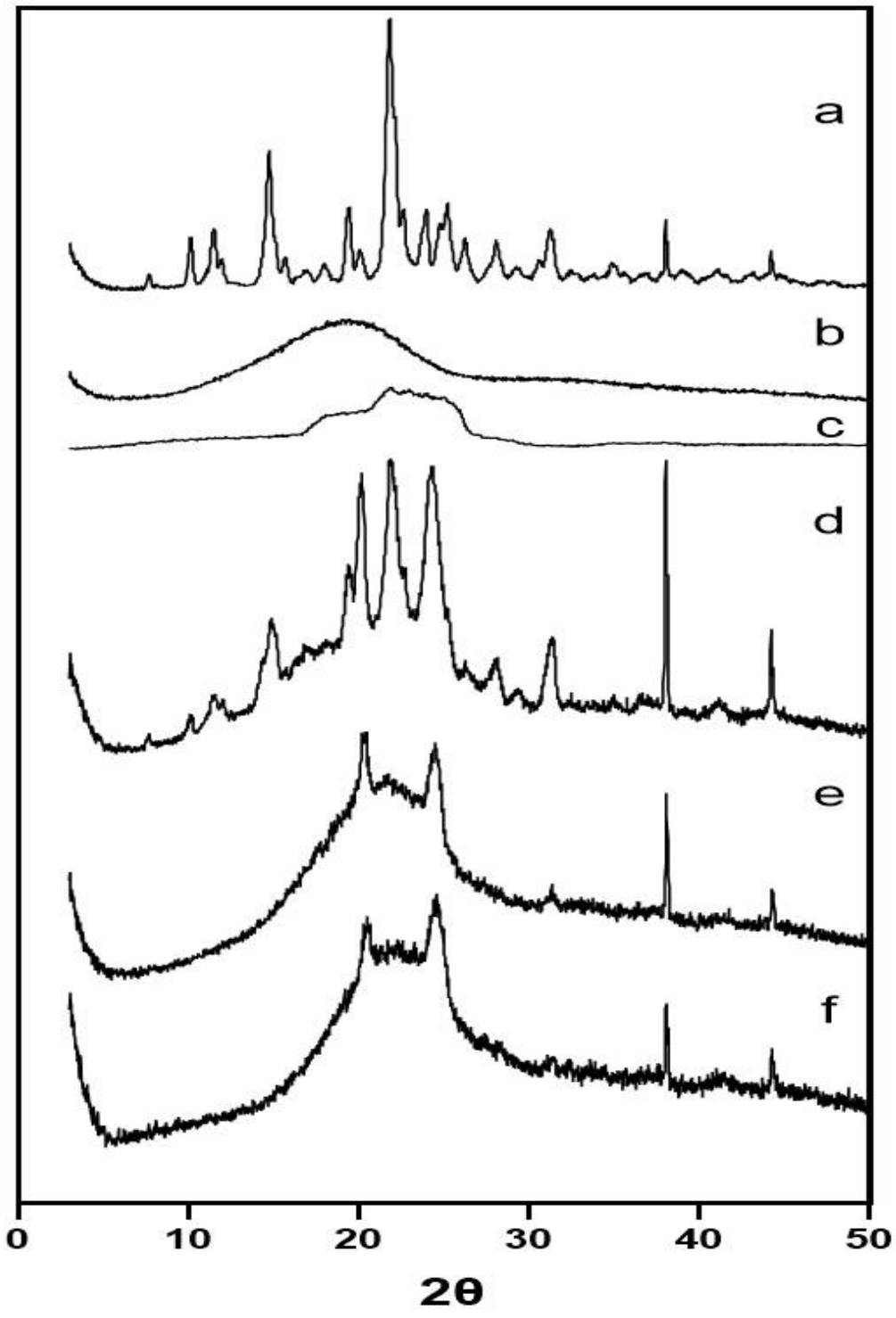

Figure 3. 6 X-ray powder diffraction spectra, pure PTV (a), PLGA (b), P188 (c), Physical mixture before extrusion (d), powdered implants of IM (e) and HME (f).

3.4.4.3 Thermal stability studies using Differential Scanning Calorimetry (DSC)

DSC was conducted to investigate the physicochemical properties of the pure materials and implants manufactured by both IM and HME. The physical form of PTV within the IM and HME implants was investigated using DSC. Figure 3.7 displays DSC thermographs for PTV, PLGA, P188 and PTV-PLGA implants (IM and HME). The PTV (Figure 3.7a) exhibited a sharp endothermic peak at 143°C corresponding to its melting point and attributed to its crystalline nature. Pure PLGA shows an endothermic peak of 43.6°C (Figure 3.7b), which corresponds to the Tg of the polymeric material (Benhabbour et al., 2019; Tseng et al., 2020). The thermogram of Kolliphor® P188 (Figure 3.7c) revealed a single, sharp endotherm peak between 50 and 55°C. This peak is typical of the melting point of poloxamer and is similar to previously reported results (Dhore et al., 2017; Moghimi et al., 2004). In the thermograms of the PTV-PLGA implants (IM and HME), the characteristic endothermic peak corresponding to the melting of the drug was not detected (Figures 3.7d & 3.7e). This suggests that the PTV drug was incorporated in an amorphous form and was molecularly dispersed in the polymeric matrices and indicates that the drug dissolved within the molten polymer during the DSC analysis (Cevher et al., 2007; Kamel & Abbas, 2018). Based on the XRD and DSC data, it is assumed that partial dissolution of PTV into the PLGA occurred during IM and HME manufacture of the implants, with the remainder dissolving in the PLGA during DSC analysis. This suggests that the PTV dissolved in the PLGA during manufacture is below saturation, and the amorphous/dissolved PTV should remain stable upon storage.

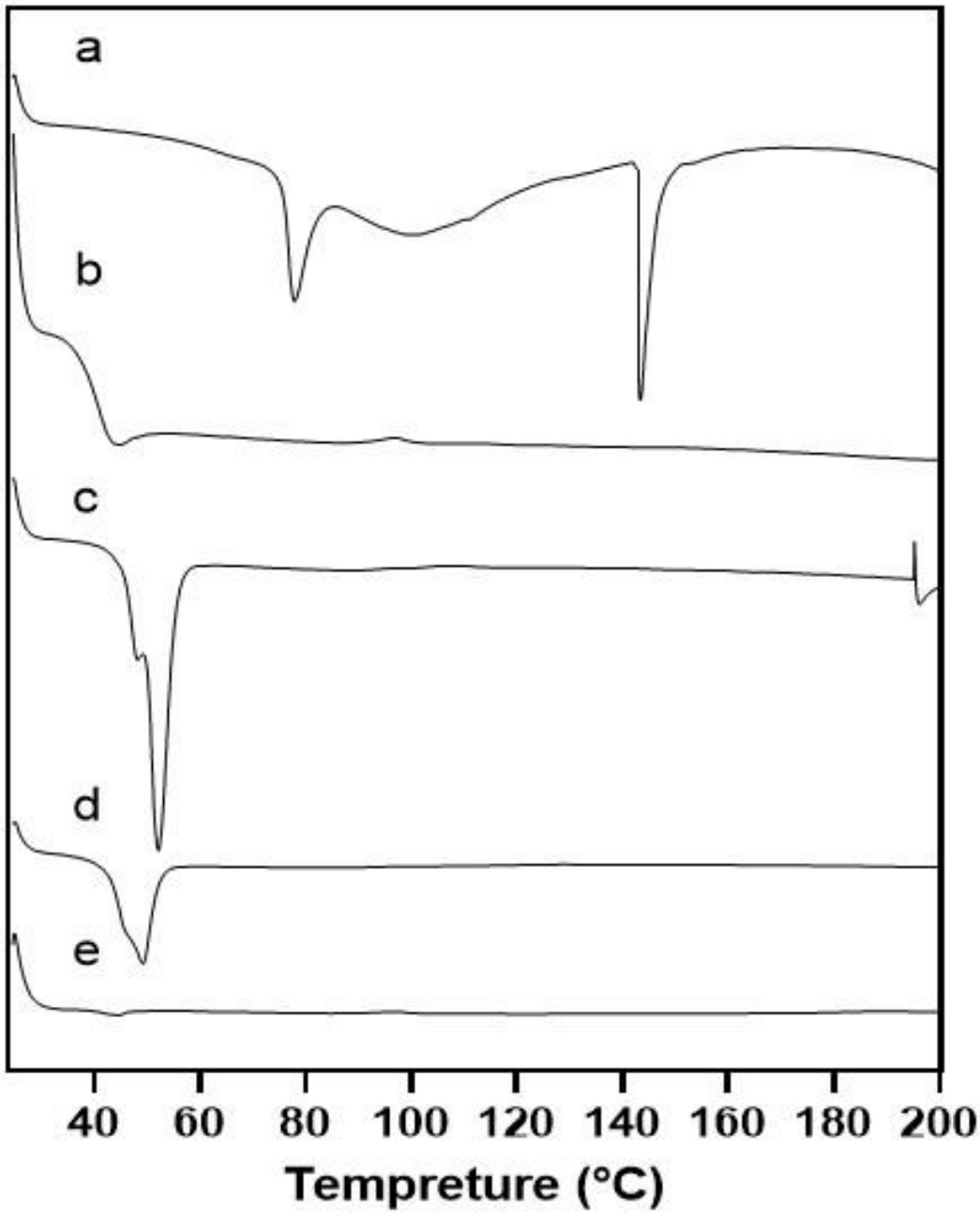

Figure 3. 7 DSC thermograms of Pure PTV (a), PLGA (b), P188 (c) and PTV-PLGA for two implants; IM implant (d) and HME implant (e).

3.4.4.4 Determination of the Physical State of PTV in the IM implants and HME implants by using Raman

Confocal Raman was used to characterise the API on the entire surface of the IM and HME implants. Single point spectra of the pure drug and the IM and HME implants are presented in Figure 3.8. In the drug spectra, high-intensity peaks were detected in the fingerprint region at 1400 cm^{-1}, confirming that PTV was in crystalline form (Figure 3.8D). In contrast, the Raman spectra of the IM and HME implants (Figures 3.8A & 3.8B) showed no PTV characteristic peaks observed, and the drug was in an amorphous state in agreement with XRD and DSC data. The results suggest that the PTV was in a crystal state and transferred to amorphous during the IM and HME process.

IM and HME involve heating and melting steps, and the API was likely dissolved in the molten PLGA.

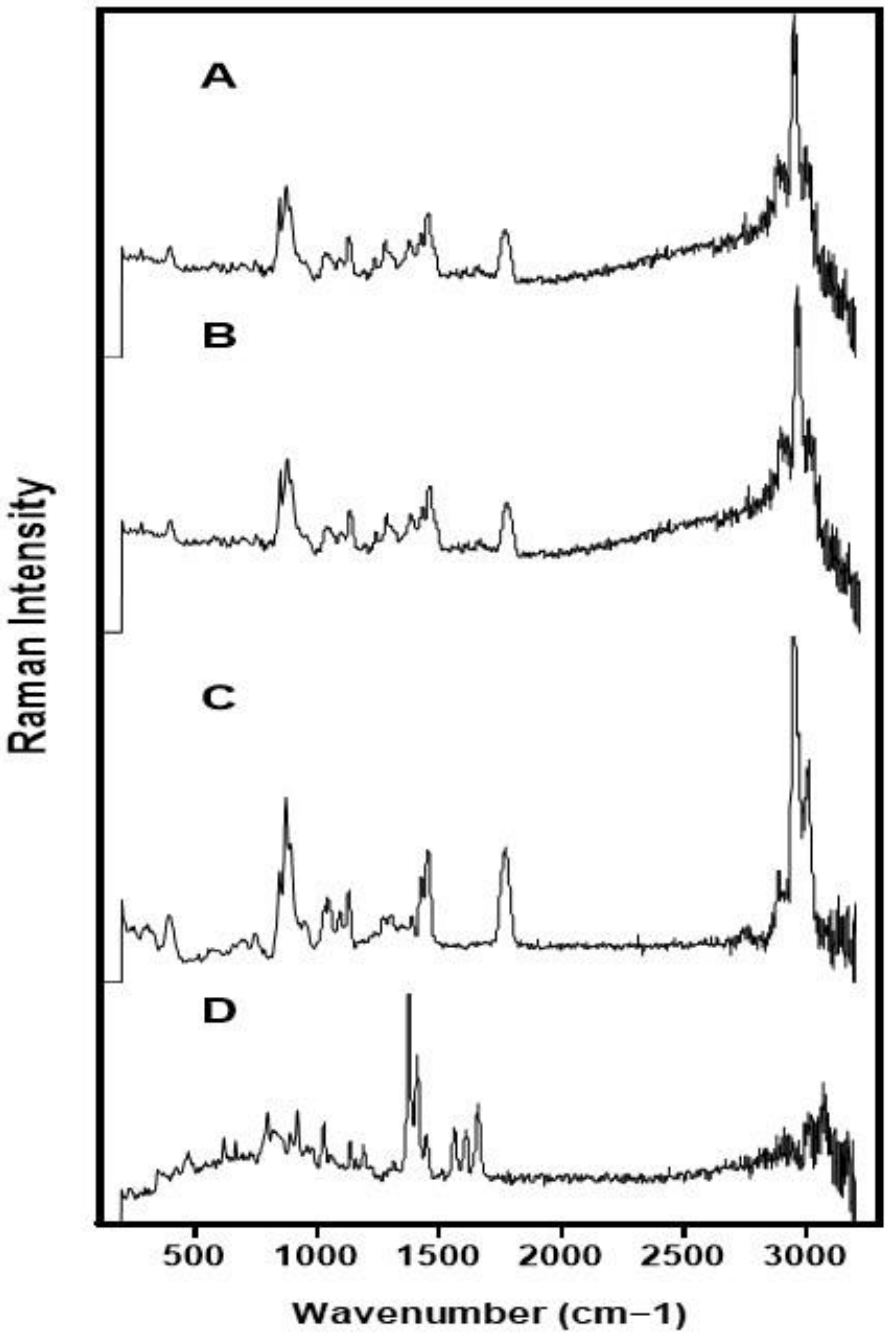

Figure 3. 8 Raman spectrogram of the IM implant (A), HME implant (B), PLGA (C) and API (PTV) (D).

3.4.4.5 Drug distribution in IM implant and HME implant by Raman mapping

Raman microscopy was used to scan the surface of the IM and HME implants. At each mapped point of the implant, reference PTV spectra (Figure 3.8D) were entered into the software and compared to the implant spectra obtained. PTV was homogenously distributed across the entire surface of the HME implant (Figure 3.9f), and the distribution of the PTV (red) was determined by Raman mapping (Figure 3.9d). In contrast, the PTV distribution was heterogeneous throughout the entire mapped area of the IM implants (Figure 3.9e), and the distribution of the PTV (blue) was determined by Raman mapping (Figure 3.9c). The drug-related peak is detected throughout the entire mapped area. However, its intensity varies. The IM and HME implants appear to have both drug-poor and drug-rich "hot spots" at the micron scale (Figures 3.9e & 3.9f).

These results can be explained by assuming that the high shear mixing of the twin-screw extruder completely dispersed the PTV within the PLGA of the HME implants. This has been reported previously (McConville et al., 2015). However, in the case of IM implants, the PTV distribution was not entirely homogeneous, and large particles were observed on the implant surface (as shown in Figure 3.9a) due to the lack of shear forces and mixing during IM.

These results conclude that PTV-PLGA HME implants were preferable implants than PTV-PLGA IM implants due to their homogenous drug distribution. As reported previously, non-homogenous drug distribution within the implant has the potential to impact the drug release kinetics (Bode et al., 2019).

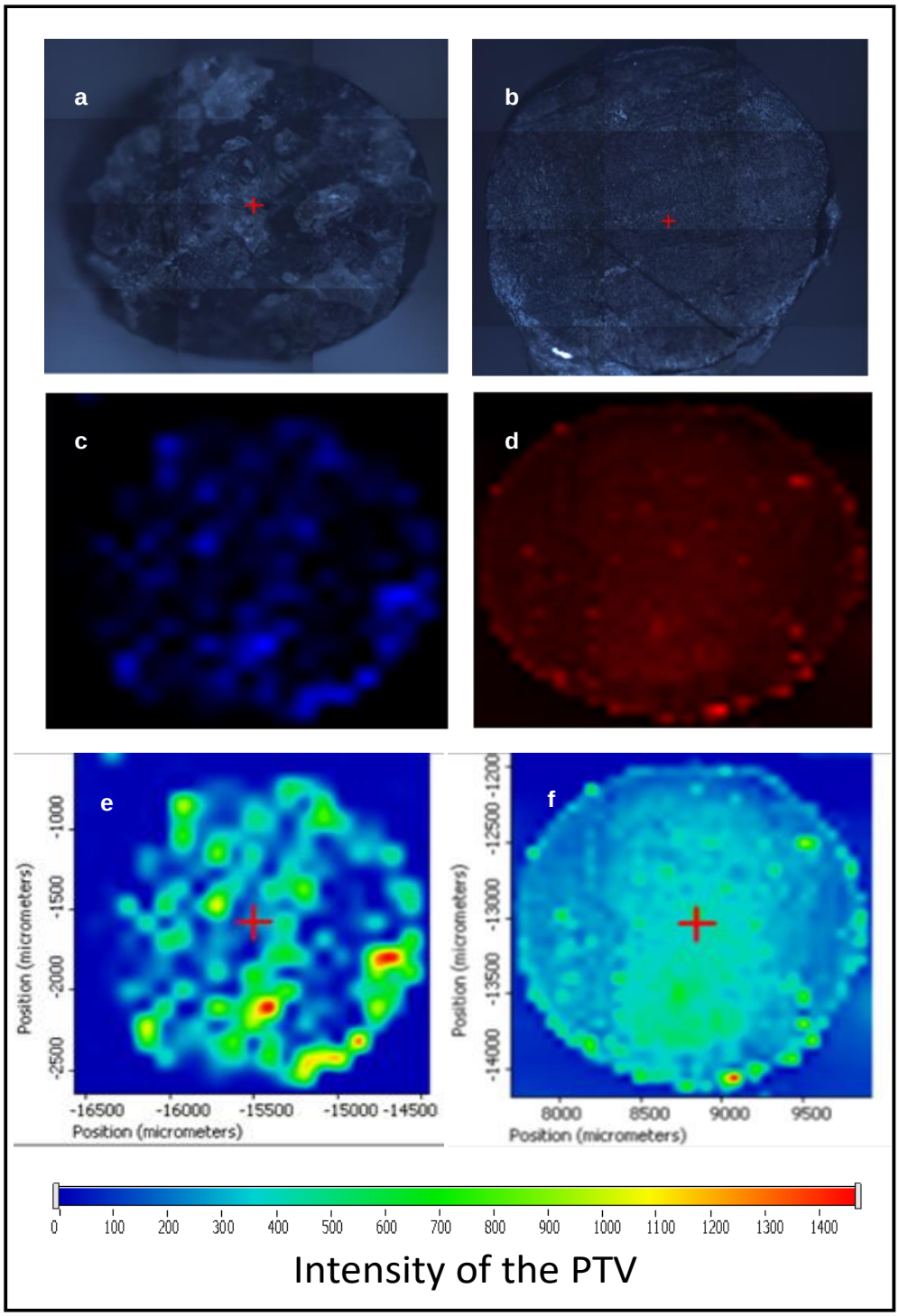

Figure 3. 9 Optical microscopy images of the investigated extrudates entire surface PTV-PLGA implants including IM implant (a) and HME implant (b), Raman mapping of IM implant (c), blue areas = PTV distribution in IM implant, Raman mapping of HME implant (d), red areas= PTV distribution in HME implant, Drug intensity on IM implant (e) and in HME implant (f).

3.4.5 In vitro dissolution studies

3.4.5.1 Solubility experiments

When selecting release media volumes, the solubility of PTV needs to be considered to ensure sink conditions throughout the release study. Therefore, before performing the drug release studies, the solubility of PTV in different dissolution media (PBS, H_2O, 50%DMSO, 70%DMSO & 80%DMSO) was determined (Figure 3.10). The solubility of PTV was found to be the highest (42.27 ± 0.28 mg/mL) in 80% DMSO, followed by 70% (18.42 ± 0.21 mg/mL) and 50% (6.76 ± 0.07 mg/mL) DMSO, while the solubility was lowest in PBS (2.33 ± 0.02 mg/mL) and dH_2O (3.27 ± 0.15 mg/mL).

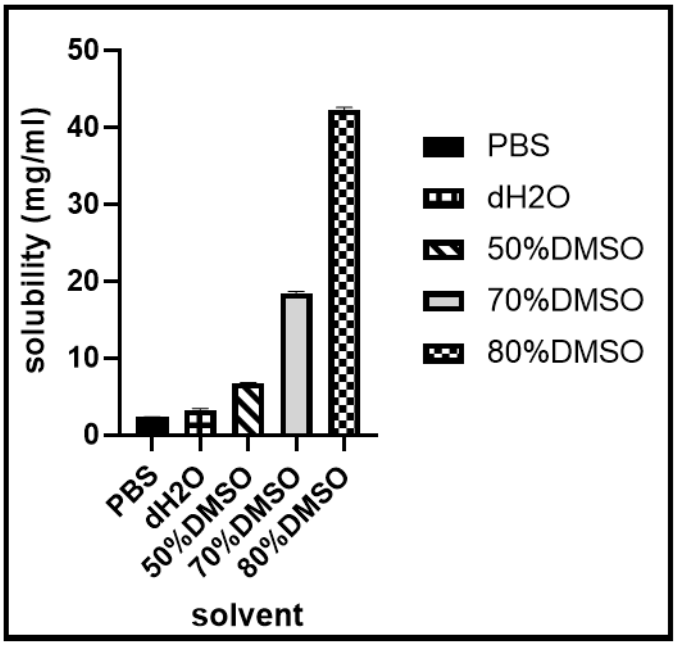

Figure 3. 10 Solubility of PTV in PBS, dH_2O, 50%DMSO, 70%DMSO and 80%DMSO (means ± S.D., n=3)

3.4.5.2 In vitro stability of PTV in the different release media

The stability of PTV in a range of in vitro release solvents (PBS, dH_2O, DMSO) was investigated (Figure 3.11). It was important to identify a suitable solvent in which PTV would remain stable for the entirety of the release study. PTV was found to be stable in all solvents over 40 days under all conditions tested (room temperature, cold room and incubator (Figure 3.11). In this study, PTV was considered stable if it retained 90% of its original concentration.

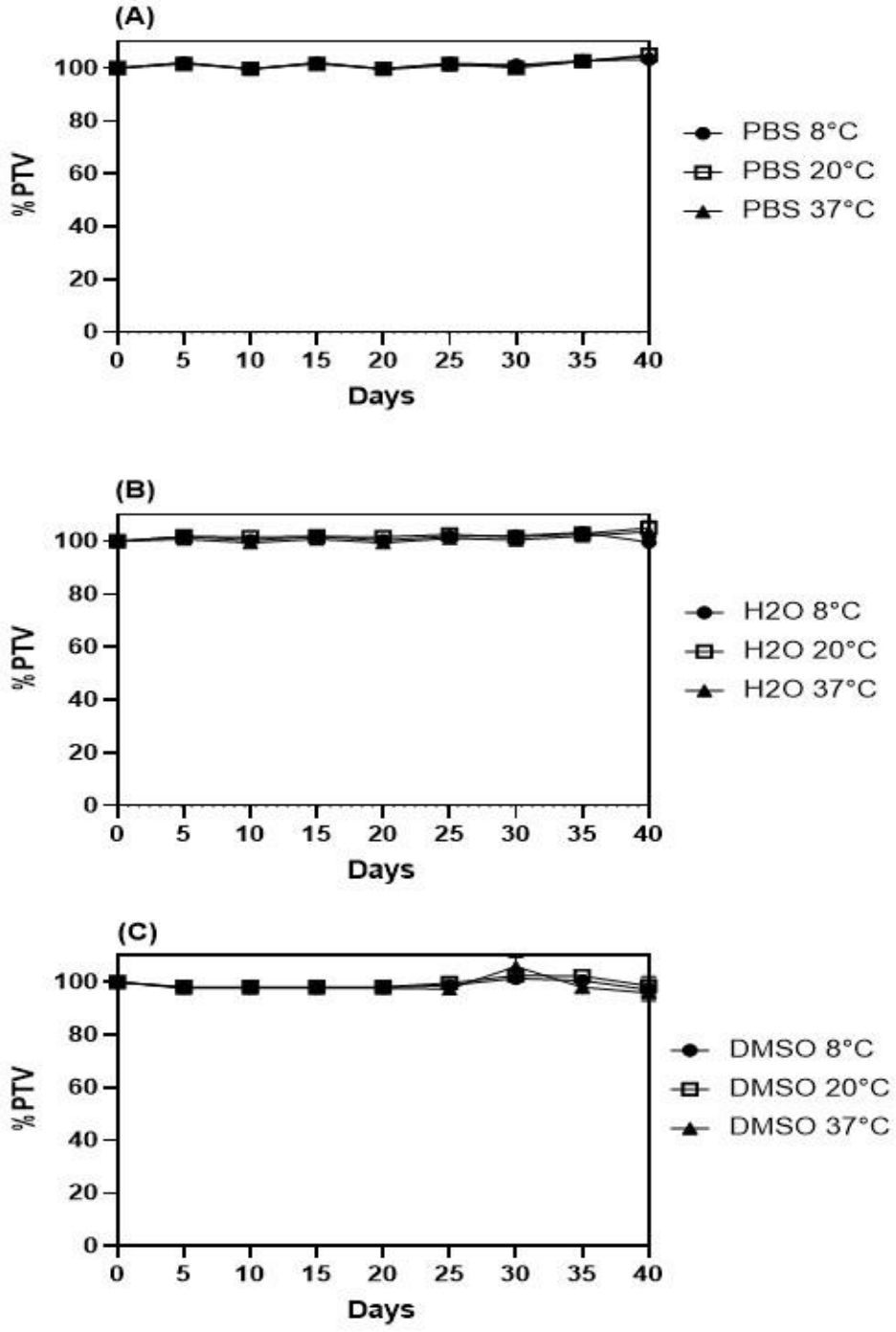

Figure 3. 11 Stability of PTV in PBS (A), H_2O (B) and DMSO (C) over 40 days at 8°C, 20°C and 37°C (means ± S.D., n=3).

3.4.6 In vitro drug release studies

3.4.6.1 Effect of manufacturing procedure on the release of PTV from PLGA implant

The effect of the manufacturing procedure on PTV release from PLGA 5004 implants containing 10% PTV was investigated. The drug release from the PTV-PLGA implants, manufactured using IM and HME techniques, was performed in PBS (pH 7.4) at 37°C over a period of 40 days, and the results are presented in Figure 3.12. The drug release data were analysed using a two-way ANOVA with Tukey's post-hoc tests. The results indicated that the drug release was significantly lower for the HME implants compared to the IM implants ($p < 0.05$) at most time points. This can be attributed to the strong shear forces of the HME process, which result in a more densely packed implant matrix evidenced by the Raman image (Figure 3.9b) and slower uptake of the dissolution medium, resulting in slower drug release. In contrast, the release from IM implants is relatively rapid during the early stage of drug release due to the lower shear forces of the IM process, which increase the porosity of the implants, allowing the release media to imbibe and the drug to diffuse out at a faster rate, subsequently enhancing degradation and overall release rate. As reported by Crowley et al. (2004) and McConville et al. (2015), the drug release rates from dosage forms prepared using HME are slower than those prepared using IM due to lower porosity and higher shear forces. The findings of this study are consistent with those of earlier research (Crowley et al., 2004; McConville et al., 2015). The drug release performance of the HME implant shows a triphasic release pattern, which is typical of PLGA implants. The initial burst release occurs in the first 24 hours, where 22.00% of the drug is released. This is followed by a lag phase where the release rate is slower due to the polymer matrix slowly degrading, leading to 41.39% release

on day 7 and 46.54% release on day 21. The final phase is the sustained release phase, where the remaining drug is gradually released over time, with 94.93% release at day 36 and 99.55% release at day 40. In contrast, the release of PTV from IM implants showed a biphasic release profile over the 7 days, with a rapid burst release 66% observed on day 1, followed by a slower release rate over a period of 7 days 98%. This indicates that PTV was released initially due to diffusion, followed by matrix degradation and that the IM implants release the drug more rapidly within the first 7 days compared to the HME implants. The initial drug release at day 1 was 66.19% for the IM implant and 22.00% for the HME implant. This significant difference ($p < 0.05$) in the initial burst release can be due to more drug on the surface of the IM being released immediately due to the absence of shear force and mixing during manufacturing. In contrast, the HME implant has lower drug on the surface as the PTV has been dispersed within the PLGA by the high shear forces of the extrusion process.

The results indicate that the manufacturing technique used can affect the drug release from PLGA implants, with the HME process resulting in a slower and tri-phasic release profile compared to the IM process.

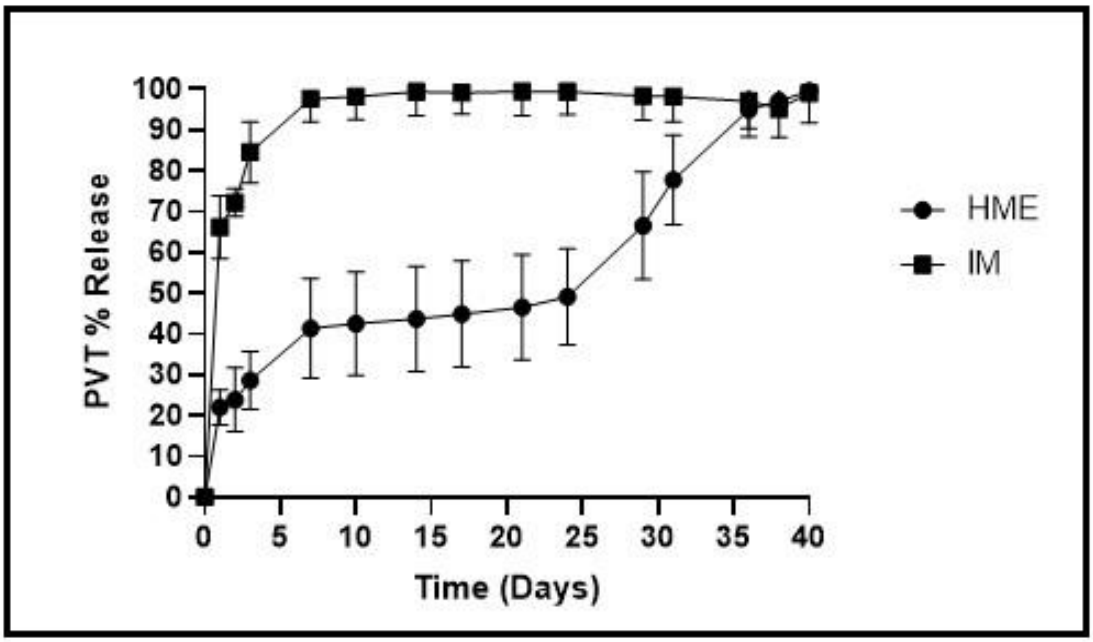

Figure 3. 12 Effect of manufacturing procedure on the release of PTV from PLGA 5004 implants (means ± S.D., n=3) significance found using a two-way ANOVA with a Tukey's post-hoc test, * = P<0.05 ** = P<0.01, *** = P<0.001, **** = P<0.0001.

3.4.6.2 Effect of the various release media on the drug release

Figure 3.13A illustrates the effect of different release media on the release profile of PTV from HME implants. In PBS, the initial burst release was observed on the first day at approximately 22%, followed by a gradual and sustained drug release from the HME implant. By day 7, the drug release increased to 41%. The drug release continued to increase, and on day 24, the drug release was 49.11%, indicating a sustained release pattern. By day 40, the drug release achieved 99.54%, indicating almost complete drug release from the HME implant. The typical release media in PBS stated above showed sustained drug release over 40 days, indicating a long-term drug release (more than a month). In order to accelerate the release rate of PTV from the HME implants, deionised water and an organic solvent (DMSO) with varied compositions (50%, 70%, and 80%) were investigated as release media. These investigations were based on the findings discussed in chapter 2 regarding the effects of different release media on IRN release from HME implants. Thus, it is expected that using dH_2O and DMSO solvents will also accelerate the PTV release rate and provide the desired drug release. A two-way ANOVA with Tukey's post-hoc test was used to compare the drug release between the different release media. The results indicated that the drug release in the medium with 80% DMSO was significantly higher ($p < 0.05$) compared to the release in PBS, dH_2O, and the medium with 50% DMSO at all time points ($p<0.05$). However, the release in the medium with 80% DMSO was not significantly ($p > 0.05$) higher than the release in 70% DMSO medium on days 1, 2, 3, 7, 10, 14 and 17. The drug release in 70% DMSO was significantly higher than PBS and H_2O at all time points ($p<0.05$). There was no significant difference in drug release between the 50% DMSO and PBS or H_2O at most time points ($p<0.05$).

Higher DMSO concentrations result in higher drug release. Therefore, DMSO 80% was selected for the accelerated drug release method as a quality control tool for HME implants. The optimised accelerated release method resulted in a complete release of PTV from the HME implant within one week (Figure 3.13C), as opposed to the real-time release period of 40 days (Figure 3.13B).

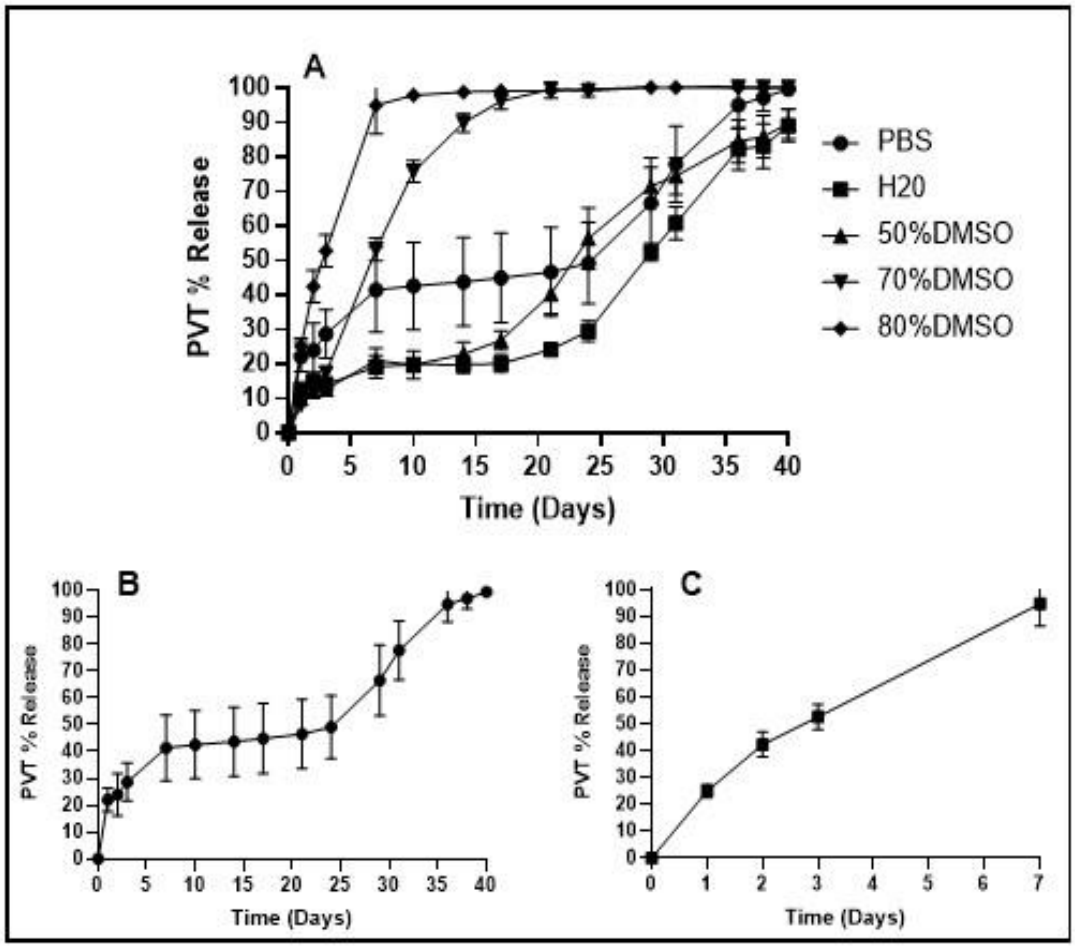

Figure 3. 13 In vitro cumulative release profiles of PTV from HME implants in various release media: dH_2O, 50%DMSO, 70%DMSO and 80%DMSO (A) significance found using a two-way ANOVA with a Tukey's post-hoc test, * = P<0.05 ** = P<0.01, *** = P<0.001, **** = P<0.0001, long-term release profile in PBS (B) and short-term release profile in 80%DMSO (C) (mean±SD; n=3).

3.5 Conclusion

This chapter investigates the effect of IM and HME techniques on the size and weight uniformity, drug content uniformity, drug content, drug distribution, stability, physical state and drug release of PTV-loaded PLGA implants (Table 3.9). The selection of formulation composition and implant manufacturing processes were investigated in the pre-screening step, including the amount of drug, type of PLGA and amount of plasticiser. Based on the rheology results, the formulations; 10%PTV+5002, 10%PTV+5004+20%P188, 20%PTV+5004+20%P188, 30%PTV+5004+20%P188 were appropriate for moulding and extrusion. The resulting IM and HME implants were characterised using various techniques, including HPLC, DSC, XRD, and Raman. The results described in this chapter demonstrate that all PTV-loaded PLGA implants manufactured by IM and HME were consistent in size (diameter and length) and weight. However, HME implants had higher drug content and good content uniformity compared to IM implants. The PTV was found to be amorphous in both HME and IM implants based on obtained Raman spectra, DSC, and XRD findings. IM and HME include heating and melting steps, and the API was likely dissolved in the PLGA and transferred to amorphous. As amorphous drugs tend to have a higher solubility and more rapid dissolution rates than crystalline, potentially resulting in better bioavailability and therapeutic efficacy. However, Raman mapping confirmed heterogeneous drug distribution within IM implants, which could result in uneven drug release and lower efficacy compared to the homogenous drug distribution observed within HME implants. HME implants were homogenously dispersed within PLGA implants due to the high shear mixing force of the twin screws of the HME. Therefore,

according to the drug content and distribution results, the HME technique is preferable to IM.

In vitro drug release of IM implants and HME implants were investigated. PTV was found to be stable in various release media (dH_2O, PBS, DMSO), which allowed for long-term release studies to be conducted. The release of PTV was affected by manufacturing techniques and the type of release media used. The drug release from HME implants is significantly lower than those manufactured by IM. This is because of high shear forces of the HME process make the implants denser, more closely packed matrix, resulting in a slower uptake of the dissolution medium and slower drug release. The completed drug release (real-time) from HME implants under physiological conditions using PBS media takes a very long time (more than a month), which is time-consuming. In comparison, the IM implants take only 7 days. Thus, accelerated release studies were investigated using various types of release media to speed up drug release from HME implants. The drug release achieved sustained release over seven days under 80%DMSO release media.

To address challenges posed by the IM technique, arising from the lack of significant shear forces found in the twin screws of the HME process, future investigations are recommended. Potential refinements such as pre-mixing or optimising the degree of grinding before IM could enhance drug content uniformity and overall performance.

Table 3. 9 Summary comparison of IM and HME techniques for the development and characterisation of PTV-loaded PLGA implants.

Parameter	IM implants	HME implants
Size and weight uniformity	Consistent in size and weight with a ± 10% deviation	Consistent in size and weight with a ± 10% deviation
Drug content uniformity	RSD % (10.1 - 16.2%) Lower drug content uniformity compared to HME implants	RSD % (0.4 - 1.4%) Higher drug content uniformity
Drug content	(62 - 77%) Low drug content level	(82 - 91%) High drug content level
Physical state of the drug	PTV found to be amorphous	PTV found to be amorphous
Drug distribution	Non-homogenous drug distribution	Homogenous drug distribution
Preferred technique	Not preferred due to lower drug content uniformity and non-homogenous drug distribution	Preferred due to higher drug content uniformity and homogenous drug distribution
Drug release profile	Faster drug release rate due to lower density matrix, complete drug release in 7 days	Slower release rate compared to IM due to denser matrix, takes more than a month (40 days) for complete release
Accelerated drug release	Not specified	Achieved sustained release over 7 days in 80% DMSO media

CHAPTER 4: DEVELOPMENT AND VALIDATION OF THE HPLC METHOD FOR THE DETERMINATION OF IRINOTECAN AND PITAVASTATIN

4.1 Background

Analytical method development plays a crucial role in drug formulation and product development, enabling the detection and quantification of APIs in dosage forms (Shrivastava et al., 2019). Numerous methods have been described in the literature for the determination of IRN and PTV individually. However, no method has been reported for the determination of these drugs mixed in a combined dosage form.

The next chapter focuses on the development of multi-layered implantable drug delivery devices (IRN-PTV-PLGA implant) specifically designed to target and treat GBM effectively. This implantable device aims to deliver IRN and PTV directly to the tumour site. The selection of IRN and PTV in combination is motivated by their synergistic effects, which can inhibit the function of MDR-1, thus allowing higher concentrations of IRN to enter the tumour cells and increase apoptosis (Jiang et al., 2014b). As a result, this combination presents a promising candidate for the development of a multi-layered implantable drug device. To ensure the success of the multi-layered implantable drug delivery device, it is essential to have a suitable analytical method capable of detecting and quantifying each compound accurately.

Therefore, this chapter describes the development of a validated HPLC method specifically designed to quantify IRN and PTV in a combined dosage form (multi-layered implantable drug delivery device). This would enable the quantification of the drug content and release from the manufactured multi-layered implant to be determined. The HPLC validation method was conducted according to the International Council for Harmonisation (ICH) guidelines. These guidelines recommend specific validation parameters, including accuracy, precision, range, linearity, specificity, limit of detection (LoD), and limit of quantification (LoQ) (Guedes

& Guedes, 2006; Harron, 2013; Shrivastava et al., 2019; Stefanini-Oresic, 2022). By employing this validated HPLC method, IRN and PTV can be confidently quantified in the multi-layered implant, ensuring its safety and efficacy for treating GBM.

4.2 Aim

This chapter aimed to develop and validate appropriate analytical methods for detecting and quantifying IRN and PTV. This would enable the quantification of drug content and release from the manufactured implantable drug delivery devices (multi-layered implant) to be determined.

4.3 Materials & Methods

4.3.1 Chemicals

The materials used in this chapter were the same as those used in chapter 2 and chapter 3.

4.3.2 Methods

4.3.2.1 Instrument and chromatographic conditions

The Separation and quantification of the IRN and PTV were performed using an Ultimate 3000 Autosampler HPLC system from Thermo Scientific Inc., Germering, Germany. A Zorbax Eclipse XDB-C18 column with dimensions of 4.6 x 150 mm and a particle size of 3 µm, manufactured by Agilent Technologies in the USA, was used for the separation. The mobile phase consisted of a mixture of acetonitrile and deionised water in a ratio of 65:35 (v/v), and the flow rate was set at 0.5 mL/min. The run time for the analysis was 10 minutes. The detection wavelength was 245 nm, and the injection volume was 10 µL. IRN and PTV retention times were 2.18 and 4.04 minutes, respectively.

4.3.2.2 Preparation of a standard stock solution and working solutions

A standard stock solution of IRN and PTV was prepared by dissolving 100 mg of each drug in a 100 ml mobile phase to give the final solution with a 1000 ug/ml concentration. The calibration curves were prepared by diluting the stock solution to give final working solutions with concentrations ranging from 10 - 400ug/ml.

4.3.2.3 Statistical Analysis

The statistical analysis was conducted using GraphPad Prism version 9 and Microsoft Excel 2016. The mean, SD and %RSD were calculated, and calibration curves were created using the least squares linear regression analysis.

4.3.2.4 HPLC validation method

The method was validated according to ICH guidelines (Harron, 2013; Reddy et al., 2013). The validation parameters were accuracy, precision-repeatability, precision (intra-day &inter-day), linearity and range, LoD and LoQ.

4.4 Results and discussion

4.4.1 Chromatographic conditions

The chromatographic conditions resulted in two sharp separate peaks with retention times of 2.1 and 4 minutes for IRN and PTV, respectively, as shown in Figure 4.1. Following this, the method was validated according to the ICH guidelines.

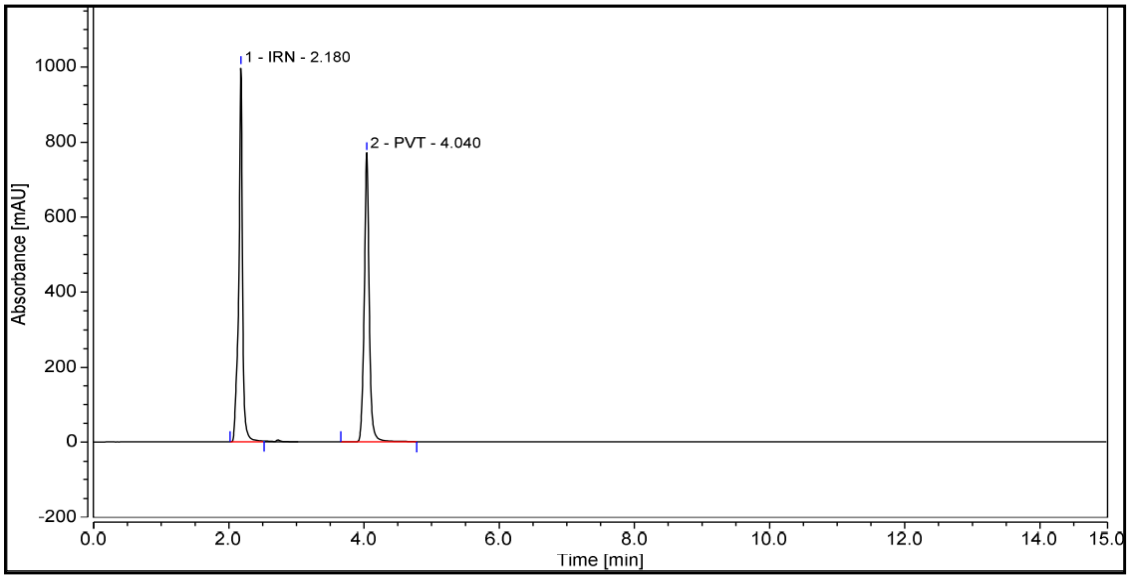

Figure 4. 1 The chromatograms of IRN (tR = 2.18 min) and PTV (tR = 4.0 min) were obtained using an HPLC system with a Zorbax Eclipse XDB-C18 column (3 µm, 4.6 x 150 mm), a mobile phase of ACN-dH_2O (65:35 v/v), a flow rate of 0.5 mL/min, and an injection volume of 10 µL.

4.4.1.1 Method validation for IRN and PTV

4.4.1.1.1 Accuracy

The accuracy of the analytical method is the closeness between the measured value to the true value (Chandran & Singh, 2007; Kowalska et al., 2022). The experiment aimed to determine the accuracy of measurements by taking three replicates for each of the six concentrations used in the calibration curve for each drug. The measured concentrations were compared to the theoretical values, and the percentage accuracy was calculated (Tables 4.1 & 4.2) by applying the following Equation (Sen et al., 2016).

$$\%\ \text{accuracy} = (\text{found concentration values}/\ \text{true values})\ \text{X}\ 100$$

The results showed that all percentage accuracy values for IRN and PTV fell within the 91% to 108% range, indicating a high accuracy level with %RSD values within the acceptable range of ≤ 2% (Tables 4.1 & 4.2).

Table 4. 1 Results of accuracy measurement of IRN.

Drug	Sample No.	Theoretical Concentration (ug/ml)	Absorbance Found	Mean Found Concentration (ug/ml)	Recovery % (Mean±SD)	%RSD
IRN	1	10	14.2	9.8	98±0.1	0.7
	2	50	51.4	50.3	100.7±0.1	0.2
	3	100	101.3	104.6	100.4±0.2	0.2
	4	200	189.5	200.7	100.3±0.3	0.1
	5	300	284.1	303.7	101.2±0.2	0.1
	6	400	368.6	395.8	98.9±1.6	0.4
Average recovery % (mean±SD)					100.6±2.3	

Table 4. 2 Results of accuracy measurement of PTV.

Drug	Sample No.	Theoretical Concentration (ug/ml)	Absorbance Found	Mean Found Concentration (ug/ml)	Recovery % (Mean±SD)	%RSD
PTV	1	10	11.9	10.5	104.9±0.1	0.8
	2	50	58.3	49.6	99.2±0.1	0.2
	3	100	118.4	100.3	100.3±0.2	0.2
	4	200	235.8	199.4	99.7±0.3	0.1
	5	300	354.7	299.7	99.9±0.5	0.1
	6	400	474.2	400.5	100.1±0.6	0.1
Average recovery % (mean±SD)					100.7±2.1	

4.4.1.1.2 Linearity, range, LoD and LoQ

Linearity refers to an analytical method's ability to generate results proportional to the analyte concentration in the sample within a specified range (Harron, 2013). The range of an analytical method refers to the range of concentrations of the analyte in the sample for which the method has been demonstrated to exhibit adequate precision, accuracy, and linearity. This range is determined through the validation process and typically includes the upper and lower limits of the concentration range (Harron, 2013).

The linearity of the analytical method for IRN and PTV drugs was determined by analysing six concentrations from the calibration curve. The experiment was repeated over three days, and the samples were prepared in triplicate. The mean values and standard deviations were used to generate a representative calibration plot (Figure 4.2). Calibration curve values for each drug are presented in Table 4.3**.** The results demonstrate high correlation coefficients (≥ 0.999) and low y-intercepts (≤ 2%), indicating an excellent linear correlation between the peak area and the concentrations of drugs over the range of 10-400 ug/ml for both IRN and PTV.

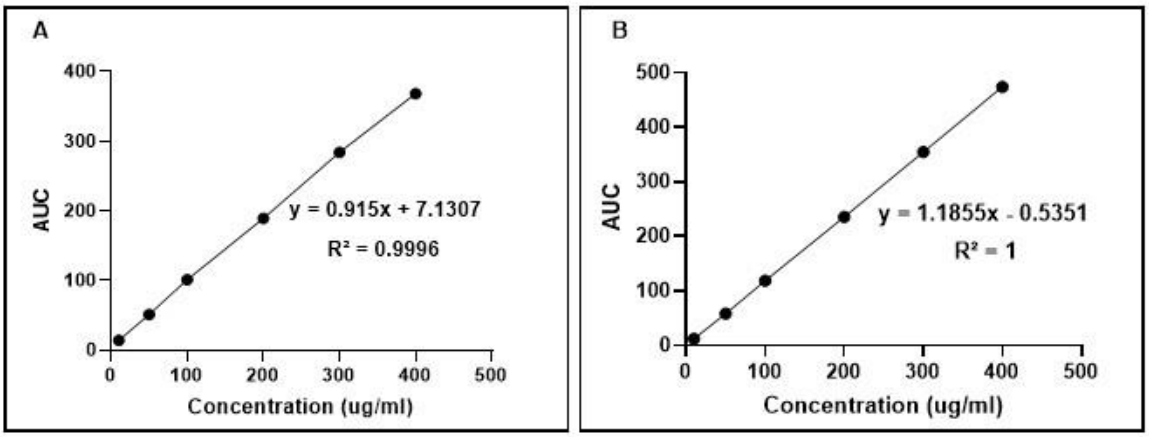

Figure 4. 2 Calibration Curve of IRN (A) and PTV (B).

Table 4. 3 Calibration curve properties for IRN and PTV drugs (means, n=9).

Drug	Linearity range	R^2	y-intercept	slope	LOD (ug/ml)	LOQ (ug/ml)
IRN	10-400 ug/ml	0.999	0.7	0.9	11.0	33.3
PTV	10-400 ug/ml	1	0.5	1.9	1.8	5.6

LoD refers to the smallest quantity of an analyte in a sample that can be detected with a certain degree of confidence but is not necessarily measured or reported as an exact value. LoQ refers to the smallest quantity of an analyte in a sample that can be measured and reported with a specific degree of precision and accuracy (Shrivastava et al., 2019).

The LOD calculation was performed using the following Equation

$$\mathrm{LoD} = 3.3\,\sigma/S$$

The LOQ calculation was performed using the following Equation

$$\mathrm{LoQ} = 10\,\sigma/S$$

'σ' refers to the standard deviation of the response, while 'S' refers to the slope of the calibration curve (Shrivastava et al., 2019; Stefanini-Oresic, 2022)

The LoD values for the IRN and PTV were 11.0 ug/mL and 1.8 ug/mL, respectively, and the LOQ values for the same analytes were 33.3 ug/ml and 5.6 ug/ml, respectively (Table 4.3).

4.4.1.1.3 Precision – Repeatability

The precision of the analytical method is the degree of agreement among a series of measurements collected from numerous sampling of the same homogeneous sample under prescribed conditions, including both repeatability (intra-day) and intermediate precision (inter-day) (Shrivastava et al., 2019).

To assess the method's repeatability, ten replicates of one concentration (100 ug/ml) from the standard solution of each drug were prepared and analysed. The retention time, peak area, and peak height were recorded, and the mean, SD, and %RSD were calculated.

The results demonstrate that the %RSD values for the means of the retention times, peak areas and peak heights for both drugs are within the acceptable range of ≤ 2% (Tables 4.4 & 4.5). Therefore, it can be concluded that the method has good repeatability.

Table 4. 4 Results of repeatability measurement of IRN.

Injection No.	Retention time (minutes)	Peak area	Peak height
Replicate 1	2.15	101.45	1,458.77
Replicate 2	2.15	102.30	1,455.26
Replicate 3	2.15	102.04	1,459.13
Replicate 4	2.15	102.46	1,462.85
Replicate 5	2.15	102.38	1,448.23
Replicate 6	2.15	101.94	1,458.38
Replicate 7	2.15	101.75	1,460.12
Replicate 8	2.15	102.04	1,459.34
Replicate 9	2.15	105.10	1,448.77
Replicate 10	2.15	100.28	1,458.43
Mean	2.15	102.17	1,456.93
SD	0.00	1.21	4.82
RSD%	0.08	1.18	0.33

Table 4. 5 Results of repeatability measurement of PTV.

Injection No.	Retention time (minutes)	Peak area	Peak height
Replicate 1	4.14	118.96	991.73
Replicate 2	4.14	119.08	994.37
Replicate 3	4.14	119.24	995.73
Replicate 4	4.14	118.55	994.74
Replicate 5	4.15	118.67	992.20
Replicate 6	4.15	118.43	992.10
Replicate 7	4.15	118.97	996.48
Replicate 8	4.16	119.41	996.66
Replicate 9	4.16	119.00	1,000.46
Replicate 10	4.16	119.10	1,002.55
Mean	4.15	118.94	995.70
SD	0.01	0.31	3.57
RSD%	0.21	0.26	0.36

4.4.1.1.4 Precision – Inter-day and Intra-day

The intraday precision of the standard method was assessed by analysing three replicates samples of three independent concentrations of IRN and PTV three times on the same day and calculating the % RSD. Inter-day precision was assessed using the same concentrations of IRN and PTV on three separate days, and % RSD was calculated. The results demonstrated that the method was found to be precise, with low %RSD values ≤ 2% for the mean found concentrations of IRN and PTV (Table 4.6).

Table 4. 6 Inter-day and intra-day precision for IRN and PTV.

Drug	Theoretical Concentration (ug/ml)	n	Intra-day precision		Inter-day precision	
			Mean Found concentration (ug/ml)	RSD%	Mean Found concentration (ug/ml)	RSD%
IRN	100	9	105.4	0.4	105.5	0.1
	200	9	213.4	0.5	213.0	0.1
	300	9	312.3	0.2	311.1	0.8
PTV	100	9	100.9	0.1	100.0	0.2
	200	9	200.0	0.2	199.6	0.6
	300	9	300.1	0.0	299.1	1.2

4.5 Conclusion

The HPLC analytical method developed for detecting and quantifying IRN and PTV is accurate, linear, precise, validated and reliable. The analytical method was verified according to the recommended principles of the ICH guidelines for the validation of analytical procedures and can be used in the following chapter. This method can be confidently used to quantify the IRN and PTV drugs in samples obtained from the drug content and in vitro release studies.

CHAPTER 5: DEVELOPMENT AND CHARACTERISATION OF MULTI-LAYER IMPLANTABLE DRUG DELIVERY DEVICE (IRINOTECAN PITAVASTATIN-LOADED PLGA) FORMULATED BY HOT MELT EXTRUSION

5.1 Background

GBM is a highly aggressive and recurrent brain tumour that has significant obstacles to successful treatment due to its heterogeneity resulting in limited responsiveness to chemotherapy as well as the difficulty of drugs crossing the BBB after systemic administration (Bastiancich et al., 2021; Trivedi et al., 2023). Localised drug delivery systems have emerged as promising methods for treating GBM to address these limitations (Bastiancich et al., 2021). This chapter aims to develop a multi-layered implantable drug delivery device that can effectively target and treat GBM. The device is designed to deliver IRN and PTV directly to the tumour site. The HME technique was selected for manufacturing the multi-layer implantable device based on the data from Chapters 2 and 3 because it allows for high drug content and ensures a homogeneous drug distribution within the PLGA matrix. This homogeneous distribution is crucial as it contributes to consistent drug release profiles from the device. The reason for choosing IRN and PTV together is their synergistic effects and ability to overcome drug resistance mechanisms commonly found in GBM (Jiang et al., 2014b). In GBM, drug resistance often results from the overexpression of the MDR-1 (Nabors et al., 1991; Nakai et al., 2009), which actively transports cytotoxic agents like IRN out of the cells (Garrigues et al., 2002; Jiang et al., 2014b). However, the combination of PTV and IRN can inhibit the function of MDR-1, allowing higher concentrations of IRN to enter the tumour cells and increase apoptosis. These synergistic effects have been validated in in-vivo studies (Jiang et al., 2014b). Moreover, high-throughput drug screening assays using GBM cell lines have shown that combining IRN and PTV treatment yields superior results to individual drug treatments (Fan et al., 2016).

This chapter will provide valuable insights into developing and characterising the multi-layer implantable drug delivery device, including size uniformity, drug content, physical state, drug distribution, and drug release kinetics. The results obtained from this investigation will contribute to advancing drug delivery systems, enhancing the overall efficacy of treatments, and improving the patient experience by offering more effective, convenient, and personalised approaches to healthcare.

5.2 Aims and objectives

This chapter aims to develop and characterise a multi-layered implantable drug delivery device loaded with IRN and PTV using the HME technique for the localised treatment of GBM.

The objectives were:

- To manufacture multi-layered implantable drug delivery devices containing IRN and PTV with different drug loadings using the HME technique.
- To evaluate the size uniformity of the multi-layered implants and ensure consistency in drug content throughout the device.
- To evaluate the thermal stability and crystallinity of the drug-loaded layers within the implants.
- To analyse the distribution of IRN and PTV within the multi-layered implants and ensure homogeneous dispersion throughout the device.
- To investigate the in vitro drug release profiles of IRN and PTV from the implants.
- To determine the mechanism of drug release from the extruded multi-layered implants by applying various mathematical models, allowing a deeper understanding of the release kinetics and factors influencing the drug release behaviour.

By achieving these objectives, we aim to comprehensively understand the developed multi-layered implantable drug delivery device, its physical and chemical properties, drug release behaviour, and its possibilities for effective localised treatment of GBM.

5.3 Materials & Methods

5.3.1 Chemicals

The materials used in this chapter were the same as those used in chapter 2, section 2.3.1 and chapter 3, section 3.3.1.

5.3.2 Methods

5.3.2.1 Manufacturing of multi-layer implant (IRN-PTV loaded PLGA) using the HME technique

A multi-layer implant was manufactured using HME to produce individual drug-loaded layers. For the IRN-loaded PLGA layer, the appropriate amounts of IRN (10%, 20%, and 30% w/w), PLGA 5004, and plasticiser (kolliphor 20% P188) were weighed into a sealed plastic container and roll mixed for approximately 10 minutes to ensure uniform blending of the API and excipients. The resulting active mix was then fed into a twin-screw minilab extruder, with the extruder's feeding, mixing, and metering zones set at specific temperatures (feeding zone: 65°C, mixing zone: 87°C, metering zone: 60°C) and a screw speed of 20 RPM. The melt obtained from the extrusion process was subsequently extruded through a 2 mm die and cut into 3 mm implant rods, thus producing the desired IRN-loaded PLGA layers. Similarly, for the PTV-loaded PLGA layer, the appropriate amounts of PTV (10%, 20%, and 30% w/w), PLGA 5004, and plasticiser (kolliphor 20% P188) were weighed, roll mixed, and processed using different extrusion parameters. The extruder's feeding, mixing, and metering zones for the PTV-loaded layer were set at specific temperatures (feeding zone: 75°C, mixing zone: 100°C, metering zone: 75°C) with a screw speed of 20 RPM. The resulting melt was extruded through a 2 mm die and cut into 3 mm implant rods to create the desired PTV-loaded PLGA layers. Finally, the individual layers containing each drug were adhered together using surgical glue (Liquid Skin®) to

create a multi-drug implant incorporating IRN and PTV, as illustrated in Figure 5.1. Liquid Skin®, purchased from Chemence Medical, Inc., was used in an amount of approximately 0.05 grams for each layer to ensure minimal excess. The two parts were gently pressed together to ensure complete contact with the adhesive. The adhesion process was completed in approximately 30 seconds.

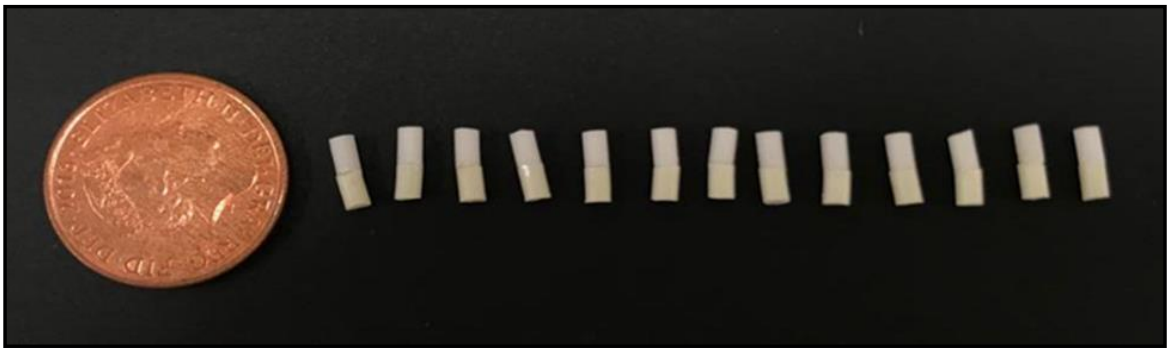

Figure 5. 1 Representative image of the multi-layered IRN-PTV loaded PLGA formulated by HME.

5.3.2.2 Physical characterisation of implants

5.3.2.2.1 Determination of the lengths, diameters and weights of multi-layered IRN-PTV-loaded PLGA implants

To determine the length, diameter, and weight of the multi-layer implant (IRN-PTV loaded PLGA), each individual layer was measured separately. The length and diameter of each layer, which had dimensions of 2x3mm, were measured using a digital vernier calliper. The average diameter and length for each layer were calculated based on these measurements (n=10). Additionally, the weight of each layer was measured using an electronic balance, and the average weight of each layer was determined (n=10).

5.3.2.3 Physiochemical characterisation

5.3.2.3.1 Determination of drug content

Each multi-layered implant was placed in a glass vial, and 5 ml of Dichloromethane (DCM) was added and left for 1 hour. Subsequently, the DCM was evaporated using a water bath at 65°C until complete dryness was achieved. The residue containing IRN, PTV, and PLGA was mixed with 10 ml of the mobile phase. The vial was placed into the ultrasonic bath for 10 minutes, followed by vortex mixing for 2-3 minutes, causing the PLGA and plasticiser to precipitate while the IRN and PTV remained soluble in the solution. The sample was filtered through a 0.45 uM syringe filter and transferred to HPLC vials for analysis. HPLC method was utilised to determine the content of IRN and PTV. The obtained results were compared to the theoretical content, calculated based on the total mass of each layer, to assess the reliability of the manufacturing process. An acceptable limit of ±10% of the theoretical content was set.

5.3.2.3.2 Crystallinity studies using X-ray Powder Diffraction (XRD)

The crystallinity studies of the multi-layered implant were conducted using X-ray Powder Diffraction (XRD). Each layer of the multi-layered implant was ground to a fine powder, and the X-ray powder diffraction patterns were obtained. The XRD patterns of the formulation blends, pure IRN, PTV, PLGA, and P188, were also measured. To perform the XRD analysis, the ground samples of each layer, formulation blends, and pure substance were filled into a flat sample holder and scanned with a 2θ range of 3–50° and step size of 0.02, and the voltage was 30 kV and 15 mA current. Samples were recorded using a Rigaku MiniFlex 600 (Rigaku, USA) with a Cu Kα X-ray source (λ=1.5418 Å) and with software Miniflex Guidance version 1.2.01.

5.3.2.3.3 Thermal stability studies using Differential Scanning Calorimetry (DSC)

To investigate the physical state of IRN and PTV in the extruded multi-layered implants, a thermal analytical study was conducted using a T.A. instrument Q200 (DSC) from T.A. Instruments (New Castle, DE, USA). The samples weighing 5 to 10 mg were placed in aluminium pans and sealed. An empty aluminium pan was used as a reference. The heating process involved raising the temperature from 25°C to 300°C at a heating rate of 10°C per minute. Nitrogen was used as a purge at a flow rate set at 50 ml/min.

5.3.2.3.4 Determination of the Physical State of IRN and PTV in the extruded multi-layered implants by using Raman

The method used for the determination of the physical state of the IRN and PTV in the extruded multi-layered implants is the same as that described in chapter 2, section 2.3.2.5.2.

5.3.2.3.5 Drug distribution in the extruded multi-layered implant by Raman mapping

A Raman mapping was employed on its internal cross-section to investigate the IRN and PTV distribution within the extruded multi-layered implant. The Raman mapping was conducted using the Thermo Scientific™ DXR Raman (Waltham, USA) with a 780 nm laser operated at 20 mW power. Each spectrum was the co-addition of three 5-second exposures collected from 200 to 3200 cm^{-1}. An Olympus 10× objective with a 25 µm confocal pinhole was used to collect the Raman signal. The spectra were collected with a step size of 106 µm in both the x- and y directions.

5.3.2.4 In vitro drug release studies

Each multi-layered implant, including 10%IRN-10%PTV-PLGA implants, 20%IRN-20%PTV-PLGA implants, and 30%IRN-30%PTV-PLGA implants, was placed inside a sealed flask containing 80% DMSO release media. The flasks were placed into an orbital shaking incubator at 37°C and 100 rpm. 1 ml samples were collected at regular time intervals of 1, 2, 3, 4, 5, 6, and 7 days, and an equivalent volume of release media was replaced in the flask after each sampling. The withdrawn samples were filtered using a 0.45 uM filter and analysed using the IRN-PTV HPLC method. All the measurements were conducted in triplicate, and the results were represented as mean % cumulative release ± SD.

5.3.2.5 Application of mathematical models on the in vitro drug release data

In this study, various models were employed to analyse the in vitro drug release of IRN and PTV from the extruded multi-layered implants. The drug release data of all drug loadings of the extruded IRN-PLGA layers and PTV-PLGA layers were fitted to the different kinetic models in order to determine the mechanism of the drug release from the extruded multi-layered implants. The selection of the most appropriate model relied on assessing the linearity between the experimental and the predicted data, as indicated by the coefficient of correlation (R^2). The mathematical equations of the models are presented in Table 5.1.

Table 5. 1 Mathematical models used for the in vitro drug release data.

Model	Equation
Zero-order	$C = K_0 t$
First-order	$logC = LogC_0 - kt/2.303$
Higuchi	$Q = Kt^{1/2}$
Korsmeyer-Peppas	$M_t/M_\infty = Kt^n$

In these equations, C represents the concentration of the drug, k_0 denotes the zero-order rate constant, k represents the rate constant, Mt/M∞ indicates the fraction of drug released at time t, and n denotes the release exponent (Enayati et al., 2017).

5.4 Results and discussion

5.4.1 Physical characterisation of the implants

5.4.1.1 Determination of the lengths, diameters and weights of multi-layered IRN-PTV-loaded PLGA implants

The physical characteristics of multi-layered IRN-PTV-PLGA implants were assessed in terms of size, weight, and content. The results are presented in Tables 5.2 and 5.3. It was observed that all multi-layered IRN-PTV-PLGA implants exhibited a ±10% deviation in size (diameter and length) and weight, indicating that the implants were consistent.

In conclusion, the physical characterisation of the multi-layered IRN-PTV-PLGA implants revealed that the manufacturing process by HME was reliable, and the implants were uniform in size and weight.

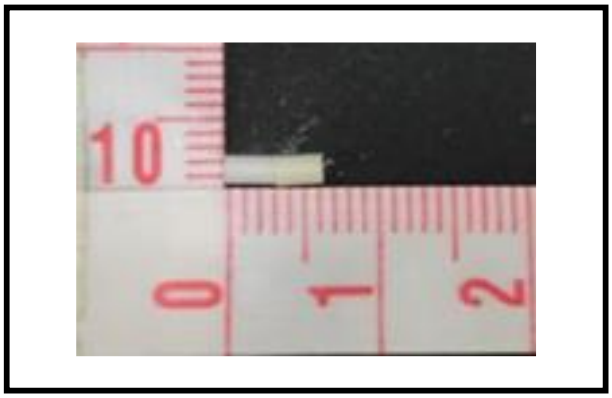

Figure 5. 2 Representative image of multi-layered IRN-PTV-PLGA implants 2X6mm formulated by HME.

Table 5. 2 Physical Appearance of the IRN-PLGA layer formulated by HME.

IRN-PLGA layer			
	10% IRN PLGA 5004 20%P188	**20% IRN** PLGA 5004 20%P188	**30% IRN** PLGA 5004 20%P188
Length (mm) Mean±SD (n=10)	3.0 ± 0.1	3.0 ± 0.1	3.0 ± 0.1
%RSD	2.3%	2.2%	2.3%
Diameter (mm) Mean±SD (n=10)	2.0± 0.1	2.0± 0.1	2.0± 0.1
%RSD	4.7%	5.2%	5.3%
Weight (mm) Mean±SD (n=10)	14.2± 0.1	14.2 ± 0.1	14.1±0.1
%RSD	1%	0.8%	0.9%

S.D is the standard deviation, %RSD is the relative standard deviation

Table 5. 3 Physical Appearance of the PTV-PLGA layer formulated by HME.

PTV-PLGA layer			
	10% PTV PLGA 5004 20%P188	**20% PTV** PLGA 5004 20%P188	**30% PTV** PLGA 5004 20%P188
Length (mm) Mean±SD (n=10)	3.0 ± 0.1	3.0 ± 0.1	3.0 ± 0.1
%RSD	2.7%	2.2%	1.7%
Diameter (mm) Mean±SD (n=10)	2.0± 0.1	2.0± 0.1	2.0± 0.1
%RSD	4.7%	6.4%	5.1%
Weight (mm) Mean±SD (n=10)	14.3± 0.1	14.2 ± 0.1	14.2±0.1
%RSD	0.5%	0.5%	0.9%

S.D is the standard deviation, %RSD is the relative standard deviation

5.4.2 Physiochemical characterisation of the implants

5.4.2.1 Determination of drug content

The drug content of multi-layered IRN-PTV-loaded PLGA implants manufactured by the HME technique was measured, and the results are summarised in Table 5.4. The implants consisted of two layers: IRN-PLGA layer and PTV-PLGA layer, both with dimensions of 2X3mm. Drug content, RSD, and %RSD were determined for three different drug concentrations of each layer (10%, 20%, and 30% w/w). The drug content of the IRN-PLGA layers was found to be 88.6%, 100.7%, and 96.9% for the 10%, 20%, and 30% w/w IRN-PLGA layers, respectively. For the PTV-PLGA layers, the drug content was determined to be 83.7%, 71.7%, and 80.6% for the 10%, 20%, and 30% w/w drug concentrations, respectively. The %RSD values for the IRN-PLGA layers were 3.2%, 5.3%, and 0.9% for the 10%, 20%, and 30% w/w drug concentrations, respectively. The %RSD values for the PTV-PLGA layers were 4.1%, 2.4%, and 3.3% for the 10%, 20%, and 30% w/w drug concentrations, respectively.

These low %RSD values indicate good content uniformity. Overall, both the IRN-PLGA and PTV-PLGA layers exhibited good content uniformity for IRN and PTV, with drug contents ranging from 81.7% to 100.7% and RSD values below 10%. These results suggest that the HME manufacturing technique achieved high and consistent drug content in the multi-layered IRN-PTV-loaded PLGA implants.

Table 5. 4 IRN and PTV contents, RSD and %RSD values for each of the 10, 20 and 30% IRN-PLGA layer and PTV-PLGA layer formulated by HME (n=6).

IRN-PLGA layer (2X3mm)			
	10%IRN	20%IRN	30%IRN
Drug content (%) (n=6)	88.6	100.7	96.9
RSD	2.8	5.4	0.8
%RSD	3.2	5.3	0.9
PTV-PLGA layer (2X3mm)			
	10%PTV	20%PTV	30%PTV
Drug content (%) (n=6)	83.7	81.7	80.6
RSD	3.5	1.9	2.6
%RSD	4.1	2.4	3.3

5.4.2.2 Crystallinity studies using X-ray Powder Diffraction (XRD)

The physical state of IRN and PTV in the multi-layered implant manufactured by the HME technique was verified through XRD analysis. The XRD diffractograms of pure IRN, PTV, PLGA, P188, the physical mixture, and each layer of the multi-layered implant (IRN-PLGA layer and PTV-PLGA layer) are presented in Figure 5.3.

The XRD diffractogram of IRN exhibited multiple strong-intensity peaks, indicating its crystalline nature. Notable peaks were observed at 2Theta values of 10°, 13°, 24°, and 26° (Figure 5.3a), which correspond to the characteristic peaks of IRN reported in previous studies (Vangara et al., 2014). The physical mixture of the IRN-PLGA layer before extrusion showed similar peaks, suggesting the presence of crystalline IRN (Figure 5.3e). In contrast, the XRD pattern of the IRN-PLGA layer from the multi-layered implant exhibited sharp diffraction peaks along with an underlying amorphous halo (Figure 5.3f). The diffraction peaks observed in the IRN-PLGA layer corresponded well to those of the crystalline IRN raw material, as indicated by the dashed red oval in Figure 5.3f. These results suggest that the extrusion process had no influence on the crystalline state of IRN in the multi-layered IRN-PTV-loaded PLGA implants.

The XRD pattern of pure PTV clearly showed strong intensity peaks at 14.28°, 21.06°, 21.86°, and 23.95° 2θ values (Figure 5.3b), indicating its crystalline state, which corresponds to the previous study (Pimple et al., 2022). These peaks were also observed in the diffraction pattern of the physical mixture (Figure 5.3g). In contrast, the XRD pattern of the PTV-PLGA layer from the multi-layered implant (Figure 5.3h) displayed halo patterns and small peaks at 21.06° and 25°. The reduction in the number of peaks intensity suggests a change in the crystallinity of

PTV due to the heating involved in the HME manufacturing process, resulting in the formation of an amorphous product. It can be hypothesised that the majority of PTV is dispersed in an amorphous form in the PLGA matrix of the HME implants, with only a small amount remaining in the crystalline form. Amorphous drug forms have higher molecular mobility than crystalline forms, improving solubility and dissolution rates (Pimple et al., 2022). Furthermore, amorphous drug forms are high-energy solids that tend to recrystallise, which can be evaluated through accelerated stability analysis (Grohganz et al., 2013). These findings indicate that the extrusion process used to produce the PTV-PLGA layer significantly influences the physical properties of PTV in the multi-layered implant.

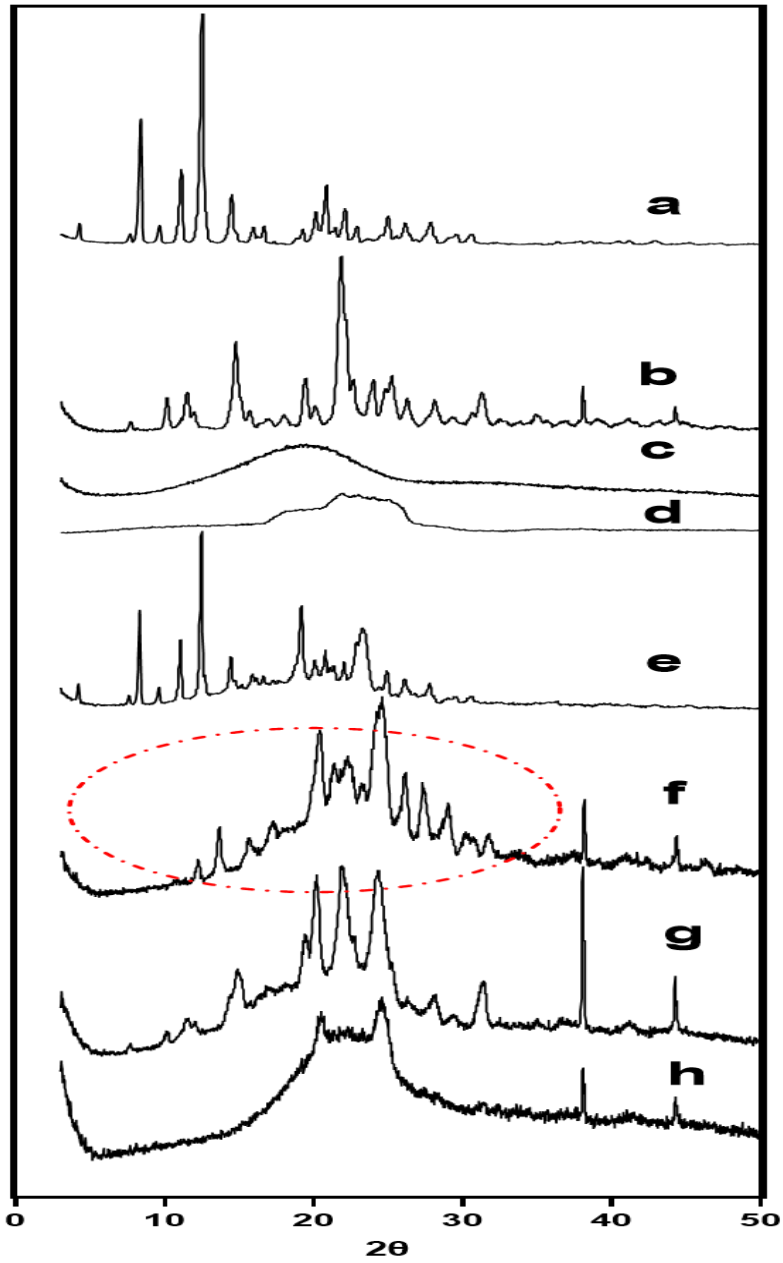

Figure 5. 3 X-ray powder diffraction spectra, pure IRN (a), PTV (b), PLGA (c), P188 (d), Physical mixture of IRN-PLGA layer (e), powdered of IRN-PLGA layer from multi-layered implant (f), Physical mixture of PTV-PLGA layer (g), powdered of PTV-PLGA layer from multi-layered implant (h).

5.4.2.3 Thermal stability studies using Differential Scanning Calorimetry (DSC)

DSC analysis was performed to investigate the physicochemical properties of the pure materials and the multi-layered implants manufactured by HME. The DSC thermograms displayed the thermal characteristics of IRN, PTV, PLGA, P188, and the extruded IRN-PLGA and PTV-PLGA layers (Figure 5.4). Pure IRN exhibited a sharp endothermic peak at 278°C, corresponding to its melting point, indicating its crystalline nature (Figure 5.4a). Similarly, PTV displayed a sharp endothermic peak at 143°C, corresponding to its melting point and confirming its crystalline nature (Figure 5.4b). The thermogram of PLGA showed an endothermic peak at 43.6°C, representing the polymeric material's Tg (Figure 5.4c). The DSC thermogram of Kolliphor® P188 revealed a single, sharp endothermic peak between 50 and 55°C, indicative of the melting point of poloxamer (Figure 5.4d). The DSC thermogram of the extruded IRN-PLGA layer exhibited the melting peak of IRN, indicating that the crystalline state of the drug was preserved, and no transition to an amorphous state occurred (Figure 5.4f). This result suggests that the drug maintained its properties and did not interact with the excipients.

Furthermore, the glass transition peak of PLGA and the melting peak of P188 were detected at the expected temperatures, indicating the absence of interactions between IRN and the excipients. These findings demonstrate that the preparation process by HME did not affect the stability of the drug and polymer. In the thermograms of the extruded PTV-PLGA layer, no characteristic endothermic peak corresponding to the melting of the PTV was observed (Figure 5.4e). This suggests that PTV was incorporated in an amorphous form and molecularly dispersed within the polymeric matrices and indicates that the drug dissolved within the molten

polymer during the DSC analysis (Cevher et al., 2007; Kamel & Abbas, 2018). Based on the XRD and DSC data, it is assumed that partial dissolution of PTV into the PLGA occurred during HME manufacture of the extruded PTV-PLGA layer, with the remainder dissolving in the PLGA during DSC analysis. This suggests that the PTV dissolved in the PLGA during manufacture is below saturation, and the amorphous/dissolved PTV should remain stable upon storage.

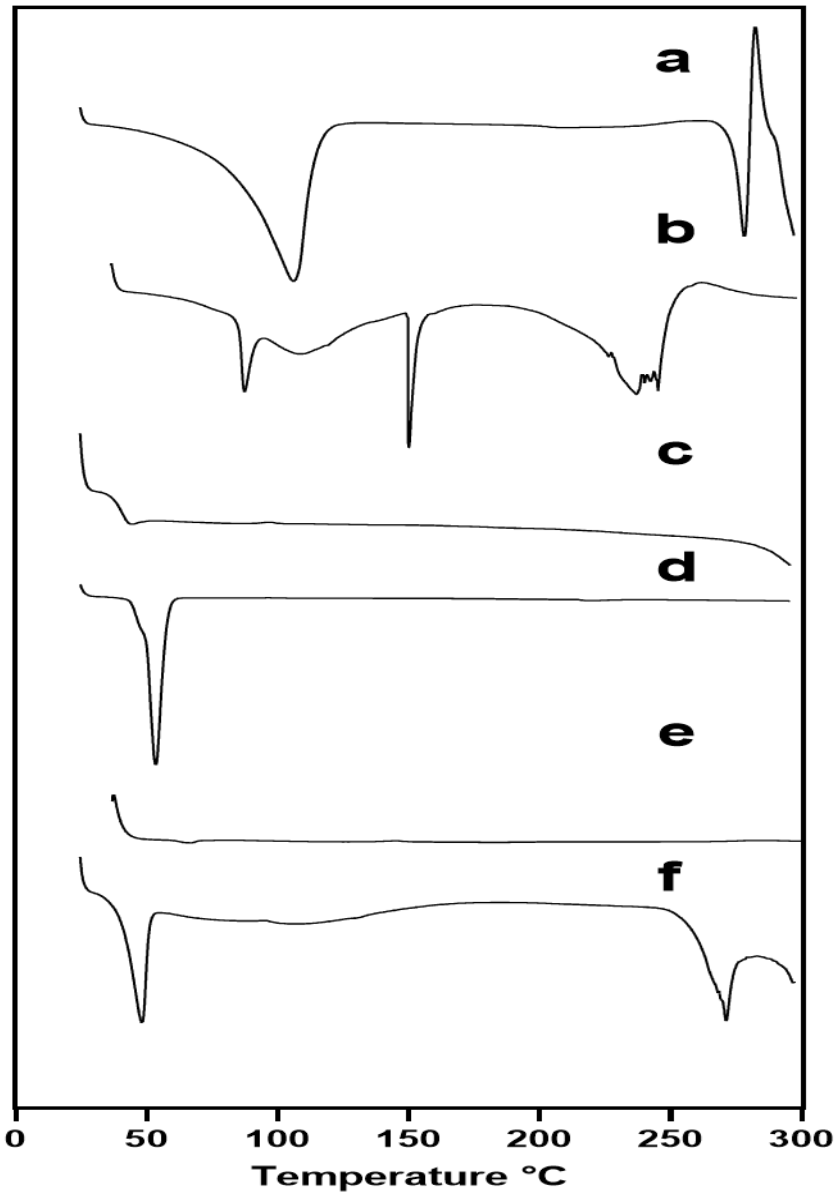

Figure 5. 4 DSC thermograms of pure IRN (a), PTV (b), PLGA (c), P188 (d), and extruded PTV-PLGA layer (e) and extruded IRN-PLGA layer (f).

5.4.2.4 Determination of the Physical State of IRN and PTV in the extruded multi-layered implants by using Raman

The physical state of IRN and PTV in the extruded multi-layered implants was determined using Raman spectroscopy. Confocal Raman analysis was performed to characterise the API across the entire surface of the extruded IRN-PLGA layer and PTV-PLGA layer of the multi-layered implant. Single point spectra of IRN, PTV, and the extruded IRN-PLGA layer and PTV-PLGA layer are presented in Figure 5.5. In the Raman spectra of IRN, high-intensity peaks were detected in the fingerprint region at 1400-1700 cm^{-1} (Figure 5.5C), confirming the presence of IRN in its crystalline form. This observation corresponds to the previous study (Chinna Babu et al., 2012). The Raman spectra of the IRN-PLGA layer (Figure 5.5B) exhibited identical features to the pure IRN reference spectrum (Figure 5.5C), indicating the presence of IRN in its solid state within the extruded IRN-PLGA layer. These results confirmed that the crystal form of IRN remained unchanged during the extrusion process, indicating its stability in the extruded IRN-PLGA layer.

In the case of PTV, the Raman spectra displayed intense peaks in the fingerprint region at 1400 cm^{-1}, confirming its crystalline form (Figure 5.5E). However, the Raman spectra of the PTV-PLGA layer (Figure 5.5D) did not exhibit any characteristic PTV peaks, indicating that PTV was in an amorphous state, consistent with XRD and DSC data. These findings suggest that PTV initially existed in a crystalline state but transformed into an amorphous state during the HME process. HME involves heating and melting steps, and the PTV was likely dissolved in the melt PLGA and transferred to amorphous.

Overall, Raman spectroscopy provided valuable insights into the physical states of IRN and PTV within the extruded multi-layered implants. The results demonstrated the stability of the crystal form of IRN during the extrusion process and the transformation of PTV from a crystalline to an amorphous state. These findings contribute to understanding pharmaceutical production methods involving melting processes and have implications for interpreting dissolution results in dosage form analysis.

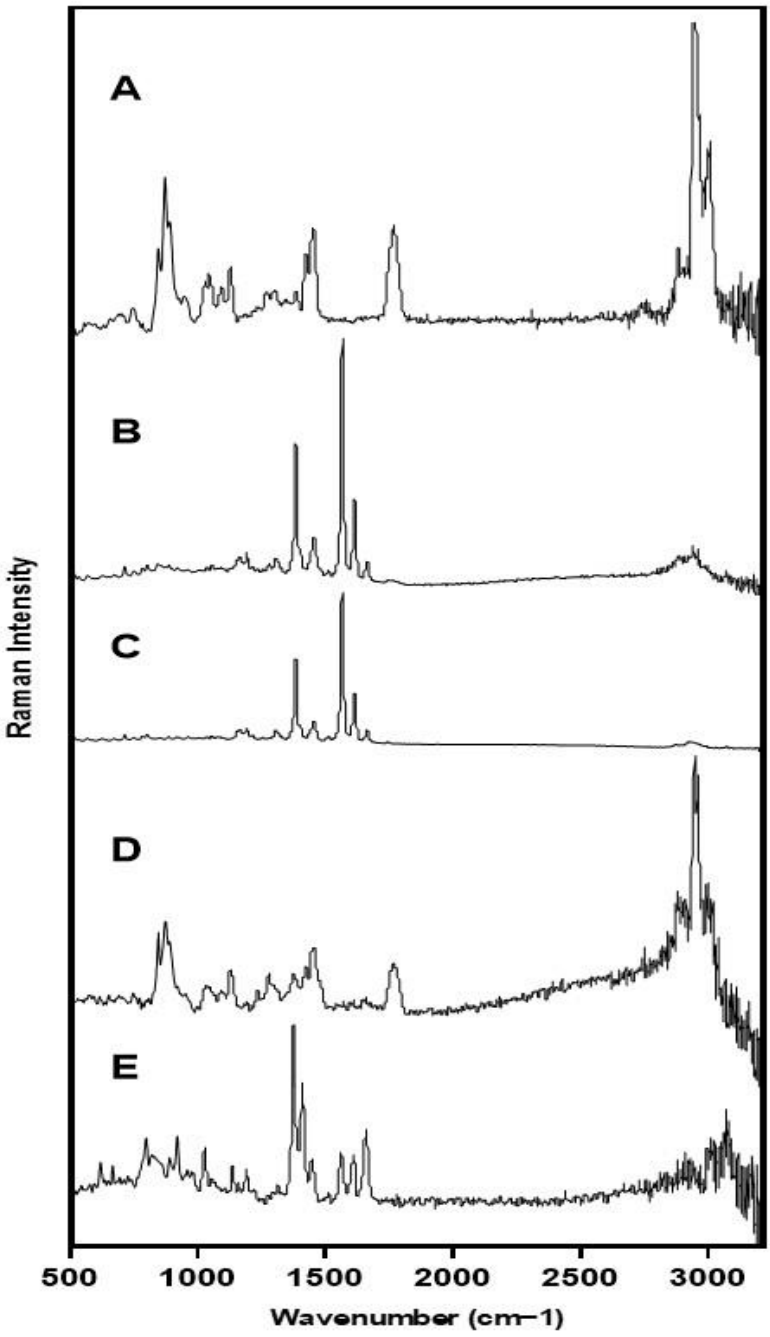

Figure 5. 5 Raman spectrogram of the PLGA (A), extruded IRN-PLGA layer (B), IRN (C), extruded PTV-PLGA layer (D) and PTV (E).

5.4.2.5 Drug distribution in the extruded multi-layered implant by Raman mapping

To ensure the homogenous distribution of IRN and PTV within the extruded multi-layered implant, Raman confocal microscopy was employed. This non-destructive method is commonly used to evaluate the drug distribution as well as the amorphous and crystalline content of pharmaceutical implants (Goyanes et al., 2015; Netchacovitch et al., 2017; Scoutaris et al., 2014). In this study, the internal cross-section of the extruded multi-layered implant was scanned using a Raman microscope. At each point of the formulation mapped, IRN and PTV reference spectra were compared to the collected implant spectra. The analysis revealed that IRN was uniformly distributed throughout the entire mapped area of the IRN-PLGA layer (Figure 5.6B). Similarly, PTV demonstrated homogenous distribution across the entire mapped area of the PTV-PLGA layer (Figure 5.6C). These results can be attributed to the efficient dispersion of IRN and PTV throughout the extruded multi-layered implant due to the high shear mixing in a twin-screw extruder. The observed homogenous distribution of IRN and PTV within the respective layers of the implant is crucial for ensuring consistent drug release and efficacy. It indicates that the HME process effectively dispersed the drugs, resulting in a formulation where the API is evenly distributed.

Overall, Raman confocal microscopy confirmed the successful homogenous distribution of IRN and PTV within the extruded multi-layered implant, validating the efficiency of the extrusion process in achieving uniform drug dispersion.

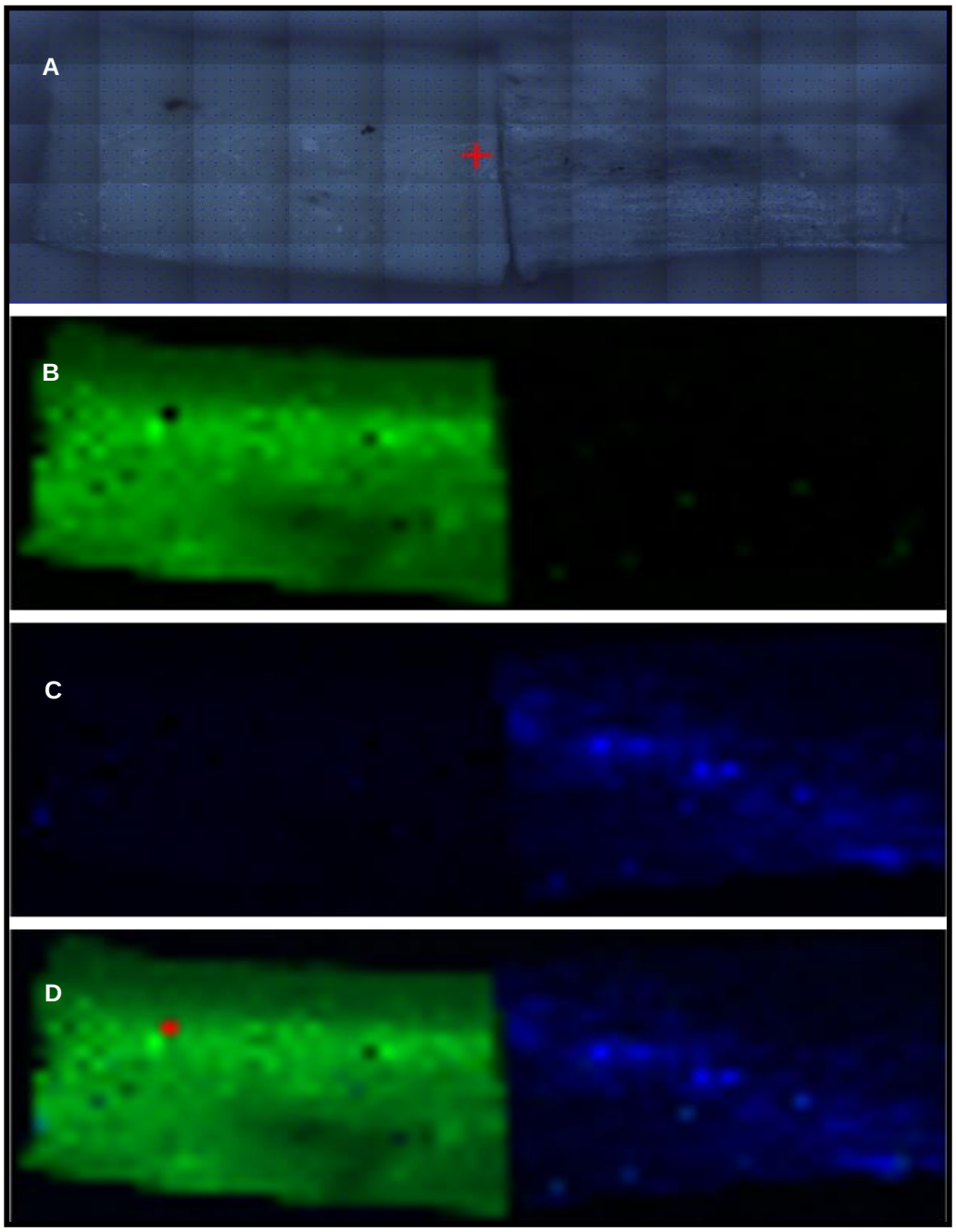

Figure 5. 6 Optical microscopy image of the extruded multi-layered implant internal cross section (A), Raman mapping of the extruded IRN-PLGA layer (B), green areas = IRN distribution, Raman mapping of the extruded PTV-PLGA layer (c), blue areas = PTV distribution.

5.4.3 In vitro drug release studies

The in vitro drug release study was conducted to evaluate the release pattern of the IRN and PTV from the IRN-loaded PLGA layers (10%, 20% & 30% w/w) and PTV-loaded PLGA layers (10%, 20% &30% w/w) of the extruded multi-layered implants. The results are presented in Figure 5.7. The study used 80% DMSO release media over seven days, which was chosen as an optimised accelerated drug release method based on the previous findings discussed in chapters 2 and 3. This method was preferred over using the PBS media as the drug released from the HME implants under physiological conditions takes a very long time (more than a month), which is time-consuming. In contrast, the drug release from the HME implants under 80%DMSO release media achieved sustained release over seven days. Accelerated release studies are used as a quality control tool, providing quicker drug release for extended-release formulations (Goel et al., 2021).

Regarding the results in Figure 5.7A, for the IRN-loaded PLGA layers: the release profiles of IRN from the PLGA layers showed a biphasic pattern over the seven days. In the initial stage, a rapid burst release was observed on day 1, accounting for approximately 30%, 27%, and 28% from the 10%, 20%, and 30% IRN-PLGA layers, respectively. Following the initial burst release, a sustained release of IRN was observed over the remaining days. The release of IRN from the PLGA layers continued gradually, with the cumulative release percentages reaching 85%, 85%, and 82.66% for the 10%, 20%, and 30% IRN-PLGA layers, respectively, at the end of the seven days. This indicates that the IRN is released initially due to diffusion, followed by gradual polymer matrix degradation.

For the PTV-loaded PLGA layers: similar to the IRN-loaded PLGA layers, the release profiles of PTV from the PLGA layers showed a biphasic pattern (Figure 5.7B). On day 1, a rapid burst release was observed, accounting for approximately 32%, 31%, and 32% from the 10%, 20%, and 30% PTV-PLGA layers, respectively. Following the initial burst release, a sustained release of PTV was observed over the remaining days. The release of PTV from the PLGA layers continued gradually, with the cumulative release percentages reaching 100%, 96.94%, and 98.56% for the 10%, 20%, and 30% PTV-PLGA layers, respectively, at the end of the seven days. This indicates that the PTV was released initially due to diffusion, followed by gradual polymer matrix degradation.

Overall, the in vitro drug release study demonstrated that both IRN and PTV-loaded PLGA layers exhibited sustained release profiles. The initial burst release was followed by a controlled and prolonged release of the drugs over seven days.

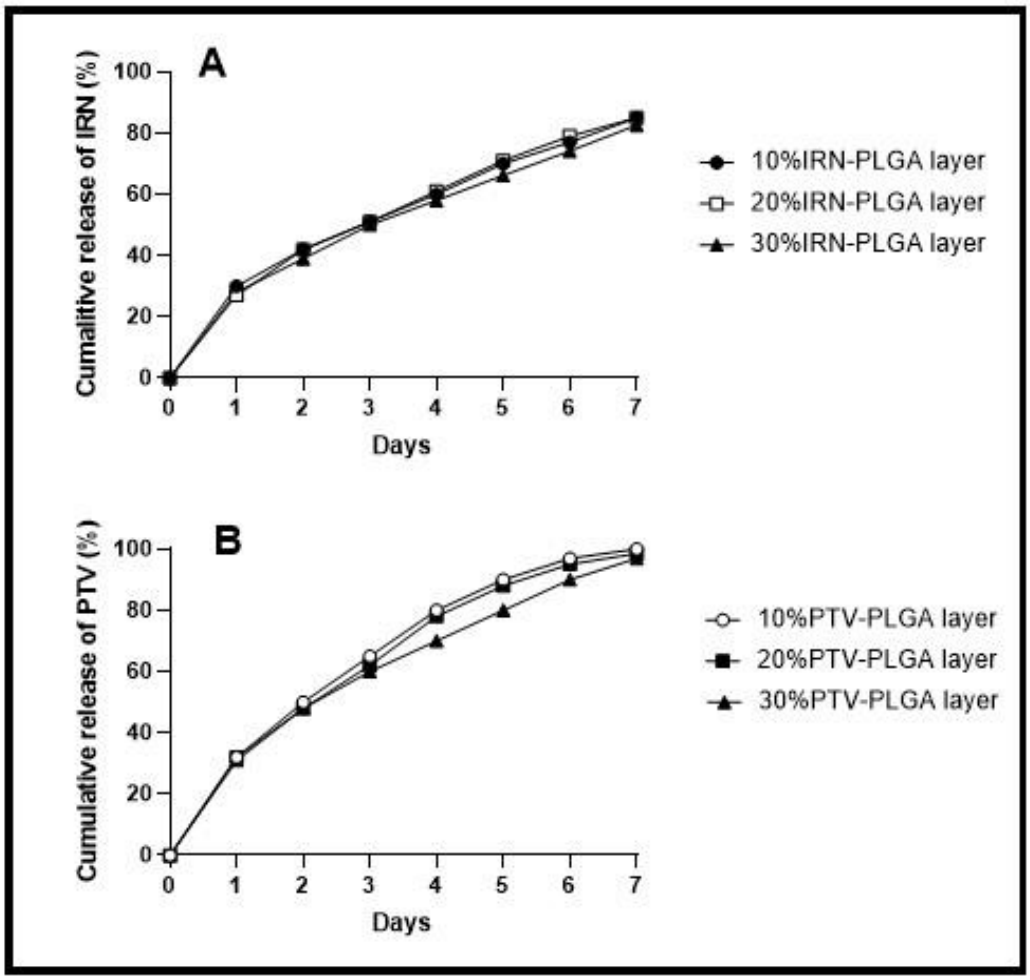

Figure 5. 7 In vitro cumulative drug release profiles of the IRN-loaded PLGA layers (10%, 20% & 30% w/w) (A) and PTV-loaded PLGA layers (10%, 20% & 30% w/w) (B) from the extruded multi-layered implant in 80% DMSO (mean±SD; n=3).

5.4.4 Application of mathematical models on the in vitro drug release data

In order to understand the drug release kinetics, various mathematical models were fitted to analyse the data. These models included zero-order (plotting cumulative percent of drug release against time), First-order (plotting the logarithm of cumulative percent of drug remaining in the matrix against time), Higuchi (plotting cumulative percent of drug release against the square root of time), and Korsmeyer-Peppas models (plotting the logarithm of cumulative percent of drug release against the natural logarithm of time) (Enayati et al., 2017). The R^2 values indicate the goodness of fit between the experimental data and the respective mathematical models, whereas the higher R^2 values indicate better fits that follow drug release kinetics (Gouda et al., 2017). In the zero-order model, drug release takes place at a constant rate over time, independent of the drug concentration (Manna et al., 2018; Tomic et al., 2016). The First-order model indicates that the amount of drug release is directly proportional to the amount of drug remaining within the matrix. As a result, the release of the drug decreases over time (Manna et al., 2018; Mello & Ricci-Júnior, 2011). In the Higuchi model, the release mechanism of the drug from the matrix is governed by diffusion through the matrix and follows the principle of Fick's law (Higuchi, 1963; Higuchi, 1961; Manna et al., 2018). Among these models, the Korsmeyer-Peppas model has been preferred as a suitable choice for characterising the release kinetics of polymeric drug delivery devices (Kini et al., 2015). The Korsmeyer-Peppas model utilises the release exponent (n) to determine the mechanism of drug release from the studied formulation. In the case of cylindrical drug delivery devices, when $n \leq 0.45$, it suggests Fickian diffusion, indicating that the drug release is primarily driven by diffusion. When $0.45 < n < 0.89$, it corresponds to anomalous (non-Fickian) diffusion, indicating that the drug release is controlled by

both diffusion and other simultaneous processes such as polymeric relaxation/erosion or swelling. When n = 0.89, it suggests zero-order release or Case-II transport, where the release mechanism is dominated by the swelling or relaxation of the polymeric chains and diffusion. When n > 0.89, it indicates Super Case-II transport (Enayati et al., 2017; Gouda et al., 2017; He et al., 2021; Manna et al., 2018; Mello & Ricci-Júnior, 2011; Ritger & Peppas, 1987; Tomic et al., 2016).

Regarding the results in Table 5.5, the 10% IRN-PLGA layer, the release data fitted all models with relatively high R^2 values of 0.941, 0.983, and 0.996, respectively, for the Zero-order, First-order, and Higuchi models. The correlation of the data to zero-order, First-order and Higuchi confirms that the drug release mechanism appears to be a combination of the diffusion and degradation of the polymer. The Korsmeyer-Peppas model provides an excellent fit with an R^2 value of 0.999, indicating a complex drug release mechanism involving both diffusion and erosion. The release exponent (n) for this model is 0.558, suggesting a non-Fickian or anomalous drug release behaviour. These findings align with previous reports that highlight the combination of drug diffusion and erosion as contributors to non-Fickian transport during the release process (Olejnik et al., 2017). Similar trends can be observed for the 20%IRN-PLGA and 30%IRN-PLGA layers, where all models provide good fits with high R^2 values (Table 5.5). The drug release mechanism for these layers appears to involve a combination of diffusion and erosion. For the 10%PTV-PLGA layer, the Zero-order, First-order and Higuchi models show reasonably good fits with R^2 values of 0.928, 0.932, and 0.991, respectively. The Korsmeyer-Peppas model also provides a good fit with an R^2 value of 0.997, suggesting a complex drug release mechanism involving both diffusion and erosion. The release exponent (n) for this

model is 0.567, indicating a non-Fickian or anomalous drug release behaviour. For the 20%PTV-PLGA and 30%PTV-PLGA layers, the Zero-order and Higuchi models exhibit relatively high R^2 values, indicating good fits. The First-order model shows lower R^2 values of 0.916 and 0.942, respectively. The Korsmeyer-Peppas model provides excellent fits with R^2 values of 1.000 and 0.996, indicating a complex drug release mechanism involving both diffusion and erosion. The release exponent (n) values for these layers are 0.678 and 0.595, respectively, suggesting a non-Fickian or anomalous drug release behaviour.

In summary, the results indicate that the Korsmeyer-Peppas model generally provides the best fit to the drug release data from the PLGA matrix implants, suggesting a complex drug release mechanism involving both diffusion and polymer erosion.

Table 5. 5 Kinetics models fitting results used to describe the IRN and PTV release from the extruded multi-layered implants.

Formulation	Zero-order	First-order	Higuchi	Korsemeyer Peppas		Release Mechanism
	Regression coefficient (R^2)				n	
10%IRN-PLGA	0.941	0.983	0.996	0.999	0.558	Non-Fickian (anomalous) diffusion
20%IRN-PLGA	0.948	0.991	0.994	1.000	0.589	
30%IRN-PLGA	0.947	0.984	0.995	0.999	0.576	
10%PTV-PLGA	0.928	0.932	0.991	0.997	0.567	
20%PTV-PLGA	0.944	0.916	0.996	1.000	0.678	
30%PTV-PLGA	0.935	0.942	0.986	0.996	0.595	

5.5 Conclusion

The physical and physiochemical characterisation of the multi-layered IRN-PTV-loaded PLGA implants has provided valuable insights into the manufacturing process and drug content. The physical characterisation confirmed that implants were consistent in size, weight and content, indicating the reliability of the HME manufacturing technique. The physiochemical characterisation revealed good content uniformity in both the IRN-PLGA and PTV-PLGA layers, with drug content ranging from 81.7% to 100% and low RSD values below 10%. XRD analysis confirmed the presence of crystalline IRN in the IRN-PLGA layer, indicating that the extrusion process did not affect the crystalline state of the IRN. However, the XRD analysis of the PTV-PLGA layer showed reduced crystallinity, suggesting that PTV was incorporated in an amorphous form and dissolved within the polymer matrix during the manufacturing process. DSC analysis confirmed these results by demonstrating the preservation of IRN crystallinity in the IRN-PLGA layer and the absence of a PTV melting peak in the PTV-PLGA layer. Raman spectroscopy further confirmed the stability of IRN in its crystalline state, as well as the transformation of PTV from a crystalline to an amorphous state within the implants. Raman mapping and microscopy provided evidence of the homogeneous distribution of IRN and PTV within their respective layers, indicating the efficient dispersion of the drugs throughout the multi-layered implants during the extrusion process. This uniform distribution is crucial for ensuring consistent drug release and effectiveness. The in vitro drug release studies exhibited a biphasic pattern for IRN and PTV, characterised by an initial burst release followed by sustained release over seven days. The release profiles indicated that drug diffusion initially occurred, followed by

gradual degradation of the polymer matrix. The application of the various mathematical models to the drug release data from the multi-layered PLGA implants revealed a complex mechanism involving both diffusion and polymer erosion. The Korsmeyer-Peppas model results provided the best fit among these models, indicating a non-Fickian or anomalous drug release behaviour from the implants. Overall, these findings further validate the effectiveness of the HME manufacturing technique in producing uniform and controlled drug delivery devices with the potential for targeted and sustained drug release. However, additional research is required to evaluate their performance in vivo and evaluate their therapeutic efficacy in relevant models or clinical trials.

CHAPTER 6: FINAL CONCLUSIONS AND FUTURE WORK

Each chapter was provided with a detailed conclusion. This conclusion summarises the overall outcomes of the thesis and outlines future work.

The first chapter highlights the challenges in treating GBM and suggests a promising solution by developing the local drug delivery system utilising PLGA implants. Overcoming the limitations of systemic chemotherapy and the BBB is crucial for effectively treating GBM. Localised drug delivery via PLGA implants presents a potential approach to improve drug delivery to the brain while avoiding systemic side effects. This work mainly focused on manufacturing and characterising implantable drug delivery devices loaded with IRN and PTV, using the IM and HME techniques. IRN has demonstrated effectiveness against GBM but faces challenges in crossing the BBB, whereas PTV has shown antitumour effects but has limited penetration through the BBB and can cause systemic adverse effects. By administering these drugs locally through PLGA implants, their concentrations can be increased at the tumour site, thereby improving therapeutic outcomes.

The second chapter aimed to develop a single-layer implantable drug delivery device loaded with IRN using the IM and HME techniques for the localised treatment of GBM. The objectives included determining the manufacturing processing parameters, producing PLGA matrix implants containing IRN, characterising the implants, investigating the IRN content and stability, and studying the impact of various factors on in vitro drug release. The study investigated the influence of IM and HME techniques on size and weight uniformity, drug content uniformity, drug distribution, stability, physical state, and drug release of IRN-loaded PLGA implants. Pre-screening experiments were carried out to determine the appropriate formulation composition and implant manufacturing processes. Rheology results identified

several formulations suitable for moulding and extrusion. Various techniques, such as HPLC, DSC, XRD, and Raman, were used to characterise the IM and HME implants. The implants demonstrated consistent size and weight, but the HME implants exhibited higher drug content and better content uniformity than IM implants. Neither technique had a negative effect on the stability of IRN within the implants. However, Raman mapping revealed heterogeneous drug distribution in IM implants. In contrast, HME implants exhibited homogeneous drug distribution due to the high shear mixing force generated by the twin screws. The study involved conducting in vitro drug release studies to evaluate the release of the IRN from the IM and HME implants. Several factors, such as the type of PLGA, drug load, implant size and manufacturing technique, influence the drug release behaviour. PLGA5004 implants showed faster drug release compared to PLGA5002 implants. Increasing the drug loading (30% w/w) resulted in a higher drug release than the lower loadings. Additionally, increasing the dimensions of the IRN-loaded PLGA5004 implants resulted in an increased drug release. The release of the drug from the HME implants was significantly lower than IM implants. This can be attributed to the denser and more closely packed matrix of HME implants, which results from high shear forces during manufacturing. This led to slower uptake of the dissolution medium and slower drug release. However, the completed drug release for both IM and HME implants in PBS media, which stimulate the physiological conditions, was time-consuming and took more than a month. Therefore, accelerated release studies were conducted using different media to accelerate the drug release. IM implants exhibited a sustained release over seven days under 70% DMSO release media, while HME implants achieved a similar sustained release period under 80% DMSO

release media. Based on the drug content, stability, and distribution results, the HME technique is considered preferable over the IM. Overall, these findings provide valuable insights into the development and characterisation of IRN-loaded PLGA implants for localised treatment of GBM, presenting potential advancements in the field of drug delivery for brain tumours.

The third chapter aimed to develop a single-layer implantable drug delivery device loaded with PTV using the IM and HME techniques for the localised treatment of GBM. The objectives included determining the manufacturing processing parameters, producing PLGA matrix implants containing PTV, characterising the implants, investigating the PTV content and stability, and investigating the in vitro drug release from the IM and HME implants. The study investigated the influence of IM and HME techniques on size and weight uniformity, drug content uniformity, drug distribution, stability, physical state, and drug release of PTV-loaded PLGA implants. Pre-screening experiments were carried out to determine the appropriate formulation composition and implant manufacturing processes. Rheology results identified several formulations suitable for moulding and extrusion. Various techniques, such as HPLC, DSC, XRD, and Raman, were used to characterise PTV-loaded PLGA implants manufactured by IM and HME. The results indicated that the implants exhibited consistent size and weight, but the HME implants exhibited higher drug content and better content uniformity than IM implants. The PTV was found to be amorphous in both HME and IM implants based on obtained Raman spectra, DSC, and XRD findings. IM and HME processes involve heating and melting steps, during which API is expected to dissolve in the PLGA and transform into an amorphous state. Amorphous drugs generally exhibit increased solubility and faster dissolution

rates than crystalline forms, leading to improved bioavailability and therapeutic effectiveness. However, Raman mapping confirmed heterogeneous drug distribution in IM implants, whereas HME implants demonstrated homogeneous drug distribution due to the high shear mixing force generated by the twin screws. The study involved conducting in vitro drug release studies to evaluate the release of the PTV from the IM and HME implants. The manufacturing technique and the type of release media were found to affect the release behaviour. HME implants demonstrated notably lower drug release than IM implants, attributed to the denser and more closely packed matrix of the HME implants, resulting from the high shear forces applied during manufacturing. This led to slower uptake of the dissolution medium and slower drug release. However, the completed drug release for both IM and HME implants in PBS media, which stimulate the physiological conditions, was time-consuming and took more than a month. Therefore, accelerated release studies were conducted using different media to accelerate the drug release. IM implants exhibited a sustained release over seven days under 70% DMSO release media, while HME implants achieved a similar sustained release period under 80% DMSO release media. Based on the drug content, stability, and distribution results, the HME technique is considered preferable over the IM. Overall, these findings provide valuable insights into the development and characterisation of PTV-loaded PLGA implants for localised treatment of GBM, providing the sustained and controlled release of PTV over an extended period.

In the fourth chapter, the developed and validated HPLC method for detecting and quantifying IRN and PTV drugs has been demonstrated to be accurate, linear, precise, validated and reliable, meeting the recommended principle outlined in the

ICH guidelines for analytical procedure validation. This method allowed precise drug release quantification, ensuring accurate safety and efficacy assessment of the devices. This method can be confidently employed in the subsequent chapter and used in the drug content and in vitro release studies to quantify the concentration of the IRN and PTV in samples.

The fifth chapter focused on developing and characterising a multi-layered implantable drug delivery device containing IRN and PTV using the HME technique. The aim was to create a device capable of targeting and treating GBM by delivering IRN and PTV directly to the tumour site. The combination of these drugs was selected because of their synergistic effects and ability to overcome the resistance mechanisms commonly found in GBM. The physical and physicochemical characterisation of the multi-layered IRN-PTV-loaded PLGA implants provided valuable insights regarding the manufacturing process and drug content. The implants consistently achieved the required size, weight, and drug content, indicating the reliability of the HME technique. Both the IRN-PLGA and PTV-PLGA layers attained content uniformity, with drug content between 81.7% and 100% and RSD values below 10%. Analysing the implants through XRD revealed that the IRN-PLGA layer maintained its crystalline form, demonstrating that the extrusion process did not affect the crystallinity of IRN. However, the XRD analysis showed decreased crystallinity in the PTV-PLGA layer, indicating that PTV was incorporated in an amorphous form and dissolved within the polymer matrix. DSC analysis supported these results by illustrating the remaining IRN crystallinity in the IRN-PLGA layer and the lack of a PTV melting peak in the PTV-PLGA layer. Raman spectroscopy provided additional evidence of IRN stability in its crystalline state and the

transformation of PTV from a crystalline to an amorphous state within the implants. Raman mapping proved the homogeneous distribution of IRN and PTV within each layer, suggesting effective drug dispersion within the multi-layered implants. This homogenous distribution is essential for ensuring consistent drug release and optimal effectiveness. In vitro drug release studies revealed a biphasic pattern for IRN and PTV, consisting of an initial burst release followed by sustained release over seven days. The release profiles demonstrated initial drug diffusion followed by gradual polymer matrix degradation. Various mathematical models were applied to the release data, providing insights into the mechanism of drug release from the multi-layered implantable drug delivery device. The Korsmeyer-Peppas model exhibited the best fit to the release data, indicating a non-Fickian or anomalous drug release behaviour from the implants. This suggests a complex drug release mechanism involving both diffusion and polymer erosion. Overall, these results confirm the success of the HME manufacturing technique in creating implantable drug delivery devices with a uniform and controlled release of drugs and capable of targeting and sustaining drug release. However, additional investigation is required to examine the performance of the devices in vivo and evaluate their efficacy in relevant models or clinical trials. The developed multi-layered implantable drug delivery device shows great promise in advancing drug delivery systems, enhancing treatment efficacy, and enhancing the overall patient experience by providing more efficient, convenient, and personalised healthcare approaches.

The work presented in this thesis indicates promising results, suggesting the need for further work and investigations. Examples of possible future investigations include:

- In vivo studies using animal models, such as rodent xenograft or orthotopic models of GBM, aim to evaluate the efficacy and toxicity of the IRN-PTV-loaded PLGA implants for the post-surgical treatment of the GBM. Tailor the selection of animal models to closely mimic the clinical scenario of GBM, focusing on parameters such as tumour size reduction, survival rates, and potential adverse effects, to provide a comprehensive understanding of implant behaviour in a relevant physiological environment and their possibilities for clinical applications.
- Performing in vivo release studies would enable a comparison with the in vitro release results, thus improving our knowledge of the correlation between in vitro and in vivo behaviour.
- Characterisation and quantification of the inflammation-mediating cells close to the IRN-PTV-loaded PLGA implants will provide insights into potential inflammation triggered by tissue injury during implantation or prolonged implant presence. Quantifying these cells will help assess the safety and compatibility of the implants in clinical applications, further advancing our understanding of their efficacy for GBM treatment.
- Accelerated stability testing, requiring exposure to higher temperatures and/or humidity, can be attempted on the formulated implantable drug delivery device to determine the type of degradation products that may arise throughout long-term storage. This investigation will also help identify the optimal storage conditions for the drug-delivery device.

- Sterilisation method such as gamma radiation is required to eliminate or deactivate a wide range of organisms, including fungi, bacteria, viruses, and spores. Additionally, it is crucial to assess the effect of radiation on drug stability and release characteristics of pharmaceutical compounds.
- To optimise the HME manufacturing technique, further optimisation of the extrusion settings, such as temperatures and screw speed, is needed to investigate their ability to predict the drug release rate and timing. This will contribute to a better understanding of the correlation between PLGA degradation and extrusion parameters. It is important to note that process parameters significantly impact the physical properties of the extruded polymeric implants, thereby influencing the behaviour of drug release.
- Explore the feasibility of 3D printing techniques for personalised drug-loaded polymeric implants, emphasising diverse patient conditions. Investigate varied sizes, drug loads, and types of PLGA using 3D printing. Assess the precision of drug release behaviours by experimenting with different printing parameters and varying implant geometries, aiming to tailor drug release to individual patient conditions.
- Explore the influence of various geometries in the design of implantable drug delivery devices on drug release kinetics and overall device performance. Employ computational modelling to predict the impact of geometry on drug diffusion and devise experiments to validate these predictions.

References

Abbott, N. J., & Romero, I. A. (1996). Transporting therapeutics across the blood-brain barrier. *Molecular Medicine Today*, *2*(3), 106–113. https://doi.org/10.1016/1357-4310(96)88720-X

Abd-Elghany, A. A., Naji, A. A., Alonazi, B., Aldosary, H., Alsufayan, M. A., Alnasser, M., Mohammad, E. A., & Mahmoud, M. Z. (2019). Radiological characteristics of glioblastoma multiforme using CT and MRI examination. *Journal of Radiation Research and Applied Sciences*, *12*(1), 289–293. https://doi.org/10.1080/16878507.2019.1655864

Adamson, C., Kanu, O. O., Mehta, A. I., Di, C., Lin, N., Mattox, A. K., & Bigner, D. D. (2009). Glioblastoma multiforme: a review of where we have been and where we are going. *Expert Opinion on Investigational Drugs*, *18*(8), 1061–1083. https://doi.org/10.1517/13543780903052764

Agarwal, S., Sane, R., Oberoi, R., Ohlfest, J. R., & Elmquist, W. F. (2011). Delivery of molecularly targeted therapy to malignant glioma, a disease of the whole brain. *Expert Reviews in Molecular Medicine*, *13*(May), 1–27. https://doi.org/10.1017/S1462399411001888

Agnihotri, S., Burrell, K. E., Wolf, A., Jalali, S., Hawkins, C., Rutka, J. T., & Zadeh, G. (2013). Glioblastoma, a brief review of history, molecular genetics, animal models and novel therapeutic strategies. *Archivum Immunologiae et Therapiae Experimentalis*, *61*(1), 25–41. https://doi.org/10.1007/s00005-012-0203-0

Alexis, F. (2005). Factors affecting the degradation and drug-release mechanism of poly(lactic acid) and poly[(lactic acid)-co-(glycolic acid)]. *Polymer International*,

54(1), 36–46. https://doi.org/10.1002/pi.1697

Amirian, E. S., Zhou, R., Wrensch, M. R., Olson, S. H., Scheurer, M. E., Il'yasova, D., Lachance, D., Armstrong, G. N., McCoy, L. S., Lau, C. C., Claus, E. B., Barnholtz-Sloan, J. S., Schildkraut, J., Ali-Osman, F., Sadetzki, S., Johansen, C., Houlston, R. S., Jenkins, R. B., Bernstein, J. L., … Bondy, M. L. (2016). Approaching a Scientific Consensus on the Association between Allergies and Glioma Risk: A Report from the Glioma International Case-Control Study. *Cancer Epidemiology, Biomarkers & Prevention*, *25*(2), 282–290. https://doi.org/10.1158/1055-9965.EPI-15-0847

Anderson, J. M., & Shive, M. S. (2012). Biodegradation and biocompatibility of PLA and PLGA microspheres. *Advanced Drug Delivery Reviews*, *64*(SUPPL.), 72–82. https://doi.org/10.1016/j.addr.2012.09.004

Andhariya, J. V., Choi, S., Wang, Y., Zou, Y., Burgess, D. J., & Shen, J. (2017). Accelerated in vitro release testing method for naltrexone loaded PLGA microspheres. *International Journal of Pharmaceutics*, *520*(1–2), 79–85. https://doi.org/10.1016/j.ijpharm.2017.01.050

Andhariya, J. V., Jog, R., Shen, J., Choi, S., Wang, Y., Zou, Y., & Burgess, D. J. (2019). Development of Level A in vitro-in vivo correlations for peptide loaded PLGA microspheres. *Journal of Controlled Release*, *308*(June), 1–13. https://doi.org/10.1016/j.jconrel.2019.07.013

Anjum, K., Shagufta, B. I., Abbas, S. Q., Patel, S., Khan, I., Shah, S. A. A., Akhter, N., & Hassan, S. S. U. (2017). Current status and future therapeutic perspectives of glioblastoma multiforme (GBM) therapy: A review. *Biomedicine &*

Pharmacotherapy = Biomedecine & Pharmacotherapie, *92*, 681–689. https://doi.org/10.1016/j.biopha.2017.05.125

Anton, K., Baehring, J. M., & Mayer, T. (2012). Glioblastoma multiforme: overview of current treatment and future perspectives. *Hematology/Oncology Clinics of North America*, *26*(4), 825–853. https://doi.org/10.1016/j.hoc.2012.04.006

Ashby, L. S., Smith, K. A., & Stea, B. (2016). Gliadel wafer implantation combined with standard radiotherapy and concurrent followed by adjuvant temozolomide for treatment of newly diagnosed high-grade glioma: A systematic literature review. *World Journal of Surgical Oncology*, *14*(1), 1–15. https://doi.org/10.1186/s12957-016-0975-5

Attenello, F., Raza, S. M., Dimeco, F., & Olivi, A. (2012). *Chemotherapy for brain tumors with polymer drug delivery* (pp. 339–353). https://doi.org/10.1016/B978-0-444-52138-5.00022-0

AVERINENI, R. K., SHAVI, G. V, GURRAM, A. K., DESHPANDE, P. B., ARUMUGAM, K., MALIYAKKAL, N., MEKA, S. R., & NAYANABHIRAMA, U. (2012). PLGA 50:50 nanoparticles of paclitaxel: Development, in vitro anti-tumor activity in BT-549 cells and in vivo evaluation. *Bulletin of Materials Science*, *35*(3), 319–326. https://doi.org/10.1007/s12034-012-0313-7

Baltes, S., Freund, I., Lewis, A. L., Nolte, I., & Brinker, T. (2010). Doxorubicin and irinotecan drug-eluting beads for treatment of glioma: A pilot study in a rat model. *Journal of Materials Science: Materials in Medicine*, *21*(4), 1393–1402. https://doi.org/10.1007/s10856-009-3803-4

Barbarite, E., Sick, J. T., Berchmans, E., Bregy, A., Shah, A. H., Elsayyad, N., &

Komotar, R. J. (2017). The role of brachytherapy in the treatment of glioblastoma multiforme. *Neurosurgical Review*, *40*(2), 195–211. https://doi.org/10.1007/s10143-016-0727-6

Bartzatt, R. (2013). Lomustine Analogous Drug Structures for Intervention of Brain and Spinal Cord Tumors: The Benefit of In Silico Substructure Search and Analysis. *Chemotherapy Research and Practice*, *2013*, 1–7. https://doi.org/10.1155/2013/360624

Bassand, C., Freitag, J., Benabed, L., Verin, J., Siepmann, F., & Siepmann, J. (2022). PLGA implants for controlled drug release: Impact of the diameter. *European Journal of Pharmaceutics and Biopharmaceutics*, *177*(March), 50–60. https://doi.org/10.1016/j.ejpb.2022.05.020

Bastiancich, C., Bozzato, E., Henley, I., & Newland, B. (2021). Does local drug delivery still hold therapeutic promise for brain cancer ? A systematic review. *Journal of Controlled Release*, *337*(March), 296–305. https://doi.org/10.1016/j.jconrel.2021.07.031

Batchelor, T. T., Gilbert, M. R., Supko, J. G., Carson, K. A., Nabors, L. B., Grossman, S. A., Lesser, G. J., Mikkelsen, T., & Phuphanich, S. (2004). Phase 2 study of weekly irinotecan in adults with recurrent malignant glioma: Final report of NABTT 97-11. *Neuro-Oncology*, *6*(1), 21–27. https://doi.org/10.1215/S1152851703000218

Batista, L. F. Z., Roos, W. P., Christmann, M., Menck, C. F. M., & Kaina, B. (2007). Differential sensitivity of malignant glioma cells to methylating and chloroethylating anticancer drugs: p53 determines the switch by regulating xpc,

ddb2, and DNA double-strand breaks. *Cancer Research*, *67*(24), 11886–11895. https://doi.org/10.1158/0008-5472.CAN-07-2964

Béduneau, A., Saulnier, P., & Benoit, J. P. (2007). Active targeting of brain tumors using nanocarriers. *Biomaterials*, *28*(33), 4947–4967. https://doi.org/10.1016/j.biomaterials.2007.06.011

Benhabbour, S. R., Kovarova, M., Jones, C., Copeland, D. J., Shrivastava, R., Swanson, M. D., Sykes, C., Ho, P. T., Cottrell, M. L., Sridharan, A., Fix, S. M., Thayer, O., Long, J. M., Hazuda, D. J., Dayton, P. A., Mumper, R. J., Kashuba, A. D. M., & Victor Garcia, J. (2019). Ultra-long-acting tunable biodegradable and removable controlled release implants for drug delivery. *Nature Communications*, *10*(1), 4324. https://doi.org/10.1038/s41467-019-12141-5

Berchane, N. S., Carson, K. H., Rice-Ficht, A. C., & Andrews, M. J. (2007). Effect of mean diameter and polydispersity of PLG microspheres on drug release: Experiment and theory. *International Journal of Pharmaceutics*, *337*(1–2), 118–126. https://doi.org/10.1016/j.ijpharm.2006.12.037

Bhandari, M., Gandhi, A. K., Devnani, B., Kumar, P., Sharma, D. N., & Julka, P. K. (2017). Comparative study of adjuvant temozolomide six cycles versus extended 12 cycles in newly diagnosed glioblastoma multiforme. *Journal of Clinical and Diagnostic Research*, *11*(5), XC04–XC08. https://doi.org/10.7860/JCDR/2017/27611.9945

Bhatti, H., & Tadi, P. (2023). Pitavastatin. In *StatPearls*. http://www.ncbi.nlm.nih.gov/pubmed/28130659

Bianco, J., Bastiancich, C., Jankovski, A., des Rieux, A., Préat, V., & Danhier, F.

(2017). On glioblastoma and the search for a cure: where do we stand? *Cellular and Molecular Life Sciences*, *74*(13), 2451–2466. https://doi.org/10.1007/s00018-017-2483-3

Bode, C., Kranz, H., Fivez, A., Siepmann, F., & Siepmann, J. (2019). Often neglected: PLGA/PLA swelling orchestrates drug release: HME implants. *Journal of Controlled Release*, *306*(May), 97–107. https://doi.org/10.1016/j.jconrel.2019.05.039

Bokstein, F., Shpigel, S., & Blumenthal, D. T. (2008). Treatment with bevacizumab and irinotecan for recurrent high-grade glial tumors. *Cancer*, *112*(10), 2267–2273. https://doi.org/10.1002/cncr.23401

Bondy, M. L., Scheurer, M. E., Malmer, B., Barnholtz-Sloan, J. S., Davis, F. G., Il'yasova, D., Kruchko, C., Mccarthy, B. J., Rajaraman, P., Schwartzbaum, J. A., Sadetzki, S., Schlehofer, B., Tihan, T., Wiemels, J. L., Wrensch, M., & Buffler, P. A. (2008). *Brain Tumor Epidemiology: Consensus From the Brain Tumor Epidemiology Consortium On behalf of the Brain Tumor Epidemiology Consortium*. https://doi.org/10.1002/cncr.23741

Bota, D. A., Desjardins, A., Quinn, J. A., Affronti, M. L., & Friedman, H. S. (2007). Interstitial chemotherapy with biodegradable BCNU (Gliadel®) wafers in the treatment of malignant gliomas. *Therapeutics and Clinical Risk Management*, *3*(5), 707–715.

Brachman, D. G., Youssef, E., Dardis, C. J., Sanai, N., Zabramski, J. M., Smith, K. A., Little, A. S., Shetter, A. G., Thomas, T., McBride, H. L., Sorensen, S., Spetzler, R. F., & Nakaji, P. (2019). Resection and permanent intracranial

brachytherapy using modular, biocompatible cesium-131 implants: Results in 20 recurrent, previously irradiated meningiomas. *Journal of Neurosurgery*, *131*(6), 1819–1828. https://doi.org/10.3171/2018.7.JNS18656

Brachman, D., Youssef, E., Dardis, C., Smith, K., Pinnaduwage, D., & Nakaji, P. (2019). Surgically Targeted Radiation Therapy: Safety Profile of Collagen Tile Brachytherapy in 79 Recurrent, Previously Irradiated Intracranial Neoplasms on a Prospective Clinical Trial. *Brachytherapy*, *18*(3), S35–S36. https://doi.org/10.1016/j.brachy.2019.04.076

Brandes, A. A., Finocchiaro, G., Zagonel, V., Reni, M., Caserta, C., Fabi, A., Clavarezza, M., Maiello, E., Eoli, M., Lombardi, G., Monteforte, M., Proietti, E., Agati, R., Eusebi, V., & Franceschi, E. (2016). AVAREG: a phase II, randomized, noncomparative study of fotemustine or bevacizumab for patients with recurrent glioblastoma. *Neuro-Oncology*, *18*(9), 1304–1312. https://doi.org/10.1093/neuonc/now035

Brandes, A. A., Tosoni, A., Basso, U., Reni, M., Valduga, F., Monfardini, S., Amistà, P., Nicolardi, L., Sotti, G., & Ermani, M. (2004). Second-Line Chemotherapy With Irinotecan Plus Carmustine in Glioblastoma Recurrent or Progressive After First-Line Temozolomide Chemotherapy: A Phase II Study of the Gruppo Italiano Cooperativo di Neuro-Oncologia (GICNO). *Journal of Clinical Oncology*, *22*(23), 4779–4786. https://doi.org/10.1200/JCO.2004.06.181

Breitenbach, J. (2002a). Melt extrusion: from process to drug delivery technology. *European Journal of Pharmaceutics and Biopharmaceutics*, *54*(2), 107–117. https://doi.org/10.1016/S0939-6411(02)00061-9

Breitenbach, J. (2002b). Melt extrusion: from process to drug delivery technology. *European Journal of Pharmaceutics and Biopharmaceutics*, *54*(2), 107–117. https://doi.org/10.1016/S0939-6411(02)00061-9

Brem, H., Piantadosi, S., Burger, P. C., Walker, M., Selker, R., Vick, N. A., Black, K., Sisti, M., Brem, S., Mohr, G., Muller, P., Morawetz, R., & Schold, S. C. (1995). Placebo-controlled trial of safety and efficacy of intraoperative controlled delivery by biodegradable polymers of chemotherapy for recurrent gliomas. *The Lancet*, *345*(8956), 1008–1012. https://doi.org/10.1016/S0140-6736(95)90755-6

Brennan, C. W., Verhaak, R. G. W., McKenna, A., Campos, B., Noushmehr, H., Salama, S. R., Zheng, S., Chakravarty, D., Sanborn, J. Z., Berman, S. H., Beroukhim, R., Bernard, B., Wu, C.-J., Genovese, G., Shmulevich, I., Barnholtz-Sloan, J., Zou, L., Vegesna, R., Shukla, S. A., … McLendon, R. (2013). The Somatic Genomic Landscape of Glioblastoma. *Cell*, *155*(2), 462–477. https://doi.org/10.1016/j.cell.2013.09.034

Brown, L., Munoz, C., Siemer, L., Edelman, E., & Langer, R. (1986). Controlled Release of Insulin From Polymer Matrices: Control of Diabetes in Rats. *Diabetes*, *35*(6), 692–697. https://doi.org/10.2337/diab.35.6.692

Buckner, J. C., Brown, P. D., O'Neill, B. P., Meyer, F. B., Wetmore, C. J., & Uhm, J. H. (2007a). Central nervous system tumors. *Mayo Clinic Proceedings*, *82*(10), 1271–1286. https://doi.org/10.4065/82.10.1271

Buckner, J. C., Brown, P. D., O'Neill, B. P., Meyer, F. B., Wetmore, C. J., & Uhm, J. H. (2007b). Central Nervous System Tumors. *Mayo Clinic Proceedings*, *82*(10), 1271–1286. https://doi.org/10.4065/82.10.1271

Buckner, J. C., Reid, J. M., Wright, K., Kaufmann, S. H., Erlichman, C., Ames, M., Cha, S., O'Fallon, J. R., Schaaf, L. J., & Miller, L. L. (2003). Irinotecan in the treatment of glioma patients. *Cancer*, *97*(S9), 2352–2358. https://doi.org/10.1002/cncr.11304

Burgess, D. J., Hussain, A. S., Ingallinera, T. S., & Chen, M.-L. (2002). Assuring quality and performance of sustained and controlled release parenterals: AAPS workshop report, co-sponsored by FDA and USP. *Pharmaceutical Research*, *19*(11), 1761–1768. https://doi.org/10.1023/a:1020730102176

Campanella, O. H., Li, P. X., Ross, K. A., & Okos, M. R. (2002). The Role of Rheology in Extrusion. In *Engineering and Food for the 21st Century* (Issue January 2003, pp. 423–444). CRC Press. https://doi.org/10.1201/9781420010169-34

Canoll, P., & Goldman, J. E. (2008). The interface between glial progenitors and gliomas. *Acta Neuropathologica*, *116*(5), 465–477. https://doi.org/10.1007/s00401-008-0432-9

Capper, D., Jones, D. T. W., Sill, M., Hovestadt, V., Schrimpf, D., Sturm, D., Koelsche, C., Sahm, F., Chavez, L., Reuss, D. E., Kratz, A., Wefers, A. K., Huang, K., Pajtler, K. W., Schweizer, L., Stichel, D., Olar, A., Engel, N. W., Lindenberg, K., … Pfister, S. M. (2018). DNA methylation-based classification of central nervous system tumours. *Nature*, *555*(7697), 469–474. https://doi.org/10.1038/nature26000

Casalini, T., Bassas-Galia, M., Girard, H., Castrovinci, A., De Carolis, A., Brianza, S., Zinn, M., & Perale, G. (2019). A systematic experimental and computational

analysis of commercially available aliphatic polyesters. *Applied Sciences (Switzerland)*, *9*(16). https://doi.org/10.3390/app9163397

Ceccarelli, M., Barthel, F. P., Malta, T. M., Sabedot, T. S., Salama, S. R., Murray, B. A., Morozova, O., Newton, Y., Radenbaugh, A., Pagnotta, S. M., Anjum, S., Wang, J., Manyam, G., Zoppoli, P., Ling, S., Rao, A. A., Grifford, M., Cherniack, A. D., Zhang, H., … Verhaak, R. G. W. (2016). Molecular Profiling Reveals Biologically Discrete Subsets and Pathways of Progression in Diffuse Glioma. *Cell*, *164*(3), 550–563. https://doi.org/10.1016/j.cell.2015.12.028

Cevher, E., Orhan, Z., Şensoy, D., Ahiskali, R., Kan, P. L., Sağirli, O., & Mülazimoğlu, L. (2007). Sodium fusidate-poly(<scp>D,L</scp> -lactide- *co* -glycolide) microspheres: Preparation, characterisation and *in vivo* evaluation of their effectiveness in the treatment of chronic osteomyelitis. *Journal of Microencapsulation*, *24*(6), 577–595. https://doi.org/10.1080/02652040701472584

Chakroun, R. W., Zhang, P., Lin, R., Schiapparelli, P., Quinones-Hinojosa, A., & Cui, H. (2018). Nanotherapeutic systems for local treatment of brain tumors. *Wiley Interdisciplinary Reviews. Nanomedicine and Nanobiotechnology*, *10*(1), 1–41. https://doi.org/10.1002/wnan.1479

Chamberlain, M. C. (2002). Salvage chemotherapy with CPT-11 for recurrent glioblastoma multiforme. *Journal of Neuro-Oncology*, *56*(2), 183–188. https://doi.org/10.1023/A:1014532202188

Chandran, S., & Singh, R. S. P. (2007). Comparison of various international guidelines for analytical method validation. *Die Pharmazie*, *62*(1), 4–14.

http://www.ncbi.nlm.nih.gov/pubmed/17294806

Chen, W. N., Shaikh, M. F., Bhuvanendran, S., Date, A., Ansari, M. T., Radhakrishnan, A. K., & Othman, I. (2022). Poloxamer 188 (P188), A Potential Polymeric Protective Agent for Central Nervous System Disorders: A Systematic Review. *Current Neuropharmacology*, *20*(4), 799–808. https://doi.org/10.2174/1570159X19666210528155801

Chinna Babu, P., Sundaraganesan, N., Sudha, S., Aroulmoji, V., & Murano, E. (2012). Molecular structure and vibrational spectra of Irinotecan: A density functional theoretical study. *Spectrochimica Acta - Part A: Molecular and Biomolecular Spectroscopy*, *98*, 1–6. https://doi.org/10.1016/j.saa.2012.08.005

Chinot, O. L., Barrié, M., Fuentes, S., Eudes, N., Lancelot, S., Metellus, P., Muracciole, X., Braguer, D., Ouafik, L., Martin, P.-M., Dufour, H., & Figarella-Branger, D. (2007). Correlation between O6-methylguanine-DNA methyltransferase and survival in inoperable newly diagnosed glioblastoma patients treated with neoadjuvant temozolomide. *Journal of Clinical Oncology : Official Journal of the American Society of Clinical Oncology*, *25*(12), 1470–1475. https://doi.org/10.1200/JCO.2006.07.4807

Clarke, J., Butowski, N., & Chang, S. (2010). Recent Advances in Therapy for Glioblastoma. *Archives of Neurology*, *67*(3). https://doi.org/10.1001/archneurol.2010.5

Cloughesy, T. F., Filka, E., Kuhn, J., Nelson, G., Kabbinavar, F., Friedman, H., Miller, L. L., & Elfring, G. L. (2003). Two studies evaluating irinotecan treatment for recurrent malignant glioma using an every-3-week regimen. *Cancer*, *97*(S9),

2381–2386. https://doi.org/10.1002/cncr.11306

Cloughesy, T. F., Filka, E., Nelson, G., Kabbinavar, F., Friedman, H., Miller, L. L., & Elfring, G. L. (2002). Irinotecan Treatment for Recurrent Malignant Glioma Using an Every-3-Week Regimen. *American Journal of Clinical Oncology*, *25*(2), 204–208. https://doi.org/10.1097/00000421-200204000-00022

Corso, C. D., & Bindra, R. S. (2016). Success and Failures of Combined Modalities in Glioblastoma Multiforme: Old Problems and New Directions. *Seminars in Radiation Oncology*, *26*(4), 281–298. https://doi.org/10.1016/j.semradonc.2016.06.003

Crowley, M. M., Schroeder, B., Fredersdorf, A., Obara, S., Talarico, M., Kucera, S., & McGinity, J. W. (2004). Physicochemical properties and mechanism of drug release from ethyl cellulose matrix tablets prepared by direct compression and hot-melt extrusion. *International Journal of Pharmaceutics*, *269*(2), 509–522. https://doi.org/10.1016/j.ijpharm.2003.09.037

Cruickshank, G., Fayeye, O., Ngoga, D., Connor, J., & Detta, A. (2015). ATNT-05INTRAOPERATIVE INTRAPARENCHYMAL INJECTION OF IRINOTECAN DRUG LOADED BEADS IN PATIENTS WITH RECURRENT GLIOBLASTOMA (GBM): A SAFE NEW DEPOT APPROACH FOR LOCO-REGIONAL THERAPY (NCT02433392). *Neuro-Oncology*, *17*(suppl 5), v11.1-v11. https://doi.org/10.1093/neuonc/nov205.05

Curry, D. J., Wright, D. A., Lee, R. C., Kang, U. J., & Frim, D. M. (2004). Poloxamer 188 Volumetrically Decreases Neuronal Loss in the Rat in a Time-dependent Manner. *Neurosurgery*, *55*(4), 943–949.

https://doi.org/10.1227/01.NEU.0000137890.29862.2C

D'Alessio, A., Proietti, G., Sica, G., & Scicchitano, B. M. (2019). Pathological and molecular features of glioblastoma and its peritumoral tissue. *Cancers*, *11*(4). https://doi.org/10.3390/cancers11040469

Dash, A., & Cudworth, G. (1998). Therapeutic applications of implantable drug delivery systems. *Journal of Pharmacological and Toxicological Methods*, *40*(1), 1–12. https://doi.org/10.1016/S1056-8719(98)00027-6

Davignon, J. (2012). Pleiotropic effects of pitavastatin. *British Journal of Clinical Pharmacology*, *73*(4), 518–535. https://doi.org/10.1111/j.1365-2125.2011.04139.x

Day, S. E., & Waziri, A. (2012). Clinical trials of small molecule inhibitors in high-grade glioma. *Neurosurgery Clinics of North America*, *23*(3), 407–416. https://doi.org/10.1016/j.nec.2012.04.004

De Bonis, P., Anile, C., Pompucci, A., Fiorentino, A., Balducci, M., Chiesa, S., Lauriola, L., Maira, G., & Mangiola, A. (2013). The influence of surgery on recurrence pattern of glioblastoma. *Clinical Neurology and Neurosurgery*, *115*(1), 37–43. https://doi.org/10.1016/j.clineuro.2012.04.005

De Souza, R., Zahedi, P., Allen, C. J., & Piquette-Miller, M. (2010). Polymeric drug delivery systems for localized cancer chemotherapy. *Drug Delivery*, *17*(6), 365–375. https://doi.org/10.3109/10717541003762854

De Wolf, E., Abdullah, M. I., Jones, S. M., Menezes, K., Moss, D. M., Drijfhout, F. P., Hart, S. R., Hoskins, C., Stronach, E. A., & Richardson, A. (2017). Dietary

geranylgeraniol can limit the activity of pitavastatin as a potential treatment for drug-resistant ovarian cancer. *Scientific Reports*, *7*(1), 1–10. https://doi.org/10.1038/s41598-017-05595-4

Desai, A., & Lee, M. (2008). Book Review: Gibaldi's Drug Delivery Systems in Pharmaceutical Care. *Annals of Pharmacotherapy*, *42*(7–8), 1149–1149. https://doi.org/10.1345/aph.1L012

DESAI, K., MALLERY, S., & SCHWENDEMAN, S. (2008). Effect of formulation parameters on 2-methoxyestradiol release from injectable cylindrical poly(dl-lactide-co-glycolide) implants. *European Journal of Pharmaceutics and Biopharmaceutics*, *70*(1), 187–198. https://doi.org/10.1016/j.ejpb.2008.03.007

Dhore, P. W., Dave, V. S., Saoji, S. D., Gupta, D., & Raut, N. A. (2017). Influence of carrier (Polymer) type and drug-carrier ratio in the development of amorphous dispersions for solubility and permeability enhancement of ritonavir. *Journal of Excipients and Food Chemicals*, *8*(3), 75–92.

Di Bonaventura, R., Montano, N., Giordano, M., Gessi, M., Gaudino, S., Izzo, A., Mattogno, P. P., Stumpo, V., Caccavella, V. M., Giordano, C., Lauretti, L., Colosimo, C., D'Alessandris, Q. G., Pallini, R., & Olivi, A. (2021). Reassessing the Role of Brain Tumor Biopsy in the Era of Advanced Surgical, Molecular, and Imaging Techniques—A Single-Center Experience with Long-Term Follow-Up. *Journal of Personalized Medicine*, *11*(9), 909. https://doi.org/10.3390/jpm11090909

Diaz, R. J., Ali, S., Qadir, M. G., De La Fuente, M. I., Ivan, M. E., & Komotar, R. J. (2017). The role of bevacizumab in the treatment of glioblastoma. *Journal of*

Neuro-Oncology, *133*(3), 455–467. https://doi.org/10.1007/s11060-017-2477-x

Dixit, S., Baker, L., Walmsley, V., & Hingorani, M. (2012). Temozolomide-related idiosyncratic and other uncommon toxicities. *Anti-Cancer Drugs*, *23*(10), 1099–1106. https://doi.org/10.1097/CAD.0b013e328356f5b0

Do, M. P., Neut, C., Metz, H., Delcourt, E., Mäder, K., Siepmann, J., & Siepmann, F. (2015). In-situ forming composite implants for periodontitis treatment: How the formulation determines system performance. *International Journal of Pharmaceutics*, *486*(1–2), 38–51. https://doi.org/10.1016/j.ijpharm.2015.03.026

Domb, A. J., Israel, Z. H., Elmalak, O., Teomim, D., & Bentolila, A. (1999). Preparation and characterization of carmustine loaded polyanhydride wafers for treating brain tumors. *Pharmaceutical Research*, *16*(5), 762–765. https://doi.org/10.1023/a:1011995728760

Domb, A. J., Rock, M., Perkin, C., Yipchuck, G., Broxup, B., & Villemure, J. G. (1995). Excretion of a radiolabelled anticancer biodegradable polymeric implant from the rabbit brain. *Biomaterials*, *16*(14), 1069–1072. https://doi.org/10.1016/0142-9612(95)98902-Q

Dorta, M. J., Santoveña, A., Llabrés, M., & Fariña, J. B. (2002). Potential applications of PLGA film-implants in modulating in vitro drugs release. *International Journal of Pharmaceutics*, *248*(1–2), 149–156. https://doi.org/10.1016/S0378-5173(02)00431-3

Dronkert, M. L. G., & Kanaar, R. (2001). Repair of DNA interstrand cross-links. In *Mutation Research - DNA Repair* (Vol. 486, Issue 4). https://doi.org/10.1016/S0921-8777(01)00092-1

Duque, L., Körber, M., & Bodmeier, R. (2018). Improving release completeness from PLGA-based implants for the acid-labile model protein ovalbumin. *International Journal of Pharmaceutics*, *538*(1–2), 139–146. https://doi.org/10.1016/j.ijpharm.2018.01.026

Duwa, R., Emami, F., Lee, S., Jeong, J.-H., & Yook, S. (2019). Polymeric and lipid-based drug delivery systems for treatment of glioblastoma multiforme. *Journal of Industrial and Engineering Chemistry*, *79*(November), 261–273. https://doi.org/10.1016/j.jiec.2019.06.050

Ellor, S. V., Pagano-Young, T. A., & Avgeropoulos, N. G. (2014). Glioblastoma: background, standard treatment paradigms, and supportive care considerations. *J Law Med Ethics.*, *42*(2), 171–182. https://doi.org/10.1111/jlme.12133

Enayati, M., Mobedi, H., Hojjati-Emami, S., Mirzadeh, H., & Jafari-Nodoushan, M. (2017). In situ forming PLGA implant for 90 days controlled release of leuprolide acetate for treatment of prostate cancer. *Polymers for Advanced Technologies*, *28*(7), 867–875. https://doi.org/10.1002/pat.3991

Engelhard, H. H. (2000). The role of interstitial BCNU chemotherapy in the treatment of malignant glioma. *Surgical Neurology*, *53*(5), 458–464. https://doi.org/10.1016/S0090-3019(00)00211-1

Esteller, M., Garcia-Foncillas, J., Andion, E., Goodman, S. N., Hidalgo, O. F., Vanaclocha, V., Baylin, S. B., & Herman, J. G. (2000). Inactivation of the DNA-repair gene MGMT and the clinical response of gliomas to alkylating agents. *The New England Journal of Medicine*, *343*(19), 1350–1354. https://doi.org/10.1056/NEJM200011093431901

Externbrink, A., Eggenreich, K., Eder, S., Mohr, S., Nickisch, K., & Klein, S. (2017). Development and evaluation of accelerated drug release testing methods for a matrix-type intravaginal ring. *European Journal of Pharmaceutics and Biopharmaceutics*, *110*, 1–12. https://doi.org/10.1016/j.ejpb.2016.10.012

Fabbro-Peray, P., Zouaoui, S., Darlix, A., Fabbro, M., Pallud, J., Rigau, V., Mathieu-Daude, H., Bessaoud, F., Bauchet, F., Riondel, A., Sorbets, E., Charissoux, M., Amelot, A., Mandonnet, E., Figarella-Branger, D., Duffau, H., Tretarre, B., Taillandier, L., & Bauchet, L. (2019). Association of patterns of care, prognostic factors, and use of radiotherapy–temozolomide therapy with survival in patients with newly diagnosed glioblastoma: a French national population-based study. *Journal of Neuro-Oncology*, *142*(1), 91–101. https://doi.org/10.1007/s11060-018-03065-z

Fan, Y., Nguyen, D. T., Akay, Y., Xu, F., & Akay, M. (2016). Engineering a Brain Cancer Chip for High-throughput Drug Screening. *Scientific Reports*, *6*(1), 25062. https://doi.org/10.1038/srep25062

Fanous, M., Gold, S., Hirsch, S., Ogorka, J., & Imanidis, G. (2020). Development of immediate release (IR) 3D-printed oral dosage forms with focus on industrial relevance. *European Journal of Pharmaceutical Sciences*, *155*(March), 105558. https://doi.org/10.1016/j.ejps.2020.105558

Fenton, O. S., Olafson, K. N., Pillai, P. S., Mitchell, M. J., & Langer, R. (2018). Advances in Biomaterials for Drug Delivery. *Advanced Materials*, *30*(29), 1705328. https://doi.org/10.1002/adma.201705328

Ferreira, C., Sterling, D., Reynolds, M., Dusenbery, K., Chen, C., & Alaei, P. (2021).

First clinical implementation of GammaTile permanent brain implants after FDA clearance. *Brachytherapy*, *20*(3), 673–685. https://doi.org/10.1016/j.brachy.2020.12.005

Fialho, S. L., & Silva Cunha, A. da. (2005). Manufacturing Techniques of Biodegradable Implants Intended for Intraocular Application. *Drug Delivery*, *12*(2), 109–116. https://doi.org/10.1080/10717540590921432

Figarella-Branger, D., Appay, R., Metais, A., Tauziède-Espariat, A., Colin, C., Rousseau, A., & Varlet, P. (2022). La classification de l'OMS 2021 des tumeurs du système nerveux central. *Annales de Pathologie*, *42*(5), 367–382. https://doi.org/10.1016/j.annpat.2021.11.005

Fisher, J. L., Schwartzbaum, J. A., Wrensch, M., & Wiemels, J. L. (2007). Epidemiology of Brain Tumors. *Neurologic Clinics*, *25*(4), 867–890. https://doi.org/10.1016/J.NCL.2007.07.002

Fița, A. C., Secăreanu, A. A., Musuc, A. M., Ozon, E. A., Sarbu, I., Atkinson, I., Rusu, A., Mati, E., Anuta, V., & Pop, A. L. (2022). The Influence of the Polymer Type on the Quality of Newly Developed Oral Immediate-Release Tablets Containing Amiodarone Solid Dispersions Obtained by Hot-Melt Extrusion. *Molecules*, *27*(19), 6600. https://doi.org/10.3390/molecules27196600

Fleming, A. B., & Saltzman, W. M. (2002). Pharmacokinetics of the carmustine implant. *Clinical Pharmacokinetics*, *41*(6), 403–419. https://doi.org/10.2165/00003088-200241060-00002

Florio, T., & Barbieri, F. (2012). The status of the art of human malignant glioma management: The promising role of targeting tumor-initiating cells. *Drug*

Discovery Today, *17*(19–20), 1103–1110. https://doi.org/10.1016/j.drudis.2012.06.001

Folkman, J., & Long, D. M. (1964). The use of silicone rubber as a carrier for prolonged drug therapy. *Journal of Surgical Research*, *4*(3), 139–142. https://doi.org/10.1016/S0022-4804(64)80040-8

Follonier, N., Doelker, E., & Cole, E. T. (1994). Evaluation of hot-melt extrusion as a new technique for the production of polymer-based pellets for sustained release capsules containing high loadings of freely soluble drugs. *Drug Development and Industrial Pharmacy*, *20*(8), 1323–1339. https://doi.org/10.3109/03639049409038373

Fonseca, C., Simões, S., & Gaspar, R. (2002). Paclitaxel-loaded PLGA nanoparticles: preparation, physicochemical characterization and in vitro anti-tumoral activity. *Journal of Controlled Release*, *83*(2), 273–286. https://doi.org/10.1016/S0168-3659(02)00212-2

Fredenberg, S., Wahlgren, M., Reslow, M., & Axelsson, A. (2011). The mechanisms of drug release in poly(lactic-co-glycolic acid)-based drug delivery systems - A review. *International Journal of Pharmaceutics*, *415*(1–2), 34–52. https://doi.org/10.1016/j.ijpharm.2011.05.049

Friedman, H S, McLendon, R. E., Kerby, T., Dugan, M., Bigner, S. H., Henry, A. J., Ashley, D. M., Krischer, J., Lovell, S., Rasheed, K., Marchev, F., Seman, A. J., Cokgor, I., Rich, J., Stewart, E., Colvin, O. M., Provenzale, J. M., Bigner, D. D., Haglund, M. M., … Modrich, P. L. (1998). DNA mismatch repair and O6-alkylguanine-DNA alkyltransferase analysis and response to Temodal in newly

diagnosed malignant glioma. *Journal of Clinical Oncology*, *16*(12), 3851–3857. https://doi.org/10.1200/JCO.1998.16.12.3851

Friedman, Henry S., Petros, W. P., Friedman, A. H., Schaaf, L. J., Kerby, T., Lawyer, J., Parry, M., Houghton, P. J., Lovell, S., Rasheed, K., Cloughsey, T., Stewart, E. S., Colvin, O. M., Provenzale, J. M., McLendon, R. E., Bigner, D. D., Cokgor, I., Haglund, M., Rich, J., … Miller, L. L. (1999). Irinotecan Therapy in Adults With Recurrent or Progressive Malignant Glioma. *Journal of Clinical Oncology*, *17*(5), 1516–1516. https://doi.org/10.1200/JCO.1999.17.5.1516

Friedman, Henry S., Prados, M. D., Wen, P. Y., Mikkelsen, T., Schiff, D., Abrey, L. E., Yung, W. K. A., Paleologos, N., Nicholas, M. K., Jensen, R., Vredenburgh, J., Huang, J., Zheng, M., & Cloughesy, T. (2009). Bevacizumab Alone and in Combination With Irinotecan in Recurrent Glioblastoma. *Journal of Clinical Oncology*, *27*(28), 4733–4740. https://doi.org/10.1200/JCO.2008.19.8721

Fung, L K, Ewend, M. G., Sills, A., Sipos, E. P., Thompson, R., Watts, M., Colvin, O. M., Brem, H., & Saltzman, W. M. (1998). Pharmacokinetics of interstitial delivery of carmustine, 4-hydroperoxycyclophosphamide, and paclitaxel from a biodegradable polymer implant in the monkey brain. *Cancer Research*, *58*(4), 672–684. http://www.ncbi.nlm.nih.gov/pubmed/9485020

Fung, Lawrence K., & Saltzman, W. M. (1997). Polymeric implants for cancer chemotherapy. *Advanced Drug Delivery Reviews*, *26*(2–3), 209–230. https://doi.org/10.1016/S0169-409X(97)00036-7

Furnari, F. B., Fenton, T., Bachoo, R. M., Mukasa, A., Stommel, J. M., Stegh, A., Hahn, W. C., Ligon, K. L., Louis, D. N., Brennan, C., Chin, L., DePinho, R. A., &

Cavenee, W. K. (2007). Malignant astrocytic glioma: Genetics, biology, and paths to treatment. *Genes and Development*, *21*(21), 2683–2710. https://doi.org/10.1101/gad.1596707

Garrigues, A., Escargueil, A. E., & Orlowski, S. (2002). The multidrug transporter, P-glycoprotein, actively mediates cholesterol redistribution in the cell membrane. *Proceedings of the National Academy of Sciences of the United States of America*, *99*(16), 10347–10352. https://doi.org/10.1073/pnas.162366399

Gawley, M., Almond, L., Daniel, S., Lastakchi, S., Kaur, S., Detta, A., Cruickshank, G., Miller, R., Hingtgen, S., Sheets, K., & McConville, C. (2020a). Development and in vivo evaluation of Irinotecan-loaded Drug Eluting Seeds (iDES) for the localised treatment of recurrent glioblastoma multiforme. *Journal of Controlled Release*, *324*(April), 1–16. https://doi.org/10.1016/j.jconrel.2020.05.012

Gawley, M., Almond, L., Daniel, S., Lastakchi, S., Kaur, S., Detta, A., Cruickshank, G., Miller, R., Hingtgen, S., Sheets, K., & McConville, C. (2020b). Development and in vivo evaluation of Irinotecan-loaded Drug Eluting Seeds (iDES) for the localised treatment of recurrent glioblastoma multiforme. *Journal of Controlled Release*, *324*(May), 1–16. https://doi.org/10.1016/j.jconrel.2020.05.012

Gerber, D. E., Grossman, S. A., Zeltzman, M., Parisi, M. A., & Kleinberg, L. (2007). The impact of thrombocytopenia from temozolomide and radiation in newly diagnosed adults with high-grade gliomas. *Neuro-Oncology*, *9*(1), 47–52. https://doi.org/10.1215/15228517-2006-024

Gessler, D. J., Ferreira, C., Dusenbery, K., & Chen, C. C. (2020). GammaTile ®: Surgically targeted radiation therapy for glioblastomas. *Future Oncology*, *16*(30),

2445–2455. https://doi.org/10.2217/fon-2020-0558

Ghalanbor, Z., Körber, M., & Bodmeier, R. (2010). Improved Lysozyme Stability and Release Properties of Poly(lactide-co-glycolide) Implants Prepared by Hot-Melt Extrusion. *Pharmaceutical Research*, *27*(2), 371–379. https://doi.org/10.1007/s11095-009-0033-x

Ghebremeskel, A. N., Vemavarapu, C., & Lodaya, M. (2007). Use of surfactants as plasticizers in preparing solid dispersions of poorly soluble API: Selection of polymer–surfactant combinations using solubility parameters and testing the processability. *International Journal of Pharmaceutics*, *328*(2), 119–129. https://doi.org/10.1016/j.ijpharm.2006.08.010

Gilbert, M. R., Supko, J. G., Batchelor, T., Lesser, G., Fisher, J. D., Piantadosi, S., & Grossman, S. (2003). Phase I clinical and pharmacokinetic study of irinotecan in adults with recurrent malignant glioma. *Clinical Cancer Research*, *9*(8), 2940–2949.

Giordano, F. A., Brehmer, S., Mürle, B., Welzel, G., Sperk, E., Keller, A., Abo-Madyan, Y., Scherzinger, E., Clausen, S., Schneider, F., Herskind, C., Glas, M., Seiz-Rosenhagen, M., Groden, C., Hänggi, D., Schmiedek, P., Emami, B., Souhami, L., Petrecca, K., & Wenz, F. (2019). Intraoperative Radiotherapy in Newly Diagnosed Glioblastoma (INTRAGO): An Open-Label, Dose-Escalation Phase I/II Trial. *Neurosurgery*, *84*(1), 41–49. https://doi.org/10.1093/neuros/nyy018

Goel, M., Leung, D., Famili, A., Chang, D., Nayak, P., & Al-Sayah, M. (2021). Accelerated in vitro release testing method for a long-acting peptide-PLGA

formulation. *European Journal of Pharmaceutics and Biopharmaceutics*, *165*(January), 185–192. https://doi.org/10.1016/j.ejpb.2021.05.008

Goli, K. J., Desjardins, A., Herndon, J. E., Rich, J. N., Reardon, D. A., Quinn, J. A., Sathornsumetee, S., Bota, D. A., Friedman, H. S., & Vredenburgh, J. J. (2007). Phase II trial of bevacizumab and irinotecan in the treatment of malignant gliomas. *Journal of Clinical Oncology*, *25*(18_suppl), 2003–2003. https://doi.org/10.1200/jco.2007.25.18_suppl.2003

Gouda, R., Baishya, H., & Qing, Z. (2017). *Journal of Developing Drugs Application of Mathematical Models in Drug Release Kinetics of Carbidopa and Levodopa ER Tablets*. *6*(2), 1–8. https://doi.org/10.4172/2329-6631.1000171

Goyanes, A., Wang, J., Buanz, A., Martínez-Pacheco, R., Telford, R., Gaisford, S., & Basit, A. W. (2015). 3D Printing of Medicines: Engineering Novel Oral Devices with Unique Design and Drug Release Characteristics. *Molecular Pharmaceutics*, *12*(11), 4077–4084. https://doi.org/10.1021/acs.molpharmaceut.5b00510

Greig, N. H. (1987). Optimizing drug delivery to brain tumors. *Cancer Treatment Reviews*, *14*(1), 1–28. https://doi.org/10.1016/0305-7372(87)90048-x

Grizić, D., & Lamprecht, A. (2020). Predictability of drug encapsulation and release from propylene carbonate/PLGA microparticles. *International Journal of Pharmaceutics*, *586*(June), 119601. https://doi.org/10.1016/j.ijpharm.2020.119601

Grizzi, I., Garreau, H., Li, S., & Vert, M. (1995). Hydrolytic degradation of devices based on poly(dl-lactic acid) size-dependence. *Biomaterials*, *16*(4), 305–311.

https://doi.org/10.1016/0142-9612(95)93258-F

Grochans, S., Cybulska, A. M., Simińska, D., Korbecki, J., Kojder, K., Chlubek, D., & Baranowska-Bosiacka, I. (2022). Epidemiology of Glioblastoma Multiforme–Literature Review. *Cancers*, *14*(10). https://doi.org/10.3390/cancers14102412

Grohganz, H., Löbmann, K., Priemel, P., Tarp Jensen, K., Graeser, K., Strachan, C., & Rades, T. (2013). Amorphous drugs and dosage forms. *Journal of Drug Delivery Science and Technology*, *23*(4), 403–408. https://doi.org/10.1016/S1773-2247(13)50057-8

Grossman, S. A., Reinhard, C., Colvin, O. M., Chasin, M., Brundrett, R., Tamargo, R. J., & Brem, H. (1992). The intracerebral distribution of BCNU delivered by surgically implanted biodegradable polymers. *Journal of Neurosurgery*, *76*(4), 640–647. https://doi.org/10.3171/jns.1992.76.4.0640

Gruber, M. L., & Buster, W. P. (2004). Temozolomide in Combination With Irinotecan for Treatment of Recurrent Malignant Glioma. *American Journal of Clinical Oncology*, *27*(1), 33–38. https://doi.org/10.1097/01.coc.0000045852.88461.80

Grund, S., Bauer, M., & Fischer, D. (2011). Polymers in Drug Delivery-State of the Art and Future Trends. *Advanced Engineering Materials*, *13*(3), B61–B87. https://doi.org/10.1002/adem.201080088

Guedes, J. da S., & Guedes, M. L. da S. (2006). Quantificação do indicador de Nelson de Moraes (curva de mortalidade proporcional). *Revista de Saúde Pública*, *40*(6), 951–961. https://doi.org/10.1590/S0034-89102006000700002

Guo, D., Reinitz, F., Youssef, M., Hong, C., Nathanson, D., Akhavan, D., Kuga, D.,

Amzajerdi, A. N., Soto, H., Zhu, S., Babic, I., Tanaka, K., Dang, J., Iwanami, A., Gini, B., DeJesus, J., Lisiero, D. D., Huang, T. T., Prins, R. M., … Mischel, P. S. (2011). An LXR Agonist Promotes Glioblastoma Cell Death through Inhibition of an EGFR/AKT/SREBP-1/LDLR–Dependent Pathway. *Cancer Discovery*, *1*(5), 442–456. https://doi.org/10.1158/2159-8290.CD-11-0102

Guo, X., Shi, Y., Liu, D., Li, Y., Chen, W., Wang, Y., Wang, Y., Xing, H., Xia, Y., Li, J., Wu, J., Liang, T., Wang, H., Liu, Q., Jin, S., Qu, T., Guo, S., Li, H., Yang, T., … Ma, W. (2023). Clinical updates on gliomas and implications of the 5th edition of the WHO classification of central nervous system tumors. *Frontiers in Oncology*, *13*(March), 1131642. https://doi.org/10.3389/fonc.2023.1131642

Gupta, S. S., Meena, A., Parikh, T., & Serajuddin, A. T. M. (2014). Investigation of thermal and viscoelastic properties of polymers relevant to hot melt extrusion - I: Polyvinylpyrrolidone and related polymers. *Journal of Excipients and Food Chemicals*, *5*(1), 32–45.

Gupta, S. S., Parikh, T., Meena, A. K., Mahajan, N., Vitez, I., & Serajuddin, A. T. M. (2015). Effect of carbamazepine on viscoelastic properties and hot melt extrudability of Soluplus®. *International Journal of Pharmaceutics*, *478*(1), 232–239. https://doi.org/10.1016/j.ijpharm.2014.11.025

Gupta, S. S., Solanki, N., & Serajuddin, A. T. M. (2016). Investigation of Thermal and Viscoelastic Properties of Polymers Relevant to Hot Melt Extrusion, IV: Affinisol™ HPMC HME Polymers. *AAPS PharmSciTech*, *17*(1), 148–157. https://doi.org/10.1208/s12249-015-0426-6

Hamoudi-Ben Yelles, M. C., Tran Tan, V., Danede, F., Willart, J. F., & Siepmann, J.

(2017). PLGA implants: How Poloxamer/PEO addition slows down or accelerates polymer degradation and drug release. *Journal of Controlled Release*, *253*, 19–29. https://doi.org/10.1016/j.jconrel.2017.03.009

Han, D., Serra, R., Gorelick, N., Fatima, U., Eberhart, C. G., Brem, H., Tyler, B., & Steckl, A. J. (2019). Multi-layered core-sheath fiber membranes for controlled drug release in the local treatment of brain tumor. *Scientific Reports*, *9*(1), 17936. https://doi.org/10.1038/s41598-019-54283-y

Hanif, F., Muzaffar, K., Perveen, K., Malhi, S. M., & Simjee, S. U. (2017). Glioblastoma multiforme: A review of its epidemiology and pathogenesis through clinical presentation and treatment. *Asian Pacific Journal of Cancer Prevention*, *18*(1), 3–9. https://doi.org/10.22034/APJCP.2017.18.1.3

Harron, D. W. G. (2013). Technical Requirements for Registration of Pharmaceuticals for Human Use: The ICH Process. In *The Textbook of Pharmaceutical Medicine* (Vol. 1994, Issue November 1996, pp. 447–460). Blackwell Publishing Ltd. https://doi.org/10.1002/9781118532331.ch23

Hasselbalch, B., Lassen, U., Hansen, S., Holmberg, M., Soørensen, M., Kosteljanetz, M., Broholm, H., Stockhausen, M. T., & Poulsen, H. S. (2010). Cetuximab, bevacizumab, and irinotecan for patients with primary glioblastoma and progression after radiation therapy and temozolomide: A phase II trial. *Neuro-Oncology*, *12*(5), 508–516. https://doi.org/10.1093/neuonc/nop063

Hauck, M., Hellmold, D., Kubelt, C., Synowitz, M., Adelung, R., Schütt, F., & Held-Feindt, J. (2022). Localized Drug Delivery Systems in High-Grade Glioma Therapy—From Construction to Application. *Advanced Therapeutics*, *5*(8),

2200013. https://doi.org/10.1002/adtp.202200013

He, X., Yuan, Z., Gaeke, S., Kao, W. W., Li, S. K., Miller, D., Williams, B., & Park, Y. C. (2021). *Laser-Activated Drug Implant for Controlled Release to the Posterior Segment of the Eye*. https://doi.org/10.1021/acsabm.0c01334

Hecht, J. R. (1998). Gastrointestinal toxicity or irinotecan. *Oncology (Williston Park, N.Y.)*, *12*(8 Suppl 6), 72–78. http://www.ncbi.nlm.nih.gov/pubmed/9726096

Hegi, M. E., Diserens, A.-C., Gorlia, T., Hamou, M.-F., de Tribolet, N., Weller, M., Kros, J. M., Hainfellner, J. A., Mason, W., Mariani, L., Bromberg, J. E. C., Hau, P., Mirimanoff, R. O., Cairncross, J. G., Janzer, R. C., & Stupp, R. (2005). MGMT gene silencing and benefit from temozolomide in glioblastoma. *The New England Journal of Medicine*, *352*(10), 997–1003. https://doi.org/10.1056/NEJMoa043331

Heiland, D. H., Masalha, W., Franco, P., Machein, M. R., & Weyerbrock, A. (2016). Progression-free and overall survival in patients with recurrent Glioblastoma multiforme treated with last-line bevacizumab versus bevacizumab/lomustine. *Journal of Neuro-Oncology*, *126*(3), 567–575. https://doi.org/10.1007/s11060-015-2002-z

Highlights of prescribing information. (2016). *NextSource Biotechnology*, 1–10.

Higuchi, T. (1963). Mechanism of sustained-action medication. Theoretical analysis of rate of release of solid drugs dispersed in solid matrices. *Journal of Pharmaceutical Sciences*, *52*(12), 1145–1149. https://doi.org/10.1002/jps.2600521210

Higuchi, Takeru. (1961). Rate of Release of Medicaments from Ointment Bases Containing Drugs in Suspension. *Journal of Pharmaceutical Sciences*, *50*(10), 874–875. https://doi.org/10.1002/jps.2600501018

Hines, D. J., & Kaplan, D. L. (2013). Poly(lactic-co-glycolic) acid-controlled-release systems: Experimental and modeling insights. *Critical Reviews in Therapeutic Drug Carrier Systems*, *30*(3), 257–276. https://doi.org/10.1615/CritRevTherDrugCarrierSyst.2013006475

Hirose, Y., Berger, M. S., & Pieper, R. O. (2001). p53 effects both the duration of G2/M arrest and the fate of temozolomide-treated human glioblastoma cells. *Cancer Research*, *61*(5), 1957–1963. http://www.ncbi.nlm.nih.gov/pubmed/11280752

Hochberg, F. H., & Pruitt, A. (1980). Assumptions in the radiotherapy of glioblastoma. *Neurology*, *30*(9), 907–911. https://doi.org/10.1212/wnl.30.9.907

Hoffman, A. S. (2008). The origins and evolution of “controlled” drug delivery systems. *Journal of Controlled Release*, *132*(3), 153–163. https://doi.org/10.1016/j.jconrel.2008.08.012

Houchin, M. L., & Topp, E. M. (2008). Chemical Degradation of Peptides and Proteins in PLGA: A Review of Reactions and Mechanisms. *Journal of Pharmaceutical Sciences*, *97*(7), 2395–2404. https://doi.org/10.1002/jps.21176

Iacob, G., & Dinca, E. B. (2009). Current data and strategy in glioblastoma multiforme. *Journal of Medicine and Life*, *2*(4), 386–393. http://www.ncbi.nlm.nih.gov/pubmed/20108752

Inskip, P., Nskip, D. I., Arone, O. E. T., Atch, L. E. H., Ilcosky, I. C. W., Hapiro, I. R. S., Elker, O. G. S., Ine, O. A. F., Lack, E. M. B., Oeffler, A. S. L., Artha, M., & Inet, S. L. (2001). The New England Journal of Medicine CELLULAR-TELEPHONE USE AND BRAIN TUMORS A BSTRACT. In *N Engl J Med* (Vol. 344, Issue 2). http://www.nejm.org

ISHIMINE, M., YOKOMIZO, T., & LEE-OKADA, H.-C. (2020). Carboxylesterase 2: A Key Enzyme in Drug and Prodrug Metabolism. *Juntendo Medical Journal*, *66*(2), 120–124. https://doi.org/10.14789/jmj.2020.66.JMJ19-R18

Iyer, S. S., Barr, W. H., & Karnes, H. T. (2006). Profilingin vitro drug release from subcutaneous implants: a review of current status and potential implications on drug product development. *Biopharmaceutics & Drug Disposition*, *27*(4), 157–170. https://doi.org/10.1002/bdd.493

Jackson, J. K., Gleave, M. E., Yago, V., Beraldi, E., Hunter, W. L., & Burt, H. M. (2000). The suppression of human prostate tumor growth mice by the intratumoral injection of a slow-release polymeric paste formulation of paclitaxel. *Cancer Research*, *60*(15), 4146–4151.

Jain, R. A. (2000). The manufacturing techniques of various drug loaded biodegradable poly(lactide-co-glycolide) (PLGA) devices. *Biomaterials*, *21*(23), 2475–2490. https://doi.org/10.1016/S0142-9612(00)00115-0

Jarmużek, D., Pedzinski, T., Hoffmann, M., Siodła, T., & Pluskota-Karwatka, D. (2020). Phototransformations of pitavastatin - The inhibitor of 3-hydroxy-3-methylglutaryl coenzyme A reductase. *Journal of Photochemistry and Photobiology A: Chemistry*, *389*(November 2019), 112243.

https://doi.org/10.1016/j.jphotochem.2019.112243

Jha, P. (2020). Effect of plasticizer and antimicrobial agents on functional properties of bionanocomposite films based on corn starch-chitosan for food packaging applications. *International Journal of Biological Macromolecules*, *160*, 571–582. https://doi.org/10.1016/j.ijbiomac.2020.05.242

Jiang, P., Mukthavaram, R., Chao, Y., Nomura, N., Bharati, I. S., Fogal, V., Pastorino, S., Teng, D., Cong, X., Pingle, S. C., Kapoor, S., Shetty, K., Aggrawal, A., Vali, S., Abbasi, T., Chien, S., & Kesari, S. (2014). In vitro and in vivo anticancer effects of mevalonate pathway modulation on human cancer cells. *British Journal of Cancer*, *111*(8), 1562–1571. https://doi.org/10.1038/bjc.2014.431

Jiang, Pengfei, Mukthavaram, R., Chao, Y., Bharati, I. S., Fogal, V., Pastorino, S., Cong, X., Nomura, N., Gallagher, M., Abbasi, T., Vali, S., Pingle, S. C., Makale, M., & Kesari, S. (2014a). Correction to novel anti-glioblastoma agents and therapeutic combinations identified from a collection of FDA approved drugs [J TranslMed (2014) 12 13]. *Journal of Translational Medicine*, *12*(1), 1. https://doi.org/10.1186/1479-5876-12-126

Jiang, Pengfei, Mukthavaram, R., Chao, Y., Bharati, I. S., Fogal, V., Pastorino, S., Cong, X., Nomura, N., Gallagher, M., Abbasi, T., Vali, S., Pingle, S. C., Makale, M., & Kesari, S. (2014b). Erratum to: novel anti-glioblastoma agents and therapeutic combinations identified from a collection of FDA approved drugs. *Journal of Translational Medicine*, *12*(1), 126. https://doi.org/10.1186/1479-5876-12-126

Jin, C., Bai, L., Wu, H., Song, W., Guo, G., & Dou, K. (2009). Cytotoxicity of Paclitaxel Incorporated in PLGA Nanoparticles on Hypoxic Human Tumor Cells. *Pharmaceutical Research*, *26*(7), 1776–1784. https://doi.org/10.1007/s11095-009-9889-z

Jivraj, M., Martini, L. G., & Thomson, C. M. (2000). An overview of the different excipients useful for the direct compression of tablets. *Pharmaceutical Science & Technology Today*, *3*(2), 58–63. https://doi.org/10.1016/S1461-5347(99)00237-0

JOVČEVSKA, I., KOČEVAR, N., & KOMEL, R. (2013). Glioma and glioblastoma - how much do we (not) know? *Molecular and Clinical Oncology*, *1*(6), 935–941. https://doi.org/10.3892/mco.2013.172

Kabat, G. C., Etgen, A. M., & Rohan, T. E. (2010). Do steroid hormones play a role in the etiology of glioma? *Cancer Epidemiology Biomarkers and Prevention*, *19*(10), 2421–2427. https://doi.org/10.1158/1055-9965.EPI-10-0658

Kaina, B., Christmann, M., Naumann, S., & Roos, W. P. (2007). MGMT: key node in the battle against genotoxicity, carcinogenicity and apoptosis induced by alkylating agents. *DNA Repair*, *6*(8), 1079–1099. https://doi.org/10.1016/j.dnarep.2007.03.008

Kamaly, N., Yameen, B., Wu, J., & Farokhzad, O. C. (2016a). Degradable controlled-release polymers and polymeric nanoparticles: Mechanisms of controlling drug release. *Chemical Reviews*, *116*(4), 2602–2663. https://doi.org/10.1021/acs.chemrev.5b00346

Kamaly, N., Yameen, B., Wu, J., & Farokhzad, O. C. (2016b). Degradable Controlled-Release Polymers and Polymeric Nanoparticles: Mechanisms of Controlling

Drug Release. *Chemical Reviews*, *116*(4), 2602–2663. https://doi.org/10.1021/acs.chemrev.5b00346

Kamel, R., & Abbas, H. (2018). PLGA-based monolithic filaments prepared by hot-melt extrusion: In-vitro comparative study. *Annales Pharmaceutiques Françaises*, *76*(2), 97–106. https://doi.org/10.1016/j.pharma.2017.09.002

Kapoor, D. N., Bhatia, A., Kaur, R., Sharma, R., Kaur, G., & Dhawan, S. (2015). PLGA: A unique polymer for drug delivery. *Therapeutic Delivery*, *6*(1), 41–58. https://doi.org/10.4155/tde.14.91

Karcher, S., Steiner, H. H., Ahmadi, R., Zoubaa, S., Vasvari, G., Bauer, H., Unterberg, A., & Herold-Mende, C. (2006). Different angiogenic phenotypes in primary and secondary glioblastomas. *International Journal of Cancer*, *118*(9), 2182–2189. https://doi.org/10.1002/ijc.21648

Kayama, T., Yoshimoto, T., Fujimoto, S., & Sakurai, Y. (1991). Intratumoral oxygen pressure in malignant brain tumor. *Journal of Neurosurgery*, *74*(1), 55–59. https://doi.org/10.3171/jns.1991.74.1.0055

Kearney, C. J., & Mooney, D. J. (2013). Macroscale delivery systems for molecular and cellular payloads. *Nature Materials*, *12*(11), 1004–1017. https://doi.org/10.1038/nmat3758

Kempe, S., & Mäder, K. (2012). In situ forming implants — an attractive formulation principle for parenteral depot formulations. *Journal of Controlled Release*, *161*(2), 668–679. https://doi.org/10.1016/j.jconrel.2012.04.016

Kemper, E. M., Van Zandbergen, A. E., Cleypool, C., Mos, H. A., Boogerd, W.,

Beijnen, J. H., & Van Tellingen, O. (2003). Increased penetration of paclitaxel into the brain by inhibition of P-glycoprotein. *Clinical Cancer Research*, *9*(7), 2849–2855.

Khan, N. A. (2010). *Development and characterization of gastroretentive floating drug delivery system*. *10*(2), 146.

Khasraw, M., Lassman, A., Wheeler, H., & Pavlakis, N. (2010). Anti-angiogenic therapy for high grade glioma. In M. Khasraw (Ed.), *Cochrane Database of Systematic Reviews*. John Wiley & Sons, Ltd. https://doi.org/10.1002/14651858.CD008218

Kini, S., Bahadur, D., & Panda, D. (2015). Mechanism of Anti-Cancer Activity of Benomyl Loaded Nanoparticles in Multidrug Resistant Cancer Cells. *Journal of Biomedical Nanotechnology*, *11*(5), 877–889. https://doi.org/10.1166/jbn.2015.1998

Kleiner, L. W., Wright, J. C., & Wang, Y. (2014). Evolution of implantable and insertable drug delivery systems. *Journal of Controlled Release*, *181*(1), 1–10. https://doi.org/10.1016/j.jconrel.2014.02.006

Klose, D., Siepmann, F., Elkharraz, K., & Siepmann, J. (2008). PLGA-based drug delivery systems: Importance of the type of drug and device geometry. *International Journal of Pharmaceutics*, *354*(1–2), 95–103. https://doi.org/10.1016/j.ijpharm.2007.10.030

Kollamaram, G., Croker, D. M., Walker, G. M., Goyanes, A., Basit, A. W., & Gaisford, S. (2018). Low temperature fused deposition modeling (FDM) 3D printing of thermolabile drugs. *International Journal of Pharmaceutics*, *545*(1–2), 144–152.

https://doi.org/10.1016/j.ijpharm.2018.04.055

Kolter, K., Karl, M., & Gryczke, A. (2012). Introduction to Solid Dispersions. In *Hot-Melt Extrusion with BASF Pharma Polymers*.

Komori, T. (2023). Update of the 2021 WHO classification of tumors of the central nervous system: adult diffuse gliomas. *Brain Tumor Pathology*, *40*(1), 1–3. https://doi.org/10.1007/s10014-022-00446-1

Koo, H., Huh, M. S., Sun, I. C., Yuk, S. H., Choi, K., Kim, K., & Kwon, I. C. (2011). In vivo targeted delivery of nanoparticles for theranosis. *Accounts of Chemical Research*, *44*(10), 1018–1028. https://doi.org/10.1021/ar2000138

Korfiatis, P., & Erickson, B. (2014). The basics of diffusion and perfusion imaging in brain tumors. *Applied Radiology*, *43*(7), 22–29. https://doi.org/10.37549/ar2093

Koshy, M., Villano, J. L., Dolecek, T. A., Howard, A., Mahmood, U., Chmura, S. J., Weichselbaum, R. R., & McCarthy, B. J. (2012). Improved survival time trends for glioblastoma using the SEER 17 population-based registries. *Journal of Neuro-Oncology*, *107*(1), 207–212. https://doi.org/10.1007/s11060-011-0738-7

Koukourakis, M. I., Mitrakas, A. G., & Giatromanolaki, A. (2016). Therapeutic interactions of autophagy with radiation and temozolomide in glioblastoma: evidence and issues to resolve. *British Journal of Cancer*, *114*(5), 485–496. https://doi.org/10.1038/bjc.2016.19

Kowalska, M., Woźniak, M., Kijek, M., Mitrosz, P., Szakiel, J., & Turek, P. (2022). Management of validation of HPLC method for determination of acetylsalicylic acid impurities in a new pharmaceutical product. *Scientific Reports*, *12*(1), 1.

https://doi.org/10.1038/s41598-021-99269-x

Kreth, F. W., Thon, N., Simon, M., Westphal, M., Schackert, G., Nikkhah, G., Hentschel, B., Reifenberger, G., Pietsch, T., Weller, M., & Tonn, J. C. (2013). Gross total but not incomplete resection of glioblastoma prolongs survival in the era of radiochemotherapy. *Annals of Oncology*, *24*(12), 3117–3123. https://doi.org/10.1093/annonc/mdt388

Kristiansen, K., Hagen, S., Kollevold, T., Torvik, A., Holme, I., Stat, M., Nesbakken, R., Hatlevoll, R., Lindgren, M., Brun, A., Lindgren, S., Notter, G., Andersen, A. P., & Elgen, K. (1981). Combined modality therapy of operated astrocytomas grade III and IV. Confirmation of the value of postoperative irradiation and lack of potentiation of bleomycin on survival time: A prospective multicenter trial of the scandinavian glioblastoma study grou. *Cancer*, *47*(4), 649–652. https://doi.org/10.1002/1097-0142(19810215)47:4<649::AID-CNCR2820470405>3.0.CO;2-W

Krupka, T. M., Weinberg, B. D., Ziats, N. P., Haaga, J. R., & Exner, A. A. (2006). Injectable polymer depot combined with radiofrequency ablation for treatment of experimental carcinoma in rat. *Investigative Radiology*, *41*(12), 890–897. https://doi.org/10.1097/01.rli.0000246102.56801.2f

Kulkarni, C., Kelly, A. L., Gough, T., Jadhav, V., Singh, K. K., & Paradkar, A. (2018). Application of hot melt extrusion for improving bioavailability of artemisinin a thermolabile drug. *Drug Development and Industrial Pharmacy*, *44*(2), 206–214. https://doi.org/10.1080/03639045.2017.1386200

Kumar, N., Sangeetha, D., & Reddy, S. P. (2012). UPLC and LC-MS studies on

degradation behavior of irinotecan hydrochloride and development of a validated stability-indicating ultra-performance liquid chromatographic method for determination of irinotecan hydrochloride and its impurities in pharmaceutic. *Journal of Chromatographic Science*, *50*(9), 810–819. https://doi.org/10.1093/chromsci/bms075

Langer, R. (1990). New Methods of Drug Delivery. *Science*, *249*(4976), 1527–1533. https://doi.org/10.1126/science.2218494

Lao, L. L., Peppas, N. A., Boey, F. Y. C., & Venkatraman, S. S. (2011). Modeling of drug release from bulk-degrading polymers. *International Journal of Pharmaceutics*, *418*(1), 28–41. https://doi.org/10.1016/j.ijpharm.2010.12.020

Laperriere, N. J., Leung, P. M. ., McKenzie, S., Milosevic, M., Wong, S., Glen, J., Pintilie, M., & Bernstein, M. (1998). Randomized study of brachytherapy in the initial management of patients with malignant astrocytoma. *International Journal of Radiation Oncology*Biology*Physics*, *41*(5), 1005–1011. https://doi.org/10.1016/S0360-3016(98)00159-X

Lapointe, S., Perry, A., & Butowski, N. A. (2018). Primary brain tumours in adults. *The Lancet*, *392*(10145), 432–446. https://doi.org/10.1016/S0140-6736(18)30990-5

Le Rhun, E., Devos, P., Houillier, C., Cartalat, S., Chinot, O., Di Stefano, A. L., Lepage, C., Reyns, N., Dubois, F., & Weller, M. (2019). Romiplostim for temozolomide-induced thrombocytopenia in glioblastoma. *Neurology*, *93*(19), e1799–e1806. https://doi.org/10.1212/WNL.0000000000008440

Lee, J. H., Lee, J. E., Kahng, J. Y., Kim, S. H., Park, J. S., Yoon, S. J., Um, J.-Y.,

Kim, W. K., Lee, J.-K., Park, J., Kim, E. H., Lee, J.-H., Lee, J.-H., Chung, W.-S., Ju, Y. S., Park, S.-H., Chang, J. H., Kang, S.-G., & Lee, J. H. (2018). Human glioblastoma arises from subventricular zone cells with low-level driver mutations. *Nature*, *560*(7717), 243–247. https://doi.org/10.1038/s41586-018-0389-3

Lee, J. H., & Wee, C. W. (2022). Treatment of Adult Gliomas: A Current Update. *Brain & Neurorehabilitation*, *15*(3). https://doi.org/10.12786/bn.2022.15.e24

Lehner, E., Gündel, D., Liebau, A., Plontke, S., & Mäder, K. (2019). Intracochlear PLGA based implants for dexamethasone release: Challenges and solutions. *International Journal of Pharmaceutics: X*, *1*(February), 100015. https://doi.org/10.1016/j.ijpx.2019.100015

Lim, H., & Hoag, S. W. (2013). Plasticizer Effects on Physical–Mechanical Properties of Solvent Cast Soluplus® Films. *AAPS PharmSciTech*, *14*(3), 903–910. https://doi.org/10.1208/s12249-013-9971-z

Lin, X., Yang, H., Su, L., Yang, Z., & Tang, X. (2018). Effect of size on the in vitro/in vivo drug release and degradation of exenatide-loaded PLGA microspheres. *Journal of Drug Delivery Science and Technology*, *45*(March), 346–356. https://doi.org/10.1016/j.jddst.2018.03.024

Louis, D. N., Perry, A., Reifenberger, G., von Deimling, A., Figarella-Branger, D., Cavenee, W. K., Ohgaki, H., Wiestler, O. D., Kleihues, P., & Ellison, D. W. (2016). The 2016 World Health Organization Classification of Tumors of the Central Nervous System: a summary. *Acta Neuropathologica*, *131*(6), 803–820. https://doi.org/10.1007/s00401-016-1545-1

Louis, D. N., Perry, A., Wesseling, P., Brat, D. J., Cree, I. A., Figarella-Branger, D., Hawkins, C., Ng, H. K., Pfister, S. M., Reifenberger, G., Soffietti, R., von Deimling, A., & Ellison, D. W. (2021). The 2021 WHO Classification of Tumors of the Central Nervous System: a summary. *Neuro-Oncology*, *23*(8), 1231–1251. https://doi.org/10.1093/neuonc/noab106

Luckachan, G. E., & Pillai, C. K. S. (2011). Biodegradable Polymers- A Review on Recent Trends and Emerging Perspectives. *Journal of Polymers and the Environment*, *19*(3), 637–676. https://doi.org/10.1007/s10924-011-0317-1

Major, I., & McConville, C. (2015). Hot Melt Extruded and Injection Moulded Dosage Forms: Recent Research and Patents. *Recent Patents on Drug Delivery & Formulation*, *9*(3), 194–200. https://doi.org/10.2174/1872211309666150512111143

Makadia, H. K., & Siegel, S. J. (2011). Poly Lactic-co-Glycolic Acid (PLGA) as Biodegradable Controlled Drug Delivery Carrier. *Polymers*, *3*(3), 1377–1397. https://doi.org/10.3390/polym3031377

Maniruzzaman, M., Boateng, J. S., Bonnefille, M., Aranyos, A., Mitchell, J. C., & Douroumis, D. (2012). Taste masking of paracetamol by hot-melt extrusion: An in vitro and in vivo evaluation. *European Journal of Pharmaceutics and Biopharmaceutics*, *80*(2), 433–442. https://doi.org/10.1016/j.ejpb.2011.10.019

Maniruzzaman, M., Boateng, J. S., Snowden, M. J., & Douroumis, D. (2012). A Review of Hot-Melt Extrusion: Process Technology to Pharmaceutical Products. *ISRN Pharmaceutics*, *2012*, 1–9. https://doi.org/10.5402/2012/436763

Manna, S., Donnell, A. M., Kaval, N., Al-Rjoub, M. F., Augsburger, J. J., & Banerjee,

R. K. (2018). Improved design and characterization of PLGA/PLA-coated Chitosan based micro-implants for controlled release of hydrophilic drugs. *International Journal of Pharmaceutics*, *547*(1–2), 122–132. https://doi.org/10.1016/j.ijpharm.2018.05.066

Mansour, H. M., Sohn, M., Al-Ghananeem, A., & DeLuca, P. P. (2010). Materials for Pharmaceutical Dosage Forms: Molecular Pharmaceutics and Controlled Release Drug Delivery Aspects. *International Journal of Molecular Sciences*, *11*(9), 3298–3322. https://doi.org/10.3390/ijms11093298

Mao, S., Guo, C., Shi, Y., & Li, L. C. (2012). Recent advances in polymeric microspheres for parenteral drug delivery – part 1. *Expert Opinion on Drug Delivery*, *9*(9), 1161–1176. https://doi.org/10.1517/17425247.2012.709844

Markland, P., & Middleton, J. (2015). Biodegradable polymers as drug carriers. In J. Swarbrick (Ed.), *Encyclopedia of Pharmaceutical Technology* (4th ed., p. 22).

Marriott, C. J. C., Thorstad, W., Akabani, G., Brown, M. T., McLendon, R. E., Hanson, M. W., & Coleman, R. E. (1998). Locally increased uptake of fluorine-18-fluorodeoxyglucose after intracavitary administration of iodine-131-labeled antibody for primary brain tumors. *Journal of Nuclear Medicine : Official Publication, Society of Nuclear Medicine*, *39*(8), 1376–1380. http://www.ncbi.nlm.nih.gov/pubmed/9708511

Martinez, R., Martin-Subero, J. I., Rohde, V., Kirsch, M., Alaminos, M., Fernandez, A. F., Ropero, S., Schockert, G., & Esteller, M. (2009). A microarray-based DNA methylation study of glioblastoma multiforme. *Epigenetics*, *4*(4), 255–264. https://doi.org/10.4161/epi.9130

Masuda, N., Fukuoka, M., Kusunoki, Y., Matsui, K., Takifuji, N., Kudoh, S., Negoro, S., Nishioka, M., Nakagawa, K., & Takada, M. (1992). CPT-11: a new derivative of camptothecin for the treatment of refractory or relapsed small-cell lung cancer. *Journal of Clinical Oncology*, *10*(8), 1225–1229. https://doi.org/10.1200/JCO.1992.10.8.1225

Masui, K., Mischel, P. S., & Reifenberger, G. (2016). *Molecular classification of gliomas* (pp. 97–120). https://doi.org/10.1016/B978-0-12-802997-8.00006-2

Maurus, P. B., & Kaeding, C. C. (2004). Bioabsorbable implant material review. *Operative Techniques in Sports Medicine*, *12*(3), 158–160. https://doi.org/10.1053/j.otsm.2004.07.015

McConville, C., Tawari, P., & Wang, W. (2015). Hot melt extruded and injection moulded disulfiram-loaded PLGA millirods for the treatment of glioblastoma multiforme via stereotactic injection. *International Journal of Pharmaceutics*, *494*(1), 73–82. https://doi.org/10.1016/j.ijpharm.2015.07.072

Melhem, J. M., Detsky, J., Lim-Fat, M. J., & Perry, J. R. (2022). Updates in IDH-Wildtype Glioblastoma. *Neurotherapeutics*, *19*(6), 1705–1723. https://doi.org/10.1007/s13311-022-01251-6

Mello, V. A. de, & Ricci-Júnior, E. (2011). Encapsulation of naproxen in nanostructured system: structural characterization and in vitro release studies. *Química Nova*, *34*(6), 933–939. https://doi.org/10.1590/S0100-40422011000600004

Menei, P., Capelle, L., Guyotat, J., Fuentes, S., Assaker, R., Bataille, B., François, P., Dorwling-Carter, D., Paquis, P., Bauchet, L., Parker, F., Sabatier, J., Faisant,

N., & Benoit, J. P. (2005). Local and sustained delivery of 5-fluorouracil from biodegradable microspheres for the radiosensitization of malignant glioma: A randomized phase II trial. *Neurosurgery*, *56*(2), 242–247. https://doi.org/10.1227/01.NEU.0000144982.82068.A2

Messali, A., Villacorta, R., & Hay, J. W. (2014). A Review of the Economic Burden of Glioblastoma and the Cost Effectiveness of Pharmacologic Treatments. *PharmacoEconomics*, *32*(12), 1201–1212. https://doi.org/10.1007/s40273-014-0198-y

Mesti, T., Ebert Moltara, M., Boc, M., Rebersek, M., & Ocvirk, J. (2015). Bevacizumab and irinotecan in recurrent malignant glioma, a single institution experience. *Radiology and Oncology*, *49*(1), 80–85. https://doi.org/10.2478/raon-2014-0021

Meyers, J. D., Doane, T., Burda, C., & Basilion, J. P. (2013). Nanoparticles for imaging and treating brain cancer. *Nanomedicine*, *8*(1), 123–143. https://doi.org/10.2217/nnm.12.185

Mikrani, I., Sarkar, M. R., Islam, M., Das, S. C., & Rahman Prattay, K. M. (2022). Development, Characterization and In vitro Evaluation of Solid Dispersion Formulations of Low Aqueous Soluble BCS Class II Drug Pitavastatin with Poloxamer 407 and HPMC. *Dhaka University Journal of Pharmaceutical Sciences*, 325–336. https://doi.org/10.3329/dujps.v20i3.59798

Minniti, G., De Sanctis, V., Muni, R., Filippone, F., Bozzao, A., Valeriani, M., Osti, M. F., De Paula, U., Lanzetta, G., Tombolini, V., & Maurizi Enrici, R. (2008). Radiotherapy plus concomitant and adjuvant temozolomide for glioblastoma in

elderly patients. *Journal of Neuro-Oncology*, *88*(1), 97–103. https://doi.org/10.1007/s11060-008-9538-0

Mitra, A., & Wu, Y. (2010). Use of In Vitro-In Vivo Correlation (IVIVC) to Facilitate the Development of Polymer-Based Controlled Release Injectable Formulations. *Recent Patents on Drug Delivery & Formulation*, *4*(2), 94–104. https://doi.org/10.2174/187221110791185024

Mitragotri, S., Burke, P. A., & Langer, R. (2014). Overcoming the challenges in administering biopharmaceuticals: formulation and delivery strategies. *Nature Reviews Drug Discovery*, *13*(9), 655–672. https://doi.org/10.1038/nrd4363

Moghimi, S. M., Hunter, A. C., Dadswell, C. M., Savay, S., Alving, C. R., & Szebeni, J. (2004). Causative factors behind poloxamer 188 (Pluronic F68, Flocor™)-induced complement activation in human sera. *Biochimica et Biophysica Acta (BBA) - Molecular Basis of Disease*, *1689*(2), 103–113. https://doi.org/10.1016/j.bbadis.2004.02.005

Moshayedi, P., Ng, G., Kwok, J. C. F., Yeo, G. S. H., Bryant, C. E., Fawcett, J. W., Franze, K., & Guck, J. (2014). The relationship between glial cell mechanosensitivity and foreign body reactions in the central nervous system. *Biomaterials*, *35*(13), 3919–3925. https://doi.org/10.1016/j.biomaterials.2014.01.038

Mrugala, M. M. (2013). Advances and challenges in the treatment of glioblastoma: a clinician’s perspective. *Discovery Medicine*, *15*(83), 221–230. http://www.ncbi.nlm.nih.gov/pubmed/23636139

Mu, L., & Feng, S. . (2003). A novel controlled release formulation for the anticancer

drug paclitaxel (Taxol®): PLGA nanoparticles containing vitamin E TPGS. *Journal of Controlled Release*, *86*(1), 33–48. https://doi.org/10.1016/S0168-3659(02)00320-6

Murphy, M. K., Piper, R. K., Greenwood, L. R., Mitch, M. G., Lamperti, P. J., Seltzer, S. M., Bales, M. J., & Phillips, M. H. (2004). Evaluation of the new cesium-131 seed for use in low-energy x-ray brachytherapy. *Medical Physics*, *31*(6), 1529–1538. https://doi.org/10.1118/1.1755182

Nabors, M. W., Griffin, C. A., Zehnbauer, B. A., Hruban, R. H., Phillips, P. C., Grossman, S. A., Brem, H., & Colvin, O. M. (1991). Multidrug resistance gene (MDR1) expression in human brain tumors. *Journal of Neurosurgery*, *75*(6), 941–946. https://doi.org/10.3171/jns.1991.75.6.0941

Nair, L. S., & Laurencin, C. T. (2007). Biodegradable polymers as biomaterials. *Progress in Polymer Science*, *32*(8–9), 762–798. https://doi.org/10.1016/j.progpolymsci.2007.05.017

Nakada, M., Kita, D., Watanabe, T., Hayashi, Y., Teng, L., Pyko, I. V, & Hamada, J.-I. (2011). Aberrant Signaling Pathways in Glioma. *Cancers*, *3*, 3242–3278. https://doi.org/10.3390/cancers3033242

Nakai, E., Park, K., Yawata, T., Chihara, T., Kumazawa, A., Nakabayashi, H., & Shimizu, K. (2009). Enhanced MDR1 expression and chemoresistance of cancer stem cells derived from glioblastoma. *Cancer Investigation*, *27*(9), 901–908. https://doi.org/10.3109/07357900801946679

Nam, L., Coll, C., Erthal, L., de la Torre, C., Serrano, D., Martínez-Máñez, R., Santos-Martínez, M., & Ruiz-Hernández, E. (2018). Drug Delivery Nanosystems

for the Localized Treatment of Glioblastoma Multiforme. *Materials*, *11*(5), 779. https://doi.org/10.3390/ma11050779

Netchacovitch, L., Dumont, E., Cailletaud, J., Thiry, J., De Bleye, C., Sacré, P. Y., Boiret, M., Evrard, B., Hubert, P., & Ziemons, E. (2017). Development of an analytical method for crystalline content determination in amorphous solid dispersions produced by hot-melt extrusion using transmission Raman spectroscopy: A feasibility study. *International Journal of Pharmaceutics*, *530*(1–2), 249–255. https://doi.org/10.1016/j.ijpharm.2017.07.052

Newton, H. B. (2016). Overview of Pathology and Treatment of Primary Brain Tumors. In *Handbook of Neuro-Oncology Neuroimaging* (Second Edi, pp. 9–22). Elsevier. https://doi.org/10.1016/B978-0-12-800945-1.00002-1

Nielsen, S. F., Nordestgaard, B. G., & Bojesen, S. E. (2012). Statin Use and Reduced Cancer-Related Mortality. *New England Journal of Medicine*, *367*(19), 1792–1802. https://doi.org/10.1056/nejmoa1201735

Norman, J., Madurawe, R. D., Moore, C. M. V., Khan, M. A., & Khairuzzaman, A. (2017). A new chapter in pharmaceutical manufacturing: 3D-printed drug products. *Advanced Drug Delivery Reviews*, *108*, 39–50. https://doi.org/10.1016/j.addr.2016.03.001

Ohgaki. (2009). Epidemiology, Cancer. In *Cancer Epidemology Vol 2 Modifiable Factors*.

Ohno, R., Okada, K., Masaoka, T., Kuramoto, A., Arima, T., Yoshida, Y., Ariyoshi, H., Ichimaru, M., Sakai, Y., & Oguro, M. (1990). An early phase II study of CPT-11: a new derivative of camptothecin, for the treatment of leukemia and lymphoma.

Journal of Clinical Oncology : Official Journal of the American Society of Clinical Oncology, *8*(11), 1907–1912. https://doi.org/10.1200/JCO.1990.8.11.1907

Olar, A., Raghunathan, A., Albarracin, C. T., Aldape, K. D., Cahill, D. P., Powell, S. Z., Goodman, J. C., & Fuller, G. N. (2012). Absence of IDH1-R132H mutation predicts rapid progression of nonenhancing diffuse glioma in older adults. *Annals of Diagnostic Pathology*, *16*(3), 161–170. https://doi.org/10.1016/j.anndiagpath.2011.08.010

Olejnik, A., Kapuscinska, A., Schroeder, G., & Nowak, I. (2017). Physico-chemical characterization of formulations containing endomorphin-2 derivatives. *Amino Acids*, *49*(10), 1719–1731. https://doi.org/10.1007/s00726-017-2470-x

Ong, B. Y. S., Ranganath, S. H., Lee, L. Y., Lu, F., Lee, H. S., Sahinidis, N. V., & Wang, C. H. (2009). Paclitaxel delivery from PLGA foams for controlled release in post-surgical chemotherapy against glioblastoma multiforme. *Biomaterials*, *30*(18), 3189–3196. https://doi.org/10.1016/j.biomaterials.2009.02.030

Osborn, A. G., Louis, D. N., Poussaint, T. Y., Linscott, L. L., & Salzman, K. L. (2022). The 2021 World Health Organization Classification of Tumors of the Central Nervous System: What Neuroradiologists Need to Know. *American Journal of Neuroradiology*, *43*(7), 928–937. https://doi.org/10.3174/ajnr.A7462

Ose, L. (2011). Pitavastatin: Finding its place in therapy. *Therapeutic Advances in Chronic Disease*, *2*(2), 101–117. https://doi.org/10.1177/2040622310389227

Ostrom, Q. T., Cioffi, G., Gittleman, H., Patil, N., Waite, K., Kruchko, C., & Barnholtz-Sloan, J. S. (2019). CBTRUS Statistical Report: Primary Brain and Other Central Nervous System Tumors Diagnosed in the United States in 2012–2016. *Neuro-*

Oncology, *21*(Supplement_5), v1–v100. https://doi.org/10.1093/neuonc/noz150

Ostrom, Q. T., Cote, D. J., Ascha, M., Kruchko, C., & Barnholtz-Sloan, J. S. (2018). Adult Glioma Incidence and Survival by Race or Ethnicity in the United States From 2000 to 2014. *JAMA Oncology*, *4*(9), 1254. https://doi.org/10.1001/jamaoncol.2018.1789

Ostrom, Q. T., Fahmideh, M. A., Cote, D. J., Muskens, I. S., Schraw, J. M., Scheurer, M. E., & Bondy, M. L. (2019). Risk factors for childhood and adult primary brain tumors. *Neuro-Oncology*, *21*(11), 1357–1375. https://doi.org/10.1093/neuonc/noz123

Ozel, O., Kurt, M., Ozdemir, O., Bayram, J., Akdeniz, H., & Koca, D. (2016a). Complete response to bevacizumab plus irinotecan in patients with rapidly progressive GBM: Cases report and literature review. *Journal of Oncological Sciences*, *2*(2–3), 87–94. https://doi.org/10.1016/j.jons.2016.07.009

Ozel, O., Kurt, M., Ozdemir, O., Bayram, J., Akdeniz, H., & Koca, D. (2016b). Complete response to bevacizumab plus irinotecan in patients with rapidly progressive GBM: Cases report and literature review. *Journal of Oncological Sciences*, *2*(2–3), 87–94. https://doi.org/10.1016/j.jons.2016.07.009

Parodi, A., Rudzińska, M., Deviatkin, A., Soond, S., Baldin, A., & Zamyatnin, A. (2019). Established and Emerging Strategies for Drug Delivery Across the Blood-Brain Barrier in Brain Cancer. *Pharmaceutics*, *11*(5), 245. https://doi.org/10.3390/pharmaceutics11050245

Patel, D. M., Agarwal, N., Tomei, K. L., Hansberry, D. R., & Goldstein, I. M. (2015). Optimal Timing of Whole-Brain Radiation Therapy Following Craniotomy for

Cerebral Malignancies. *World Neurosurgery*, *84*(2), 412–419. https://doi.org/10.1016/j.wneu.2015.03.052

Patil, H., Tiwari, R. V., & Repka, M. A. (2016). Hot-Melt Extrusion: from Theory to Application in Pharmaceutical Formulation. *AAPS PharmSciTech*, *17*(1), 20–42. https://doi.org/10.1208/s12249-015-0360-7

Perry, A., & Wesseling, P. (2016). Histologic classification of gliomas. *Handbook of Clinical Neurology*, *134*, 71–95. https://doi.org/10.1016/B978-0-12-802997-8.00005-0

Phan-Thien, N., & Mai-Duy, N. (2017). *Understanding Viscoelasticity*. Springer International Publishing. https://doi.org/10.1007/978-3-319-62000-8

Pimple, P., Singh, P., Prabhu, A., & Gupta, S. (2022). Development and Optimization of HP-β-CD Inclusion Complex-Based Fast Orally Disintegrating Tablet of Pitavastatin Calcium. *Journal of Pharmaceutical Innovation*, *17*(3), 993–1010. https://doi.org/10.1007/s12247-022-09661-x

Potmesil, M. (1994). Camptothecins: from bench research to hospital wards. *Cancer Research*, *54*(6), 1431–1439. http://www.ncbi.nlm.nih.gov/pubmed/8137244

Poudel, B. K., Gupta, B., Ramasamy, T., Thapa, R. K., Youn, Y. S., Choi, H. G., Yong, C. S., & Kim, J. O. (2016). Development of polymeric irinotecan nanoparticles using a novel lactone preservation strategy. *International Journal of Pharmaceutics*, *512*(1), 75–86. https://doi.org/10.1016/j.ijpharm.2016.08.018

Pradhan, D. K., Choudhary, R. N. P., Samantaray, B. K., Karan, N. K., & Katiyar, R. S. (2007). Effect of Plasticizer on Structural and Electrical Properties of Polymer

Nanocompsoite Electrolytes. *International Journal of Electrochemical Science*, *2*(11), 861–871. https://doi.org/10.1016/S1452-3981(23)17118-5

Prados, M. D., Lamborn, K., Yung, W. K. A., Jaeckle, K., Robins, H. I., Mehta, M., Fine, H. A., Wen, P. Y., Cloughesy, T., Chang, S., Nicholas, M. K., Schiff, D., Greenberg, H., Junck, L., Fink, K., Hess, K., & Kuhn, J. (2006). A phase 2 trial of irinotecan (CPT-11) in patients with recurrent malignant glioma: A North American Brain Tumor Consortium study1. *Neuro-Oncology*, *8*(2), 189–193. https://doi.org/10.1215/15228517-2005-010

Prados, M. D., Yung, W. K. A., Jaeckle, K. A., Robins, H. I., Mehta, M. P., Fine, H. A., Wen, P. Y., Cloughesy, T. F., Chang, S. M., Nicholas, M. K., Schiff, D., Greenberg, H. S., Junck, L., Fink, K. L., Hess, K. R., & Kuhn, J. (2004). Phase 1 trial of irinotecan (CPT-11) in patients with recurrent malignant glioma: A North American brain tumor consortium study. *Neuro-Oncology*, *6*(1), 44–54. https://doi.org/10.1215/S1152851703000292

Prasad, G., & Haas-Kogan, D. A. (2009). Radiation-induced gliomas. *Expert Review of Neurotherapeutics*, *9*(10), 1511–1517. https://doi.org/10.1002/pmic.200800802

Purow, B., & Fine, H. A. (2004). Antiangiogenic therapy for primary and metastatic brain tumors. *Hematology/Oncology Clinics of North America*, *18*(5), 1161–1181. https://doi.org/10.1016/j.hoc.2004.05.003

Qian, F., Szymanski, A., & Gao, J. (2001). Fabrication and characterization of controlled release poly(D,L-lactide-co-glycolide) millirods. *Journal of Biomedical Materials Research*, *55*(4), 512–522. https://doi.org/10.1002/1097-

4636(20010615)55:4<512::aid-jbm1044>3.0.co;2-n

Quinn, J. A., Reardon, D. A., Friedman, A. H., Rich, J. N., Sampson, J. H., Vredenburgh, J., Gururangan, S., Provenzale, J. M., Walker, A., Schweitzer, H., Bigner, D. D., Tourt-Uhlig, S., Herndon, J. E., Affronti, M. Lou, Jackson, S., Allen, D., Ziegler, K., Bohlin, C., Lentz, C., & Friedman, H. S. (2004). Phase 1 trial of irinotecan plus BCNU in patients with progressive or recurrent malignant glioma. *Neuro-Oncology*, *6*(2), 145–153. https://doi.org/10.1215/S1152851703000498

QUINTEN, T., BEER, T., VERVAET, C., & REMON, J. (2009). Evaluation of injection moulding as a pharmaceutical technology to produce matrix tablets. *European Journal of Pharmaceutics and Biopharmaceutics*, *71*(1), 145–154. https://doi.org/10.1016/j.ejpb.2008.02.025

Rabin, C., Liang, Y., Ehrlichman, R. S., Budhian, A., Metzger, K. L., Majewski-Tiedeken, C., Winey, K. I., & Siegel, S. J. (2008). In vitro and in vivo demonstration of risperidone implants in mice. *Schizophrenia Research*, *98*(1–3), 66–78. https://doi.org/10.1016/j.schres.2007.08.003

Rajgor, N., Bhaskar, V., & Patel, M. (2011). Implantable drug delivery systems: An overview. *Systematic Reviews in Pharmacy*, *2*(2), 91. https://doi.org/10.4103/0975-8453.86297

Ramesh, M., Ahlawat, P., & Srinivas, N. R. (2010). Irinotecan and its active metabolite, SN-38: review of bioanalytical methods and recent update from clinical pharmacology perspectives. *Biomedical Chromatography*, *24*(1), 104–123. https://doi.org/10.1002/bmc.1345

Raval, S., Hwang, S., & Dorsett, L. (2007). Bevacizumab and irinotecan in patients

(pts) with recurrent glioblastoma multiforme (GBM). *Journal of Clinical Oncology*, *25*(18_suppl), 2078–2078. https://doi.org/10.1200/jco.2007.25.18_suppl.2078

Raymond, E., Fabbro, M., Boige, V., Rixe, O., Frenay, M., Vassal, G., Faivre, S., Sicard, E., Germa, C., Rodier, J. M., Vernillet, L., & Armand, J. P. (2003). Multicentre phase II study and pharmacokinetic analysis of irinotecan in chemotherapy-naïve patients with glioblastoma. *Annals of Oncology*, *14*(4), 603–614. https://doi.org/10.1093/annonc/mdg159

Razavi, S. M., Lee, K. E., Jin, B. E., Aujla, P. S., Gholamin, S., & Li, G. (2016). Immune Evasion Strategies of Glioblastoma. *Frontiers in Surgery*, *3*(March), 1–9. https://doi.org/10.3389/fsurg.2016.00011

Reardon, D. A., Quinn, J. A., Rich, J. N., Gururangan, S., Vredenburgh, J., Sampson, J. H., Provenzale, J. M., Walker, A., Badruddoja, M., Tourt-Uhlig, S., Herndon, J. E., Dowell, J. M., Affronti, M. Lou, Jackson, S., Allen, D., Ziegler, K., Silverman, S., Bohlin, C., Friedman, A. H., … Friedman, H. S. (2004). Phase 2 trial of BCNU plus irinotecan in adults with malignant glioma. *Neuro-Oncology*, *6*(2), 134–144. https://doi.org/10.1215/S1152851703000413

Reddy, P. S., Babu, K. S., & Kumar, N. (2013). *ARTÍCULOS ORIGINALES A validated RP-HPLC method for the determination of Irinotecan hydrochloride residues for cleaning validation in production area Método RP- HPLC validado para la determinación de residuos de*. *47*(1), 41–50.

Reese, T. S., & Karnovsky, M. J. (1967). Fine structural localization of a blood-brain barrier to exogenous peroxidase. *The Journal of Cell Biology*, *34*(1), 207–217. https://doi.org/10.1083/jcb.34.1.207

Reguera-Nuñez, E., Roca, C., Hardy, E., de la Fuente, M., Csaba, N., & Garcia-Fuentes, M. (2014). Implantable controlled release devices for BMP-7 delivery and suppression of glioblastoma initiating cells. *Biomaterials*, *35*(9), 2859–2867. https://doi.org/10.1016/j.biomaterials.2013.12.001

Repka, M. A., Battu, S. K., Upadhye, S. B., Thumma, S., Crowley, M. M., Zhang, F., Martin, C., & McGinity, J. W. (2007). Pharmaceutical Applications of Hot-Melt Extrusion: Part II. *Drug Development and Industrial Pharmacy*, *33*(10), 1043–1057. https://doi.org/10.1080/03639040701525627

Repka, M. A., Majumdar, S., Kumar Battu, S., Srirangam, R., & Upadhye, S. B. (2008). Applications of hot-melt extrusion for drug delivery. *Expert Opinion on Drug Delivery*, *5*(12), 1357–1376. https://doi.org/10.1517/17425240802583421

Repka, M. A., Shah, S., Lu, J., Maddineni, S., Morott, J., Patwardhan, K., & Mohammed, N. N. (2012). Melt extrusion: process to product. *Expert Opinion on Drug Delivery*, *9*(1), 105–125. https://doi.org/10.1517/17425247.2012.642365

Ritger, P. L., & Peppas, N. A. (1987). *A simple equation for description of solute release II. Fickian and anomalous release from swellable devices*. *5*, 37–42. https://doi.org/10.1016/0168-3659(87)90035-6.

Rivard, M. J. (2007). Brachytherapy dosimetry parameters calculated for a Cs131 source. *Medical Physics*, *34*(2), 754–762. https://doi.org/10.1118/1.2432162

Rivard, M. J., Ballester, F., Butler, W. M., DeWerd, L. A., Ibbott, G. S., Meigooni, A. S., Melhus, C. S., Mitch, M. G., Nath, R., & Papagiannis, P. (2017). Supplement 2 for the 2004 update of the AAPM Task Group No. 43 Report: Joint recommendations by the AAPM and GEC-ESTRO. *Medical Physics*, *44*(9),

e297–e338. https://doi.org/10.1002/mp.12430

Rothen-Weinhold, A. (1999). Stability studies of a somatostatin analogue in biodegradable implants. *International Journal of Pharmaceutics*, *178*(2), 213–221. https://doi.org/10.1016/S0378-5173(98)00376-7

Rothen-Weinhold, A., Besseghir, K., Vuaridel, E., Sublet, E., Oudry, N., Kubel, F., & Gurny, R. (1999). Injection-molding versus extrusion as manufacturing technique for the preparation of biodegradable implants. *European Journal of Pharmaceutics and Biopharmaceutics*, *48*(2), 113–121. https://doi.org/10.1016/S0939-6411(99)00034-X

Rothen-Weinhold, Alexandra, Besseghir, K., & Gurny, R. (1997). Analysis of the influence of polymer characteristics and core loading on the in vivo release of a somatostatin analogue. *European Journal of Pharmaceutical Sciences*, *5*(6), 303–313. https://doi.org/10.1016/S0928-0987(97)00022-5

Rothenberg, M. L. (2001). Irinotecan (CPT-11): recent developments and future directions--colorectal cancer and beyond. *The Oncologist*, *6*(1), 66–80. https://doi.org/10.1634/theoncologist.6-1-66

Salvati, M., Frati, A., Russo, N., Caroli, E., Polli, F. M., Minniti, G., & Delfini, R. (2003). Radiation-induced gliomas: report of 10 cases and review of the literature. *Surgical Neurology*, *60*(1), 60–67. https://doi.org/10.1016/S0090-3019(03)00137-X

Santoveña, A., García, J. T., Oliva, A., Llabrés, M., & Fariña, J. B. (2006). A mathematical model for interpreting in vitro rhGH release from laminar implants. *International Journal of Pharmaceutics*, *309*(1–2), 38–43.

https://doi.org/10.1016/j.ijpharm.2005.10.045

Schjesvold, F., & Oriol, A. (2021). Current and Novel Alkylators in Multiple Myeloma. *Cancers*, *13*(10), 2465. https://doi.org/10.3390/cancers13102465

Schliecker, G., Schmidt, C., Fuchs, S., Ehinger, A., Sandow, J., & Kissel, T. (2004). In vitro and in vivo correlation of buserelin release from biodegradable implants using statistical moment analysis. *Journal of Controlled Release*, *94*(1), 25–37. https://doi.org/10.1016/j.jconrel.2003.09.003

Schreiner, V., Detampel, P., Jirkof, P., Puchkov, M., & Huwyler, J. (2021). Buprenorphine loaded PLGA microparticles: Characterization of a sustained-release formulation. *Journal of Drug Delivery Science and Technology*, *63*(April), 102558. https://doi.org/10.1016/j.jddst.2021.102558

Schwartzbaum, J. A., Fisher, J. L., Aldape, K. D., & Wrensch, M. (2006). Epidemiology and molecular pathology of glioma. *Nature Clinical Practice Neurology*, *2*(9), 494–503. https://doi.org/10.1038/ncpneuro0289

Scoutaris, N., Vithani, K., Slipper, I., Chowdhry, B., & Douroumis, D. (2014). SEM/EDX and confocal Raman microscopy as complementary tools for the characterization of pharmaceutical tablets. *International Journal of Pharmaceutics*, *470*(1–2), 88–98. https://doi.org/10.1016/j.ijpharm.2014.05.007

Seelig, A., Gottschlich, R., & Devant, R. M. (1994). A method to determine the ability of drugs to diffuse through the blood- brain barrier. *Proceedings of the National Academy of Sciences of the United States of America*, *91*(1), 68–72. https://doi.org/10.1073/pnas.91.1.68

Sen, A., Hinsu, D., Sen, D., Zanwar, A., Maheshwari, R., & Chandrakar, V. (2016). Analytical method development and validation for simultaneous estimation of Teneligliptin hydrobromide hydrate and Metformin hydrochloride from it's pharmaceutical dosage form by three different UV spectrophotometric methods. *Journal of Applied Pharmaceutical Science*, *6*(9), 157–165. https://doi.org/10.7324/JAPS.2016.60924

Sepehri, N., Rouhani, H., Tavassolian, F., Montazeri, H., Khoshayand, M. R., Ghahremani, M. H., Ostad, S. N., Atyabi, F., & Dinarvand, R. (2014). SN38 polymeric nanoparticles: In vitro cytotoxicity and in vivo antitumor efficacy in xenograft balb/c model with breast cancer versus irinotecan. *International Journal of Pharmaceutics*, *471*(1–2), 485–497. https://doi.org/10.1016/j.ijpharm.2014.05.046

Sequeira, J. A. D., Santos, A. C., Serra, J., Veiga, F., & Ribeiro, A. J. (2018). Poly(lactic- co -glycolic acid) (PLGA) matrix implants. In *Nanostructures for the Engineering of Cells, Tissues and Organs* (pp. 375–402). Elsevier. https://doi.org/10.1016/B978-0-12-813665-2.00010-7

Shameem, M., Lee, H., & DeLuca, P. P. (1999). A short-term (accelerated release) approach to evaluate peptide release from PLGA depot formulations. *AAPS PharmSci*, *1*(3), 1–6. https://doi.org/10.1208/ps010307

Shi, Y., Kramer, G., Schröder, A., Kirkpatrick, C., Seekamp, A., Schmidt, H., & Fuchs, S. (2014). Early endothelial progenitor cells as a source of myeloid cells to improve the pre-vascularisation of bone constructs. *European Cells and Materials*, *27*, 64–80. https://doi.org/10.22203/eCM.v027a06

SHIM, W., KIM, J., KIM, K., KIM, Y., PARK, R., KIM, I., KWON, I., & LEE, D. (2007). pH- and temperature-sensitive, injectable, biodegradable block copolymer hydrogels as carriers for paclitaxel. *International Journal of Pharmaceutics*, *331*(1), 11–18. https://doi.org/10.1016/j.ijpharm.2006.09.027

Shimada, Y., Yoshino, M., Wakui, A., Nakao, I., Futatsuki, K., Sakata, Y., Kambe, M., Taguchi, T., & Ogawa, N. (1993). Phase II study of CPT-11, a new camptothecin derivative, in metastatic colorectal cancer. CPT-11 Gastrointestinal Cancer Study Group. *Journal of Clinical Oncology : Official Journal of the American Society of Clinical Oncology*, *11*(5), 909–913. https://doi.org/10.1200/JCO.1993.11.5.909

Shrivastava, S., Deshpande, P., & Daharwal, S. J. (2019). Key Aspects of Analytical Method Development and Validation. *Journal of Ravishankar University (PART-B)*, *31*(1), 32–39. https://doi.org/10.52228/JRUB.2018-31-1-6

SIEGEL, S., KAHN, J., METZGER, K., WINEY, K., WERNER, K., & DAN, N. (2006). Effect of drug type on the degradation rate of PLGA matrices. *European Journal of Pharmaceutics and Biopharmaceutics*, *64*(3), 287–293. https://doi.org/10.1016/j.ejpb.2006.06.009

Siepmann, J, Siepmann, F., & Florence, A. T. (2006). Local controlled drug delivery to the brain: mathematical modeling of the underlying mass transport mechanisms. *International Journal of Pharmaceutics*, *314*(2), 101–119. https://doi.org/10.1016/j.ijpharm.2005.07.027

Siepmann, Juergen, & Siepmann, F. (2012). Modeling of diffusion controlled drug delivery. *Journal of Controlled Release*, *161*(2), 351–362.

https://doi.org/10.1016/j.jconrel.2011.10.006

Sinha, B. K. (1995). Topoisomerase Inhibitors: A Review of their Therapeutic Potential in Cancer. *Drugs*, *49*(1), 11–19. https://doi.org/10.2165/00003495-199549010-00002

Solanki, N. G., Tahsin, M., Shah, A. V., & Serajuddin, A. T. M. (2018). Formulation of 3D Printed Tablet for Rapid Drug Release by Fused Deposition Modeling: Screening Polymers for Drug Release, Drug-Polymer Miscibility and Printability. *Journal of Pharmaceutical Sciences*, *107*(1), 390–401. https://doi.org/10.1016/j.xphs.2017.10.021

Steele, T. W. J., Huang, C. L., Widjaja, E., Boey, F. Y. C., Loo, J. S. C., & Venkatraman, S. S. (2011). The effect of polyethylene glycol structure on paclitaxel drug release and mechanical properties of PLGA thin films. *Acta Biomaterialia*, *7*(5), 1973–1983. https://doi.org/10.1016/j.actbio.2011.02.002

Stefanini-Oresic, L. (2022). Validation of analytical procedures: ICH guidelines Q2(R2). *Farmaceutski Glasnik*, *2*(0), 1–34.

Stein, E. A. (2003). The power of statins: Aggressive lipid lowering. *Clinical Cardiology*, *26*(S3), 25–31. https://doi.org/10.1002/clc.4960261506

Stewart, L. A. (2002). Chemotherapy in adult high-grade glioma: a systematic review and meta-analysis of individual patient data from 12 randomised trials. *Lancet (London, England)*, *359*(9311), 1011–1018. https://doi.org/10.1016/s0140-6736(02)08091-1

Stewart, S., Domínguez-Robles, J., Donnelly, R., & Larrañeta, E. (2018). Implantable

Polymeric Drug Delivery Devices: Classification, Manufacture, Materials, and Clinical Applications. *Polymers*, *10*(12), 1379. https://doi.org/10.3390/polym10121379

Stupp, R, Brada, M., Van Den Bent, M. J., Tonn, J.-C., & Pentheroudakis, & G. (2014). High-grade glioma: ESMO Clinical Practice Guidelines for diagnosis, treatment and follow-up † on behalf of the ESMO Guidelines Working Group * incidence and epidemiology. *Annals of Oncology*, *25*(April), iii93–iii101. https://doi.org/10.1093/annonc/mdu050

Stupp, Roger, Hegi, M. E., van den Bent, M. J., Mason, W. P., Weller, M., Mirimanoff, R. O., & Cairncross, J. G. (2006). Changing Paradigms—An Update on the Multidisciplinary Management of Malignant Glioma. *The Oncologist*, *11*(2), 165–180. https://doi.org/10.1634/theoncologist.11-2-165

Suh, M. S., Kastellorizios, M., Tipnis, N., Zou, Y., Wang, Y., Choi, S., & Burgess, D. J. (2021). Effect of implant formation on drug release kinetics of in situ forming implants. *International Journal of Pharmaceutics*, *592*(July 2020), 120105. https://doi.org/10.1016/j.ijpharm.2020.120105

Tabet, A., Jensen, M. P., Parkins, C. C., Patil, P. G., Watts, C., & Scherman, O. A. (2019). Designing Next-Generation Local Drug Delivery Vehicles for Glioblastoma Adjuvant Chemotherapy: Lessons from the Clinic. *Advanced Healthcare Materials*, *8*(3), 1801391. https://doi.org/10.1002/adhm.201801391

Takahashi, M., Onishi, H., & Machida, Y. (2004). Development of implant tablet for a week-long sustained release. *Journal of Controlled Release*, *100*(1), 63–74. https://doi.org/10.1016/j.jconrel.2004.07.031

Thakkar, J. P., Dolecek, T. A., Horbinski, C., Ostrom, Q. T., Lightner, D. D., Barnholtz-Sloan, J. S., & Villano, J. L. (2014). Epidemiologic and molecular prognostic review of glioblastoma. *Cancer Epidemiology Biomarkers and Prevention*, *23*(10), 1985–1996. https://doi.org/10.1158/1055-9965.EPI-14-0275

Thalhauser, S., Peterhoff, D., Wagner, R., & Breunig, M. (2020). Silica particles incorporated into PLGA-based in situ-forming implants exploit the dual advantage of sustained release and particulate delivery. *European Journal of Pharmaceutics and Biopharmaceutics*, *156*(February), 1–10. https://doi.org/10.1016/j.ejpb.2020.08.020

Thurnher, M., Nussbaumer, O., & Gruenbacher, G. (2012). Novel aspects of mevalonate pathway inhibitors as antitumor agents. *Clinical Cancer Research*, *18*(13), 3524–3531. https://doi.org/10.1158/1078-0432.CCR-12-0489

Tomar, M. S., Kumar, A., Srivastava, C., & Shrivastava, A. (2021). Elucidating the mechanisms of Temozolomide resistance in gliomas and the strategies to overcome the resistance. *Biochimica et Biophysica Acta (BBA) - Reviews on Cancer*, *1876*(2), 188616. https://doi.org/10.1016/j.bbcan.2021.188616

Tomic, I., Vidis-Millward, A., Mueller-Zsigmondy, M., & Cardot, J.-M. (2016). Setting accelerated dissolution test for PLGA microspheres containing peptide, investigation of critical parameters affecting drug release rate and mechanism. *International Journal of Pharmaceutics*, *505*(1–2), 42–51. https://doi.org/10.1016/j.ijpharm.2016.03.048

Tracy, M. A., Ward, K. L., Firouzabadian, L., Wang, Y., Dong, N., Qian, R., & Zhang, Y. (1999). Factors affecting the degradation rate of poly(lactide-co-glycolide)

microspheres in vivo and in vitro. *Biomaterials*, *20*(11), 1057–1062. https://doi.org/10.1016/S0142-9612(99)00002-2

Trivedi, S., Bhoyar, V., Akojwar, N., & Belgamwar, V. (2023). *Nano Trends Transport of nanocarriers to brain for treatment of glioblastoma multiforme : Routes and challenges*. *1*(February). https://doi.org/10.1016/j.nwnano.2023.100005

Tseng, Y. Y., Yang, T. C., Chen, S. M., Yang, S. T., Tang, Y. L., & Liu, S. J. (2020). Injectable SN-38-embedded polymeric microparticles promote antitumor efficacy against malignant glioma in an animal model. *Pharmaceutics*, *12*(5). https://doi.org/10.3390/pharmaceutics12050479

Tsuboi, Y., Kurimoto, M., Nagai, S., Hayakawa, Y., Kamiyama, H., Hayashi, N., Kitajima, I., & Endo, S. (2009). Induction of autophagic cell death and radiosensitization by the pharmacological inhibition of nuclear factor-kappa B activation in human glioma cell lines. *Journal of Neurosurgery*, *110*(3), 594–604. https://doi.org/10.3171/2008.8.JNS17648

Turner, C. D. (2002). Phase II study of irinotecan (CPT-11) in children with high-risk malignant brain tumors: The Duke experience. *Neuro-Oncology*, *4*(2), 102–108. https://doi.org/10.1215/15228517-4-2-102

Umeki, N., Sato, T., Harada, M., Takeda, J., Saito, S., Iwao, Y., & Itai, S. (2011). Preparation and evaluation of biodegradable films containing the potent osteogenic compound BFB0261 for localized delivery. *International Journal of Pharmaceutics*, *404*(1–2), 10–18. https://doi.org/10.1016/j.ijpharm.2010.10.043

Valtonen, S., Timonen, U., Toivanen, P., Kalimo, H., Kivipelto, L., Heiskanen, O., Unsgaard, G., & Kuurne, T. (1997). Interstitial chemotherapy with carmustine-

loaded polymers for high- grade gliomas: A randomized double-blind study. *Neurosurgery*, *41*(1), 44–49. https://doi.org/10.1097/00006123-199707000-00011

van den Bent, M. J., Dubbink, H. J., Sanson, M., van der Lee-Haarloo, C. R., Hegi, M., Jeuken, J. W. M., Ibdaih, A., Brandes, A. A., Taphoorn, M. J. B., Frenay, M., Lacombe, D., Gorlia, T., Dinjens, W. N. M., & Kros, J. M. (2009). MGMT promoter methylation is prognostic but not predictive for outcome to adjuvant PCV chemotherapy in anaplastic oligodendroglial tumors: a report from EORTC Brain Tumor Group Study 26951. *Journal of Clinical Oncology : Official Journal of the American Society of Clinical Oncology*, *27*(35), 5881–5886. https://doi.org/10.1200/JCO.2009.24.1034

Vangara, K. K., Ali, H. I., Lu, D., Liu, J. L., Kolluru, S., & Palakurthi, S. (2014). SN-38-cyclodextrin complexation and its influence on the solubility, stability, and in vitro anticancer activity against ovarian cancer. *AAPS PharmSciTech*, *15*(2), 472–482. https://doi.org/10.1208/s12249-013-0068-5

Vay, K., Scheler, S., & Frieß, W. (2011). Application of Hansen solubility parameters for understanding and prediction of drug distribution in microspheres. *International Journal of Pharmaceutics*, *416*(1), 202–209. https://doi.org/10.1016/j.ijpharm.2011.06.047

Villalva, C., Cortes, U., Wager, M., Tourani, J.-M., Rivet, P., Marquant, C., Martin, S., Turhan, A. G., & Karayan-Tapon, L. (2012). O6-Methylguanine-Methyltransferase (MGMT) Promoter Methylation Status in Glioma Stem-Like Cells is Correlated to Temozolomide Sensitivity Under Differentiation-Promoting

Conditions. *International Journal of Molecular Sciences*, *13*(6), 6983–6994. https://doi.org/10.3390/ijms13066983

Vitaz, T. W., Warnke, P. C., Tabar, V., & Gutin, P. H. (2005). Brachytherapy for brain tumors. *Journal of Neuro-Oncology*, *73*(1), 71–86. https://doi.org/10.1007/s11060-004-2352-4

Vogl, T. J., Engelmann, K., Mack, M. G., Straub, R., Zangos, S., Eichler, K., Hochmuth, K., & Orenberg, E. (2002). CT-guided intratumoural administration of cisplatin/epinephrine gel for treatment of malignant liver tumours. *British Journal of Cancer*, *86*(4), 524–529. https://doi.org/10.1038/sj.bjc.6600116

Voss, L., Guttek, K., Reddig, A., Reinhold, A., Voss, M., Simeoni, L., Schraven, B., & Reinhold, D. (2021). Pitavastatin is a highly potent inhibitor of t-cell proliferation. *Pharmaceuticals*, *14*(8), 1–19. https://doi.org/10.3390/ph14080727

Vredenburgh, J. J., Desjardins, A., Herndon, J. E., Dowell, J. M., Reardon, D. A., Quinn, J. A., Rich, J. N., Sathornsumetee, S., Gururangan, S., Wagner, M., Bigner, D. D., Friedman, A. H., & Friedman, H. S. (2007). Phase II Trial of Bevacizumab and Irinotecan in Recurrent Malignant Glioma. *Clinical Cancer Research*, *13*(4), 1253–1259. https://doi.org/10.1158/1078-0432.CCR-06-2309

Vredenburgh, J. J., Desjardins, A., Herndon, J. E., Marcello, J., Reardon, D. A., Quinn, J. A., Rich, J. N., Sathornsumetee, S., Gururangan, S., Sampson, J., Wagner, M., Bailey, L., Bigner, D. D., Friedman, A. H., & Friedman, H. S. (2007). Bevacizumab plus irinotecan in recurrent glioblastoma multiforme. *Journal of Clinical Oncology*, *25*(30), 4722–4729. https://doi.org/10.1200/JCO.2007.12.2440

Vredenburgh, J. J., Desjardins, A., Reardon, D. A., & Friedman, H. S. (2009). Experience with irinotecan for the treatment of malignant glioma. *Neuro-Oncology*, *11*(1), 80–91. https://doi.org/10.1215/15228517-2008-075

Vukelja, S. J., Anthony, S. P., Arseneau, J. C., Berman, B. S., Cunningham, C. C., Nemunaitis, J. J., Samlowski, W. E., & Fowers, K. D. (2007). Phase 1 study of escalating-dose OncoGel (ReGel/paclitaxel) depot injection, a controlled-release formulation of paclitaxel, for local management of superficial solid tumor lesions. *Anti-Cancer Drugs*, *18*(3), 283–289. https://doi.org/10.1097/CAD.0b013e328011a51d

Wait, S. D., Prabhu, R. S., Burri, S. H., Atkins, T. G., & Asher, A. L. (2015). Polymeric drug delivery for the treatment of glioblastoma. *Neuro-Oncology*, *17*(October 2014), ii9–ii23. https://doi.org/10.1093/neuonc/nou360

Wald, L. L., Nelson, S. J., Day, M. R., Noworolski, S. E., Henry, R. G., Huhn, S. L., Chang, S., Prados, M. D., Sneed, P. K., Larson, D. A., Wara, W. M., McDermott, M., Dillon, W. P., Gutin, P. H., & Vigneron, D. B. (1997). Serial proton magnetic resonance spectroscopy imaging of glioblastoma multiforme after brachytherapy. *Journal of Neurosurgery*, *87*(4), 525–534. https://doi.org/10.3171/jns.1997.87.4.0525

Walker, M. D., Alexander, E., Hunt, W. E., MacCarty, C. S., Mahaley, M. S., Mealey, J., Norrell, H. A., Owens, G., Ransohoff, J., Wilson, C. B., Gehan, E. A., & Strike, T. A. (1978). Evaluation of BCNU and/or radiotherapy in the treatment of anaplastic gliomas. *Journal of Neurosurgery*, *49*(3), 333–343. https://doi.org/10.3171/jns.1978.49.3.0333

Walker, M. D., Green, S. B., Byar, D. P., Alexander, E., Batzdorf, U., Brooks, W. H., Hunt, W. E., MacCarty, C. S., Mahaley, M. S., Mealey, J., Owens, G., Ransohoff, J., Robertson, J. T., Shapiro, W. R., Smith, K. R., Wilson, C. B., & Strike, T. A. (1980). Randomized comparisons of radiotherapy and nitrosoureas for the treatment of malignant glioma after surgery. *The New England Journal of Medicine*, *303*(23), 1323–1329. https://doi.org/10.1056/NEJM198012043032303

Wan, B., Andhariya, J. V., Bao, Q., Wang, Y., Zou, Y., & Burgess, D. J. (2021). Effect of polymer source on in vitro drug release from PLGA microspheres. *International Journal of Pharmaceutics*, *607*(July), 120907. https://doi.org/10.1016/j.ijpharm.2021.120907

Wang, A. Z. (2012). Nanoparticle drug delivery: Focusing on the therapeutic cargo. *Nanomedicine*, *7*(10), 1463–1465. https://doi.org/10.2217/nnm.12.114

Wang, C.-K., Wang, W.-Y., Meyer, R. F., Liang, Y., Winey, K. I., & Siegel, S. J. (2010). A rapid method for creating drug implants: Translating laboratory-based methods into a scalable manufacturing process. *Journal of Biomedical Materials Research Part B: Applied Biomaterials*, *93B*(2), 562–572. https://doi.org/10.1002/jbm.b.31617

Wang, P. P., Frazier, J., & Brem, H. (2002). Local drug delivery to the brain. *Advanced Drug Delivery Reviews*, *54*(7), 987–1013. https://doi.org/10.1016/s0169-409x(02)00054-6

Wang, W., Ghandi, A., Liebes, L., Louie, S. G., Hofman, F. M., Schönthal, A. H., & Chen, T. C. (2011). Effective conversion of irinotecan to SN-38 after intratumoral drug delivery to an intracranial murine glioma model in vivo. *Journal of*

Neurosurgery, *114*(3), 689–694. https://doi.org/10.3171/2010.2.JNS09719

Wang, Y., & Burgess, D. J. (2012). Microsphere Technologies. In *Long Acting Injections and Implants* (pp. 167–194). Springer US. https://doi.org/10.1007/978-1-4614-0554-2_10

Waqar, M., Trifiletti, D. M., McBain, C., O'Connor, J., Coope, D. J., Akkari, L., Quinones-Hinojosa, A., & Borst, G. R. (2022). Early Therapeutic Interventions for Newly Diagnosed Glioblastoma: Rationale and Review of the Literature. *Current Oncology Reports*, *24*(3), 311–324. https://doi.org/10.1007/s11912-021-01157-0

Washington, M. A., Swiner, D. J., Bell, K. R., Fedorchak, M. V., Little, S. R., & Meyer, T. Y. (2017). The impact of monomer sequence and stereochemistry on the swelling and erosion of biodegradable poly(lactic-co-glycolic acid) matrices. *Biomaterials*, *117*, 66–76. https://doi.org/10.1016/j.biomaterials.2016.11.037

Wedge, S. R., & Newlands, E. S. (1996). O6-benzylguanine enhances the sensitivity of a glioma xenograft with low O6-alkylguanine-DNA alkyltransferase activity to temozolomide and BCNU. *British Journal of Cancer*, *73*(9), 1049–1052. https://doi.org/10.1038/bjc.1996.203

Weinberg, B. D., Blanco, E., & Gao, J. (2008). Polymer implants for intratumoral drug delivery and cancer therapy. *Journal of Pharmaceutical Sciences*, *97*(5), 1681–1702. https://doi.org/10.1002/jps.21038

Wen, P. Y., & Kesari, S. (2008). Malignant Gliomas in Adults. *New England Journal of Medicine*, *359*(5), 492–507. https://doi.org/10.1056/NEJMra0708126

Westphal, M., Hilt, D. C., Bortey, E., Delavault, P., Olivares, R., Warnke, P. C.,

Whittle, I. R., Jääskeläinen, J., & Ram, Z. (2003). A phase 3 trial of local chemotherapy with biodegradable carmustine (BCNU) wafers (Gliadel wafers) in patients with primary malignant glioma. *Neuro-Oncology*, *5*(2), 79–88. https://doi.org/10.1215/15228517-5-2-79

Wick, W., Osswald, M., Wick, A., & Winkler, F. (2018). Treatment of glioblastoma in adults. *Therapeutic Advances in Neurological Disorders*, *11*(14), 1756286418790452. https://doi.org/10.1177/1756286418790452

Wilson, T., Karajannis, M., & Harter, D. (2014). Glioblastoma multiforme: State of the art and future therapeutics. *Surgical Neurology International*, *5*(1), 64. https://doi.org/10.4103/2152-7806.132138

Wolinsky, J. B., Colson, Y. L., & Grinstaff, M. W. (2012). Local drug delivery strategies for cancer treatment: Gels, nanoparticles, polymeric films, rods, and wafers. *Journal of Controlled Release*, *159*(1), 14–26. https://doi.org/10.1016/j.jconrel.2011.11.031

Wrensch, M., Minn, Y., Chew, T., Bondy, M., & Berger, M. S. (2002). Epidemiology of primary brain tumors: Current concepts and review of the literature. *Neuro-Oncology*, *4*(4), 278–299. https://doi.org/10.1215/S152285170200011X

Wu, C., Baldursdottir, S., Yang, M., & Mu, H. (2018). Lipid and PLGA hybrid microparticles as carriers for protein delivery. *Journal of Drug Delivery Science and Technology*, *43*, 65–72. https://doi.org/10.1016/j.jddst.2017.09.006

Wu, W., Klockow, J. L., Zhang, M., Lafortune, F., Chang, E., Jin, L., Wu, Y., & Daldrup-Link, H. E. (2021). Glioblastoma multiforme (GBM): An overview of current therapies and mechanisms of resistance. *Pharmacological Research*,

171, 105780. https://doi.org/10.1016/j.phrs.2021.105780

Xiao, P., Qi, P., Chen, J., Song, Z., Wang, Y., He, H., Tang, X., & Wang, P. (2020). The effect of polymer blends on initial release regulation and in vitro-in vivo relationship of peptides loaded PLGA-Hydrogel Microspheres. *International Journal of Pharmaceutics*, *591*(September), 119964. https://doi.org/10.1016/j.ijpharm.2020.119964

Xie, J., & Wang, C. H. (2006). Electrospun micro- and nanofibers for sustained delivery of paclitaxel to treat C6 glioma in vitro. *Pharmaceutical Research*, *23*(8), 1817–1826. https://doi.org/10.1007/s11095-006-9036-z

Xie, X., Li, Z., Zhang, L., Chi, Q., Yang, Y., Zhang, H., Yang, Y., & Mei, X. (2015). A novel accelerated in vitro release method to evaluate the release of thymopentin from PLGA microspheres. *Pharmaceutical Development and Technology*, *20*(5), 633–640. https://doi.org/10.3109/10837450.2014.892131

Xu, Q., & Czernuszka, J. T. (2008). Controlled release of amoxicillin from hydroxyapatite-coated poly(lactic-co-glycolic acid) microspheres. *Journal of Controlled Release*, *127*(2), 146–153. https://doi.org/10.1016/j.jconrel.2008.01.017

Xu, Y., & Villalona-Calero, M. A. (2002a). Irinotecan: Mechanisms of tumor resistance and novel strategies for modulating its activity. *Annals of Oncology*, *13*(12), 1841–1851. https://doi.org/10.1093/annonc/mdf337

Xu, Y., & Villalona-Calero, M. A. (2002b). Irinotecan: mechanisms of tumor resistance and novel strategies for modulating its activity. *Annals of Oncology*, *13*(12), 1841–1851. https://doi.org/10.1093/annonc/mdf337

Yanae, M., Tsubaki, M., Satou, T., Itoh, T., Imano, M., Yamazoe, Y., & Nishida, S. (2011). Statin-induced apoptosis via the suppression of ERK1/2 and Akt activation by inhibition of the geranylgeranyl-pyrophosphate biosynthesis in glioblastoma. *Journal of Experimental & Clinical Cancer Research*, *30*(1), 74. https://doi.org/10.1186/1756-9966-30-74

Youssef, E., Nakaji, P., Thomas, T., McBride, H., Fram, E., & Brachman, D. (2017). SCDT-36. NOVEL MODULAR, PERMANENTLY IMPLANTED COLLAGEN-BASED DEVICE FOR INTRAOPERATIVE BRACHYTHERAPY IN PATIENTS WITH CENTRAL NERVOUS SYSTEM TUMORS. *Neuro-Oncology*, *19*(suppl_6), vi272–vi272. https://doi.org/10.1093/neuonc/nox168.1117

Yung, W. K. A., Lieberman, F. S., Wen, P., Robin, I., Gilbert, M., Chang, S., Junck, L., Cloughesy, T., Lamborn, K., & Prados, M. (2005). Combination of temozolomide (TMZ) and irinotecan (CPT-11) showed enhanced activity for recurrent malignant gliomas: A North American Brain Tumor Consortium (NABTC) phase II study. *Journal of Clinical Oncology*, *23*(16_suppl), 1521–1521. https://doi.org/10.1200/jco.2005.23.16_suppl.1521

Zackrisson, G., Östling, G., Skagerberg, B., & Anfält, T. (1995). ACcelerated Dissolution Rate Analysis (ACDRA) for controlled release drugs. Application to Roxiam®. *Journal of Pharmaceutical and Biomedical Analysis*, *13*(4–5), 377–383. https://doi.org/10.1016/0731-7085(95)01293-T

Zembko, I., Ahmed, I., Farooq, A., Dail, J., Tawari, P., Wang, W., & Mcconville, C. (2015). Development of Disulfiram-Loaded Poly(Lactic-co-Glycolic Acid) Wafers for the Localised Treatment of Glioblastoma Multiforme: A Comparison of

Manufacturing Techniques. *Journal of Pharmaceutical Sciences*, *104*(3), 1076–1086. https://doi.org/10.1002/jps.24304

Zhang, J., Stevens, M. F. G., & Bradshaw, T. D. (2012). Temozolomide: mechanisms of action, repair and resistance. *Current Molecular Pharmacology*, *5*(1), 102–114. https://doi.org/10.2174/1874467211205010102

Zhang, Y., Chan, H. F., & Leong, K. W. (2013). Advanced materials and processing for drug delivery: The past and the future. *Advanced Drug Delivery Reviews*, *65*(1), 104–120. https://doi.org/10.1016/j.addr.2012.10.003

Zhang, Z.-Y., Zheng, S.-H., Yang, W.-G., Yang, C., & Yuan, W.-T. (2017). Targeting colon cancer stem cells with novel blood cholesterol drug pitavastatin. *European Review for Medical and Pharmacological Sciences*, *21*(6), 1226–1233. http://www.ncbi.nlm.nih.gov/pubmed/28387909

Zhou, T., Lewis, H., Foster, R. E., & Schwendeman, S. P. (1998). Development of a multiple-drug delivery implant for intraocular management of proliferative vitreoretinopathy. *Journal of Controlled Release*, *55*(2–3), 281–295. https://doi.org/10.1016/S0168-3659(98)00061-3

Zolnik, B. S., & Burgess, D. J. (2008). Evaluation of in vivo–in vitro release of dexamethasone from PLGA microspheres. *Journal of Controlled Release*, *127*(2), 137–145. https://doi.org/10.1016/j.jconrel.2008.01.004

Zolnik, B. S., Leary, P. E., & Burgess, D. J. (2006). Elevated temperature accelerated release testing of PLGA microspheres. *Journal of Controlled Release*, *112*(3), 293–300. https://doi.org/10.1016/j.jconrel.2006.02.015